THIN FILM ELECTROLYTE ELECTROCHEMISTRY FOR THE STUDY OF ATMOSPHERIC CORROSION

by

Shi Hua Zhang

A Thesis Presented to the
University of Manchester
for the Degree of
Doctor of Philosophy

Corrosion and Protection Centre
University of Manchester
Institute of Science and Technology

February 1995

To
My Parents
My Lovely Wife Lin Zhang for Her
Understanding, Encouragement and
Patiently Typing This Thesis

DECLARATION

No portion of the work referred to in the thesis has been submitted in support of an application for another degree or qualification of this or any other university or other institution of learning.

Zhang Shi Hua Shi Hua Zhang

PUBLICATIONS

Some of the work described in this thesis has been published as follows:

(1) The Electrochemistry of Iron, Zinc and Copper in Thin Layer Electrolytes

S.H. Zhang and S.B. Lyon, ***Corrosion Science***, 35, 713 (1993)

(2) Anodic Processes on Iron Covered by Thin, Dilute Electrolyte Layers (I)-Anodic Polarization

S.H. Zhang and S.B. Lyon, ***Corrosion Science***, 36, 1289(1994)

(3) Anodic Processes on Iron Covered by Thin, Dilute Electrolyte Layers (II)-A.C. Impedance Measurements

S.H. Zhang and S.B. Lyon, ***Corrosion Science***, 36, 1309(1994)

(4) Problems in A.C. Impedance Measurements of High Resistance System in Thin-film Electrolytes

S.H. Zhang and S.B. Lyon, Electronics Division Colloquium on Electrochemical Measurements, The Institution of Electrical Engineers, London (1994)

(5) Retention of Passivity on Selected Iron Samples After Several Months Atmospheric Exposure

S.H. Zhang and S.B. Lyon, Electronic Journal of Corrosion Science and Engineering at http://www.cp.umist.ac.uk.(1995)

ACKNOWLEDGEMENTS

The author wishes to express his gratitude to the following:

Dr S.B. Lyon	For his personal supervision, consistent encouragement, helpful suggestions and detailed discussion of this work.
Dr R.C. Newman Dr S.Turgoose	For their helpful suggestions and discussion.
British Council ORS Award Hardstone Foundation	For the financial support of this work

Thanks also to all the technicians and other staffs in the Corrosion and Protection Centre for their helpful assistance, and especially to all the students in laboratory D26 for their friendship and help during my stay in the Centre.

ABSTRACT

Atmospheric corrosion can be regarded as wet corrosion of materials under a thin water film, produced either by condensation in high humidity conditions or by direct precipitation of rain or snow etc. This kind of corrosion is usually considered to be electrochemical in nature. So, the general electrochemical law which holds for metal corrosion in bulk electrolytes also holds for the special case of atmospheric corrosion. However, the conventional investigation methods used in bulk solution electrochemistry can obviously be used in thin layer electrolyte electrochemistry only after major modification. Although an early study of corrosion in thin electrolytes by electrochemical techniques dates from the 1950's, relatively little fundamental work has been performed using electrochemical techniques in the study of atmospheric corrosion. This is mainly due to the difficulties and complexities in the electrochemical measurements under thin film electrolyte conditions.

In this investigation, the possibilities for a successful application of conventional electrochemical methods for the studies of atmospheric corrosion were explored. An electrochemical cell, suitable for the study of electrochemistry in thin-layer electrolytes, has been designed and produced. Comprehensive electrochemical research on this electrochemical cell under various thicknesses of electrolyte (10^{-4} to 10^{-1} M Na_2SO_4, thickness form 50 μm to bulk solution) has been carried out using d.c. (potentiodynamic polarization) and a.c. (a.c. impedance) electrochemical techniques.

With regard to the mechanism of atmospheric corrosion, it was suggested that it is impossible for atmospheric corrosion of iron to be controlled by the cathodic reduction process, i.e. the diffusion of oxygen through a thin film of electrolyte. In many cases, and particularly when the thin layer of electrolyte is relatively dilute (e.g. 10^{-4} Na_2SO_4),

passivation of the iron is a prevalent phenomenon. During the initial period of atmospheric corrosion of iron, the establishment of a passive film is dependent on the composition, concentration and the thickness of the electrolyte layer. In the early stages of atmospheric corrosion, and possibly during normal conditions, iron corrodes in the atmosphere in alternative passive and active stages, corresponding to changes in the external stage (wet/dry) of the surface. It is also stated that in the initial stage of atmospheric corrosion, the corrosion rate of iron is mainly controlled by the anodic process, i.e. the passivation of the material. The ohmic resistance polarization is not very significant.

In addition, the results also show that even in the relatively high concentrated electrolyte layers (0.1 M Na_2SO_4), passivity of iron is still the dominant anodic process. The passive properties of iron covered with concentrated electrolyte layers are significantly affected by the thickness of electrolytes. The beneficial effect of the alloying element Cu on the protective properties of weathering steel in atmospheric corrosion is mainly on the anodic processes, e.g. enhancing the passivity of iron by accumulated Cu on the surface during long time exposure.

CONTENTS

CHAPTER 2: LITERATURE REVIEW

INTRODUCTION

INTRODUCTION

Since most metallic structures are exposed to atmospheric environments, atmospheric corrosion is the most wide-spread form of metal deterioration. Due to the complexity of the variables, which determine the kinetics of the corrosion reactions, corrosion mechanisms of metals in atmospheric environments are not fully understood. Equally important, this complexity makes it difficult to simulate the corrosion process under simple laboratory conditions. Therefore, previous studies of atmospheric corrosion have concentrated on the following aspects[1,2,3,4]:

(1) Long term exposure tests have been utilized to rank corrosion behaviour of materials in various atmospheric environments, normally classified as "rural", "industrial" and "marine" by their locations. These experiments have also been used to characterize the atmosphere with regard to its corrosivity. Information obtained by these investigations is valuable to engineers and designers selecting systems for providing corrosion protection as well as those concerned with the performance of products and devices exposed to the atmosphere.

(2) Accelerated laboratory experiments were used to assess the durability of materials used in environments in terms of general corrosion rates and morphology of corrosion products. Additionally, this type of investigation has also been used, usually combined with advanced physical microanalysis methods, to investigate the mechanism of atmospheric corrosion, especially the kinetics of atmospheric corrosion as determined by the variation of specific active species (e.g. SO_2, CO_2 etc.) in the atmosphere.

(3) To develop better systems for classifying the corrosivity of the atmospheres, including the use of electrochemical testing methods to characterize atmospheric corrosion

behaviour. One of the methods is using electrochemical corrosion monitoring systems to monitor atmospheric exposure sites.

The atmospheric corrosion investigations mentioned above give general information on material performance and corrosivity of a particular atmospheric environment. Thus, a widespread knowledge of the general corrosion rates of metals in a variety of environments and of corrosion aggressivity of various atmospheric environments has been obtained. Although this information is useful in practice the approach does not easily lend itself to a mechanistic understanding of the atmospheric corrosion, which is significantly important to control or at least slow down this highly destructive process.

Atmospheric corrosion occurs on a metal surface covered by a thin, dilute electrolyte layer, produced either by condensation process in high humidity conditions or by direct precipitation of rain or snow etc. This kind of corrosion is usually considered to be electrochemical in nature. So, the general electrochemical law which holds for metal corrosion in bulk electrolytes also holds for the special case of atmospheric corrosion. The conventional investigation method used in bulk solution electrochemistry can obviously be used in thin layer electrolyte electrochemistry only after major modification. However, although an early study of corrosion in thin electrolytes by electrochemical techniques dates from the 1950's in work done by Rozenfeld and co-workers[5,6], relatively little fundamental work has been performed using electrochemical techniques in the study of atmospheric corrosion. This is mainly due to the difficulties and complexities in the electrochemical measurements under thin film electrolyte conditions.

In this investigation, the possibilities for a successful application of conventional electrochemical methods for the studies of atmospheric corrosion were explored. From the technical viewpoint, an electrochemical cell suitable for the study of atmospheric corrosion

should have a similar electrochemical function to that of the electrochemical corrosion cell operating on metals in the atmosphere, i.e. the current path between anode to cathode in the electrochemical cell is parallel with the surface of the sample, oxygen diffusion is perpendicular to the metal surface and a variety of thicknesses of electrolyte layer can be provided. From these considerations, a novel electrochemical cell assembly was produced, with which drying (evaporation) and wetting (condensation) processes, as well as maintenance of a constant thickness of electrolyte on the surface, can be accomplished to simulate the processes occurring during atmospheric corrosion. Electrochemical behaviour related to cathodic processes, anodic processes and resistance polarization of materials (mainly iron, as well as copper and zinc) covered with thin layer of electrolytes were studied using D.C. and A.C. electrochemical techniques. The purposes of this investigation are aimed to study the suitability of thin electrolyte electrochemical methods for studies of atmospheric corrosion, to find out what information can be obtained on the mechanisms of reactions occurring in thin layers of electrolyte and to what degree the results obtained can be extended to the research of atmospheric corrosion. Finally, and hopefully with this study, a new clue in relation to the mechanism of atmospheric corrosion can be found, allowing better understanding of this most widespread corrosion form and a new research method of atmospheric corrosion can be provided, supplementing other existing investigation methods.

CHAPTER 1
BASIC KNOWLEDGE OF ATMOSPHERIC CORROSION

CHAPTER 1 BASIC KNOWLEDGE OF ATMOSPHERIC CORROSION

1.1 The Economic Importance of Atmospheric Corrosion

Due to the fact that a large number of products, devices and engineering structures, such as buildings, bridges and cars are in general used in the atmosphere, atmospheric corrosion is perhaps one of the most pervasive corrosion problems. Although the economic importance of corrosion has already been emphasized in several reports[7,8,9], there seem to have been no recent attempts to assess the cost attributed specifically to atmospheric corrosion. Barton[10] quoted the assessment by Uhlig[11] to suggest that approximately half the total cost of corrosion protection in the United States in 1949 (over $US 2.8 M) was spent on measures against atmospheric corrosion effects. In another estimation of the cost caused by atmospheric corrosion, Daeves and Trapp[12] who are also quoted by Barton[10], calculated that 2% of steel production in Germany in 1937 was being converted back to rust by atmospheric corrosion each year. In the Hoar Report[7], an estimate was made of the national annual cost of corrosion and protection measures in the U.K. The total cost was considered to be £1365 M, of which £250 M is connected with building and construction, £280 M with marine problems and £350 M with transport. It seems to be reasonable to suggest that about half the cost caused by corrosion is related to the atmospheric corrosion. Fontana[13] claimed that an estimated cost of atmospheric corrosion in the United States is $US 2 billion. For the U.K. alone, the annual cost of atmospheric corrosion is several hundred millions of pounds[14]. More recently Duncan[15] pointed out that from the most basic community to the most sophisticated, atmospheric corrosion has the ability to influence a nation's economic health.

An improved understanding of the mechanisms of atmospheric corrosion will undoubtedly be beneficial for both academic and economic aspects.

1.2 Concept of Atmospheric Corrosion

Atmospheric corrosion is an electrochemical process which occurs in thin films or adsorbed layers of electrolyte formed either by direct precipitation, e.g. rain or snow, or by condensation processes in relatively high humidity environments. Due to the characteristic of the thin film electrolyte formed by a limited amount of electrolyte present on the metal surface, the process is influenced sensitively by external environmental factors, such as temperature, relative humidity, chemical composition of the atmosphere (including airborne pollutants), and dust or particulates etc; and by the properties of the corrosion products formed.

In addition, the atmospheric corrosion conditions will change frequently and periodically during wetting (condensation) and drying (evaporation) of metal surfaces. For instance, the diffusion of oxygen, which is considered to be the main reactant of the cathodic process in atmospheric corrosion, is greatly enhanced during evaporation of surface electrolyte. The accumulation of corrosion products promotes the formation of solid corrosion products on metals because the solubility product of the corrosion products is easily exceeded in so small volume of electrolyte. In subsequent drying processes, crystallization in the corrosion product layer will occur, which changes its protective properties significantly. Periodic renewal of electrolyte by rain, alongside changes in the concentration of electrolyte on the surface, can wash out the soluble component of the corrosion product from the surface, which again modifies the corrosion process.

Therefore, atmospheric corrosion is an extremely complex process, which occurs in the metal/corrosion product/water/environment system under frequently changed conditions. This process, in most circumstances, should include the adsorption of pollutants on the metal surface (or incorporation of pollutants in various forms of precipitation), formation of water films on the metal surface, chemical and electrochemical reactions and crystallization and phase transformation processes in corrosion products.

1.3 Brief Description of Atmosphere

Atmospheric corrosivities are normally simply clarified as "desert", "rural", "urban" "industrial" and "marine" environments determined with respect to the quantities of pollutants present in the air, the water content and solid particulate content of the air etc., which have a deteriorating effect on the corrosion of materials. Obviously this classification which is usually identified by the corrosion rates of commonly used engineering materials from long term field exposure experiments, is inadequate for an academic purpose. However, it has been proven to be difficult to obtain an universally accepted clarification of atmospheres in terms of corrosivity because of the complexities of the variables concerned, although many efforts have been made to develop a relatively standardized method to assess the atmosphere in relation to its aggressivity[16,17]. Consequently, the atmosphere is briefly described here with several meterological and pollution parameters which are thought important in deciding the kinetics of atmospheric corrosion.

(1) Oxygen

The concentration of oxygen in the atmosphere (23%) is relatively constant, although

it varies with the altitude of the location. Undoubtedly, oxygen is a very important atmospheric component for atmospheric corrosion because in most cases atmospheric corrosion occurs with the reduction of oxygen as the main cathodic process. Normally, provision of oxygen in atmospheric corrosion process is adequate because of its high partial pressure in the air and generally saturated existence in the water phases, e.g. rain water drops, fog, etc, as well as the favoured diffusion through thin electrolyte films on the metal surface.

(2) Water

The water content of the atmosphere must be discussed in terms of precipitation and absolute humidity (atmospheric vapour content), both of which are dependent on geographical position. The presence of liquid water on the surface is an important condition where accelerated atmospheric corrosion occurs because it provides the electrolytic path and facilitates the electrochemical reactions. The liquid water film can be formed on the surface not only directly by precipitation but also by adsorption and condensation processes which are determined jointly by the absolute humidity and the temperature, or the relative humidity (R.H.). The relative humidity is defined as the percentage ratio of water vapour in the atmosphere compared to that which would saturate the atmosphere at the same temperature. At equilibrium, when the relative humidity is at 100%, representing the condition where the atmosphere is saturated with water vapour, the water vapour will condense on the surface as liquid water until a new equilibrium is established. However, in some cases below 100% relative humidity, condensation of water can still occur. This phenomenon is related to the lowering of the dew point caused by chemical contamination of surface with hygroscopic substances or physical condensation within a porous structure e.g. of corrosion products. These will be discussed in more detail

in section 1.4 of this chapter.

(3) Temperature

Since an increase in temperature causes acceleration of all chemical reaction rates, according to the Arrhenius equation[18], it might be expected that atmospheric corrosion should proceed more rapidly at higher temperatures. However, in practice, the effect of increased temperature on atmospheric corrosion rates is usually overridden by other factors which have a stronger influence. For instance, it was often observed[19] that in some areas the atmospheric corrosion rate was highest in winter. This was caused by the higher concentration of SO_2 in the atmosphere due to the heating systems with combustion of sulphur-containing fuels, although the temperature is relatively low in this season.

Generally speaking, at high temperature the relative humidity is always low and atmospheric corrosion is thus unlikely. However, at high humidity and high temperature, a rapid small temperature drop results in the dew point being exceeded, which often promotes atmospheric corrosion by condensation of water films onto a metal surface.

One of the critical temperature dependent factors concerns the duration of presence of moisture (or water film) on the metal surface. Clearly, this influence of temperature is related to the evaporation rate of water film on the metal surface, which is also affected by other factors with respect to the thermal capacity of metal structure, its orientation, and wind velocity. Normally, the higher the temperature, the shorter the duration of existence of water film on the metal.

Various important measurements of temperature can be made. These are the ambient air temperature, the dew point temperature, and the metal surface temperature, all of which affect persistence of water on a surface and, hence, atmospheric corrosion.

(4) Sulphur Dioxide and Chlorides

There are various kinds of polluting substances in the atmosphere, e.g. CO_2, CO, NH_3, NO_x, H_2S, and some organic substances. However, two primary pollutants which are considered to have a significant effect on atmospheric corrosion, and are usually monitored in exposure sites, are sulphur dioxide and sodium chloride respectively.

One of the major stimulants of metallic atmospheric corrosion is sulphur dioxide. The mechanisms of the effect of sulphur dioxide on iron atmospheric corrosion will be examined in detail in chapter 2. Here, attention is paid to the concentration of sulphur dioxide in the air because it was found that a far higher concentration of SO_2 was often used to simulate atmospheric corrosion in the laboratory, which is unlikely to represent the practical situation. The normal concentration of SO_2 for urban atmospheres has been reported to be 0.11 to 2.3 mg m^{-3} (about 0.1 to 1.96 ppm) and 10 to 50 mg m^{-3} (about 8.5 to 42 ppm) for industrial atmosphere in 1957[20]. However, it must be noted that atmospheric concentrations of sulphur dioxide have decreased significantly over the past decade. Eisenbud[21] reports that the annual maximum hourly concentration was reduced from 2.2 to 0.8 ppm between 1965 and 1969. In 1970, the total sulphur emission expressed in terms of gaseous mass, from burnt fuel in the U.K. was about 7 million tonnes. In 1985 this figure had reduced to about 4 million tonnes[22], mainly due to burning of low-sulphur fuels. Therefore, it was reported that the typical urban concentration of SO_2 was 50 μg m^{-3} and 300 μg m^{-3} at high concentrations in 1985 in the U.K.[22].

The acceleration of corrosion by chloride ions in coastal areas has long been known. The severity of atmospheric corrosion of metals is largely a function of the quantity of salt deposited and decreases rapidly with increasing distance from the surf line[23]. However, the mechanism of effect of Cl^- on atmospheric corrosion is still far from clear. One of the

obvious reason for this effect concerns the hygroscopic properties of chloride species, which facilitate the electrochemical process of atmospheric corrosion by favouring electrolyte formation at relatively low relative humidity. It was also thought that a threshold level of chloride is always present at all sites, giving a constant effect, and that only when this level is greatly increased does the effect of corrosion increase significantly[24].

(5) Dust and Particulate

The deposition of particulate or dust onto metal surfaces is also important in atmospheric corrosion. In urban and industrial area, the dusts contain some water-soluble inorganic components, for example, up to 3 % soluble sulphate in industrial dust was reported[25]. Particulates which exist in atmosphere include ammonium sulphate, sodium chloride, sand, charcoal and soot. These particulates deposite on the metal surface and can promote corrosion either by decreasing of the dew point with hygroscopic chemical species on the surface or by physical adsorption of water.

1.4 Critical Relative Humidity

Critical relative humidity is often referred to as the relative humidity at which sufficient wetting of a metal surface occurs to cause a significant increase in the corrosion rate. The importance of the critical relative humidity in atmospheric corrosion was discovered by Vernon[26] as early as 1930's. This gives the evidence that atmospheric corrosion is a type of electrochemical corrosion process. The presence of liquid water on the surface is an important prerequisite for the electrochemical path of the corrosion process.

The factor linking critical relative humidity with the atmospheric corrosion of metals

is the time of wetness[27] which is defined as the period when the critical humidity is exceeded. In a more strict sense, time of wetness is related to the condition of relative humidity that would result in an adequate film of water on a metal surface to accelerate corrosion significantly. However, although extensive studies have been carried out to measure the time of wetness[28,29,30,31], there is not an universally accepted criterion to assess this phenomenon. The reason for this is mainly concerned with the variables that locally change relative humidity such as surface contaminants (e.g. soluble ions which depress vapour pressure), the nature of the corrosion products that may render the surfaces hygroscopic or provide pores into which water may condense, and the microclimate.

1.5 Formation of Electrolyte Layers on the Metal Surface

In atmospheric corrosion, the necessary condition for active electrochemical reaction is the presence of an electrolyte on the metal surface. Generally, there are two ways in which the water film on the surface of metals are formed, i.e. by precipitation or by adsorption and condensation.

1.5.1 Precipitation

The water film on the metal surfaces can be formed by precipitation, e.g. rain, fog, dew or snow. In the case where the water film is formed by rain, the thickness of the electrolyte layer can reach up to 200 μm[10,32], which is enough for the operation of the electrochemical corrosion process. During raining, the water-soluble components of the atmosphere is absorbed in the water, which changes the composition and concentration of

the electrolyte and promotes corrosion. On the other hand, prolonged raining can wash away the accumulated corrosion stimulator from the surface or dilute the concentration of electrolyte on the surface, which can retard the corrosion. In some cases, the previously-formed corrosion products which are sparingly soluble and provide a protective layer to some extent can also be washed away by rain which, in this case, increases the corrosion.

In the case of precipitation of very small water drops (e.g. from a mist or fog), a discontinuous liquid layer is formed by a large number of isolated water drops and later a continuous water film may be formed on the surface after prolonged exposure by coalescence of these isolated drops. The layer of electrolyte formed in this way is more aggressive to the metals because of the large surface area of the water drops, which are easily saturated with atmospheric oxygen and all other species important for corrosion. In Graedel's study[33],it was shown that the concentration of constituents (in terms of H^+, NH_4^+, NO_3^- and SO_4^{2-}, respectively) in fog was the highest among these in the other precipitation forms e.g. dew, rain and snow. Obviously, this observation is generally in line with the above explanation.

1.5.2 Capillary Condensation

The vapour pressure above a concave meniscus of water is less than that over a plane water surface. The relative lowering of the saturated vapour pressure is related to r, the radius of the concave meniscus[34]. Thus, as the value of r decreases, the humidity at which condensation takes place within the capillary also decreases. Therefore, electrolytes may be formed by capillary condensation into small micropores and valleys on metal surfaces. However, it is thought that this process is unlikely since capillary condensation will occur

only slightly below the saturation value for atmospheric humidity[10,35]. But it is really difficult to rule out the possibility of capillary condensation on the metal surface covered by rust with a microporous structure.

1.5.3 Chemical Condensation

The more important consideration for the formation of electrolyte layers on the metal surface concerns the lowering of the dew point by hygroscopic water soluble species. These species are present on the metal surface as the soluble corrosion products or soluble solid salts precipitated from the environment. When the humidity exceeds that in equilibrium with a saturated solution of the soluble species, a solution, initially saturated, is formed until equilibrium is established with the ambient humidity.

1.5.4 Thickness of Water Film Formed on the Metal Surface

In laboratory studies of thin film electrolyte electrochemistry to simulate processes occurring in atmospheric corrosion, one of the important factors is the thickness of the electrolyte layer on the metal surface, which affects the oxygen diffusion, solution resistance and crystallization of corrosion products.

Relatively thicker layers, reported as up to 200 μm[10,32], can be formed by atmospheric precipitation, e.g. rain. This formation is determined by gravity, hydrological behaviour of the layer, and the properties of the surface (e.g. surface tension). It has been observed by the author that on an epoxy surface in which is centred a small iron electrode (dia. 0.5 mm), the thickness of water layers formed by rain can reach up to 500 - 600 μm. This

may be explained by the high surface tension of the epoxy resin surface which prevents the water from spreading out. In addition, the water layer formed on paint surfaces by rain is composed of a relatively large number of isolated water drops with hemispherical shape whose diameter being about 2 cm and height of meniscus more than 300 μm. On the other hand, on a rusted steel surface, a very uniform water film can be formed by rain. In thin film electrolyte electrochemistry, the simulation of the water film formed by rain can be achieved easily because as thin as 100 μm thick uniform electrolyte layer can be formed on the metal electrode without effort.

In regard to the water film formed by condensation processes, there have been variously reported magnitudes of thickness of water layers. Bowden and Throssell[36] examined the thickness of water film on gold and aluminium respectively. It was found that even at 90% relative humidity the thickness of the water film was not greater than about two molecules, and that it was only about one molecule at 60% relative humidity. However, even a small contamination with a hygroscopic substance can change the situation completely; 10^{-7} g.cm^{-2} of potassium hydroxide on the surface would produce 5 molecular layer of water film from an atmosphere of 50% relative humidity before the establishment of equilibrium, whilst 25 molecular layers would built up if the relative humidity was 90%. A thicker water film was reported[37] to be formed by adsorption on a clean polished iron surface. From the relationship of atmosphere relative humidity to the thickness of an adsorbed film of moisture on a clean, finely polished iron surface, it could be seen that at 90% relative humidity, the thickness of water film was about 65 molecular layers and about 20 molecular layers at 60% relative humidity. Both values are significantly greater than those discussed previously, and this may be due to the different surface conditions which affect significantly the thickness of the water film adsorbed. The

other magnitudes of thickness of water film formed by condensation on to iron have been reported as about 25-30 molecules on pure iron at 100 % relative humidity[38] and $< 4\ \mu m$ on iron with a sulphate-free rust layer at 100 % relative humidity[39]. In contrast to the situation where the water film is formed by rain, the simulation of water films formed by adsorption, in thin electrolyte electrochemical techniques, is really difficult due to this extremely thin water film. Perhaps the most practicable method to fulfil this process is through controlled evaporation.

Finally, it must be mentioned that in practice the thickness of water film on the surface is always changing with the variation in the external environmental factors, e.g. temperature, humidity and precipitation etc. For example, during the evaporation process, alongside with the alteration of water film thickness, other physical properties of the water film, e.g. the concentration of electrolyte, conductivity, resistance, and rate of oxygen diffusion in the electrochemical cell will also be changed, which ultimately will alter the course of the electrochemical process controlling the atmospheric corrosion. More detailed discussion of these effects can be found in a recent paper [40] which uses a computer simulation of atmospheric corrosion from a model based on a condensed droplet with a central anode and a peripheral cathode. Considerations were given to the effects of evaporation on the concentration of electrolyte, its conductivity and the effects of reducing droplet size on the variation in limiting oxygen reduction current.

1.6 The Destruction of Electrolyte layers

In contrast to a number of mechanisms of formation of electrolyte layers for atmospheric corrosion, there are only two possible mechanisms of destruction of water

film on the metal surface, namely, evaporation and chemical reaction of water on the surface. Evaporation can occur only at relative humidity below 100%, and thus is dependent on the environmental relative humidity and ambient temperature. In addition, during atmospheric corrosion occurring in a limited volume of electrolyte, chemical reactions, e.g. hydrolysis of corrosion products, need the participation of water, thus removing part of water on the surface. The solid corrosion products produced also have more or less ability to bind the water.

In practice, the destruction mechanisms of water layers on the surface are much more complicated than can be expected.

During evaporation, the thickness of water film will be reduced and thus the diffusion of oxygen through the thin water film will be enhanced. But at the same time, the concentration of electrolyte layer will also be increased, which affects the water partial pressure in equilibrium with the surface solution and the solubility of oxygen in the surface solution. When the evaporation process proceeds to a certain extent (or the concentration of surface electrolyte increases to a certain point), the evaporation rate may decrease because of the establishment of new equilibrium between the concentrated solution and ambient relative humidity, and the diffusion of oxygen may be controlled by the transport process through the interface of air/electrolyte because of the strongly reduced solubility of oxygen in high concentration solutions. If the presence of colloidal, hygroscopic, and porous corrosion products are involved in the consideration of destruction of electrolyte layer, the situation would become more complicated.

1.7 Microclimate

Microclimate is referred to as climatic conditions around a "micro environment" on the metal surface. The importance of microclimate for atmospheric corrosion can be seen from the observation that batch of samples, all produced under the same generally defined conditions, may corrode quite differently. Generally, the conditions of the atmosphere at a specific exposure site are defined by general meteorological and chemical (including pollutants) parameters which are measured by more or less standard methods all over the world. However, the corrosion behaviour of metals will be affected, besides the generally defined condition, more importantly by another factors, namely the microclimate. Although the effects of micro climate on atmospheric corrosion are complex, these factors can be classified into respective groups according to the ultimate effect on the corrosion. The factors which will ultimately affect the time of wetness on a metal surface include the distance of the samples from the earth's surface, heat-conducting or heat-insulating connections with the earth, heat capacities of the sample, corrosion products on the sample, the distance from a heating or cooling source, the slope of the surface and geographical orientation of the sample, etc. In these cases, the measurements of the time of wetness on the surface appears to be very important for the assessment of the environmental corrosivity although this measurement is also sensitively affected by many factors which will be discussed in Chapter 3. Other factors include the surface roughness, deposition of dust, design configuration etc. On the other hand, it must be pointed out that many efforts have been devoted to find the relation of long term corrosion behaviour of metals as the function of factors in relation to the general meteorological and pollution properties of atmosphere. Clearly, the validity of this relation normally described by a

equation is significantly deteriorated by the effect of microclimate.

1.8 Effect of Corrosion Product on the Processes of Atmospheric Corrosion

The corrosion products formed on the metal surface undoubtedly play an important role in the long term course of atmospheric corrosion because during the majority of exposure time, metals are covered with corrosion products which are formed after initiation of corrosion. Therefore, a lot of research on atmospheric corrosion concerns the corrosion products, e.g. structure, morphology, chemical composition, phase transformation etc. These aspects will be examined in more detail in Chapter 3.

The corrosion products formed in damp and wet atmospheres may be soluble or insoluble. Normally, insoluble corrosion products provide more protection than soluble corrosion products by isolating the electrode from the corrosion environment. Soluble corrosion products may increase corrosion rates either by increasing the conductivity of the electrolyte solution thereby decreasing the internal resistance of the corrosion cell, or by acting as hygroscopic species to form solutions at a humidity below that in equilibrium with the saturated solution; i.e. decrease the critical humidity.

On the other hand, due to the large surface area (51 m^2g^{-1})[41] and porous structure of many corrosion products (e.g. rust), the adsorption of SO_2 has been shown to considerably increase, which may be attributed to the increased amount of electrolyte present in the more porous corrosion products[42]. It was also shown that the soluble component of the corrosion product significantly accelerated the reaction $SO_2 \rightarrow SO_4^{2-}$ [32]. In addition, the corrosion products may affect the cathodic reduction processes of the atmospheric corrosion. Evans[43] postulated that FeOOH in the rust may be reduced to produce Fe_3O_4

as an alternative cathodic reduction reaction in atmospheric corrosion when the surface is covered by thicker water films. Stratmann also pointed out that the oxygen reduction reaction can take place at the oxide/electrolyte interface as the rust layer behaves like a large surface area cathode[44].

In the case of mild steels (including weathering steels), the corrosion products formed on steel surfaces always provide more or less protection in the long term exposure to the environment. This can be proven by many observations in long term exposure experiments[45,46] that corrosion rates decrease with increase in the time of exposure. Thus, a sharp decrease in corrosion rates generally occurs in the initial 3 to 5 years of exposure, indicating the time required for the establishment of relatively stable systems composed of the metal substrate and the corrosion products.

CHAPTER 2
LITERATURE REVIEW

CHAPTER 2 LITERATURE REVIEW

2.1 SO_2 Effect on the Atmospheric Corrosion of Iron

2.1.1. SO_2 as a Corrosion Stimulator

Significant effects of sulphur dioxide on atmospheric corrosion have long been known. The extensive work of Hudson[1,47] in several parts of the world has shown that atmospheric corrosion is most rapid in places where the sulphur dioxide content of the atmosphere is high. Schikorr[19] has also shown that in a given locality, rusting is more rapid at seasons of the year when the sulphur dioxide is highest. Vernon[26] was the first worker to show the serious corrosion-accelerating effect of sulphur dioxide in conjunction with humidity. It was shown that in comparatively dry air with a relative humidity of less than 70 %, very little rusting occurred whether the atmosphere was polluted or not. However, in atmospheres containing some sulphur dioxide, there was a pronounced increase in the rate of rusting when the relative humidity exceeded 80 %. In the case of weathering steels which normally exhibit higher corrosion-resistant properties than that of carbon steels, their corrosion resistances are also sensitively affected by the content of sulphur dioxide present in the atmosphere. In a recent study by Cermakova[46], et al, atmospheric exposures of weathering steels were carried out for five years to determine the corrosion behaviour of these steels in specific industrial atmospheres. The results have shown that the corrosion rates of weathering steels were proportional to the amount of sulphur dioxide presented, although their absolute corrosion rates were less than those of comparative carbon steels. In this investigation, a maximum level of SO_2 in the

atmosphere (or critical SO_2 level e.g. 90 mg/m²/day annual average value) was also specified, under which weathering steels may be used without protective coatings. When weathering steels are used without protection in atmospheres exceeding this limit of SO_2 pollution, consideration must be given to the service life of the structure. Similar results were obtained by Haynie, et al[48], who studied effects of air pollutants (SO_2, NO_2 and O_3) on the corrosion behaviour of weathering steel and galvanized steel, using controlled environment exposure chambers. In this work, attention was paid to the direct and synergistic effect of relative humidity, sulphur dioxide, nitrogen dioxide, and ozone in a programmed dew/light cycle. The low level and high level concentrations of SO_2 used in the chamber were 79 $\mu g/m^3$ (0.03 ppm) and 1310 $\mu g/m^3$ (0.50 ppm) respectively. The results showed that the concentration of SO_2 was a major factor in accelerating the corrosion rates of weathering steel and galvanized steel. For weathering steel, sulphur dioxide, relative humidity, and interaction between the two were the important corrosion rate factors. For galvanized steel, only the direct effect of sulphur dioxide and relative humidity were important. The remainder of the fifteen possible direct and synergistic effects were statistically insignificant. This result is indeed in agreement with the viewpoint that the sulphur dioxide and relative humidity are two very important factors determining the corrosion behaviour of materials.

2.1.2 Dry and Wet Deposition on Metal Surface

Before discussing dry and wet deposition, it must be mentioned that due to increasingly heavier pollution worldwide which led to the acidification of rain, rivers and lakes, a relatively detailed study of acid rain began in the 1970's with the OECD (Organization for

Economic Co-operation and Development) programme[49,50]. Since then, extensive work has been carried out internationally to study the formation of acid rain and its effects, including the corrosion of materials. Therefore, more comprehensive information is available now in books[51] and proceedings[52,53], about the emission, dispersion and deposition of pollutants (SO_2 and NO_x), and the chemistry of deposition. Undoubtedly, these data are also valuable for the study of atmospheric corrosion because a better understanding of atmospheric corrosion depends on fully understanding the atmosphere and the corrosion processes respectively. For example, it has been shown, that with respect to corrosion, the conventional classification of climates into marine, inland, industrial, etc., types is not sufficient. More accurate specification should include the actual chemical component in the atmosphere, as well as humidity and other factors[54]. This is because pollutants (SO_2 and others) emitted from the source can transport for hundreds of kilometres before being deposited[51]. The mechanisms of transport and deposition of pollutants are more complex than expected and not fully understood yet.

Two principal mechanisms are responsible for transporting sulphur dioxide and other pollutants to surfaces, dry deposition and wet deposition, respectively.

Dry deposition refers to transport of pollutants between and during precipitation events. Particles may deposit by sedimentation, inertial impaction, interception, diffusion, or a combination of these mechanisms. Gases generally deposit by diffusion from the atmosphere onto surfaces, with subsequent adsorption or chemical reactions. Some species present as gases and partially oxidized aerosols are also deposited by dry deposition.

Wet deposition refers to scavenging during precipitation, and may include in-cloud processes as well as uptake of pollutants by falling raindrops and snowflakes. For particles, wet deposition often involves scavenging during formation of cloud condensation

nuclei or ice nuclei. Collection of particles, as polluted air masses sweep through clouds, may also be important. For wet deposition of gases, diffusion to cloud droplets or ice crystals, with subsequent chemical reactions, is an important process. Oxidized materials e.g. SO_4^{2-}, NO_3^{2-}, are more soluble and are deposited during rain episodes.

Generally, in areas nearer to pollution sources, dry deposition dominates, but with progressive oxidation downwind more soluble constituents are formed, so that in the areas far from the pollution sources wet deposition becomes important. At any site, however, both local and distance sources will contribute to deposition.

From the perspective of atmospheric corrosion, the most interested pollutant in the air is SO_2, which can be deposited onto metal surfaces by both dry and wet deposition. It was reported that dry deposition of sulphur dioxide is a significant factor in the central part of central Europe, and is responsible for the removal of about 50 % of the total emissions, while about 30 % of the total sulphur emission is removal by precipitation scavenging[54].

Dry deposition is a process that is still not fully understood. The dry deposition fluxes for a specific species are expressed with the dry deposition velocity V_d (cm/sec.). In many cases, the airborne concentrations (g/cm^3) have been measured simultaneously with deposition rates (g/cm^3.sec.), permitting estimation of the dry deposition velocity (cm/sec.)[55]. However, the processes of dry deposition are affected by many factors in relation to the wind velocity, nature of surfaces, as well as atmospheric conditions. There is no single agreed-upon method for its measurement.

For wet deposition, the processes may include the atmospheric oxidation of sulphur dioxide gas to sulphate (or similar reactions of nitric oxide (NO) to nitrate (NO_3^-)), then dissolution of sulphate (or nitrate) in the rain droplets. Besides this, a small amount of the gases dissolve directly without reaction in the rain water. However, this is limited by the

partial pressure of the gas and self-limited by the increasing acidity which results. Therefore, the chemical composition of rain water always includes the SO_4^{2-}, NO_3^-, NH_4^+, Na^+, Mg^{2+}, Cl^-, etc components. Barrett, et al[88] reported the concentration of major ions in 'typical' rain (annual mean) and in cloud, mist and fog water in the U.K. It is clear that cloud, mist and fog water have significantly higher concentrations of major ions, often by as much as an order of magnitude. The total concentrations of rain and cloud water, calculated by the concentrations of anion are 122 μEq/l and 3884 μEq/l respectively. In a recent paper, Graedel[21] has reviewed the effect of chemical composition (i.e. including the species H^+, NH_4^+, NO_3^-, SO_4^{2-}, Cl^-, HCHO, RCOOH) of the different atmospheric precipitation forms on atmospheric corrosion. With the chemical concentration and the typical annual durations of the precipitation forms in four cities in the USA, the contribution of each precipitation type to annual exposures of materials surfaces to corrodents was deduced. Among the results of interest were that the nitrate exposure of surfaces appears to be predominantly due to gaseous deposition (dry deposition), that materials exposure to the sulphate ion may occur more from dew than from other forms of precipitation, and that under some circumstances fog, rain and perhaps snow can contribute substantial fractions of corrodent exposure burdens. Consequently, the amount of ions produced on the metal surface by wet deposition is equally important, compared with that by dry deposition, and may be more important if the increased thickness of water films produced by rain and subsequent evaporation, which increases further the concentration, are considered.

In summary, SO_2 and other pollutants can transport to the metal surface by dry deposition and wet deposition. During dry deposition, gases (SO_2 or others) diffuse directly to the metal surface, with subsequent absorption and chemical reaction. The two

important factors which affect dry deposition concern the airborne concentration and deposition rate. However, in corrosion research, the main attention is paid to the relationship between the severity of corrosion and the concentration of airborne pollutant, e.g. SO_2. Clearly, this is not adequate because dry deposition is significantly affected, beside the concentration of pollutants, by the natural of the surface, humidity, geographical condition and wind speed etc. Therefore, a comparatively detailed knowledge of the atmosphere in relation to the emission, transportation, deposition of pollutants and chemistry of rain, obtained from the research of environmental science, is valuable for studies of atmospheric corrosion. For wet deposition, it must be born in mind that with changes in pollution of the air (although the level of SO_2 in the air was reduced during last decade, the level of NO_x was increased at the same time), the rain water can contain a quantity of ions, and serves as the dilute electrolyte on the metal surface. This trend will continue and may change the causes of atmospheric corrosion significantly.

2.1.3 Initial Stage of SO_2 Reaction on the Metal Surface

In this section, the emphasize will be focused on the adsorption process of SO_2 on the metal surfaces, which belongs to the dry deposition process as discussed previously.

In the work by Spedding[56], the adsorption by aluminium of sulphur dioxide at atmospheric concentrations has been investigated using S-35 sulphur dioxide. It has been shown that in all cases the amount of SO_2 absorbed by the Al increased linearly with time. The important result was that the uptake of SO_2 was always linear and strongly dependent on humidity. Generally, the amount of SO_2 adsorbed increased with increasing relative humidity. However, it was found that the velocity of deposition of SO_2 ($cm.s^{-1}$) obtained

remained relatively constant in the range 50-90 % R.H. and increased very rapidly in the range 90-100 %. This suggested that there was a close relationship between SO_2 sorption by an Al surface and the amount of water on that surface. It is likely that this relationship reflected the ease of access of SO_2 to the surface water which, below 90 % R.H., was probably confined to capillary pores in the surface oxide layer. Above 90 % R.H. an increasing coverage of the surface with a water film would allow the increasing SO_2 uptake observed. It was also found that much of the SO_2 (60 %) absorbed in the range 50-53 % R.H. was physically adsorbed and released to the surrounding air when the SO_2 concentration is decreased. The fraction of absorbed sulphur dioxide desorbed when the partial pressure of sulphur dioxide was reduced was found to increase with decreasing humidity.

In the investigation by Sydberger and Vannerberg[57], the effect of the relative humidity and the corrosion products on the rate of adsorption of sulphur dioxide on metal surface was also studied using an S-35 isotope. The experiments were performed with 0.10 ppm SO_2 at relative humidity between 50 and 98 percent. The adsorption of SO_2 on polished iron, zinc, copper and aluminium samples have been compared with those of pre-exposed samples of these metals. For different polished metal samples, it was shown that, at 90 percent relative humidity, the initial adsorption rate was relatively high on the zinc and copper but decreases with increasing time, finally approaching a constant value. The aluminium sample always showed a markedly lower adsorption rate. For iron, during the first hour of exposure, the adsorption rate is low, but after about 1 hour, the adsorption rate increases rapidly, finally approaching a high constant value. In regard to the effect of relative humidity on the adsorption of SO_2, it was found that for all metals tested (Fe, Cu, Al, Zn), the adsorption rate is markedly dependent on the humidity, namely, the

adsorption rate increases with increase of the relative humidity, although the adsorption behaviours for respective metals are different. In the case of polished iron, the initial adsorption rate decreases at all humidities and approaches zero at humidities < 80 %. However, at humidities exceeding 90 % the rate of adsorption soon increases rapidly. This phenomenon may be related to the critical humidity. For polished aluminium, an extremely low adsorption was shown; even at a relative humidity of 98 %, only a small fraction of the sulphur dioxide molecules impinging on the aluminium surface were adsorbed. In this work, the significant effect of corrosion products on the adsorption of SO_2 was also observed. It was shown that at the same relative humidity, the adsorption rate of SO_2 on corroded iron was significantly higher than that on polished iron. On the other hand, the adsorption behaviour of SO_2 on rusted samples was also different from that on polished samples, indicated by the different shape of the adsorption rate-time curves in the respective cases. The high adsorption rate on iron with corrosion products was explained by a rapid oxidation of adsorbed sulphur dioxide due to the catalytic effect of the corrosion products of iron[32]. Conversely, copper, aluminium, and their corrosion products exhibited a high resistance to the adsorption of SO_2. Consequently, from this work, it is clear that the adsorption of SO_2 is affected by the humidity, corrosion products, and the kind of metal.

In later work by Duncan and Spedding[59], a similar result as discussed previously[57] was obtained concerning the effect of relative humidity on adsorption of sulphur dioxide on to metal surfaces. However, in this paper there is definite evidence for desorption from zinc and apparently irregular desorption of SO_2 from iron.

However, the distribution of SO_2 adsorbed on the metal surfaces is not uniform. Duncan and co-workers[58] reported that most of the $^{35}SO_2$ was adsorbed in specific areas

up to 0.5 mm in diameter on the iron surface. It was claimed that no differences in the physical structure of the surface of the iron samples could be detected by electron microscopy. No surface heterogeneities were found on these surfaces. For the formation of the discrete areas of adsorption of SO_2, Duncan, et al attributed it to the differential adsorption onto different types of oxide surface.

The observed evidence of effects of relative humidity and corrosion products formed on the adsorption of SO_2 on the metal surfaces, as discussed above, can be explained by two models, one being based on traditional theories of reaction in an electrolyte solution at the surface and other based on specific adsorption of the SO_2 at the solution/metal oxide interface. Those two models have been discussed in detail in a review by Duncan and Spedding[60]. In the following sections, both models are to be examined briefly.

2.1.3.1 Surface Electrolyte Solution Reaction (SESR) Model

This model assumes that there exists an electrolyte layer on the metal surfaces exposed to the atmosphere. This electrolyte layer can be formed directly by precipitation (e.g. rain, fog, snow, etc) or by condensation of atmospheric moisture at high relative humidity. Indeed, there are many reported values in relation to the thickness of electrolyte layer formed on the metal surfaces by different mechanisms, as discussed in section 1.5.4[10,32,36-39]. Also in section 1.5, a relatively detailed discussion can be found about the various factors affecting the formation of electrolyte layers on the metal surface. Undoubtedly, the values and observations reported previously in the literature support this model.

The assumption which is most easily subjected to criticism in this model is that the reactions taking place in the electrolyte layer present on the surface are those occur in an

ordinary bulk solution, with the exception that there is now a constant and homogeneous oxygen concentration throughout the solution.

2.1.3.2 Specific Adsorption Site (SAS) Model

The basic assumption of this model is that there is a number of particular sites on a metal surface exposed to the atmosphere. Chemisorption can occur only at these sites, and reactions which occur at the surface also at these available sites. Because there is only a limited number of such sites, the surface may become saturated by blocking of all sites by chemisorbed molecules. When this occurs, sites on the surface can be freed for further adsorption only by reaction of the adsorbed species. Those favourable sites for adsorption of SO_2, which have still not been defined, are supposed to be related to the different types of oxides or oxyhydroxides with favourable geometric and/or chemical properties for sulphate formation, or to the cracking of the oxide layer, exposing the base metal, or at inclusions or trace impurities in the oxide film.

However, in reality it is not appropriate to rule out one model and prefer the other because it is difficult to distinguish the effect of these two models. The best model, as Duncan and Spedding pointed out[60], may be one which combines the characteristics of both the SAS and SESR models.

It can be imagined that at very beginning of condensation, the water film should be formed at the specific areas, like the situations discussed in the section 1.4. It is unlikely that a very uniform thin water film covers the whole area of the surface. Thus, this specific adsorbed water film itself can lead to the subsequent specific adsorption of SO_2 due to the dissolution of SO_2 in water as explained in the SESR model. However, with

subsequent chemical reactions involving the water, SO_2 and metal in this specific area, the corrosion products formed change the properties of the water film significantly. On the one hand, the hygroscopic properties of corrosion products formed in the water film will adsorb more water by lowering the critical humidity. This, in turn, leads to more adsorption of SO_2 as in the SESR model. On the other hand, the corrosion products (oxides or oxyhydroxides) formed in so limited volume of water may adsorb the SO_2 directly from the air as described in the SAS model. Thus, the adsorption of SO_2 may increase rapidly due to the greater surface area of corrosion product, e.g. rust, or to the catalytic action of the corrosion product ion e.g. Fe(III) for the reaction $SO_2 \rightarrow SO_4^{2-}$. In addition, the oxidative reaction of SO_2 by O_2 to from the SO_4^{2-} ($SO_2 + O_2 + 2e \rightarrow SO_4^{2-}$) ion needs electrons, either coming from the oxidation of ferrous; $2Fe^{2+} \rightarrow 2Fe^{3+} + 2e$ or from dissolution of iron; $Fe \rightarrow Fe^{2+} + 2e$ [10]. The existence of the water film on metal surfaces facilitates this electrochemical reaction, increasing the transformation of SO_2 to SO_4^{2-}, hence increasing the adsorption ability of SO_2 of the metal surface by both models. Therefore, this positive feed back system (water film → adsorption of SO_2 → corrosion reactions → corrosion products → more water adsorption → more adsorption of SO_2 → more .....) makes it difficult to distinguish the SESR and SAS models from the real situation.

Finally, a mention must be made of the sulphate nests observed and reported by many workers[10,67,68]. One of the reasons for the formation of sulphate nests may be related to the initially specific adsorption of the water film, as discussed above. It may be likely that with the evaporation of dilute water film which is already initially formed at specific areas, the concentration of electrolyte film is increased and finally, when nearly dry, a number of concentrated water clusters are formed on specific areas of the surface. Under these water clusters, corrosion is easily initiated due to the high concentration of the solution.

When the corrosion proceeds, the sulphate nests are formed.

2.1.4 Electrolytes for Simulating Atmospheric Corrosion

One of the important considerations in utilizing laboratory experiments, especially with thin layer electrolyte electrochemical methods for the study of atmospheric corrosion, is the choice of the type and the concentration of the electrolyte used.

With regard to the effect of SO_2 in air on atmospheric corrosion, it is suggested that SO_2 is rapidly oxidized by oxygen to form SO_4^{2-}, following primary adsorption of SO_2 and O_2. The accelerating effect of sulphur dioxide is not due to the amount of gas dissolved in the electrolyte or the acidification of the electrolyte, but involves the sulphate ions formed by conversion of sulphur dioxide[10]. Therefore, for the simplest case, the Na_2SO_4 solutions are often used in laboratory experiments to simulate atmospheric corrosion[5,14,41,44].

However, as to the concentration of the electrolyte chosen to represent the real situation of atmospheric corrosion, the more detailed consideration must be given, concerning the mechanisms of adsorption of SO_2 on the surfaces, reactions of SO_2 with metal or oxygen on the surfaces, and the formation of water film on the surfaces. In normal conditions, at least three possibilities must be considered:

First, the SO_2 gas may dissolve in a water film condensed on the surface of a material by the mechanism as described in the SESR model in the section 2.1.3.1. The concentration of the gas in the water film is governed by Henry's law, which describes the equilibrium of the gaseous and the aqueous phases. Although the solubility of SO_2 in water is relatively high (16.2 g SO_2/100 g H_2O), Graedel[33] reports relatively low surface water

layer concentrations ($8.0x10^{-3}$ to 0.35 μeq/l) resulting from sulphur dioxide dissolution. In the real situation, much higher concentrations of sulphur oxyanions in the water film might be expected due to the fact that much of the SO_2 dissolved in the water film may be converted to the SO_4^{2-} by the reactions reported above.

Secondly, the wet deposition of pollutants on the metal surface as described in section 2.1.2 must be considered. The compositions of precipitation have been variously reported in many papers and books[33,51,52]. Here, cited in Table 2.1, is the composition of the solution which is used in UMIST as an artificial acid rain simulating the acid rain occurrence in the Manchester area. It contains Na_2SO_4, NaCl, NH_4Cl, etc, and its equivalent concentration is about $4x10^{-4}$ M.

Table 2.1 The Chemical Composition of the Artificial Acid Rain in Manchester Area*

Nitric acid	15.75 (mg/l)
Sulphuric acid	31.85 (mg/l)
Ammonium sulphate	46.20 (mg/l)
Sodium sulphate	31.95 (mg/l)
Sodium chloride	84.83 (mg/l)
Sodium nitrate	21.25 (mg/l)

(* N.B. This solution is 10 times the average concentration of chemicals in rain falling in the Manchester area)

Thirdly, the evaporation of the water layer initially formed by precipitation on the

metal surface will significantly change the concentration of electrolyte on the surface, although the initial concentration of the precipitation is relatively low.

Finally, from the typical values for deposition of SO_2 on to metal surfaces, listed in the Table 1 of the paper[60], a gross estimation of concentration of SO_2 in the water film can be made by calculation. For instance, the adsorbed SO_2 on the iron surface at 90 % R.H. is about $23x10^{-5}$ μg mm^{-2}. It can be calculated that the concentration of SO_2 in the electrolyte layer (1 μm thick) on an iron surface is approximately $3.59x10^{-3}$ M, while a very high concentration (about 0.75 M) of SO_2 in the electrolyte layer on aluminium surface was obtained[60], using $75x10^{-5}$ $\mu g.mm^{-2}$ adsorbed. This higher concentration obtained by the calculation may be due to estimates of a much thinner electrolyte layer, although this was not mentioned in the original paper[60].

In the experiment by Justo and Ferreira[63], $FeSO_4 7H_2O$ solution with concentration of $3.1x10^{-4}$, $7.8x10^{-4}$ and $1.2x10^{-3}$ M was used as experimental electrolytes for the study of atmospheric corrosion. It was claimed that these concentrations correspond respectively to concentrations of 20, 50, 75 μgm^{-3} of SO_2 in the air. However, there was no more detailed explanation for this choice of the concentration of electrolytes in the original paper.

In the recent study by Stratmann et al[64], Na_2SO_4 solution with 10^{-2} to 1 M concentration respectively was used to cover the metal surface for the investigation of electrochemical behaviour under thin film electrolyte conditions.

Therefore, according to the above discussion, it seems to be reasonable to chose a Na_2SO_4 solution with the concentration range from 10^{-4} to 1 M as the experimental electrolyte for stimulating the atmospheric corrosion processes in laboratory studies.

2.1.5 Mechanistic Roles of Sulphur Dioxide in the Atmospheric Corrosion of Iron

2.1.5.1 Electrochemical Reduction of Sulphur Dioxide

The mechanism of effect of SO_2 on the cathodic reaction of the atmospheric corrosion was proposed by Rosenfeld[5,6]. In the measurements of cathodic polarization curves for various sulphur dioxide concentrations (0.1 % - 1.0 %) in air on several metals including iron and aluminium, Rosenfeld found that the cathodic reaction rate was increased with increasing sulphur dioxide concentration. Therefore, it was thought that sulphur dioxide was reduced at cathodic sites as a new cathodic depolarizer, due to the greater solubility of the gas in water than oxygen (about 1300 times more soluble than oxygen) explaining its stimulating action on the atmospheric corrosion of iron. The most likely scheme of its reduction was assumed to be:

$$2\ HSO_3^- + 2\ H^+ + 2\ e \rightarrow S_2O_4^{2-} + 2\ H_2O \qquad (2\text{-}1)$$

Although the cathodic reaction of sulphur dioxide is thermodynamically feasible, the problem remains as to whether this process can occur under conditions of atmospheric exposure, in view of the low concentration of SO_2 (normally 0.1 - 1 ppm). In Rosenfeld's investigation, the SO_2 concentration (0.1 % to 1 %) was a few thousand times higher than the practical environment. Subsequently, Koschelev and Klark[65] have shown that the electrochemical reduction of sulphur dioxide via the cathodic reaction:

$$2\ SO_2 + 2\ e \rightarrow S_2O_4^{2-} \qquad (2\text{-}2)$$

can occur only at high partial pressures of sulphur dioxide in air, i.e. at concentrations of

0.5 % more.

2.1.5.2 Acid Regeneration Cycle

The Acid Regeneration Cycle was mentioned in the early writing of Vernon[26] and later proposed by Schikorr[19] based on observations of naturally occurring corrosion. This mechanism can be described by the following overall reactions,

$$Fe + SO_2 + O_2 = FeSO_4 \quad (2\text{-}3)$$

$$4\ FeSO_4 + 6\ H_2O + O_2 = 4\ FeOOH + 4\ H_2SO_4 \quad (2\text{-}4)$$

$$4\ H_2SO_4 + 4\ Fe + 2\ O_2 = 4\ FeSO_4 + 4\ H_2O \quad (2\text{-}5)$$

and consisted of three basic steps. First, there was the uptake of sulphur dioxide on the iron surface, which was affected by the surface conditions. It was found that virtually all the sulphur dioxide arriving at the rust was adsorbed, and also noted that unrusted iron adsorbed much less sulphur dioxide than rusty iron surfaces, as qualified by Sydberger et al[57]. The second step was reaction of the adsorbed sulphur dioxide with atmospheric oxygen and iron to give ferrous sulphate (reaction 2-3). Mayne[66] had previously observed that the oxidation of sulphur dioxide to sulphuric acid was catalysed by rust. Thirdly, oxidation of ferrous sulphate and hydrolysis lead to formation of hydroxides as the chief component of rust and reliberation of sulphuric acid (reaction 2-4). Thus, reliberated acid attacks iron to give fresh ferrous sulphate (reaction 2-5), which, by oxidation and hydrolysis, produces yet more acid-and so on. However, it should be borne in mind that

hydrolysis will not necessarily liberate all the acid; some may become insoluble as basic ferric sulphate, or may be leached out from the rust by rain.

2.1.5.3 The Theory of "Sulphate Nest"

The presence of sulphate nests in rusts formed on steel in atmospheres polluted with sulphur dioxide has been recognized for a long time. Tanner[67], studying the atmospheric corrosion of steel exposed at different localities in Britain for several years, found crystals of $FeSO_4 4H_2O$ in shallow pits. Schwarz[68] claimed that the $FeSO_4$, formed as a result of the sulphur dioxide content of the atmosphere, was present in the rust at the metal surface as a non-uniform accumulation of finely divided crystals that form a "nest". The growth of such a "nest" was accelerated by moisture. Ross and Callaghan[69], studying the rust formed by exposing mild steel sheets in the atmosphere in Manchester, considered that the formation of sulphate nests was a later stage of the atmospheric corrosion, before this stage a more band-like distribution of sulphate being likely. Evans[70] suggested that during electrochemical rusting sulphate ions are driven towards the anodic portions of the corroding surface by the potential gradient. The influence of the potential would be such as to overcome the tendency for sulphate to diffuse outwards under the concentration gradient.

A relatively detailed illustration of the "sulphate nest" mechanism of atmospheric corrosion of iron can be found in the book[10] and the paper[71] by Barton, et al. The main features of this theory are that after adsorption of SO_2 on metal surfaces, sulphate formed by the reaction of adsorbed SO_2 exists in the form of a nest in the rust, the primary reason for the formation of the nest remaining unknown[71]. The difficulty of dissolving sulphate

from rust[66] and the stability of $FeSO_4$ nests seem to be related to the presence of membranes covering the single nests acting as a kind of "reservoir" of soluble SO_4^{2-} ions. In the course of the corrosion process this membrane cracks periodically and releases a drop of concentrated $FeSO_4$ solution or even a solid crystal, which originates a new centre of corrosion. For example, after steel samples with rust containing known amounts of sulphate (labelled with S^{35}) were leached with distilled water until no sulphate was detected in the leachant, the samples were then transferred to a humid atmosphere (96% R.H., 25 °C) for 14 days, no new sulphate or sulphur dioxide being added during this period. Thereafter the dissolution was repeated and a similar leaching-out characteristic of the system was found. This confirms that during the second corrosion period new sulphate had come from the nests only, mainly in consequence of the periodic cracking of the membranes around the sulphate nests.

However, in a recent paper by Graedel and Frankenthal[72], it was suggested that the scenario (description of "sulphate nests") is only an overview and not a complete mechanistic description, because (i) the mechanism cannot explain the finding[19,73,74] that steel exposed initially during the winter tends to corrode more rapidly than does steel initially exposed in the summer, and (ii) no analytical evidence exists for the constraining hydroxide "membranes". One can do no better at present than acknowledge that corrosion is spatially heterogeneous, that sulphur tends to concentrate at specific sites, and that the details of the interaction between the chemistry of rusting and the physics of rust layer morphological change cannot yet be specified.

2.2 An Anodic Dissolution Mechanism for the Atmospheric Corrosion of Iron

Although the total atmospheric corrosion process of iron is related to the combination of cathodic, anodic, and resistance polarization processes caused by the thin film electrolytes, the single anodic dissolution process, which is usually investigated in bulk electrolytes by traditional electrochemical methods, is pertinent to the understanding of atmospheric corrosion of iron.

In the investigation by Florianovich, et al[75], the mechanism of the anodic dissolution of iron in acid solution was studied. The anodic polarization curves were measured for iron in sulphuric acid solution with sodium sulphate at various pH (0 - 5) and various sulphate concentrations (10^{-3} to 1 N) in the range of potentials corresponding to the active dissolution of iron. It was shown that at constant electrode potential (- 0.35 V (NHE)), the anodic dissolution current of iron, log i, linearly depends on pH (at a constant sulphate activity a_s) and log i on the sulphate activity log a_s (at pH = const.). This means that both the OH^- ions and SO_4^{2-} ions directly participate in the reaction of iron dissolution.

In order to explain these results, Florianovich, et al postulated a mechanism described as follows: at first the iron reacts electrochemically with the surface water molecules to lead to the formation of $(FeOH)_{ads}$ complexes adsorbed on the surface, according to the reactions

$$Fe + H_2O \rightleftharpoons Fe(OH^-)_{ads} + H^+ \qquad (2\text{-}6)$$

$$Fe(OH^-)_{ads} \rightleftharpoons (FeOH)_{ads} + e \qquad (2\text{-}7)$$

These reactions are followed by the interaction of $(FeOH)_{ads}$ with the anions of the

solution,

$$(FeOH)_{ads} + HSO_4^- \rightarrow FeSO_4 + H_2O + e \quad (2\text{-}8)$$

or

$$(FeOH)_{ads} + SO_4^{2-} \rightarrow FeSO_4 + OH^- + e \quad (2\text{-}9)$$

with subsequent dissociation:

$$FeSO_4 \rightleftharpoons Fe^{2+} + SO_4^{2-} \quad (2\text{-}10)$$

or

$$FeSO_4 + H_2O \rightleftharpoons FeHSO_4^{2-} + OH^- \quad (2\text{-}11)$$

If reactions (2-6) and (2-7) are assumed to be equilibrium ones, and reactions (2-8) or (2-9) to be slow, and the HSO_4^{2-} or SO_4^{2-} anions are designated as A^{n-}, then for the rate of iron dissolution i we can write

$$i = k' a_{(FeOH)_{ads}} a_{A^{n-}} \exp\left(\frac{\beta \Phi F}{RT}\right) \quad (2\text{-}12)$$

where a is the activity of the relevant particles and ß the coefficient of potential effect.

Expressing $a_{Fe(OH)ads}$ on the basis of (2-6) and (2-7) as

$$a_{(FeOH)_{ads}} = k'' a_{H^+}^{-1} \exp\left(\frac{\Phi F}{RT}\right) \quad (2\text{-}13)$$

and substituting $a_{(FeOH)ads}$ from (2-13) into (2-12), we obtain

$$i = k a_{H^+}^{-1} a_{A^{n-}} \exp\left[(1+\beta)\frac{\Phi F}{RT}\right] \quad (2\text{-}14)$$

or

$$\log i = k + pH + \log a_{A^{n-}} + (1 + \beta)\frac{\Phi F}{2.3RT} \qquad (2\text{-}15)$$

where: i is the anodic dissolution current

k is the rate constant

a_A^{n-} is the activity of SO_4 or HSO_4^-

ß is the coefficient of potential effect factor

Φ is the electrode potential

F is the Faraday constant

R is the Molar gas constant

T is the absolute temperature

This proposed mechanism indicates that the anodic dissolution of iron at constant electrode potential is affected not only by the OH^- activity, but also by the SO_4^{2-} activity.

Extensive work[10,39,76] has been done by Barton and Bartonova concerning the mechanism of atmospheric corrosion of iron. A mechanism of atmospheric corrosion of steel under the effect of SO_2, was proposed by them using the analogy of Florianovich's work in bulk solution[75]. It is described by the following reactions:

$$Fe + H_2O \rightarrow Fe(OH^-)_{ads} + H^+ \qquad (2\text{-}16)$$

$$Fe(OH^-)_{ads} \rightarrow Fe(OH)_{ads} + e \qquad (2\text{-}17)$$

$$Fe(OH)_{ads} + SO_4^{2-} \rightarrow FeSO_4 + OH^- + e \qquad (2\text{-}18)$$

$$FeSO_4 + H_2O \rightarrow FeOOH + SO_4^{2-} + 3H^+ + e \quad (2\text{-}19)$$

It was assumed that reaction (2-18) and (2-19) are slow, and hence kinetically significant. The surface concentration of the $Fe(OH)^-_{ads}$ complex (in reaction (2-16)) and the course of reaction (2-19) are thus dependent on the water activity in the system. One should therefore expect a second-order dependence on water activity (i.e. relative humidity).

In investigations of the rusting kinetics in the presence of varying initial surface sulphate concentrations, in the form of $FeSO_4$, it was shown that the corrosion process is affected by the activity of this stimulator, actually by the free sulphate remaining because of the binding of a certain amount of the sulphate by the rust. Therefore, a critical sulphate concentration was proposed, above which the faster mechanism described above by reaction (2-16 to 2-19) was thought to occur.

Below the critical sulphate concentration, the overall reaction (2-20) in a slower rate will occur:

$$4Fe + O_2 + 2H_2O \rightarrow 4FeOOH \quad (2\text{-}20)$$

There are several mechanisms for this reaction which have been proposed, most of which involves the following as initial steps;

$$Fe + H_2O \rightarrow Fe(OH^-)_{ads} + H^+ \quad (2\text{-}21)$$

$$Fe(OH^-)_{ads} \rightarrow Fe(OH)_{ads} + e \quad (2\text{-}22)$$

$$Fe(OH)_{ads} \rightarrow Fe(OH)^+ + e \quad (2\text{-}23)$$

If this mechanism were not interrupted it would lead to the formation of a protective passive layer[77].

Therefore, it was claimed that the accelerating effect of sulphur dioxide is not due to the amount of gas dissolved in the electrolyte or the acidification of the electrolyte, but involves the sulphate ions formed by conversion of sulphur dioxide. The acidification of the electrolyte which should result from the reaction (2-19) is probably counteracted by the buffer capacity of the oxide and hydroxide corrosion products already existing on the surface, so that it may be regarded as insignificant.

2.3 An Electrochemical Mechanism for the Atmospheric Corrosion of Iron

In this mechanism, first suggested by Evans[78] and later qualified by Evans and Taylor[43] with a detailed quantitative investigation, it was postulated that ferric oxyhydroxide present in rust, in the presence of ferrous sulphate (formed from dissolved SO_2 or sulphate-containing salts present in the electrolyte) could form an electrolyte cell;

$$Fe \mid FeSO_4 \mid FeOOH$$

with iron behaving as anode and ferric oxyhydroxide as a cathode.

At certain points the anodic reaction

$$Fe = Fe^{2+} + 2e \tag{2-24}$$

would occur, whilst at another point the two electrons would be used up in the cathodic reduction of the rust to magnetite

$$Fe^{2+} + 8FeOOH + 2e \rightarrow 3Fe_3O_4 + 4H_2O \tag{2-25}$$

The magnetite would quickly be re-converted by atmospheric oxygen to rust

$$3Fe_3O_4 + 0.75O_2 + 4.5H_2O = 9FeOOH \tag{2-26}$$

but now there are nine molecules of FeOOH instead of only eight - a net gain of one, due to the entry of one Fe^{2+} ion. The amount of Fe^{2+} used up is equal to that regenerated by the anodic reaction.

The following experimental observations support this mechanism:

(1) The cell Fe | $FeSO_4$ solution | Fe_2O_3 (on a copper substrate) can generate a current which dies away when the whole of the orange-brown ferric rust has been converted to black ferrous-ferric matter[79].

(2) In the experiment weighted pieces of unrusted iron were covered with filter paper soaked in ferrous sulphate solution (10 M), on which rested iron carrying rust on both sides. When the two iron specimens were joined through a milliammeter, initially, the current was high, but fell off with time, as the brown rust on the lower side of the upper specimen was supposedly reduced to magnetite. When the specimen was turned upside down so that a fresh supply of ferric rust was available; the current was again initially high, but soon decayed. Further inversions restored the current, since the magnetite formed in the first cycle had been re-oxidised to ferric rust by atmospheric oxygen. It was

also found that the milliampere-hours were roughly equivalent to the weight-loss of the lower specimen in the sense of Faraday's law[43].

(3) Once ferrous sulphate has appeared, the presence of sulphur dioxide in the gas-phase is not needed for rusting[43,78]. Thus the specimens moved after 4 hours in moist air containing SO_2 to moist air without SO_2 give practically the same performance as those left in the original atmosphere with SO_2; but the specimens from which ferrous sulphate has been removed by a day in water suffer practically no rusting, behaving more like specimens exposed from the outset to moist air free from sulphur dioxide.

Correlating this mechanism with the real situation of the atmospheric corrosion of iron, Evans and Taylor proposed that when iron was exposed outdoors in a position where it remained covered with liquid during precipitation, and then dried up, the brown rust would probably be reduced to black magnetite under rain and then during the succeeding dry period the black would be re-oxidized to brown rust. Thus the two stages of the process will occur alternatively.

For indoor conditions, it was claimed that the ferrous irons formed from anodic dissolution were immediately oxidised to magnetite which, since air was present, also instantaneously re-oxidized to ferric oxyhydroxide. This resulted in the iron ions being formed at one place and removed at another, so the solid produced was not protective, explaining why rusting continued at a nearly constant rate.

However, by carefully analyzing this mechanism, it can be found that after one cycle, the net reactions are only related to the reduction of oxygen in the air and the anodic dissolution of iron, while the magnetite takes part in the reactions just as a catalyst. Therefore, the questions arise as to if it is possible for Fe_3O_4 to be re-oxidised to FeOOH by the oxygen in the air; which reaction is faster between the direct reduction of oxygen

on the iron surface and the reduction of FeOOH to Fe_3O_4 which is subsequently re-oxidized by the oxygen. With regard to these questions, Evans and Taylor[43] pointed out that doubtless a perfect magnetite crystal does resist oxidation in damp air, but newly formed magnetite (produced, for instance, by the action of alkali on a solution containing Fe^{2+} and Fe^{3+}) soon loses its magnetism and changes it colour when exposed to water with access of air. It was also suggested that the cathodic reduction of ferric to ferroso-ferric material proceeds more rapidly than the cathodic reduction of oxygen[80].

As proposed by Evans[43,78], the electrochemical reduction of rust on steel acts as an important cathodic reaction and promotes the atmospheric corrosion of steel. Therefore, in order to elucidate the electrochemical properties of iron rust, Suzuki and co-workers[81] examined galvanostatic cathodic polarization of rusted steel and rust electrodes, prepared by fixing a piece of rust plate on an acrylic plate with conductive adhesive. The change in the amount of crystalline substances in the rust layer was observed by X-ray diffraction.

X-ray analysis of the rust plate separated from iron exposed in an urban environment for 4 months indicated that crystalline parts of pure iron rust plate were composed of γ-FeOOH, α-FeOOH, and Fe_3O_4. During the galvanostatic reduction of the rust electrode in 0.1M Na_2SO_4 (current density, 100 $\mu A.cm^{-2}$), γ-FeOOH was reduced directly to Fe_3O_4 but α-FeOOH in the surface layer was not reduced. By analyzing the relationship between the amount of γ-FeOOH and Fe_3O_4 during the reduction, Suzuki et al pointed out that in addition to γ-FeOOH in the rust layer, there were reducible amorphous substances, referred to as intermediate substances. Fe_3O_4 was also formed from these intermediate substances. Later, by examining the cathodic reduction of rusted plain steel and rusted weathering steel, it was found that the rust layers on weathering steel contained less intermediate substances than those on plain steel. Suzuki concluded that the intermediate

substances in the rust on weathering steel were difficult to convert to crystalline magnetite by cathodic reduction as compared to those on plain steel. Therefore, beneficial elements added to steel inhibited the formation of crystalline magnetite in the cathodic reaction process of rust and thereby increased the electrical resistance of the rust layer.

In another experiment, it was shown that the dissolved oxygen had no significant effects on the galvanic current of pure iron/rust electrode. This indicates that the dissolved oxygen did not contribute to cathodic reaction of the rust layer and that galvanic current between the pure iron and rust electrode can only be explained as the reduction of the rust layer, rather than the reduction of dissolved oxygen. This best demonstrates the importance of reduction of rust layer in the process of iron atmospheric corrosion.

Clearly, in the experiments of Suzuki et al, two points related to Evans' proposed electrochemical cycle have been proven; first, the reduction of γ-FeOOH in the rust layer to Fe_3O_4 is possible, although Fe_3O_4 was also formed from the intermediate substances. Secondly, and more important, is that reduction of the rust layer provides the majority of galvanic current between the pure iron and the rust layer, while the dissolved oxygen has little contribution, at least in the bulk solution condition.

In the research reported by Matsushima and Ueno[82], cathodic polarization curves of rusted weathering steel (exposure time, 5 months) in aerated and deaerated 0.1 M Na_2SO_4 indicated that reduction of some species other than O_2 predominated in the cathodic reaction. The reaction was presumably the reduction of ferric rust to lower oxide(s) as proposed by Evans[43,78]. It is an interesting fact, as observed by Suzuki et al[81], that cathodic current of a rusted steel in aqueous environment is mostly supplied by the reduction of ferric rust, and that dissolved O_2 contributes only to a minor extent.

M. Stratmann, et al[41] investigated isolated rust layers by electrochemical methods to

find out whether their reduction and re-oxidation can affect the atmospheric corrosion of iron.

A thin electroplated layer of iron, after about 150 hrs exposure in oxygen of 99 % r.h. with addition of 1.5 g SO_2 /m^2 Fe, was completely oxidized to nearly equal amounts of γ-FeOOH and α-FeOOH. The rust layers thus obtained were further characterized by electrochemical polarization in oxygen-free 0.2 M Na_2SO_4, X-ray, magnetic and chemical methods and by BET measurements to determine their phase composition, their amount of ferromagnetic components such as α-Fe and Fe_3O_4, the amount of Fe^{2+} and Fe^{3+} and the specific surface of the layers.

The possible reduction reactions of the FeOOH species[43,83,84,85] depend kinetically on various parameters: electrode potential, Fe^{2+} concentration and pH. It was shown that in a first reduction stage, a Fe^{2+} intermediate was formed, whose chemical nature could not be determined by a X-ray analysis and that the magnetite formation was a succeeding reaction. It was very likely that the intermediate was a reduced surface layer on the γ-FeOOH and perhaps also on the α-FeOOH crystal. The amount of α-FeOOH in the rust layer was not influenced during the electrochemical polarization reduction. A lower pH value accelerated the formation of free Fe^{2+}, whereas a high Fe^{2+} concentration and high pH value promoted the build up of Fe_3O_4. Stratmann, et al explained these phenomena by the following reactions:

$$\gamma\text{-}FeOOH + H^+ + e^- \rightarrow (Fe.OH.OH) \qquad (2\text{-}27)$$

$$(Fe.OH.OH) + 2H^+ \rightarrow Fe^{2+}(aqu.) + 2H_2O \qquad (2\text{-}28)$$

$$Fe^{2+} + 2\gamma\text{-}FeOOH \rightarrow Fe_3O_4 + 2H^+ \quad (2\text{-}29)$$

$$(Fe.OH.OH) + 2\gamma\text{-}FeOOH \rightarrow Fe_3O_4 + 2H_2O \quad (2\text{-}30)$$

In the initial reduction stage, the Fe^{3+} within a surface region of the FeOOH was reduced to Fe^{2+} accompanied by protonation of O^{2+} to OH^- (equation 2-27). The Fe^{2+} ions may also cross the solid/electrolyte interface to enter the solution (equation 2-28). Reaction (2-28) was strongly enhanced by a more acid pH. Later, rather alkaline pH values should result in the pore system of the rust layer due to the occurrence of the reaction (2-27) and pH change had two consequences. First, the velocity of the reaction (2-27) and (2-28) would be slowed down and secondly, magnetite became the thermodynamic stable phase. However, the formation of Fe_3O_4 through eq.2-29 and eq.2-30 was eventually reduced in more alkaline conditions because of the reduced amount of Fe^{2+} and Fe(OH.OH) as mentioned above. In this condition, the formation of α-FeOOH from γ-FeOOH was facilitated. At higher pH (=13), reduction of the rust was completely retarded at a potential of -400 mV(SHE). Furthermore, the reaction (2-29) and (2-30) could also be interpreted from a crystallographic point of view in terms of the similar lattice between Fe_3O_4 and γ-Fe_2O_3 which could be formed by dehydration of γ-FeOOH at about 180 °C.

In the oxidative condition, it was indicated that the reduced surface layer could be reversibly reoxidized. During potentiodynamic polarization up to +800 mV Fe_3O_4 can only partly be re-oxidized to γ-Fe_2O_3. However, the formation of γ-Fe_2O_3 by oxidation of Fe_3O_4 was reversible; i.e. at -400 mV(SHE) Fe_3O_4 was reformed.

Thus, Stratmann proposed that the Fe^{2+} intermediate and Fe_3O_4 as the reduced, γ-FeOOH and γ-Fe_2O_3 as the oxidized components, were the constituents of the oxidation-reduction cycle within the rust layer which was proposed by U. R. Evans[43,78].

Like Stratmann et al[41], J. Dunnwald and A. Otto[86] used isolated rust layers on gold substrate for an electrochemical investigation of reduction and re-oxidation, combined with in-situ Raman spectroscopy methods.

After several days exposure in the environment (saturated humidity provided by 0.5 M NaCl solution and 0.5 % SO_2), the rust layer consisted of a mixture of α-FeOOH, γ-FeOOH, $Fe(OH)_3$ and amorphous FeOOH. The cathodic polarization measurements of the rust layer in 0.2 M Na_2SO_4 indicated that at a potential of -0.3 V(SCE) for 24 hours, the spectra showed that α- and γ-FeOOH were stable in this potential range compared with $Fe(OH)_3$ and amorphous FeOOH which vanish. It may be that the latter species were transformed by water loss into crystalline FeOOH. No Raman signal for Fe_3O_4 appeared. The formation of an $Fe(OH)_2$ surface layer, not observable by Raman spectroscopy, was therefore assumed. At -0.5 V(SCE) α-FeOOH was stable and γ-FeOOH was reduced to Fe_3O_4. At potentials more negative than -0.6 V(SCE) α-FeOOH was reduced to Fe_3O_4. Now, mainly Fe_3O_4 was present in the sample with a small amount of α-FeOOH remaining. After anodic polarization and exposure to air for several weeks, Fe_3O_4 itself could not be oxidized. Accordingly, a minor modification of the Evans[43,78] model of atmospheric corrosion was proposed replacing Fe_3O_4 by $Fe(OH)_2$ as the reduced state.

Thus, it was suggested that the primary product of iron atmospheric corrosion was $Fe(OH)_3$. Water loss and crystallization of $Fe(OH)_3$ resulted in α- or γ-FeOOH. Reduction of γ-FeOOH during wetting leaded to the formation of partly Fe_3O_4 and mainly $Fe(OH)_2$ which could be oxidized again to $Fe(OH)_3$ during drying.

In further research by M. Stratmann and co-workers[87], the atmospheric corrosion of pure iron and the binary alloy Fe-0.5Cu was studied by a simultaneous measurement of the anodic current density of the metal dissolution and the cathodic current density of the

O_2 reduction reaction during several wet/dry cycles using a magnetic and a gas volumetric technique, respectively. Although the monitoring of iron dissolution by the magnetic method used in this investigation suffered from errors, especially when the rust layer on the surface was rather thick and rich in magnetite, as mentioned in the paper, the measurements of O_2 consumption during wet/dry period still showed that the atmospheric corrosion of iron occurred in three typical stages, i.e. stage 1, wetting of a dry surface where the rust may be reduced as the cathodic process of the corrosion; stage 2, wet surface where slow corrosion occurred with O_2 reduction as cathodic process; and stage 3, drying out of the surface where very rapid corrosion happened with O_2 reduction as the cathodic process during critical wetting of the surface.

2.4 Phase Composition and Transformations in Rust

2.4.1 Research Methods for Detecting the Phase Composition and Transformations in Rust

From the 1970s, much interest has been shown in detecting the various compounds present in rust and in elucidating the variation of phase compositions in rust with time of exposure. Generally, in these investigations, the research methods used include modern physical analytic methods, e.g. X-ray powder diffraction, Mossbauer spectroscopy, Raman spectroscopy, infrared spectroscopy and far-infrared spectroscopy, to detect the composition of the rusts formed on steels exposed to different environments for different periods of time (from a few weeks to a few years). The information provided by those investigations are mostly related to the later stages of atmospheric corrosion after long

periods of exposure. At these times, when a stable rust layer has been formed on the samples, the rust is relatively less sensitive to the effect of SO_2. On the other hand, the compositions and mechanisms of formation of rust layers have been subject to much disagreement. Other than the complexities of mechanisms of atmospheric corrosion, leading to the formation of different rust products in different locations and on different steels, the analytical methods used to determine rust products could themselves also produce problems relative to the interpretation of the results. There are many reports about the similarities between the spectra of different species. For example, it has been claimed that since the X-ray diffraction patterns of Fe_3O_4 and γ-Fe_2O_3 are so similar, reports about the presence of Fe_3O_4 in atmospheric corrosion products on the basis of X-ray diffraction data are suspect[94]. In Keiser's work[91], it was found that the infrared spectra of the two compounds (amorphous FeOOH and δ-FeOOH) were identical and that a mixture of approximately 2:1 Fe_3O_4:α-FeOOH has a similar Raman spectrum to δ-FeOOH. In the work by Misawa[97], a similar phenomenon was observed that the characteristic infrared adsorption bands of amorphous FeOOH showed a striking resemblance to those of δ-FeOOH. In the work of Singh et al[98], the same question was put forwards in connection with interpretation of the results obtained by X-ray or Mossbauer. It is difficult to distinguish between the presence of Fe_3O_4 and γ-Fe_2O_3 in rust samples with the aid of Mossbauer spectroscopy if the proportion of these phases and the grain size was small, especially if the rust contained α-FeOOH. Therefore, the problem of accurate determination of rust compositions was mainly caused by the difficulties of spectroscopy measurements on the mixture of oxides[89,90], in conjunction with the interference of oxide structure distortion[90], amorphous materials[89] and the small particle sizes of the crystalline material[91,92], variation in the cation distribution, incorporation of different chemical

groups and varieties in stoichiometry. So, this is one of the reasons why until now, there is no close agreement about the composition of rust products on steels.

2.4.2 Phase Composition and Transformations in Rust

It has been known that the main products formed on both mild steels and low alloy steels by atmospheric corrosion are α-FeOOH (goethite), τ-FeOOH (lepidocrocite), Fe_3O_4 (magnetite) and amorphous matter[89,91,93,98]. ß-FeOOH (akaganeite) is sometimes found in the corrosion products of Fe when Cl^- is present[99]. γ-Fe_2O_3 (maghemite)[94] and δ-FeOOH (ferroxyhite)[89,91] were also reported to be present in the rust layer.

Prior to the formation of stable oxide and hydroxide products, transitory green rusts, called as green rust I (in the presence of Cl^-) and green rust II (in the presence of SO_4^{2-}) respectively according to the environmental conditions, are formed[100,101]. Misawa and co-workers[96] has identified the green complexes I and II (precursor of green rust) as $[Fe(II)_2Fe(III)_1O_x(OH)_y]^{(7-2x+y)+}$ and $[Fe(II)_1Fe(III)_1O_x(OH)_y]^{(5-2x-y)+}$ respectively. Presumably these cations are bound to the coexisting anions in the solutions. Recently, a more specific chemical formula for green rust I was proposed to be $3Fe(OH)_2Fe(OH)_2ClnH_2O$ $(3 \geq n \geq 2)$[102] with an oxidation number of +2.25 and for green rust II the formula was suggested by Olowe et al[103] to be $4Fe(OH)_2FeSO_4nH_2O$ (n is probably 4) with an oxidation number of +2.29. In the conditions with the combined influence of Cl^- and SO_4^{2-} ions, as in actual atmospheric corrosion, green rust II, normally formed in the sulphate-containing medium, would also be formed by transformation of green rust I[104]. Therefore, the overall oxidation processes of ferrous hydroxide was proposed by Ph. Refait, et al as ferrous hydroxide → green rust I → green rust II → α and

γ ferric oxyhydroxides[104]. However, the formation processes of corrosion products in a Fe - H_2O system at room temperature are very complex, being determined not only by thermodynamic relationships[105] but also by the oxidation rate, pH and the structure and composition of initial and intermediate species of iron[96]. Misawa and co-workers[96] have studied the mechanism of formation of green rusts, Fe_3O_4, α-FeOOH, ß-FeOOH, γ-FeOOH, δ-FeOOH and amorphous ferric oxyhydroxde in aqueous solution at room temperature. The detailed discussion of these mechanisms can be found in the original paper. Here, the mechanism of atmospheric corrosion of iron is discussed, proposed by Misawa et al using the results of atmospheric exposure of mild and alloys steels in semi-rural site for 2.5 years[97], aided with the results of mechanism of formation of various iron corrosion products in the aqueous solution[96]. In their study, it was found that the main corrosion products in both inner and outer rust layers on mild and low alloy steels were α-FeOOH, -FeOOH and a large quantity of amorphous ferric oxyhydroxide ($FeO_x(OH)_{3-2x}$). δ-FeOOH was not detected in the rust samples and some Fe_3O_4 was found by electron diffraction methods, residing at the rust/steel interface. It was proposed that rusting began with the formation of -FeOOH directly precipitated by oxidation of $FeOH^+$ in slightly acidic solution. Then a low pH water layer dissolved γ-FeOOH and resulted in the precipitation of amorphous ferric oxyhydroxide with drying. The amorphous ferric oxyhydroxide transformed to α-FeOOH by deprotonation using hydroxyl provided by rain. The wet-dry cycle accelerated this rusting process, especially precipitation and transformation with deprotonation and dehydration. Fe_3O_4 detected by electron diffraction at the rust/steel interface was regarded as formed under poor oxygen supply after the steel surface was covered with dense oxyhydroxide rust layer.

However, the results obtained and discussed above and the mechanism proposed by

Misawa et al, are slightly different from that obtained in an earlier investigation by themselves[89]. In this case, rust from steels exposed to industrial or urban sites for 9, 12 or 43 months respectively was powdered and analyzed by i.r. spectroscopy, allied with the study of the oxidation process of Fe(II) hydroxy-complexes. For both mild steel and low alloy steel, it was found that the main products of atmospheric rusting were α-FeOOH, γ-FeOOH, Fe_3O_4 and a large quantity of δ-FeOOH and sulphate. It was suggested that after initial corrosion, $Fe(OH)_2$ was formed. In strongly basic conditions, α-FeOOH could be formed by the oxidation of $Fe(OH)_2$ by O_2, which was thought to be unlikely to be realized in atmospheric corrosion. However, α-FeOOH was always one of the main products of atmospheric rusting. This fact can be explained because γ-FeOOH formed in neutral or slightly acidic solutions may transform easily to α-FeOOH by dissolution and reprecipitation in aqueous solutions. In slightly basic condition, Fe_3O_4 could be formed from the oxidation of $Fe(OH)_2$. In higher temperature or at lower relative humidity, the freshly precipitated $Fe(OH)_2$ could be dehydrated and consequently oxidized directly by oxygen to form the δ-FeOOH. Furthermore, the formation of H_2O_2, which had been reported as an intermediate product in the atmospheric corrosion of Fe[106], would also result in oxidation of $Fe(OH)_2$ to δ-FeOOH. However, the δ-FeOOH formed in this way (dehydration-oxidation or rapid oxidation with H_2O_2) could not be protective in atmospheric corrosion due to the resultant mixture of amorphous δ-FeOOH and coarse grains of Fe_3O_4 or α-, ß-, or γ-FeOOH. In contrast, it was claimed that δ-FeOOH formed on low alloy steels was produced from Fe(II)-complexes by catalytic reaction with Cu^{2+} and PO_4^{3-} concentrated in the interface of rust/metal, providing a cohesive and compact rust layer.

A similar result was found by Keiser and co-workers[91], who investigated the passive

film (inner layer of the rust) formed on weathering steels, which were exposed to a industrial environment for 4.5 and 8 years, by using Raman spectroscopy, infra-red spectroscopy and electrochemical techniques. It was found that in both cases the passive film was composed predominantly of δ-FeOOH with 10-20% γ-FeOOH and possibly some α-FeOOH. Raman spectra from different depths of the surface were identical which implied that the film composition was homogeneous.

In the work by A.K. Singh et al[98], the phase analysis of rusts on mild steels by Mossbauer spectroscopy and X-ray powder diffraction was reported. In the investigation, the mild steel panels were exposed in environments including subarctic, rural, urban, and marine with different deposition rates of chloride, for four years and one years respectively. It was found that in all samples, α-FeOOH and γ-FeOOH were the main constituents (> 70%). Only in the marine samples were ß-FeOOH and $Fe_{3-\delta}O_4$ found.

In addition it was evident that the α-FeOOH/γ-FeOOH radio obtained increased with increasing SO_2 concentration at the test sites, which was in agreement with the suggestion by Misawa et al[96,97] that dissolution of SO_2 in the surface electrolyte on corroding surfaces promoted the conversion of γ-FeOOH into α-FeOOH. No indication was obtained of δ-FeOOH or amorphous rust component in the rust.

Henry Leidheiser, Jr. and Svetozar Music[94] reported research on the composition of rusts on the surface of steel panels, determined by Mossbauer spectroscopy after atmospheric exposure times of 2 weeks, 2 months and 6 months and estimated 25 years for the purpose of better understanding of the initial stages of rusting of steel during atmospheric exposure. It was shown that the initial product was γ-FeOOH which converted in time to a mixture of α-FeOOH and γ-Fe_2O_3. The rate at which these processes occurred apparently was a function of the time of wetness as well as solids that settled on the

surface since the processes occurred much more rapidly on the panel in the horizontal position than on the vertical panel. Steel exposed for times of the order of 25 years was covered with corrosion products consisting largely of γ-Fe_2O_3. However, in this research, there was no evidence for the presence of Fe_3O_4.

Later in another investigation, Henry Leidheiser, Jr and Ilona Czako-Nagy[15] studied the rust formed during simulated atmospheric corrosion by using Mossbauer spectroscopy. They paid particular attention to the differences in the earliest stages of corrosion occurring in the natural atmospheric environment and in the simulated laboratory environment respectively.

In the simulated laboratory experiments, steel coupons were subject to 100 % relative humidity and were inoculated every day with 100 μl of 0.01 N solutions of NaCl, Na_2SO_4, LiCl, or CsCl. In some cases, distilled water rather than the salts solution were used during wet-dry cycles.

It was found that during the earliest stage of corrosion in laboratory experiment with salt water, the first solid rust constituent formed contained significant amounts of both τ-FeOOH and ferrihydrite. The authors did not give exactly the formula of ferrihydrite (with the bulk composition $5Fe_2O_3.9H_2O$) because different formulas had been proposed for ferrihydrite by different researchers, e.g. $Fe_5HO_8.4H_2O$[16], $Fe_5(O_4H_3)_3$[17], and $Fe_2O_3.2FeOOH.2.6H_2O$[18] etc. In contrast, only γ-FeOOH was observed in the rust formed during atmospheric corrosion. It was interesting that the corrosion product of steel in the simulated experiment using distilled water, rather than salt water, was γ-FeOOH, identical to that detected during atmospheric exposure. Therefore, it was concluded that inoculating the surface with significant quantities of salts, a practice often used to increase the rate of rusting in accelerated laboratory experiments, does not properly reflect the conditions

which exist during atmospheric exposure.

In a recent paper by Yamashita, et al[107], the rust layers formed on weathering and mild steels by atmospheric corrosion in an industrial region for 26 years have been characterized using various analytical techniques. It has been shown that the rust layers formed on both the weathering and mild steels are mainly composed of α-FeOOH and γ-FeOOH as crystalline constituents. The presence of a little Fe_3O_4 can also be detected. In addition, both of the corrosion products contain a considerable amount of bound water. However, there is no clear evidence for the presence of amorphous substances. For the weathering steel, it was found that the surface rust consists of the outer layer which mainly comprises -FeOOH and inner layer mainly composed of densely packed nano-particles of α-FeOOH, while the corrosion products formed on the mild steel is composed of a mottled structure of mixture of γ- and α-FeOOH. It is also noted that Cr is accumulated only in the inner layer. No enrichment of P or Cu in the inner layer of rust was observed. According to these observations, it was proposed that γ-FeOOH is formed on the steel surface at the initial stage of corrosion. The inner portion of the initial corrosion product may then change to amorphous ferric oxyhydroxde, via the dissolution of γ-FeOOH accelerated by acid rain and the precipitation of amorphous ferric oxyhydroxide by wet-dry cycles in an industrial atmosphere. In this stage, it is supposed that Cr, P and Cu which dissolved out from the steel matrix exert a favourable influence on the uniform formation of the protective rust layer. Finally, during a long period of exposure, the amorphous inner layer can transform to a densely packed aggregate of nano-particle α-FeOOH which is stable both electrochemically and thermodynamically.

2.4.3 The Principal Protective Constituents in Rust

One of the aims for investigating atmospheric corrosion is in trying to find which constituent in rust provides the most effective protection against further corrosion. However, up to now, these is little consensus on this matter with various propositions about this aspect of atmospheric corrosion.

Suzuki and co-workers[81] proposed that during atmospheric corrosion, Fe_3O_4 can be formed from the reducible amorphous substance they referred to as the intermediate substance, with rust layers on weathering steel containing less intermediate substance than those on plain steel. Suzuki concluded that the intermediate substances in the rust on weathering steel were difficult to convert to crystalline magnetite by cathodic reduction as compared to those on plain steel. Therefore, beneficial elements added to weathering steel, (eg. Cr, Cu, P), inhibited the formation of crystalline magnetite in the cathodic reaction process of rust and thereby increased the electrical resistance of the rust layer.

Matsushima and Ueno[82], measuring the polarization curves of weathering and carbon steels exposed to the atmosphere for various times, found that the corrosion current on weathering steel was smaller than that on carbon steel and, although the corrosion current of both steels decreased with exposure time, the tendency was greater with the weathering steel. Furthermore, it was shown that the decrease in the corrosion current of the weathering steel was due to a smaller passive current (during anodic polarization)than that of carbon steel, although both of the steels exhibited a passive tendency.

Matsushima and Ueno also found that the amount of sulphate formed by oxidation of adsorbed SO_2, presumably by the catalytic action of rust was much smaller for the weathering steel than for the carbon steel. The authors attributed this observation to the

different chemical nature of the rust formed on the weathering steel.

Stratmann and co-workers[87], studying the atmospheric corrosion of pure iron and the binary alloy Fe - 0.5Cu, pointed out that the effect of copper in the steel was restricted to the drying stage, where the corrosion rate was much smaller for the Fe-0.5Cu alloy than for pure iron. Stratmann et al explained this observation by two models based on different assumptions. One model assumed that Cu changed the kinetics of the cathodic reaction. Thus, if the addition of copper retarded the kinetics of the O_2 reduction until the overall reaction was under kinetic control, then the enhancement of the transport of O_2 during drying out period would have no influence on the corrosion rate. Thus, the corrosion potential would stay rather negative during the period of drying-out. The other model proposed that Cu changed the kinetics of the anodic reaction. If during corrosion copper was enriched at the metal-electrolyte interface, it would change the kinetics of the metal dissolution, or cause the metal to passivate more easily than for the pure iron. In this case, the corrosion potential should stay rather positive during the drying period. Although it seems impossible to prefer one to the other, experimentally, both models could be distinguished by a measurement of the corrosion potential during the time of critical wetting.

In the earlier study[89], Misawa et al attributed the better protective properties of weathering steel to the uniform formation of δ-FeOOH by catalytic reaction with Cu^{2+} and PO_4^{3-} concentrated in the interface of rust/metal, providing a cohesive and compact rust layer.

In the later investigation[97], it was found that the amorphous ferric oxyhydroxide rust on low alloy steel was dense and uniform and contained a considerable amount of bound water. Misawa et al explained this observation by stating that the amorphous ferric

oxyhydroxide rust acted as a protective barrier against atmospheric corrosion of the steels. Cu, P, and Cr in low alloy steels favoured the formation of crack-free, uniform rust layer and helped to produce uniform amorphous ferric oxyhydroxide.

In recent work[107], Yamashita et al have shown that the final stable corrosion product, nano-size α-FeOOH, which is formed in association with enriched Cr in the inner layer, is the densely packed uniform rust layer. This final stable product of nano-size α-FeOOH rust possesses an extremely high protective ability against atmospheric corrosion.

For the comments on this aspect of investigation, it is appropriate to cite Evans's saying[108] that "Without underestimating the value of such investigation, it should be pointed out that the position of the formation of a compound may be of greater importance than its composition or structure; a compound formed in physical continuity with the metal phase is most likely to be protective. Moreover, the protective character of a compound is likely to be affected more by the presence or absence of defects (such vacant sites or dislocations) than by the stucture which would exist if defects were absent."

2.5 Thin Film Electrolyte Electrochemistry for the Study of Atmospheric Corrosion

2.5.1 Introduction

As early as the 1930's Vernon[26] found the importance of the critical relative humidity in atmospheric corrosion, beyond which rapid acceleration of corrosion occurs. This implies that an adequate film of water on a metal surface will facilitate the highest rate of electrochemical reaction. Therefore, studies of corrosion reactions occurring in a thin electrolyte film should provide unique data in revealing the complex mechanisms of

atmospheric corrosion. However, compared with the abundant knowledge of exposure behaviour of materials in atmospheric environments, relatively little information on corrosion behaviour of materials covered by a thin layer electrolyte can be found in the literature.

In the early work done by Bengough[109], the effect of depth of immersion (0.35 mm to 15 mm) on corrosion rate was studied by measuring the rate of oxygen uptake volumetrically. Later in 1950's, Whitton[110] became one of the first workers to investigate the corrosion of iron covered by a thin film of neutral salt solution. The corrosion rate was determined by the consumption of oxygen by a volumetrical method. It was shown that the corrosion rate of iron was not a linear, but a square root function of external oxygen concentration. This indicated that the rate controlling step for the atmospheric corrosion of iron is not solely oxygen diffusion through the rust layers.

However, a relatively detailed, comprehensive research of corrosion of materials covered with a controlled thickness of electrolyte layer by electrochemical methods only began in 1950's from the work done by I. R. Rosenfel'D[5,6]. In this study, Rosenfeld developed a method of electrochemical research in thin electrolyte layers (0.1 N NaCl, thicknesses range from 30 to 640 μm), with which the electrochemical kinetics and mechanism of corrosion were studied. Since then, although much effort has been applied to the development of electrochemically-based atmospheric corrosion monitors[28-31], relatively little fundamental work has been performed using electrochemical techniques in the study of atmospheric corrosion. Then in 1977, Fishman and Crowe[111] attempted to study the effect of relative humidity on corrosion rate using potential transients, with some degree of success. Up to the 1980's, much more interest was shown in using thin film electrochemical methods for the study of atmospheric corrosion. Fiaud, et al[112,113] made

a detailed study of film thickness on corrosion rate using A.C. impedance analysis. Most recently, Cox and Lyon[114-116] have presented a relatively detailed study of atmospheric corrosion of mild steel covered by thin film electrolytes. While in the last few years, Stratmann and co-workers have introduced novel non-electrochemical techniques to the study of atmospheric corrosion of iron which have addressed some of the mechanistic questions[117-120].

2.5.2 Thin Film Electrolyte Electrochemical Cells

In the study of corrosion processes occurring in thin layer electrolytes, one of the important questions concerned is the configuration of the thin film electrolyte electrochemical cell. Ideally, the electrochemical cell which is suitable for the study of atmospheric corrosion should have a constant, precisely measurable layer of electrolyte which does not change in thickness with time. In addition, this cell should reasonably simulate the processes similar to these occurring in the actual situation of atmospheric corrosion, i.e. the process of drying or wetting of the surface, the transport of oxygen from air to the sample covered with thin electrolyte, and the current flow between the anode and the cathode.

Generally, there are two kinds of configuration of the electrochemical cells, namely, the open-air and closed-air cells used, although a variety of thin electrolyte electrochemical cells have been reported in the literature.

The so-called open-air cell, like these used by Rosenfeld[5,6], Fishman et al[111], Gladkikh et al[121], and Basman[122,123], is composed of a specimen, which is fixed into a resin or glass substrate. The working electrode and the counter electrode are in the same

plane. The upper flat surface of the assembly is covered with a thin layer electrolyte which is open to air. This configuration of the cell allows the oxygen to transport from air to the surface of the sample through a thin electrolyte, which is similar to that occurring in the real situation of the atmospheric corrosion. The limited volume of electrolyte used in the cell can also simulate the accumulation of ions produced in the electrode reactions which has a significant effect on the whole process of atmospheric corrosion. More importantly, drying and wetting of the sample surface are easily realized in this kind of cell. However, one of the disadvantages of this kind of cell is that of evaporation of the electrolyte on the sample which changes the thickness of the electrolyte layer during the experiment, unless a high humidity is kept in the chamber of the experiment.

The kind of closed air cell, which has been used by Fiaud[112,113] et al, Keddam et al[124], and modified by Cox and Lyon[114-116], is composed of an upper section (a parallel insulating plane) and a lower section (a working electrode), between them a thin film of electrolyte is formed. The whole assembly is immersed in bulk solution, with the reference electrode and the counter electrode in the bulk solution outside the assembly. In some cases, in order to simulate atmospheric corrosion, the upper insulating plane is constituted by a waterproof membrane permeable to oxygen supplied by a air flux on the rear face at a slight overpressure.

Compared with the open cell, the advantage of this kind of cell is the convenience and the accuracy of the maintenance and the measurement of the thickness of the electrolyte layer. However, the way in which this kind of cell works is different from that in the atmospheric corrosion. It is also far more difficult to realise the processes of drying and wetting of the sample surface in this system, as often occur in real atmospheric corrosion.

Finally, it is worth mentioning the Kelvin electrode technique, which has been

introduced and used by Stratmann and co-workers[117-120] to study the atmospheric corrosion of iron. Unlike traditional electrochemical methods in which a Luggin capillary has to be used in order to measure the potential of the corroding surface, this unique technique employs a Kelvin probe as a reference electrode for the measurement of electrode potentials without touching the surface under investigation. This technique allied with the gas volumetric measurement provides the possibility that corrosion rates and corrosion potentials of atmospherically corroding iron surfaces during wet/dry transitions can be measured simultaneously, which is difficult to be realized by conventional electrochemical techniques. However, due to the oscillating Kelvin probe on the surface of the electrolyte, the mass transfer process, e.g. the diffusion of oxygen in the thin film of solution, may be changed, especially in thicker film solution. This may change the experimental conditions from the practical environment of atmospheric corrosion.

2.5.3 D.C. Electrochemical Measurement

2.5.3.1 Cathodic Process Occurring on the Metal Covered by Thin Film Electrolyte

In most cases of atmospheric corrosion, where the surface electrolyte on the metal is neutral or, occasionally, slightly acid, reduction of oxygen occurs as the main cathodic reaction. The whole process should include the dissolution of oxygen in the thin electrolyte layer, like that in the bulk solution, diffusion of oxygen through a sluggish layer to the surface of the sample, the thickness of the sluggish layer being less than the total thickness of the electrolyte layer covering the sample and diffusion being governed by Fick's first law, and then electrochemical reduction of oxygen on the metal surface.

Rosenfeld[5] has conducted experiments varying the electrolyte film thickness and measuring the oxygen diffusion current from polarization curves. It was generally indicated that the limiting reduction current of oxygen was increased with decrease of the thickness of the electrolyte layer on the surface, as expected if the reduction of oxygen was controlled by the diffusion of oxygen. However, by quantitative examination of results obtained, it was found that experimental values of the oxygen reduction rate were some 5 times larger than theoretical values which were estimated using Fick's law at the total thickness of 640 μm. The difference between the latter and experimental values decreased as the total thickness approached about 70 μm, becoming almost identical at the thickness of 30 μm. Rosenfeld attributed the observations to the self-mixing of the thin electrolyte layer, caused by a change in the surface tension of electrolyte film, either due to the non-uniformity of evaporation or to the variation in the temperature and concentration of the electrolyte in different parts of the film. It was claimed that oxygen may be transferred through thin electrolyte layers to the electrode not only by diffusion but also by convection. The true thickness of diffusion layers in thin films were far smaller than those in bulk due to self-mixing of the film.

In addition, as already discussed in the section 2.1.5.1, in the measurements of cathodic polarization curves for various sulphur dioxide (0.1 %- 1.0 %) in air, Rosenfeld found that the cathodic reaction rate was increased with increasing sulphur dioxide concentration. Therefore, it was thought that sulphur dioxide was reduced in the cathodic reduction process as a new cathodic depolarizer.

In Stratmann, et al's investigation[118,119], the gas volumetric method was used to measure the consumption of oxygen as the corrosion rate of the iron covered with the thin layer of electrolyte at the open potential conditions during wet/dry transitions. Therefore,

the results obtained in this way should concern the whole corrosion process of iron, including both the cathodic and anodic processes, instead of only the cathodic process. The typical result of the time dependence of corrosion potential and corrosion rate (consumption of oxygen) during drying is described as follows. As long as the surface was visibly wet, the corrosion potential was rather negative, the corrosion rate being given by the diffusion limited oxygen reduction. Then a sharp rise in the corrosion rate was observed, the electrolyte layer being invisibly thin during this stage. Simultaneously, the corrosion potential was shifted anodically by more than 0.5 V. After approaching a maximum corrosion rate of 1 mA cm^{-2} (values depending on the number of wet/dry transition and materials in investigation), the corrosion rate showed a sharp decay until very small rates of less than 10 μA cm^{-2} were observed. The corrosion potential was shifted further anodically up to values of +0.2 V(SHE).

This characteristic phenomena was explained by Stratmann and co-workers in terms of three competing reactions: the acceleration of diffusion limited oxygen reduction in the beginning, the passivation of the surfaces as drying continues and the decrease of the rate of the oxygen reduction during the last stage of drying.

It was thought that as the cathodic reaction during drying of the corroding metal surface was given by the O_2 reduction, its rate can easily be affected by the thickness of the electrolyte layer, if the rate of the oxygen reduction was controlled by the diffusion of O_2 through the electrolyte layer. When the thickness of the electrolyte layer became thinner, rates of the oxygen reduction were increased due to an acceleration of the transport of oxygen through the thinner electrolyte layer. As a consequence of the O_2 reduction, highly alkaline conditions would prevail in the thin electrolyte layer, therefore allowing the surface to passivate easily. In addition to this, the ion generated by a dissolution rate of

about 1 mA cm^{-2} would precipitate immediately at the metal/electrolyte interface because the limit of solubility was reached. As result of the precipitation large parts of the surface were rapidly blocked and the anodic metal dissolution was retarded.

The extremely high rates of the O_2 reduction at potentials of 0 to +0.2 V(SHE) were explained by the assumption that during the oxygen reduction the electron transfer reaction takes place at the oxide/electrolyte and not at the metal/electrolyte interface. During rust layer reduction, Fe^{2+} species are created within the lattice of the γ-FeOOH, therefore increasing the conductivity of the n-type semiconducting oxide and the density of electrons at the interface oxide/electrolyte. During subsequent drying, the thickness of the electrolyte layer decreased and oxygen would be reduced with high rates on the rust layer, which behaves like a large surface area cathode. The current density, which was normalized on the real surface area, was orders of magnitude smaller, as the specific surface area of the rust film was about 50 m^2g^{-2}.

Later on, Stratmann and co-workers[120] measured the cathodic polarization curves of oxygen reduction on platinum and iron electrodes respectively, using the modified Kelvin electrode device. Generally, the limiting diffusion current densities of oxygen are increased with decreasing the thickness of electrolyte layer covering the electrode. However, two important points, which are different from the observations of Rosenfeld's investigation, should be mentioned . First, the range of thickness of electrolyte layer can be divided into three groups, according to the mechanism of transport of oxygen to the surface of electrode. For a thickness $> 100\ \mu m$ the rate of the oxygen reduction is independent of the thickness. This was due to a strong convection induced by the vibrating Kelvin probe just above the electrolyte. For a thickness $< 100\ \mu m$ this convection no longer limits the thickness of the adherent diffusion layer but the rate is now inversely proportional to the

thickness of the electrolyte layer according to Fick's first law. For very thin electrolyte layers the diffusion - limited current density is again independent of the electrolyte thickness. This was due to the fact that in this case, the reduction of oxygen was controlled by the limiting transport of oxygen through the phase boundary of electrolyte/gas. The correspondent maximum oxygen reduction current in this case was reported to be about 8000 $\mu A/cm^2$, which is one order of magnitude larger than that (620 $\mu m/cm^2$ in 30 μm thickness) observed under the diffusion control mechanism[5]. Secondly, a much larger oxygen reduction current density in the respective thickness of electrolyte was observed in this investigation. For instance, 2500 $\mu A/cm^2$ oxygen reduction current in a 33 μm thick electrolyte layer was observed, about three times larger than that (620 $\mu A/cm^2$ in 30 μm thick electrolyte layer) observed by Rosenfeld[5].

Most recently, Cox and Lyon[114-116] have reported the results of cathodic reduction of oxygen on the iron surface covered by thin layer electrolyte. A variety of experiments were carried out, including limiting diffusion current measurements in a 300 μm electrolyte film under different oxygen concentrations, cathodic polarization curves with nitrogen, air and oxygen ventilation respectively, the limiting oxygen reduction current measurements as a function of electrolyte film thickness and oxygen limiting current measurements under evaporation and retained conditions. Generally, the oxygen reduction current density was sensitively affected by the concentration of oxygen, the variation of the thickness of electrolyte layer, and the condition of evaporation and condensation. However, in most cases, a relatively lower oxygen reduction current (63 $\mu A/cm^2$ in 300 μm thick electrolyte film) was observed, compared with the results of Rosenfeld (155 $\mu A/cm^2$ in 320 μm thick electrolyte film). This is partly because when the thickness of electrolyte film was below about 300 μm, the main source of oxygen was at the edges of

the electrolyte film rather than, as intended, from the top of the film via the ventilating housing.

With regard to the cathodic reduction of SO_2, as suggested by Rosenfeld[5], Cox and Lyon have investigated the effect of SO_2 pollutant at a gas concentration of 1 ppm, using cyclic voltammetry in a thin film electrolyte on iron. Results showed that although the reduction of bisulphite to thionite, and its re-oxidation, occurred during polarization in an oxygen-free atmosphere between -600 and -1200 mV (SCE), no evidence for such a redox process was found in the electrolyte film in air. Only sulphate species were found in the electrolyte film, implying relatively rapid oxidation of dissolved SO_2 to sulphate in the presence of ferric species as catalyst. Thus, it was concluded that the Rozenfeld mechanism[5,6] of the effect of SO_2 is invalid.

More importantly, Cox and Lyon, measuring the cathodic polarization and voltammetry response on pre-corroded and uncorroded iron, confirmed the Stratmann modifications to the Evan's electrochemical cycle for atmospheric corrosion. Thus, FeOOH and Fe^{2+} or $Fe(OH)_2$ comprise the oxidised and reduced species respectively. The reversibility of this reaction depends very much on the pH of the electrolyte. No evidence for oxidation of Fe_3O_4 to FeOOH was found. However, there was evidence for a redox couple involving Fe_3O_4 or Fe_2O_3 and $Fe(OH)_2$ as the oxidised and reduced species.

2.5.3.2 Anodic Processes Occurring on the Metal Covered by Thin Film Electrolyte

There has been little fundamental work carried out on the studies of anodic processes of metals covered with thin layer electrolytes, compared with the relatively detailed knowledge of cathodic processes of metals, as obtained and discussed above. Probably,

the reason for this may be related to the much more complicated anodic processes. For example, an anodic process may include the dissolution of metal in the electrolyte, accumulation and hydrolysis of metal ions, deposition of metal oxides, and variation of pH value in the solution, while in most cases, the cathodic process (reduction of oxygen) mainly causes a change of pH value in the solution. The other reason may concern the difficulties in obtaining reproducible results of anodic processes because in this case, the results are more sensitively affected by the other factors, i.e. crevice corrosion.

In Rosenfeld's[5] investigation of the anodic reaction, it has been shown that in the case of copper, the more rapid saturation of thin layers with anodic reaction products impeded somewhat the anodic process of copper corrosion, and the anodic overvoltage increased. Copper displayed the phenomenon of anodic passivity which occurred in bulk solution and in thin layers at identical potential values. This indicated that the nature of the passive state was the same in both cases and was due to the attainment of the potential of formation of the same chemical compound (CuO).

An entirely different behaviour was displayed by iron, steel and zinc. These metals did not undergo any marked polarization, either under thin electrolyte layers or in bulk solution and remained in the active state over a considerable range of current densities.

Fishman and Crowe[111], studying atmospheric corrosion processes of iron at three different condition of relative humidity (67, 78, 98 % R.H.), showed that the measurement of polarization curves (anodic and cathodic) in condensed film condition was largely dictated by the cell resistance. This made it difficult to give a meaningful explanation to the results obtained. A detailed discussion about the effect of cell resistance will be given in the next section.

Stratmann and co-workers[119], using volumetric methods to study the corrosion

processes of iron and steels, indicated that during the evaporation of electrolyte, when the surface of iron became nearly dry, after approaching 1 mA/cm^2 which corresponds to a metal loss of 1 cm/year, the corrosion rate showed a sharp decay until very small rates of less than 10 μA/cm^2 were observed. This very small corrosion rate is clearly attributed to the occurrence of passivation. Stratmann explained this passivation as due to the change of pH value in the solution caused by the preceding high rate of reduction of oxygen or to the accumulation of anodic products in the limited volume of solution. However, for the pure iron, this passivation is not stable. In the subsequent wet condition, an activation of iron corrosion can be observed, indicated by a relatively large corrosion rate. The important observation is that unlike the case of pure iron, Fe-3.4Cu steel exhibits a very stable passivation and no activation of corrosion is observed after 8th wet/dry transition. This observation was explained as that the rust layers formed on the Fe-3.4Cu steel are more dense, perhaps by the enrichment of Cu at the interface metal/electrolyte.

In later measurements[120], the anodic polarization curves clearly showed a passivation feature. The critical passivation current and passivated current are all decreased with a decrease in thickness of the electrolyte layer. However, by quantitative analysis, it can be found that although the phenomenon of passivation was observed, the passivated current densities are still relatively large (more than 100 μA/cm^2 for 2-3 μm thickness electrolyte and more than 1000 μA/cm^2 for 10 μm thickness of electrolyte), which could not provide full protection for iron under atmospheric corrosion.

2.5.3.3 Solution Resistance Polarization

Solution resistance polarization here should be referred to the polarization caused by

the solution resistance between the anode and the cathode. However, due to the difficulty of identification of this polarization, the general aspect of solution resistance caused by the thin layer electrolyte is discussed here.

The theoretical analysis about the relationship between the solution resistance (R) and the thickness of the electrolyte layer (δ) was examined by Basman, et al[122], using a formula for electrolyte resistance between two coaxial cylindrical electrodes[125]:

$$R = (2\pi\lambda\delta)^{-1}\ln(\frac{r_2}{r_1})$$

where λ is the conductivity of the solution; δ the height of the cylinder (in the present case thickness of electrolyte layer); r_1 the radius of the internal cylinder (in the present case the radius of the working electrode); r_2 the radius of the external cylinder (in the present case distance between the working electrode and the counter electrode). From this equation, it was revealed that the solution resistance R has a linear relation with the reciprocal of the thickness of the solution. Therefore, this relation can be used as one of the criteria to judge the validity of the methods for determination of the solution resistance.

In the investigation of Fishman and Crowe, a concept of cell resistance of the electrochemical system was introduced, which consists of the solution resistance R_s between the Luggin probe and working electrode and the interface resistance R_i.

The individual values of the solution and interface resistances were independently determined by applying a step voltage impulse to the cell and measuring the voltage-time characteristic across a known series resistance R_p. This was so because the voltage drop across the interface was zero at the first instant that the step voltage was applied. The solution resistance, R_s, can then be calculated using quantities measured from the oscilloscope trace and the relation:

$$\frac{E_{p1}}{E_{applied}} = \frac{R_p}{R_p + R_s}$$

as shown schematically in Fig.2-1. At a later time, the interface capacitance charged so the interface resistance, R_i, was calculated using the relation:

$$\frac{E_{p2}}{E_{applied}} = \frac{R_p}{R_p + R_s + R_i}$$

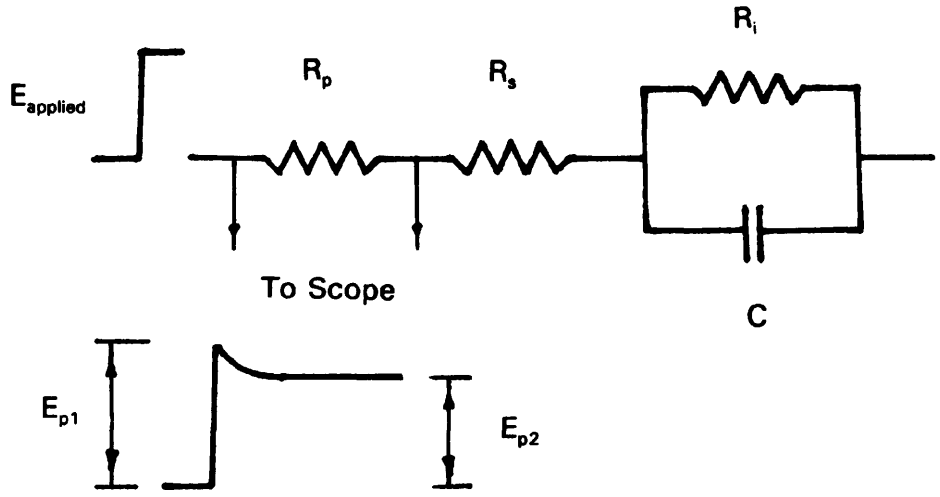

Figure 2-1 Electric analogue of cell solution and interface.

By using the technique and the equivalent circuit in Fig.2-1, it was found that the measured solution resistances varied from 28 kohm (93% R.H.) to 141 kohm (67% R.H.) and interface resistances from 1.4 kohm (93% R.H.) to 397 kohm (67% R.H.) were very high, meaning that measured polarisation curves contained a large contribution from IR drops. It was this characteristic which differentiated the thin film electrolyte measurements from polarization measurements obtained for bulk electrolytes.

Additionally, Fishman also derived the minimum expected corrosion current from measurements of polarisation curves by taking the current where the anodic and cathodic curve separation equals the calculated ohmic potential drop. Minimum expected corrosion

current densities for the three relative humidities were 2 μAcm^{-2} (67% R.H.), 13 μAcm^{-2} (78% R.H.) and 77 μAcm^{-2} (93% R.H.) respectively. It was seen that the humidity was extremely important in the atmospheric corrosion process with a decrease in corrosion current of almost two orders in magnitude with a decrease in R.H. from 93% to 67%.

However, it was clear that the polarization curves obtained in three humidities (67%, 78%, 93% RH) were significantly dominated by the effects of the IR drop, as the applied potential can reach as high as 5 to 6 volts when the applied current remains as little as few micro ampere per square centimetre (67%). The authors ascribed this effect to the existence of high solution resistance R_s and interface resistance R_i and, as stated before, derived the equivalent circuit in Fig.2-1 to explain the results. Now, the problem perhaps arises from the definition of the interface resistance R_i in this system. If the interface resistance did not include the charge transfer resistance R_t and double layer capacitance C_d, an R_t in parallel with C_d should be added to the circuit to represent a complete electrochemical system. In this case, the technique used in this investigation for the measurements of R_s and R_i would be valid just only when R_t is much less than R_i, which was not mentioned in the paper. More importantly, the very high interface resistance obtained at 67% RH (379 kohm) and at 78% RH (14.5 kohm), for whatever reason, should passivate the system.

In contrast, to elucidate the controlling steps in corrosion processes under thin layer electrolyte, Rozenfeld measured the potential distribution curves on anodic and cathodic areas of a bimetallic cell under thin film conditions. An analysis of the corrosion cell work showed that in invisible electrolyte layers (to 70 μm) the operation of the macrocell model was controlled by the cathodic process both in highly conducting and poorly conducting media. The role of ohmic factor was negligible. These results obtained on macromodels

was claimed can be extended to atmospheric corrosion due to microcell activity.

2.5.4 A.C. Impedance Measurements on Metals Covered with Thin Layer Electrolyte

C.Fiaud, et al[112] used a specially-designed electrochemical cell to perform impedance and polarization resistance measurements on various metals (aluminium, iron and nickel) covered by electrolyte layers of thicknesses between 30 and 3000 μm, in deaerated or aerated conditions. Experimental results were interpreted successfully on the basis of a model taking into account potential and concentration distribution in the liquid film.

The electrochemical cell, which was composed of an upper section (a parallel insulating plane) and a lower section (a working electrode), between them a thin film of electrolyte formed, was immersed in bulk solution (0.05 M Na_2SO_4 + 0.05 M H_2SO_4). In order to simulate atmospheric corrosion, the insulating plane constituted a waterproof membrane permeable to oxygen supplied by a air flux on the rear face at a slight overpressure.

In the case of aluminium, whose corrosion current was very low provided pitting corrosion was not initiated, the experiment was focused on the dependence of potential distributions on the thickness of the electrolyte layer. At frequencies lower than 5 kHz, the impedance results were presented by a slightly depressed semi-circle, which can be explained by frequency distributed R and C. As the electrolyte thickness decreased, the general shape of the impedance loop was not significantly modified, except at high frequencies, where there appeared an additional straight branch exhibiting a 1.2 slope. If R_D was defined as the projection on the X axis of the additional branch and R_s as the high frequency limit of the impedance, the real part of the impedance is the sum of R_s, R_D and

Rp which was approximately independent of the electrolyte thickness (ϵ). Whereas, both R_s and R_D were proportional to the reciprocal of ϵ. The above phenomena were interpreted by Fiaud and co-workers using the following procedure. The Al disk electrode was divided into 1000 narrow concentric rings. Impedance of an elementary ring was simulated by a partial double layer capacitance in parallel with a partial resistance, both functions of the ring radius. The total impedance was integrated numerically from the centre to the exterior of the disk for each frequency. The Rp contribution, in parallel with each partial double layer capacitance, was taken into account in the calculation but its effect was quite negligible at high frequencies and did not mask the potential distribution effect on the shape of the impedance diagram. R_S was calculated by cancelling the capacitive admittance in front of the plastic embedding. It was found that the result calculated by taking into account the effect of potential distribution on the a.c. impedance was in good agreement with the experimental result obtained.

In contrast with the case of aluminium in the electrolyte, metals like iron or nickel were subject to faster corrosion at their rest potentials. Correspondingly, impedance diagrams were very sensitive to any variation of the electrolyte layer thickness ϵ. In the case of iron, a decrease of ϵ caused (i) a shift of the diagram toward the right due to an increase of Rs, (ii) a deformation of the loop due to potential distribution effects, (iii) and moreover an important enlargement of the loop diameter Rt. Obviously, in the electrochemical cell used the diffusion path way of reacting species participating in reactions of corrosion was from the bulk of electrolyte to the corroding surface. Therefore, the corrosion rate was expected to be proportional to the layer thickness. However, the experimental data showed that the corrosion rate was proportional to the square root thickness $\epsilon^{-1/2}$. This was explained by the existence of concentration distribution, that is,

the concentration of the reacting species and consequently the corrosion rate at the electrode surface depends on the radial position of the point considered.

In aerated conditions for metals, iron and nickel, the variation in electrolyte thickness lead to the contribution of opposite effects respectively at high, intermediate and small ϵ values.

For $\epsilon > 1000\ \mu m$, both aerated and deaerated conditions give the same behaviour. The $\epsilon^{-1/2}$ law was interpreted by radial diffusion of reacting species within the layer. At ϵ values below 1000 μm, oxygen supply through the membrane controlled the corrosion rate by diffusion normal to the metal surface, giving as a rule a linear relationship between Rt (diameter of depressed semi-circle on impedance plot) and ϵ. The slight increase of Rt at the smallest ϵ values investigated ($\epsilon < 100\ \mu m$) was probably of poor significance since a distortion of the impedance diagram was clearly seen. This distortion was likely to arise from potential distribution effects and leads to an overestimation of Rt.

Using similar methods but with Fe-36Ni alloy, C. Fiaud et al[113] investigated the effect of the potential distribution on the impedance diagram of the thin layer electrolyte covering electrodes as a function of the reference tip position and layer thickness. The influence of the potential probe position was studied by using two different configurations of the thin layer electrolyte arrangement, one of them locating the probe outside the electrolyte layer, and other inserting the reference electrode through the upper part of the cell in order to reduce and possibly cancel out the ohmic drop contribution to the measurements. It was shown that when the potential probe was outside the thin layer, in the low frequency domain the impedance was close to a capacitive arc corresponding to a parallel R-C circle. An increase in the charge transfer resistance was observed in the experiments when the electrolyte layer was made thinner and thinner.

As the thickness (ϵ) of electrolyte layers was decreased, a typical feature appeared more and more clearly in the high frequency range, namely a straight line of unit slope (45°), as found and discussed previously in the paper[112]. If R_D was defined as the contribution of this region to the real part of the impedance and Rs as the high frequency limit of the impedance, the Rs was ascribed to the resistance of the ring shape electrolyte path outside the working electrode zone and R_D to the ohmic component of the impedance distribution in the electrolyte layer over the working electrode surface.

Where the potential probe was placed at the centre of the layer, the dc and ac potential measurements were also referred to the centre of the electrolyte layer. The high frequency feature mentioned above was found to disappear, which agreed with the removal of the potential distribution due to ohmic drop. In the same high frequency domain, the impedance diagrams intersected the imaginary axis and travelled through the second and third quadrants (negative real part). This behaviour was interpreted on the basis of the following model.

If it is assumed that the open circuit corrosion rate of the Fe-36Ni was small and that no differential aeration took place, the electrolyte composition and corrosion potential are uniform all over the electrode surface. In contrast, the ac components gradually reduced down as the signal penetrated more and more deeply from the edge towards the centre of the active area, due to the combined effects of the parallel short circuit by the surface impedance and the series ohmic drop in the electrolyte path resistance. The resulting frequency dependent potential distribution was dealt with by de Levie in terms of a transmission line model for a cylindrical pore[13] and shown to provide analytically the potential and current distributions and therefore the impedance referred to the local potential measured at the pore mouth.

The complex mathematical calculation about the effect of the potential distribution on the a.c. impedance measurements, based on the de Levie model can be found in the original paper[12]. For brevity, the main points obtained in this paper were that the impedance of a distributed system was strongly dependent on the location of the potential probe. A simple model which was derived by mathematical calculation and discussed in detail in the paper[12] could be used to interpret the data and to optimize the position of the reference tip with respect to the effect of the frequency dependent potential distribution. It was claimed that the results obtained were, at least qualitatively, valid for any distribution arising from one-dimensional or two-dimensional geometries.

As discussed above, C.Fiaud, et al work has focused on the problems concerning the potential and concentration distribution effects in thin layer electrolyte electrochemical cell on the a.c. impedance measurements. Clearly, proper consideration of these problems is important in interpreting the A.C. impedance results obtained in the condition of thin layer electrolytes. However, these investigations may be more suitable for studies of pitting or crevice corrosion which occur in the occluded cell than that of atmospheric corrosion in terms of the configuration of the cell used. Normally, in atmospheric corrosion the diffusion of some species (O_2 and SO_2 etc) normal to the surface of the electrolyte layer on the sample is the primary mass transfer process. In the cell used by C.Fiaud, et al the diffusion process normal to the surface of the sample may be slightly impeded by the additional solid surface of the upper plane or membrane. If this situation is true, then radial diffusion through the edge of the sample will supplement the mass transfer process, which has a different relation with the thickness of the electrolyte.

CHAPTER 3
EXPERIMENTAL METHOD

CHAPTER 3 EXPERIMENTAL METHOD

3.1 The Electrochemical Cell

3.1.1 The Configuration and the Fabrication of the Electrochemical Cells

The two kinds of thin layer electrolyte electrochemical cells, i.e. three electrode and two electrode, used in this study are shown in Figure 3-1 and Figure 3-2 respectively. In the three electrode system, two different sizes of working electrodes, i.e. 0.5 mm and 3 mm in diameter respectively, were used. The reason for this will be discussed later in the relevant part of the thesis. The sample material (99.99 % iron, 0.5 mm diameter or bright mild steel, 3 mm diameter) of 15 mm length was polished with 1200 and 4000 grade emery papers, washed with acetone and deionized water, dried with a cold air stream. A piece of copper wire was welded to the edge of the electrode to provide electrical contact. The electrode was coated with thin layers of a two component epoxy and allowed to cure for 48 hours at 25 $^{\circ}$C before embedded with epoxy resin. This procedure avoided crevice corrosion of the iron.

The electrode was then embedded vertically and centrally in a perspex ring containing epoxy resin to form a working electrode, according to the illustration in Figure 3-3. A piece of perspex tubing of length 15 mm and diameter 25 mm was placed on a greased perspex mould, in the centre of which a hole with the correct diameter was drilled for the purpose of supporting the electrode in the centre of the perspex tubing vertically. The electrode was then placed centrally into the tube. The electrical wire was threaded through a 1 mm (dia.) hole drilled centrally into the side of the tube (as step 1 in Fig. 3-3).

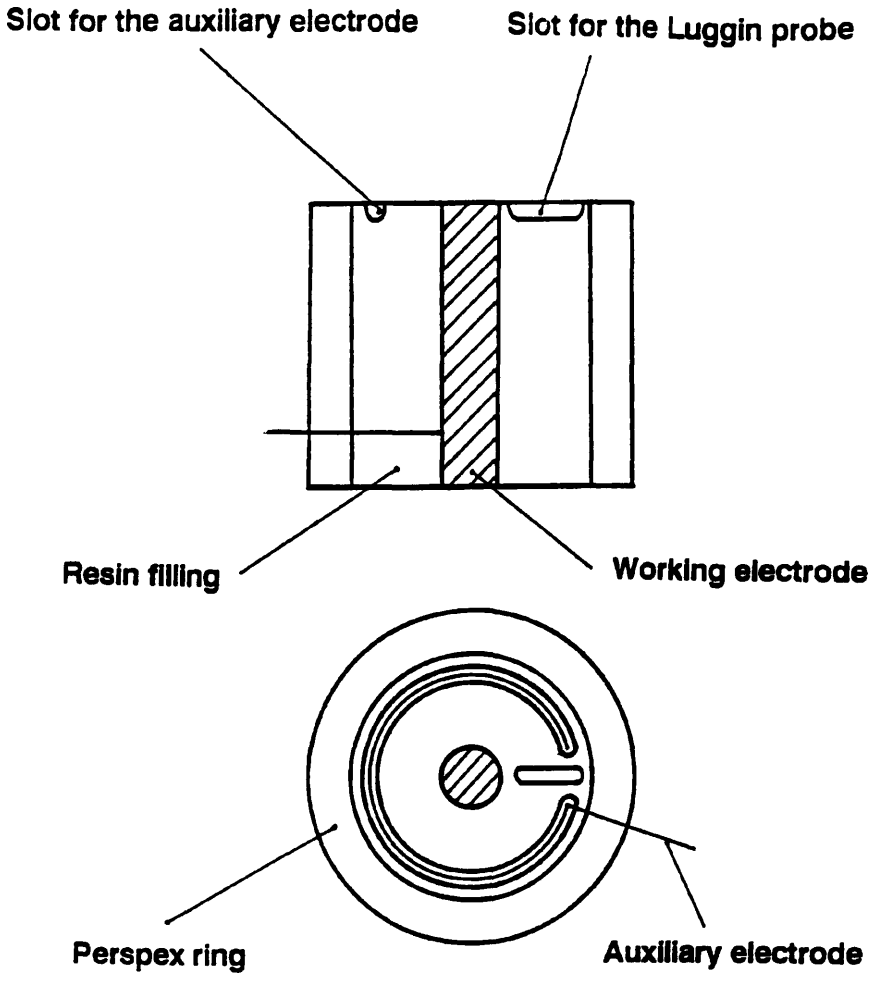

Figure 3-1 The three-electrode thin electrolyte electrochemical cell.

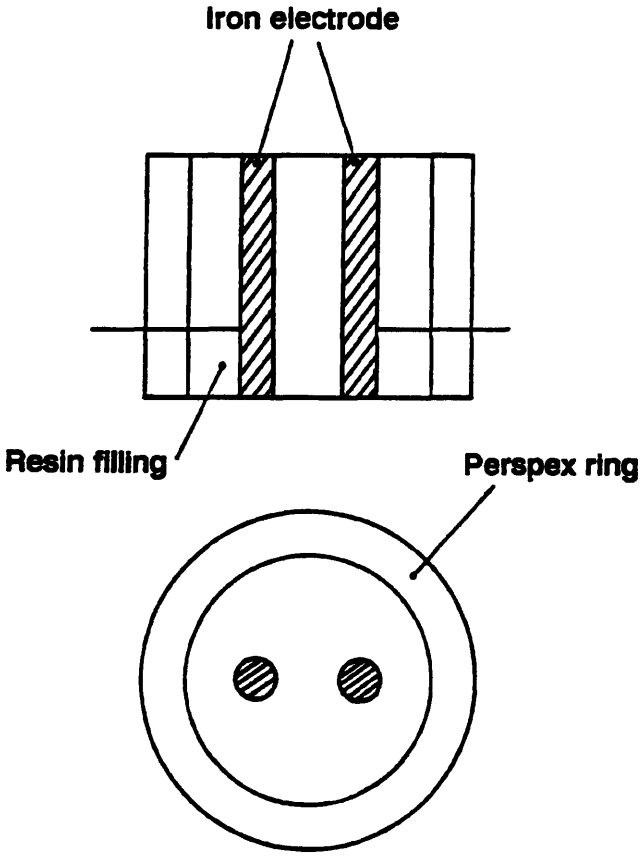

Figure 3-2 The two-electrode thin electrolyte electrochemical cell.

Plasticine was used to seal the edge of the tube and liquid "Araldite" poured into the cavity to fill the tube. After 24 hours curing, the mount was prised from the mould and the grease was removed from the tube. Then the liquid resin was poured into the remaining cavity in the other end of the tube to finish embedding (as step 2 in Fig. 3-3).

The mount was polished to exposed the electrode on the lower and upper faces which were successively wet ground with 240, 400, 800, 1200, 4000 grade emery papers respectively. Circular and straight slots were made around the working electrode on the upper face of sample, using a ball end milling cutter (as step 3 in Fig. 3-3), for the auxiliary electrode (a piece of platinum wire, diameter 0.5 mm) and a Luggin probe, respectively. The thin electrolyte layer was formed by eluting a few droplets of dilute electrolyte on the surface of the sample.

The electrolyte contact from the working electrode to the reference electrode was accomplished by a series connection using a plastic tubing with a Luggin probe at its end filled with agar + 0.001 M Na_2SO_4, a bottle containing 0.001 M Na_2SO_4 solution, the salt bridge (agar + saturated KCl) and a bottle containing saturated KCl solution, illustrated in Figure 3-4.

The two electrode system (in Fig. 3-2) is composed of the two electrodes (99.99 % iron, 0.5 mm diameter and 15 mm length) which were embedded vertically, parallel with each other, in a perspex ring with epoxy resin to form the electrode pair. The distance between the two electrodes was 2.8 mm. Procedures in fabrication of the two electrode samples were similar to those as discussed above and illustrated in Figure 3-3.

Finally, it must be noted that prior to the embedding, axial grooves must be cut inside the perspex tube, as shown in Figure 3-5, in order to reinforce adherence of the resin onto the inner face of the tube. Otherwise, a crevice would be produced in the interface

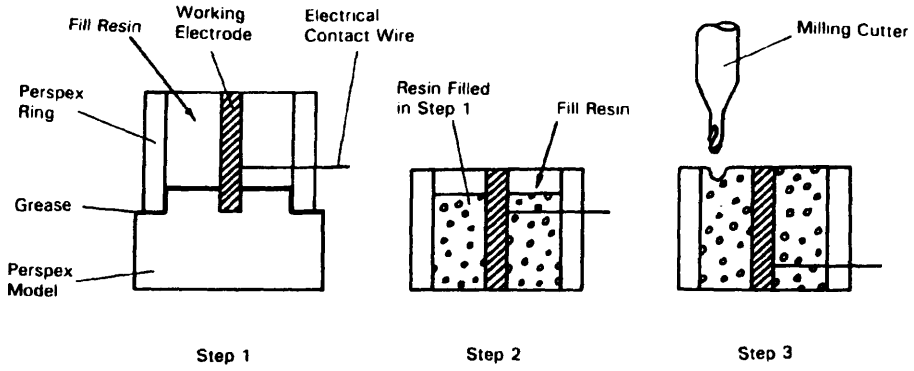

Figure 3-3 Procedures for the fabrication of the electrochemical cell.

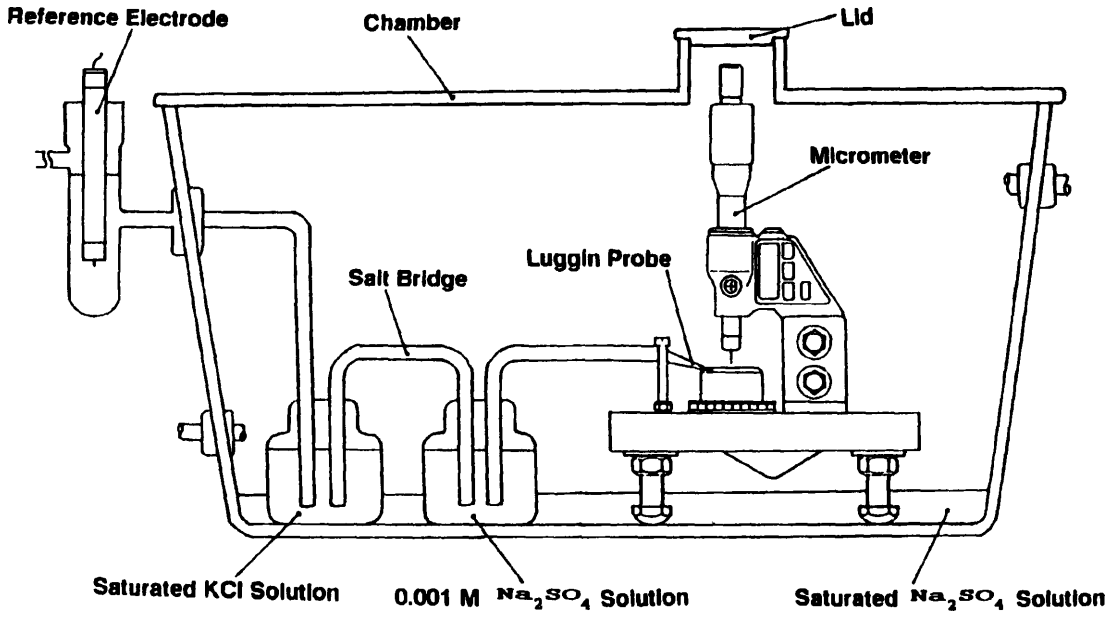

Figure 3-4 Complete Experimental Arrangement.

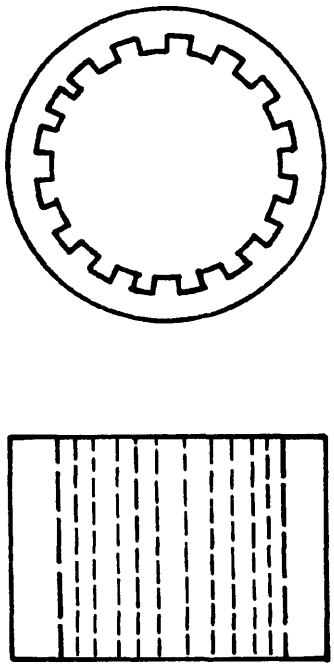

Figure 3-5 The perspex ring with axial grooves.

between the resin and the inside of the tube during the heating or cooling of the sample (in order to affect the evaporation and the condensation processes). Unless avoided, this crevice was found to affect the experimental results significantly, probably due to the accumulation and release of ions inside the crevice during the heating or cooling process.

3.1.2 The Features of the Electrochemical Cell

(a) The Reduction of IR Drop

The uncompensated solution resistance R_s, i.e. the resistance between the working electrode and the tip of the Luggin probe, is a serious problem in making the electrochemical measurements due to the poor conductivity and the thin layer characteristics of the electrolyte. Thus, in order to reduce the magnitude of this IR drop a small area working electrode (e.g. 0.5 mm diameter) and a correct configuration of the thin layer electrolyte electrochemical cell was chosen. In this specially designed electrochemical cell, the current required for the polarization of the working electrode is provided radially from a circular electrode. Only a fraction of the polarization current passes through the uncompensated solution resistance. In addition, the Luggin probe was put in a deep slot, not a thin layer electrolyte. This also leads to the further reduction of the solution resistance. The problem of IR drop encountered in the study of thin electrolyte electrochemistry will be discussed in more detail in the section 3.5.1.

(b) The Simulation of Atmospheric Corrosion Processes

In this electrochemical arrangement, the working electrode is surrounded by a circular counter electrode. Thus, the current flows radially from a circular counter electrode to the working electrode within the thin film electrolyte on the surface of the sample. In addition,

this arrangement also allows open access of surrounding air to the top of the electrolyte meniscus. These processes allow conditions similar to those of atmospheric corrosion, in which a small anode is surrounded by a number of small cathodes distributed in a circular form and oxygen, the main reactant of the corrosion process, gets access to the surface of the sample through a thin film of electrolyte.

Furthermore, evaporation and condensation of the electrolyte layer on the surface of the working electrode can be accomplished using a semiconductor heat pump underneath the sample by changing the polarity of the power source to provide a heating and a cooling source, as shown in Figure 3-6.

3.2 Measurements of the Thickness of the Electrolyte Layer

In this study, the thickness of the electrolyte layer on the surface of the working electrode is an important factor affecting the results of the experiments. The device used for the measurements of the thickness of the electrolyte layer is shown in Figure 3-6. A needle micrometer (Mitutoyo Digimatic Micrometer) and an ohmmeter were used to locate the position of the electrolyte meniscus and the surface of the sample. When the needle was slowly moved down and touched the meniscus of the electrolyte, the resistance monitored by the ohmmeter suddenly dropped down from infinity to some high value, depending on the thickness and the concentration of the electrolyte layer. Later, when the needle was moved down further and touched the meal surface, the resistance would be nearly zero, if the metal surface was rust-free or just covered with loose corrosion products. This technique allow the measurement of electrolyte thickness with an accuracy of $\pm$ 5 μm. This error takes into account the lowering down speed of the needle and the

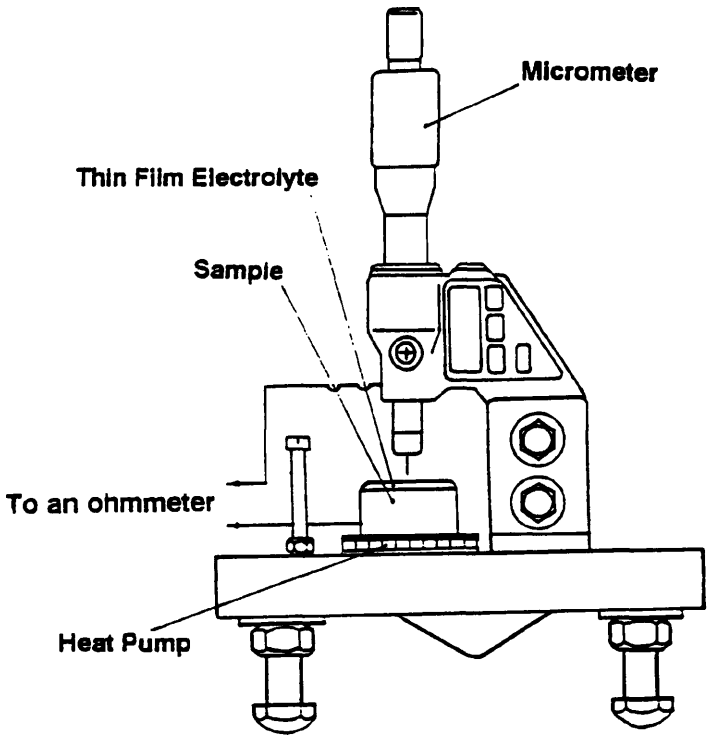

Figure 3-6 The device used for the measurements of the thickness of the electrolyte layer.

accuracy of measurements of the micrometer.

Additionally, care must be taken to place the sample in a level position and the working electrode just under the needle, in order to obtain a uniformly thick electrolyte layer on the sample and an accurate thickness measurement which represents the thickness of electrolyte layer just on the surface of the working electrode.

With this arrangement in situ measurements of the thickness of the electrolyte layer on the top of the sample can be carried out at any time during experiments by opening the small lid on top of the experimental chamber (shown in Figure 3-4) without disturbing the thickness of the electrolyte layer and changing the humidity inside the chamber significantly.

3.3 The Complete Experimental Arrangement

The complete experimental arrangement used in this study is shown in Figure 3-4. The thin layer electrolyte electrochemical cell was placed into a plastic box, the bottom of which was covered with saturated Na_2SO_4 solution to keep a constant humidity in the box and prevent significant change in the thickness of the electrolyte layer on the surface of the sample during the test. By introducing a thermometer and a digital humidometer in the box, the temperature and the humidity inside the box can be monitored. Furthermore, the environmental conditions in respect to the composition of gas and the humidity in the box can also be altered using a gas blender and a humidifier, according to the purpose of the experiment.

The rate of evaporation or condensation of the electrolyte layer on the surface of the working electrode can be controlled by changing the magnitude of the current supplied to

the semiconductor heat pump underneath the sample by a power source.

3.4 Experimental Process

3.4.1 The Preparation of the Sample

3.4.1.1 The Working Electrode

The working electrodes were wet polished with 600, 800, 1200 and 4000 grade emery papers respectively, then washed in running water, degreased with acetone and further cleaned by deionized water, dried with a cold air stream prior to each electrochemical run. Before and after the experiment the sample was carefully examined under the optical microscope (200-500x) to check whether there is a possibility for the occurrence of crevice corrosion. This is very important to ensure that the results obtained would not be degraded by the existence of crevice corrosion.

3.4.1.2 The Counter Electrode

In bulk electrochemistry, the counter electrode, far away from the working electrode or kept in another compartment, is rarely contaminated by the products produced on the working electrode. However, in thin film electrolyte electrochemistry, due to the fact that the counter electrode is kept in close to the working electrode, as shown in Figure 3-1, the products produced on the working electrode during experiments are easily deposited on the counter electrode, especially in the anodic polarization experiment. In this study,

it was found that this occurrence has significant effects on the stability of the system, for example, sometimes causing oscillation. Therefore, after several experiments, especially the anodic polarization experiment (judged from the colour of the counter electrode), the counter electrode (platinum wire) should be washed in the mixture of ethanol and NaOH (10% each) for about 5 minutes and in hot concentrated nitric acid (80 °C) for about 5 minutes respectively.

3.4.1.3 Agar + Na_2SO_4 Solution in the Luggin Probe

0.60 gram agar was added to 40 ml 0.001 M Na_2SO_4 solution under stirring. The mixture obtained was heated on a hot plate with occasional stirring until it became boiled and gelled.

The gel with Na_2SO_4 was then naturally cooled and drawn into the tube with a Luggin probe at its end by a syringe. The tube with gel inside was naturally cooled again at room temperature until the gel was fixed completely.

The preparation of salt bridge (agar +saturated KCl) can be made in the similar way to that described above. But more agar was needed in this case due to the higher concentration of the solution used.

3.4.2 Electrochemical Polarization Measurements

Electrochemical polarization was performed using a Ministat precision potentiostat (H. B. Thompson) and linear sweep generator (Chemical Electronics Ltd). The corrosion potential of the sample was monitored using a HP-3478A digital multimeter (Hewlett-

Packard). Potential-current curves were automatically recorded on an x-t recorder (Servoscribe).

Unless otherwise stated, all polarization curves were obtained at a potential sweep rate of 30 mV/min and all potentials reported with reference to a saturated calomel electrode (SCE). The tests were conducted at room temperature and the exposed areas of the working electrode were 1.963×10^{-3} cm^2 (diameter 0.5 mm) and 7.06×10^{-2} cm^2 (diameter 3 mm) respectively.

After the pretreatment as described in section 3.4.1.1, the sample was placed on the surface of the Peltier-effect heat pump inside the box and the thin film of electrolyte was formed on the surface of the sample by eluting a few droplets of dilute electrolyte. The film was left approximately 30 minutes to reach a relatively stable condition in respect to the thickness of electrolyte layer and the corrosion potential. During this period, the corrosion potential-time and the electrolytic thickness-time relations were measured simultaneously. Then the polarization measurements were performed from the corrosion potential, either cathodically or anodically. After each electrochemical run, the thickness of electrolyte layer was measured again to insure that the experiment was conducted at constant electrolytic thickness condition.

The same procedure was adopted for the A.C. impedance measurements

3.4.3 Corrosion Potential - Time Measurements

Corrosion potential - time curves during evaporation and condensation period were obtained by using a HP-3478A digital multimeter and a computer to acquire the data by HB-IB interface bus.

3.4.4 A.C. Impedance Measurements

The equipment used in measurements of a.c. impedance included a Solartron 1250 frequency response analyzer, a "Ministat" potentiostat and a computer for data acquisition.

The following instrumental parameters were used in all experiments, unless otherwise stated;

Amplitude of perturbation signal:	15-20 mV
Maximum frequency:	10 kHz
Minimum frequency:	10 mHz

All A.C. impedance measurements were carried out at the corrosion potential.

In this measurement, the three electrode system (as in Fig. 3-1) with potentiostatic control and the two electrode system (as in Fig. 3-2) with galvanostatic control were used. The detailed discussion about the circuit connections and the advantages of the two electrode system, etc will be made in Chapter 6.

3.5 Preliminary Examination of the Electrochemical Arrangement

Unlike bulk electrochemistry, the success of thin layer electrolyte electrochemistry in atmospheric corrosion research depends on, to a great extent, the suitability and the availability of the electrochemical arrangement used, probably due to the difficulties and complexities in making electrochemical arrangements and measurements under very thin film of electrolyte. Therefore, it is appropriate to examine the aspects and problems encountered in the thin film electrolyte electrochemical arrangement, before discussing the details of the results obtained. The discussion in the following section will be focused on

the uncompensated IR drop, the avoidance of crevice corrosion and the change of the thickness of electrolyte during test, although the volume of electrolyte, pH changes caused by reactions, and diffusion of species in the electrochemical cell will also be mentioned.

3.5.1 Uncompensated IR Drop

When the potential of a working electrode is measured against a reference electrode during the passage of current, a voltage drop equal to IR_s (called IR drop) will always be included in the measured potential. Here R_s is the solution resistance between the working and reference electrodes. The effects of the uncompensated IR drop on the experiments may be substantially significant or negligible, depending on the experimental conditions and the requirements of the experiment. However, in most cases, at least three possibilities for the effect of IR drop on the results of experiments must be considered. First, the measured electrode potentials always involve a IR drop, which leads to an error reading of the true electrode potential and a potential control error. When the current I and the solution resistance R_s are constant, then this means simply a constant error, like in polarization measurements in bulk solution electrochemistry, which may be allowed correction after the experiments by arithmetical substraction. Secondly, when linear sweep techniques, e.g. linear sweep voltammetry, are used, the current will vary in a nonlinear way with time so that, for a constant value of R_s, the actual electrode potential will be a non-linear function of time ($E_{true} = E_{appl} - IR_s$). This makes it difficult to explain the results obtained by using linear-sweep theory[126,127]. Thirdly, in pulse techniques, e.g. voltage step experiments, the existence of a significant IR drop makes the rise in potential at the working electrode interface in the form of an exponential, which is controlled by the cell

time constant, R_sC_d. Thus, transient experiments will not be meaningful unless the cell time constant is small compared to the time scales of the measurements[126].

IR drop in experiments can be minimized by three main approaches[126,127]:

(1) Cell Design

(a) Using a Luggin capillary and positioning the Luggin probe in close vicinity of the working electrode

(b) Using a smaller working electrode

(c) Using more concentrated supporting electrolyte

(d) Other means

(2) Simple Arithmetic Correction

If R_s is time - invariant and known by other methods, e.g. A.C. impedance measurements and voltage pulse techniques, the real electrode potential for each current can be obtained by subtracting IR_s from the applied potential. This is often applied to D.C polarization measurements.

(3) Instrumental Correction

One of the most common instrumental methods of IR compensation is the positive feed-back method. The idea for this method is that a correction voltage proportional to the IR_s is added into the input of the potentiostat, so that the total applied electrode potential is equal to the $E_{true} + IR_s$. In this case, the electrode potential obtained by the working electrode is exactly E_{true}.

In practice, however, there are problems with this scheme because the elements of the cell and the amplifiers in the control circuit introduce phase shifts. Thus, there are significant time lags in the application of a correction signal, the establishment of a correction, and the sensing that the correction has been applied. These delays can cause

the whole feed-back system to over-correct for changes in the input signal.

In severe cases the potentiostat will break into a high-frequency oscillation and therefore lose control completely over the cell[126]. In addition, there is a problem in knowing the value of R_s. It can be measured in A.C. experiments, but in most cases it is unknown.

Due to the dilute electrolytes used mostly in this research and the characteristics of thin film electrolytes, one of the major problems, encountered and recognized from the very beginning of this investigation, is the uncompensated resistance of electrolyte between the working electrode and the Luggin probe. This problem, when the relatively large working electrode (dia. 3 mm) was used, had given rise to a great deal of difficulty in interpreting some experimental results (e.g. voltammetry) obtained in this investigation. Now, the questions are, the possibility and necessity of a complete compensation of IR-drop in the research reported here, and the extent of the uncompensated IR-drop effect on the validity of the results discussed in this thesis.

Compared with normal bulk electrolyte electrochemistry research, thin layer electrolyte electrochemistry research incurs more instability characteristics, caused by the high input impedance of measuring circuit between reference electrode and working electrode, and especially due to the diluted and thin layer electrolytes. The electrochemical measurements are very sensitive to the noise produced either by the electrochemical cell itself or by the measuring circuitry and oscillation happens occasionally even when the system is slightly disturbed. On the other hand, the concentration of species in the electrolytes, especially in the vicinity of the working electrode, may vary significantly with polarization time during experiment, since the volume of electrolytes in the working electrode area is small. This concentration variation, in some cases, e.g. active dissolution of iron, is

comparatively large. This means that the solution resistance R_s is not constant and varies with time. Thus, by taking these two aspects into account, it was thought that positive feedback methods for elimination of IR-drops, normally used in the potentiostats with IR-drop compensation function, is not an appropriate way to attack IR-drop problem in this situation.

For the reason of the poor conductivity of the electrolyte in investigation and the thin film electrolyte characteristic of this study, the determination of the electrolyte resistance between the working electrode and the Luggin probe by A.C. impedance measurement become rather difficult when a three electrode electrochemical system is used. Partially, this problem may arise from the participation and the interference of the reference electrode with the system A.C. impedance response in high resistance systems, which will be discussed in the Chapter 6 in detail.

In addition, because the mechanisms of atmospheric corrosion are sensitively affected by the concentration, the conductivity and the kind of the electrolyte on the metal surface, the addition of a supporting electrolyte into the electrolyte for the reduction of IR drop is also not a reasonable method in this study.

Therefore, the appropriate approach to the minimisation of the effects of IR-drop in this investigation is by proper cell design, e.g. the small working electrode (diameter 0.5 mm) and the configuration of the thin layer electrolyte electrochemical cell, as discussed previously in the section 3.1.2.

The question about the validity of the results obtained in this investigation under the effect of uncompensated IR drop will be discussed in the respective sections below.

3.5.2 Avoidance of Crevice Corrosion

From the perspective of reduction of IR drop, the smaller the electrode used, the less the effect of IR drop on the results obtained because of the reduction of total polarization current. However, besides the restraints of electrode fabrication on the further reduction of the size of the working electrode, the smaller electrode will give rise to another problem, i.e. the occurrence of crevice corrosion. This is because the ratio ($\alpha = 2/r$ of electrode periphery ($l = 2\pi r$) to electrode area ($S = \pi r^2$) is increased with decreasing the radius of electrode for a circular sample. Here r is the radius of electrode; S is the area of electrode and l is the periphery of electrode. In severe cases, the results of experiment will be completely dictated by the occurrence of crevice corrosion, which makes it impossible to get meaningful results. Therefore, measures must be taken to avoid the occurrence of crevice corrosion as far as possible in the fabrication of the electrode and during the experiments, as discussed in the section 3.1.1 and section 3.4.1.1 respectively. This is one of the important aspects to insure that the results obtained in thin electrolyte electrochemistry can be successfully extended to the study of atmospheric corrosion.

3.5.3 The Change of Thickness of Electrolyte Layers

Although some previous work has been reported, as discussed in the literature review of this thesis, among them little mention was made of the change in the thickness of electrolyte layers during experiments. However, in practice, water layers can evaporate from metal surfaces at below 100 % relative humidity and evaporation will result in the reduction of the thickness of electrolyte layers. The change in the thickness of electrolyte

layers, on one hand, will affect the experimental results in thin film electrolyte electrochemistry, and, on the other hand, affect the duration of electrolyte presence on the metal surface in practice. Therefore, for both the research and the practical purposes, the topic about the change of electrolyte layers during experiment deserves consideration.

The relationship between the thickness of electrolyte layers (0.001 M Na_2SO_4) and exposure time at laboratory air condition (T = 25 °C; R.H. = 35 %) during natural evaporation is shown in Figure 3-7. It is clear that at a given relative humidity the change of thickness of electrolyte layers has an approximately linear dependence on the evaporation time, indicated by a straight line on the Figure 3-7. From this straight line, the evaporation rate of the electrolyte layers can be estimated by the slope of the line. In the case of T = 25 °C, R.H. = 35 %, the evaporation rate of electrolyte layer (0.001 M Na_2SO_4) is about 6.44 μm/min, obtained by the way as described above. This linear relationship indicates that at a given temperature and relative humidity, the evaporating rate is constant in a range of thickness of electrolyte layers and the evaporation process is thus dependent above all on the environmental relative humidity. This point can also be verified by thickness - time measurements (Fig. 3-8) carried out inside the box, as shown in Figure 3-4. Because the bottom of the box is covered with the saturated Na_2SO_4 solution, the relative humidity inside the box is higher (60 - 90 %) than that in the laboratory air (35 %). In addition, it will need some time for the relative humidity to reach its equilibrium value with this solution (e.g. 90 % equilibrium relative humidity for the saturated Na_2SO_4 solution) due to relatively large space of the box. During this period (0 - about 200 minutes), the evaporation rate of the surface electrolyte layers changes according to different relative humidity inside the box. At the first 40 minutes, the evaporation rate is about 1.41 μm /min under the relative humidity range of 60 % to 87

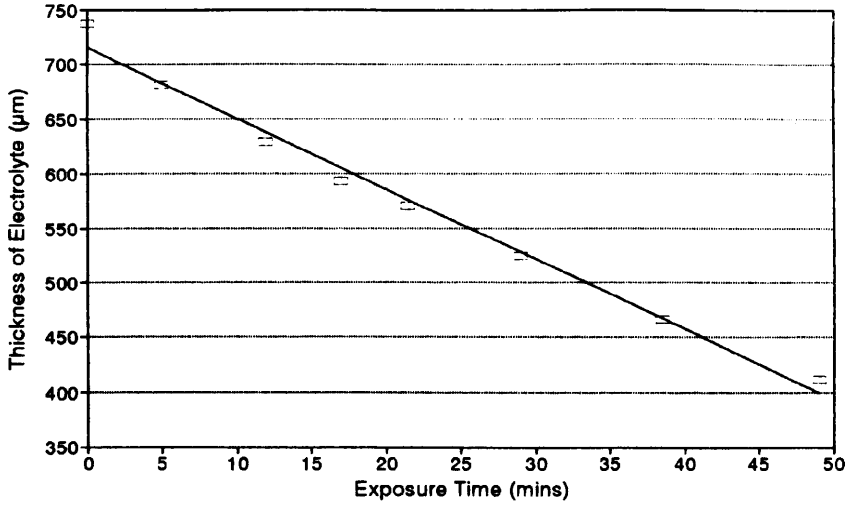

Figure 3-7 Thickness change with time at laboratory air during natural evaporation; electrolyte: 0.001 M Na_2SO_4, R.H. = 35%, T = 25 °C, thickness reduction rate: 6.44 μm/min.

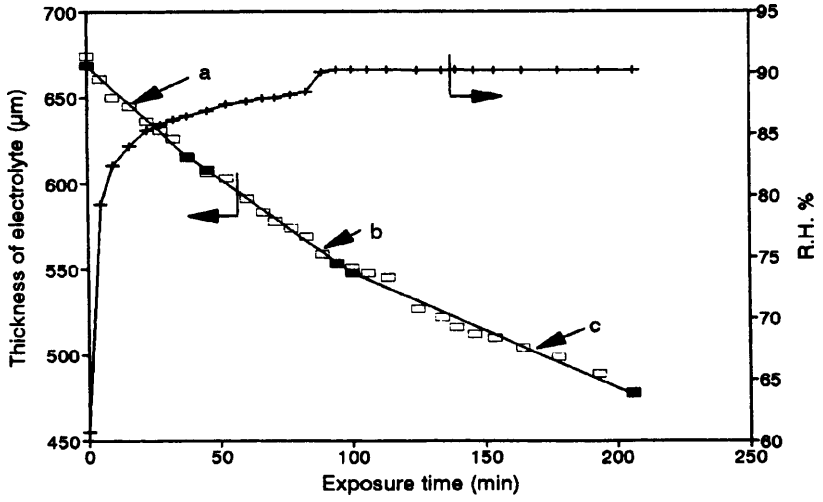

Figure 3-8 Thickness change with time inside the box during natural evaporation; electrolyte: 0.001 M Na_2SO_4, T = 22.1 °C, room R.H. = 35%, thickness reduction rate: (a) 1.41 μm/min; (b) 1.10 μm/min; (c) 0.67 μm/min.

%. Then the evaporation rate is reduced to about 1.10 μm/min as the relative humidity is from 87 % to 90 %. At the equilibrium relative humidity (90 %), the evaporation rate is about 0.67 μm/min. Thus, the evaporation rate is dependent on the relative humidity and decreases with increasing relative humidity.

At a relative humidity of 75 % (22.1 $^{\circ}$C), the evaporation rate obtained in this investigation (Fig.3-8) is about 84 μm/h, much higher than 35 μm/h at 20 $^{\circ}$C and 75 % r.h. reported in the literature[128]. More importantly, it can be seen that the thickness of electrolyte layer changes significantly by evaporation during the experimental period even though the relative humidity inside the experimental chamber is kept relatively high. For instance, one experiment will spend at least one hour, including half a hour stabilization and half a hour polarization. During this time, the thickness will reduce about 40 μm at the equilibrium relative humidity (90 % r.h), which introduces some error in the measurement of the thickness in experiments . In some cases, as shown in Figure 3-8, this error will be more severe as the establishment of the equilibrium relative humidity inside the box need some time.

Therefore, in order to keep the thickness of electrolyte layers constant during experiment, a semi-conductor cooling pump underneath the sample is needed to reduce the temperature of the sample to a point, for pure water theoretically the dew point temperature at a given humidity and temperature (e.g. t_d = 20.4 $^{\circ}$C at T = 22.1 $^{\circ}$C and R.H. = 90.2 %). The change in the thickness of electrolyte layers with time under the control of the cooling pump is shown in Figure 3-9. At the beginning , the thickness of the electrolyte layer reduces by about 30 μm by evaporation due to the lag of the cooling effect on the surface of the sample. Afterwards, the thickness begins to increase due to the effect of condensation. Finally, a relatively constant thickness of electrolyte film can be

obtained under the control of the cooling pump with a 0.8 A current. In this way, it can be assured that the whole experiment can be carried out under a relatively constant thickness of electrolyte layer, regardless of the duration of the experiment.

In contrast, the evaporation rate of the electrolyte layers can be increased by using a heating pump underneath the sample, or can be controlled by changing the magnitude of the current supplied to the heating pump. Figure 3-10 shows the change of the thickness of electrolyte layers with heating time under the effect of the heating pump with a 0.6 A current at 20.4 $^{\circ}$C and the relative humidities indicated in the Figure. In this case, evaporation rate intensified by the heating pump is about 4.60 μm/min, much higher than that (0.67 μm/min in Fig. 3-8) of natural evaporation.

In summary, the evaporation rate of electrolyte layers is linearly dependent on the relative humidity, increasing with the decrease in the relative humidity. The change of thickness of electrolyte layers may be significant during experiment even at a relatively high relative humidity provided by a saturated solution. This thickness change will affect the accuracy of the experiment greatly, unless other measures, e.g. using a cooling pump, are taken to prevent this change during the experiment.

3.5.4 Other Aspects

With reference to the configuration of the thin layer electrolyte electrochemical cell presented in Figure 3-1, besides the features which have already been described in the section 3.1.2, some other aspects, e.g. the ratio of counter electrode area to the working electrode area and the ratio of total volume of solution to the area of working electrode etc, must be examined because the analysis of the results obtained on the electrochemical

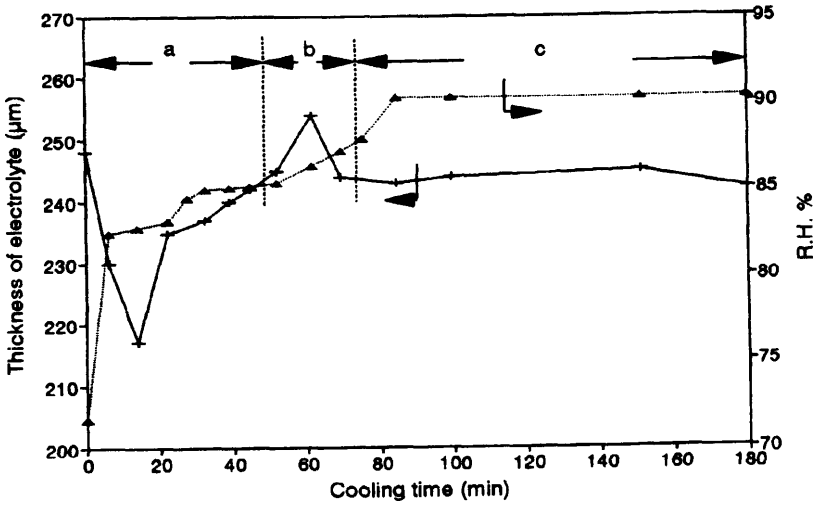

Figure 3-9 Thickness change with time inside the box during cooling by a peltier effect heat pump (PEHP); electrolyte: 0.001 M Na_2SO_4, room temperature: 22.4 °C, room R.H. = 40.1%, current to the PEHP: (a) 1 A; (b) 0.4 A; (c) 0.8 A.

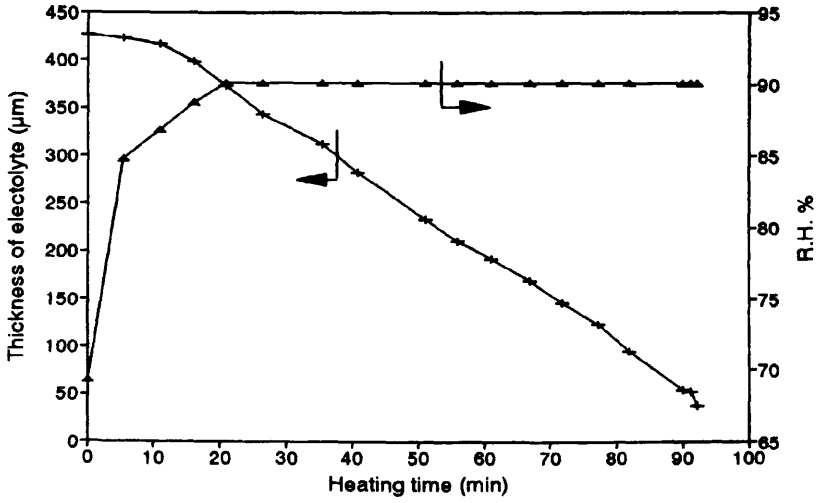

Figure 3-10 Thickness change with time inside the box during heating by a peltier effect heat pump (PEHP); electrolyte: 0.001 M Na_2SO_4, room temperature: 20.4 °C, current to the PEHP: 0.6 A, initial R.H. = 64%, thickness reduction rate: 4.60 μ/min.

cell are related to these aspects.

The ratios of the counter electrode area to the working electrode area in the cell of Figure 3-1 are 333.60 for the 0.5 m diameter working electrode and 9.26 for the 3 m diameter working electrode respectively, obtained by the calculation using a 0.5 m diameter platinum wire as a counter electrode. This ratio is big enough to satisfy the criteria of general electrochemistry which requires a larger area of counter electrode compared to the working electrode (normally, 3 :1).

The relationship between the total volume of electrolyte and the thickness of electrolyte layer is shown in Figure 3-11, obtained by calculation using the configuration of cell in Figure 3-1. In the case of 50 μm thickness, the volume of the electrolyte on the surface of sample is about 0.185 cm^3, and increases to about 0.397 cm^3 when the thickness increases to 800 μm. The ratio of the total volume of electrolyte to the area of the working electrode (0.5 m diameter) is about 94.2 cm^3/cm^2 for the thickness of 50 μm and is 202.2 cm^3/cm^2 for the thickness of 800 μm. From this point of view, the electrochemical study on the electrochemical cell used in this investigation can still be grossly considered to belong to the normal electrochemistry regime, although this study is so called thin film electrolyte electrochemistry. Therefore, the basic knowledge for bulk electrochemistry can also be applied to the study of thin layer electrolyte electrochemistry in this investigation without appreciable problems.

However, it must be noted that although the total volume of electrolyte is apparently fairly large, the majority of the solution is located in the counter electrode area due to the deep cut slot for the counter electrode. This feature and the comparatively larger area of counter electrode indeed reduce the possibility of contamination from the products produced on the counter electrode. However, the working electrode is necessarily covered

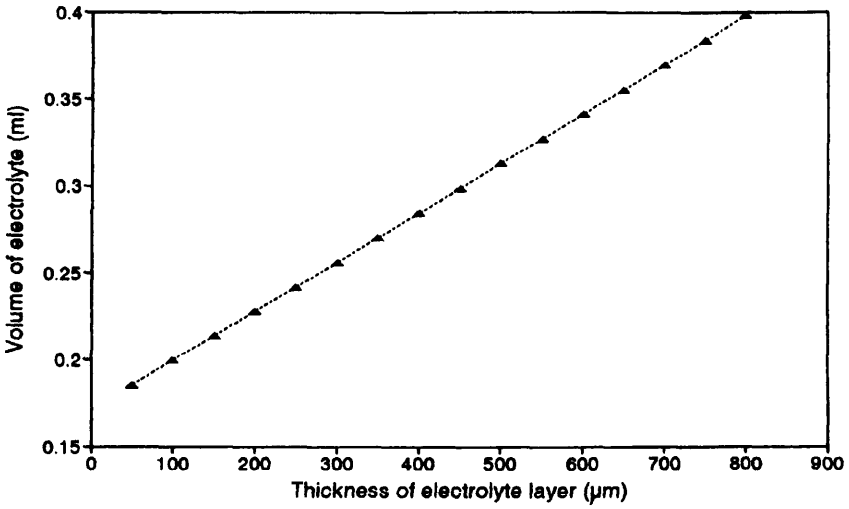

Figure 3-11 Relationship between the volume of electrolyte and the thickness of electrolyte layer.

by a thin film of electrolyte. The relatively smaller volume of solution in the working electrode area makes the accumulation of products from the working electrode more possible. This accumulation of products (or pH change in working electrode area) is related to the diffusion process of species in a very thin film of electrolyte, which has not been fully understood yet.

CHAPTER 4
CATHODIC PROCESSES ON MATERIALS COVERED BY THIN ELECTROLYTE LAYERS

CHAPTER 4 CATHODIC PROCESSES ON MATERIALS COVERED BY THIN ELECTROLYTE LAYERS

4.1 Introduction

In this chapter, attention is paid to the cathodic process of materials covered by thin electrolyte layers. Generally, compared with anodic processes which involve the production of metallic ions, the accumulation of ions and deposition of oxides etc, the cathodic processes are relatively simple, mainly involving the reduction of oxygen and subsequent change in conditions caused by this reaction, such as the change of pH value of the electrolyte near the surface of the electrode. Therefore, a preliminary study was made of the cathodic oxygen reduction on Cu, Zn and Fe samples (3 mm diameter) covered with dilute electrolyte layers 100 - 1132 μm in thickness, in respect to the cathodic reduction current as a function of the electrolyte thickness and the oxygen activity, in order to verify the suitability and validity of this experimental method in this investigation. Then, a smaller sample (0.5 mm diameter) and a more concentrated electrolyte (10^{-1} M Na_2SO_4) are used to investigate the cathodic processes on pure iron covered by thin electrolyte layers under more specific conditions (eliminating the effect of IR drop and providing more uniform current distribution due to the use of the smaller electrode and more concentrated electrolyte). Finally, the cathodic processes on pre-corroded iron, exposed for 4 months in Manchester environment, covered with electrolyte layers (10^{-4} M Na_2SO_4) are studied under evaporation conditions.

The emphasis of this chapter will be focused on the following questions:

(1) The suitability and the validity of thin electrolyte electrochemistry for the study of

atmospheric corrosion.

(2) The effect of the electrode size and the concentration of electrolyte layer on the electrochemical measurements under thin film electrolyte conditions.

(3) The mechanism of oxygen transport to the electrode in thin electrolyte films.

(4) Whether it is possible for atmospheric corrosion to be controlled by the oxygen diffusion process through the electrolyte layer and thus by the cathodic process.

(5) The effect of rust components on atmospheric corrosion, especially on its cathodic processes.

4.2 Preliminary Study of the Cathodic Oxygen Reduction on Cu, Fe and Zn Covered with Dilute Electrolyte Layers

4.2.1 Experimental

In this sub-section, all the experiments were carried out on a relatively large electrode (3 mm diameter). The thin electrolyte layer was formed by dropping a few droplets of deionized water on the surface of the sample. The Luggin probe and the solution bridge were filled with 0.2 M Na_2SO_4 solution in agar for the purpose of reducing the resistance of the measurement circuit between the reference electrode and the working electrode, which is important for the stability of the measurements when an X -Y recorder was used to record the potential - current curves.

4.2.2 Experimental Results

4.2.2.1 The Cathodic Polarization Curves for Iron, Copper and Zinc Covered by Thin Dilute Electrolyte Films

The cathodic polarization curves for iron covered with different thickness of water layers (from about 100 to 1118 μm) under the normal condition (laboratory air) are shown in Figures 4-1 and 4-2 respectively.

Except in the very thin film condition, e.g, 100 μm, the cathodic polarization curves reveal the obvious characteristics of concentration polarization with a limiting diffusion current range appearing, i.e. a nearly vertical line in the polarization curve. The limiting diffusion current densities increase with a decrease of the thickness of water layer, as would be expected if the cathodic reaction rate were controlled by the reactant oxygen diffusion to the surface of the electrode. In the case of very thin electrolyte layer, e.g. 100 μm in Figure 4-1, a limiting diffusion current was not observed, probably due to either the increased oxygen transport rate in the thinner electrolyte layer, causing the change in the controlling step from oxygen diffusion control to mixed control (electrochemical and diffusion control), or the increased IR drop caused by a larger electrolyte resistance in the thinner electrolyte layer, outweighing the effect of the oxygen diffusion process on the polarization curve. When the thickness of the electrolyte layer increases to greater than 736 μm (in Fig. 4-2), the effect of the change in the thickness of electrolyte on the shape of the polarization curves, especially on the magnitude of the limiting diffusion current, is not significant, indicating that, in these conditions, the thicker electrolyte layers (> 736 μm) behave effectively like a bulk electrolyte and that further increased total

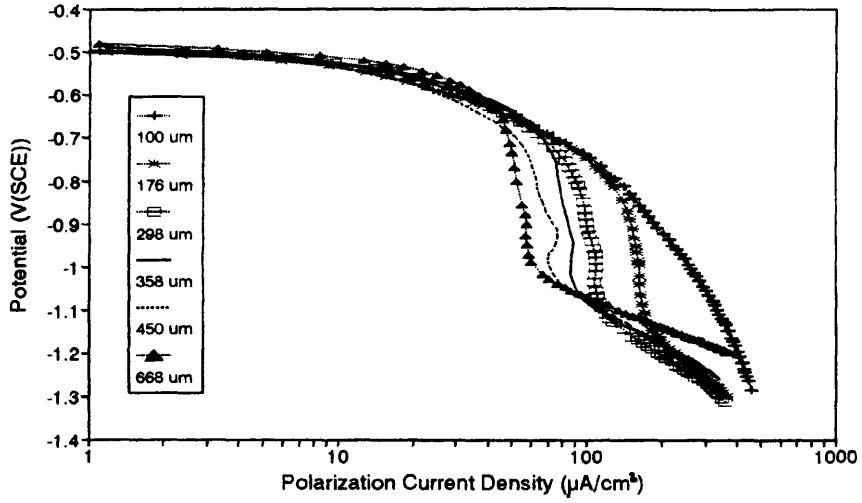

Figure 4-1 Cathodic polarization curves for iron covered with different thickness of water layers (from 100 to 668 μm) under normal conditions (laboratory air).

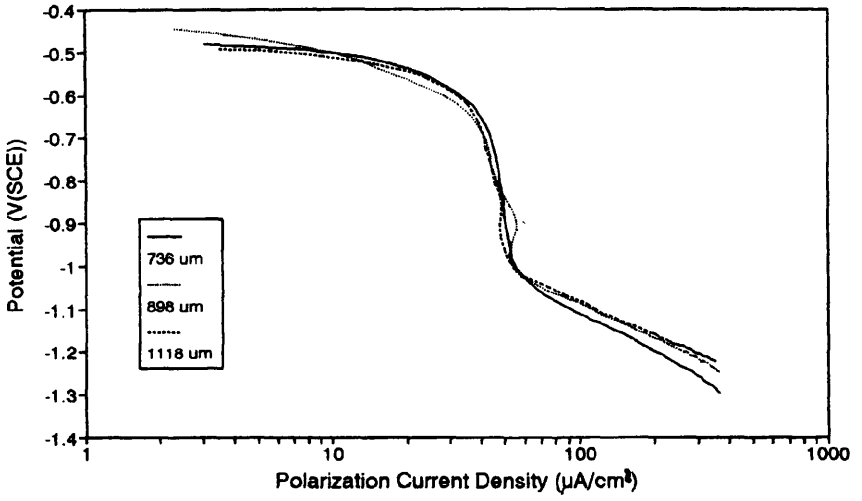

Figure 4-2 Cathodic polarization curves for iron covered with different thickness of water layers (from 736 to 1118 μm) under normal conditions (laboratory air).

thickness of electrolyte layer does not change the thickness of the diffusion layer significantly.

The cathodic polarization curves for copper covered with various thickness layers of water (from about 112 μm to 1132 μm) under similar conditions to that of iron polarization as discussed above are presented in Figure 4-3 and 4-4 respectively.

In this case, similar cathodic polarization curves to those of iron, discussed above, were found, also showing a limiting diffusion current range when the thickness of electrolyte layers is greater than 112 μm. However, at 112 μm, although the polarization curve is still dominated by a large IR drop as in the case of iron, an obscure limiting diffusion current range can be revealed when the polarization is beyond -1.0 V (SCE). This may indicate that, even in very thin electrolyte layers (about 100 μm), the cathodic processes may still be controlled by the slowing of oxygen diffusion through a thin diffusion layer under strong cathodic polarization. In addition, due to the more positive corrosion potential of copper, a larger potential range where the electrochemical processes are controlled by the diffusion process of oxygen can be observed in the polarization curves. Hence, there is a more clear concentration polarization characteristic in the cathodic polarization curves for copper. Similarly, when the thickness is beyond 836 μm, the effect of change in the total thickness of electrolyte on the shape of the curves is not great. The same explanation as described in the case of iron can be given to this phenomena, i.e. that the diffusion layer is less than the electrolyte thickness.

The cathodic polarization curves for zinc covered with various thickness of water layers (from 144 μm to 1072 μm) under laboratory air environment are given in Figure 4-5 and 4-6 respectively.

Unlike the cathodic polarization curves for iron and copper, it is not easy to determine

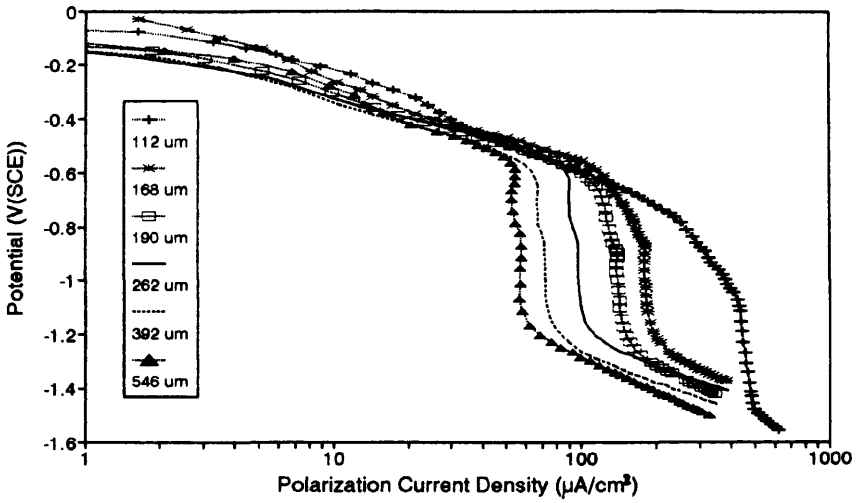

Figure 4-3 Cathodic polarization curves for copper covered with various thickness layers of water (from 112 to 546 μm) under normal conditions (laboratory air).

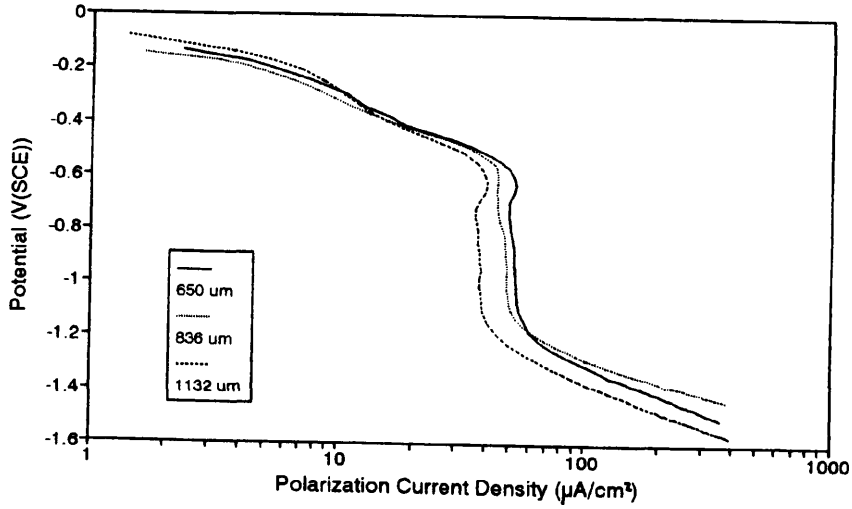

Figure 4-4 Cathodic polarization curves for copper covered with various thickness layers of water (from 650 to 1132 μm) under normal conditions (laboratory air).

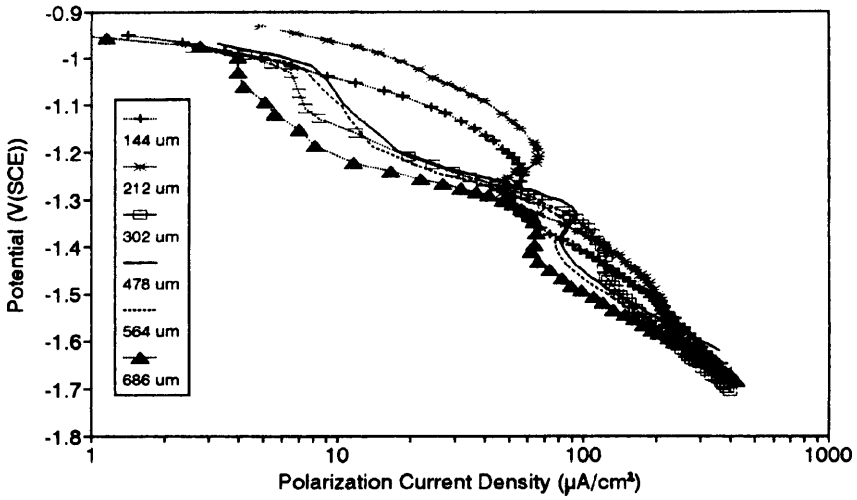

Figure 4-5 Cathodic polarization curves for zinc covered with various thickness of water layers (from 144 to 686 μm) under normal conditions (laboratory air).

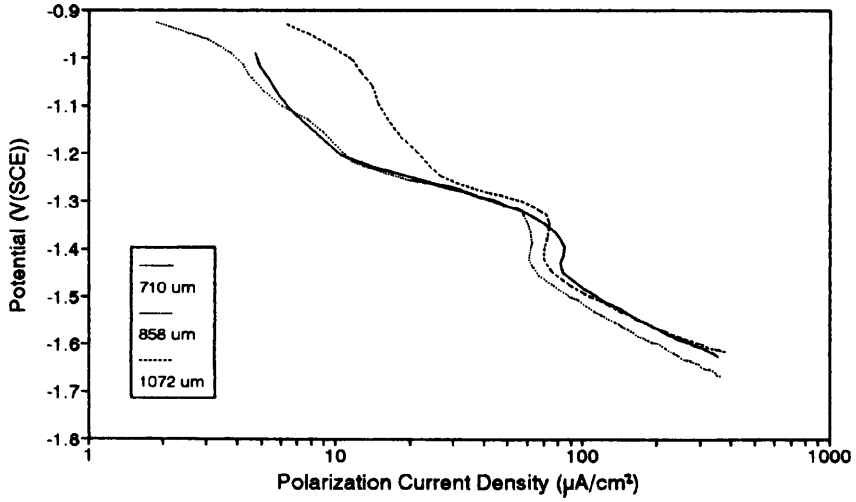

Figure 4-6 Cathodic polarization curves for zinc covered with various thickness of water layers (from 710 to 1072 μm) under normal conditions (laboratory air).

any regular behaviour from the zinc cathodic polarization curves with respect to the thickness of the electrolyte layer. This may be attributed to its relatively negative corrosion potential, which makes the hydrogen evolution process more likely when the electrode potential is polarized to a similar cathodic overpotential. If the cathodic process on zinc is dominated by hydrogen evolution rather than oxygen diffusion (which has relation to the thickness of the water layer), it is understandable that the zinc cathodic process under the condition of a thin water layer is relatively independent of the thickness of the water layer and not sensitive to the wet and dry cycles of the environment. In addition, besides the hydrogen evolution processes, reduction of zinc oxide, which may be identified by a current peak in the cathodic polarization curves, also contributes a amount of cathodic current in the polarization process.

In order to examine the effect of oxygen activity on the cathodic polarization of materials and verify that the vertical lines in the cathodic polarization curves of iron and copper are related to the oxygen diffusion process, a number of supplementary experiments were carried out to measure the cathodic polarization curves of materials under nitrogen purged conditions.

The cathodic polarization curves of iron covered with the thin electrolyte layers in the nitrogen purged condition, compared with the results obtained under normal laboratory air condition, are shown in Figure 4-7. Also Figure 4-8 shows the results of this kind experiment on copper in the similar conditions.

In respect to the effect of activity of oxygen on the cathodic process, two kinds of situation can be observed, according to the reduced activity of oxygen in the experimental environment. If the oxygen was removed relatively completely from the environment by either a stronger nitrogen purge or a nitrogen purge for a longer time, the reactant of the

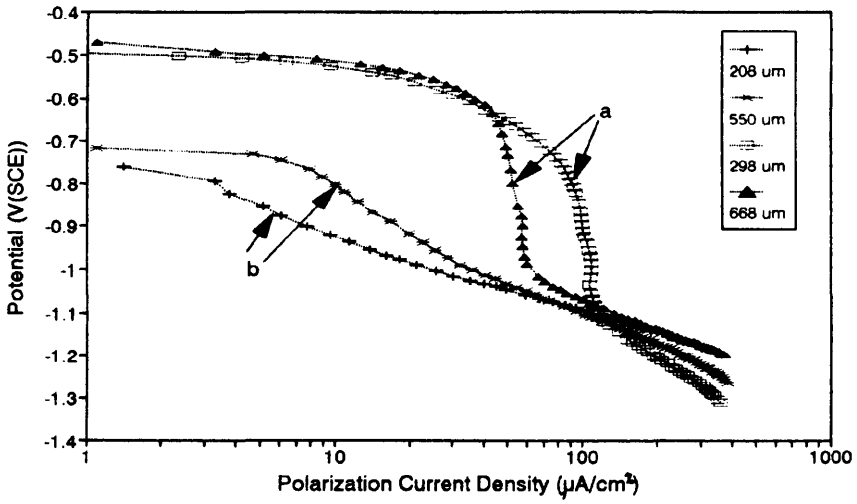

Figure 4-7 Cathodic polarization curves of iron covered with the thin water layers in the conditions of (a) normal laboratory air; (b) nitrogen purged.

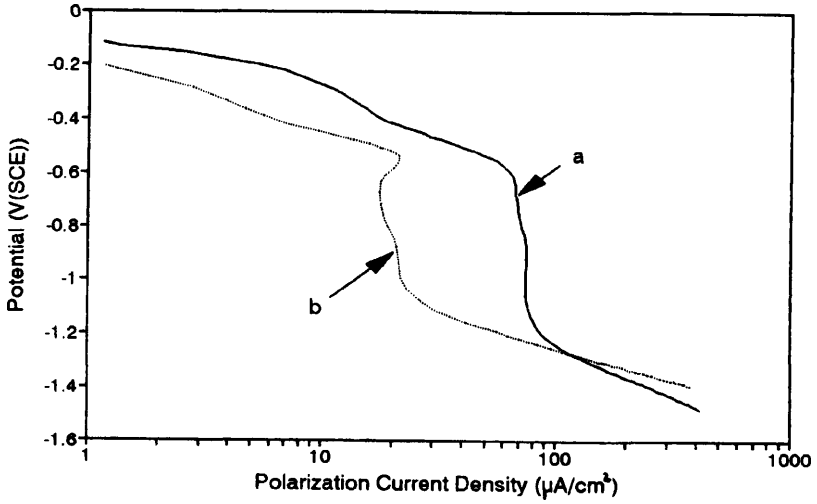

Figure 4-8 Cathodic polarization curves of copper covered with thin water layers in the conditions of (a) normal laboratory air; (b) nitrogen purged.

cathodic process would change from one species to the other, e.g. from oxygen reduction to hydrogen evolution. In this case, as observed in Figure 4-7, the feature of limiting oxygen diffusion current disappears from the curves because the main cathodic reaction now involves the hydrogen evolution rather than the reduction of oxygen. This change can be clearly observed in Figure 4-7, indicating the sensitivity of the experimental set up used in this investigation to the change in the environmental parameters. In the other case, if the nitrogen purge is not enough to remove all the residual oxygen in the experimental environment, the cathodic polarization is still controlled by the oxygen diffusion process. But due to the decrease of the oxygen activity by the nitrogen purge, the limiting oxygen diffusion current will be reduced also. This case is clearly represented in Figure 4-8. As expected, under the similar thickness of electrolyte layers (410 μm and 420 μm respectively in Fig. 4-8), the limiting oxygen diffusion current densities are reduced from about 80 $\mu m/cm^2$ in normal air to about 20 $\mu A/cm^2$ in the nitrogen purged condition due to the reduced activity of oxygen. This verifies that the vertical lines in the polarization curves are indeed related to the oxygen diffusion process, which is dependent on both the activity of the oxygen and the thickness of the electrolyte layers.

For zinc cathodic polarization curves under the nitrogen purge condition, presented in Figure 4-9, the reduction of cathodic reaction current in some areas of the cathodic polarization curves can still be observed. However, the reduction of zinc oxides confuses the interpretation. Thus, the current peak in relation to the reduction of zinc oxides is more clearly distinguished, probably due to the decrease of the oxygen reduction current which overlaps partly this region.

4.2.2.2 The Effect of Oxygen Concentration on the Cathodic Reduction Process

After confirming the existence of the oxygen diffusion process during cathodic polarization, the effect of gaseous oxygen concentration in the experimental environment on the limiting cathodic reduction current of materials covered with a constant thickness of electrolyte layer was investigated. This was done by keeping the electrode potential at -0.851 V (SCE) to record the limiting cathodic current under different conditions (laboratory air, nitrogen purged and oxygen purged). Figure 4-10 illustrates the relationship between the limiting cathodic current on iron covered with a 614 μm electrolyte film and the concentration of oxygen (air, and nitrogen - purged) at the electrode potential of - 0.851 V (SCE). In the normal condition (laboratory air), the limiting cathodic current is about 55 $\mu A/cm^2$, very close to the value obtained in the polarization curves measurements in the same thickness of electrolyte layer. However, the limiting cathodic current gradually decreases during nitrogen purging of the experimental chamber to a residual value, i.e. 2-3 $\mu A/cm^2$, which is probably due to the reduction of residual oxygen in the electrolyte. Similar experiments were carried out on a copper electrode and the typical result is shown in Figure 4-11. In similar way, the initial limiting cathodic current density is dependent on the thickness of the electrolyte layer as observed in the polarization measurements in laboratory air. Later, as the concentration of oxygen was changed by nitrogen purge, pure oxygen purge and air purge, respectively, the limiting cathodic current is dependant on the concentration of oxygen in the experimental chamber. It decreases gradually to a small value during nitrogen purge due to decreased oxygen concentration and increases rapidly again to about 190 $\mu A/cm^2$ as pure oxygen was ventilated to the chamber, then decreases again to the nearly same value as the beginning

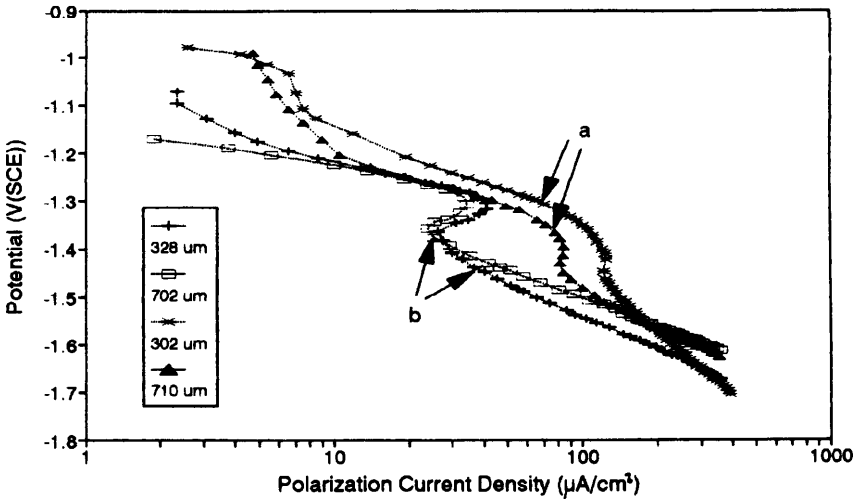

Figure 4-9 Zinc cathodic polarization curves under various thickness of water layers in the conditions of (a) normal laboratory air; (b) nitrogen purged.

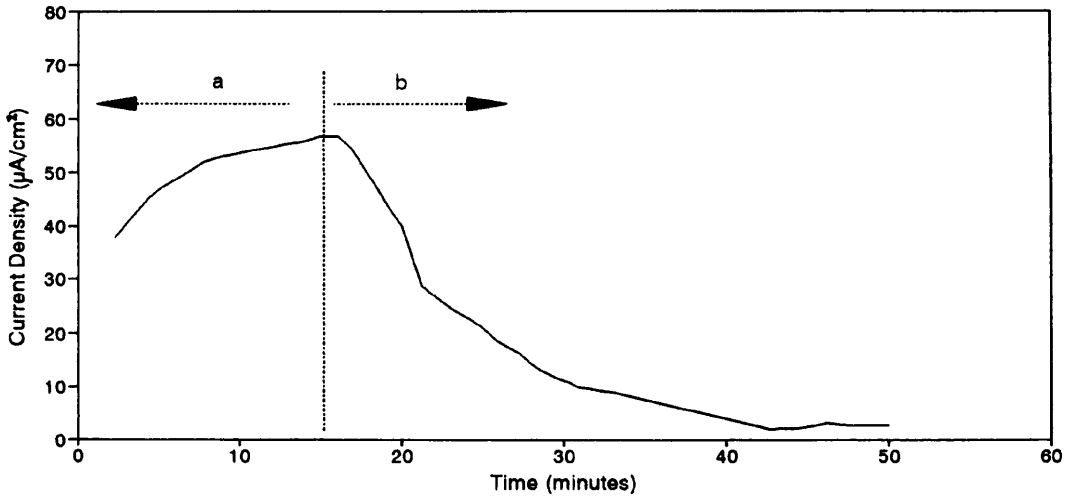

Figure 4-10 The relationship between the limiting cathodic current on iron covered with a 614 μm water film and the concentration of oxygen: (a) in laboratory air; (b) in nitrogen purged condition, at - 0.851 V(SCE).

when laboratory air was purged to the chamber.

4.2.2.3 The Cathodic Reduction Process During Evaporation of Electrolyte Layers

In the cathodic polarization experiments (the results shown in Figure 4-1 to Figure 4-6), the minimum thickness of electrolyte layers which can be applied to the surface of electrode without much difficulty by the present method is approximately 100 μm. This minimum thickness (100 μm) is still several times greater than that ($<$ 20 μm) in the practical situation (referred to the literature survey section of this thesis). Therefore, in order to investigate the cathodic reduction process of oxygen in thinner electrolyte films, e.g. $<$ 100 μm, experiments were undertaken to record the cathodic current when the electrolyte layer on the surface of the electrode was evaporated from wet up to dry conditions, while keeping the electrode at - 0.851 V (SCE).

Figure 4-12 and Figure 4-13 show the change of oxygen reduction current with the change of the thickness of the water layer covering the surface of iron and copper respectively. Evaporation of the water layer was achieved by heating the sample with a semiconductor heating pump (Peltier device). As the time of heating the sample increased, the water layer on the surface of the sample became thinner and the oxygen reduction current increased first. If the sample was heated for longer, the surface of the sample became dry and the oxygen reduction current declined sharply. This process may be explained in more detail as follows. In the wet condition, the sample is covered by a relatively thick water layer (e.g. thickness 800 μm in Figure 4-12 and 600 μm in Figure 4-13) and the oxygen reduction rate is controlled by the diffusion rate of oxygen through this water layer. However, due to the heating of the sample and the evaporation of the

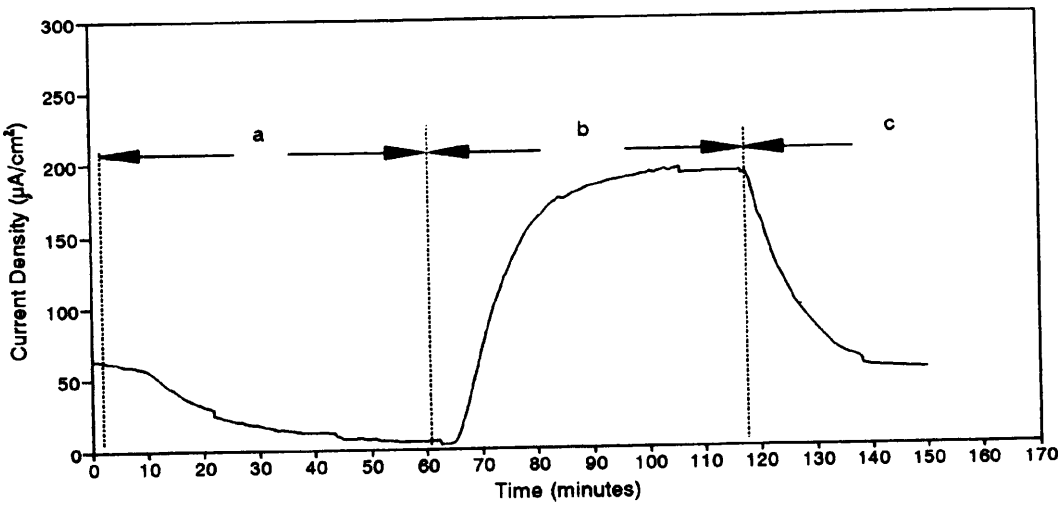

Figure 4-11 The limiting cathodic current on copper covered with a 800 μm water film as a function of oxygen concentrations: (a) nitrogen purged; (b) oxygen purged; (c) air-purged, at - 0.851 V (SCE).

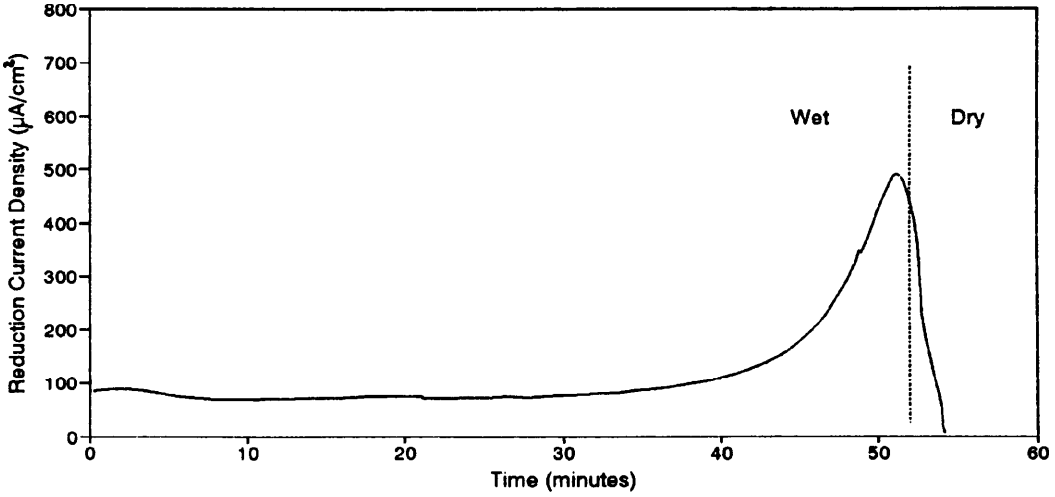

Figure 4-12 The change of oxygen reduction current with the change of the thickness of water layer indicated by the time spent to heat the iron sample (at - 0.851 V (SCE) with the initial water layer of 800 μm).

water layer on the sample, there is a strong convective action in the thin water film and the real diffusion layer in the water film is far less than that in the normal condition (i.e. without the heating and evaporation as in Figures 4-1 to 4-4). This can be justified by comparing the initial current densities (about 100 $\mu A/cm^2$ at 600 μm thickness in Figure 4-13 and about 90 $\mu A/cm^2$ at 800 μm thickness in Figure 4-12) with the current densities obtained in Figure 4-1 and Figure 4-3 respectively. Thus, in order to achieve these current densities, thicknesses of about 262 μm to 358 μm respectively, would be required. During the initial period of heating or evaporation of the water layers, the cathodic reduction current densities do not change significantly because the decrease of the total thickness of the water layer by evaporation does not change the real diffusion layer greatly in a relatively thick water film. A nearly constant current density is therefore observed during this initial period of evaporation. When the water layer becomes sufficiently thin that the total thickness of the water layer is nearly equal to that of the diffusion layer, the oxygen reduction rate increases with continued evaporation due to the decrease of the real diffusion layer and reaches a maximum value at a certain water layer thickness at a nearly dry condition. When the surface of the sample is dried further the oxygen reduction rate declines sharply because there is not enough electrolyte to maintain the proper electrochemical process for the reduction of oxygen. In these experiments, the most important information obtained concerns the maximum oxygen reduction current density which is about 560 $\mu A/cm^2$ on iron in Figure 4-12 and about 520 $\mu A/cm^2$ on copper in Figure 4-13.

4.2.2.4 The Change of Corrosion Potential During Nitrogen Purge

The change of corrosion potential of iron, copper and zinc covered with thin electrolyte layers during nitrogen purge is shown in Figures 4-14, 4-15 and 4-16 respectively. In all cases, the corrosion potentials show negative shifts with the decreasing oxygen concentration during nitrogen ventilation, although the magnitudes of negative shifts are different with different materials. The biggest shift occurs on the iron from about - 0.47 V to - 0.725 V (SCE) during the nitrogen purge. Three aspects may be considered for the explanation to this phenomenon.

First, the equilibrium potential of oxygen on all materials which can be described by the Nernst equation:

$$E = E^0 + \frac{RT}{nF}\ln\frac{[O_2]}{[OH]^4} \qquad (4\text{-}1)$$

will decrease with decreasing of oxygen partial pressure in the system. The decrease of the equilibrium potential of cathodic process will lead to the final decrease of the mixed potential, i.e. the corrosion potential, of the corrosion system. However, the decrease of corrosion potential caused in this way is unlikely to be great (14.75 mV reduction for each unit reduction of oxygen concentration). This explanation is likely to be suitable for the case of copper and zinc.

Secondly, for easily passivated materials like iron, the reduced oxygen concentration in the environment will transfer the material from the partial passive state which may be identified by a relatively positive corrosion potential to the active state which may be identified by a negative corrosion potential. The corrosion potential change of iron during nitrogen purge probably belongs to this category.

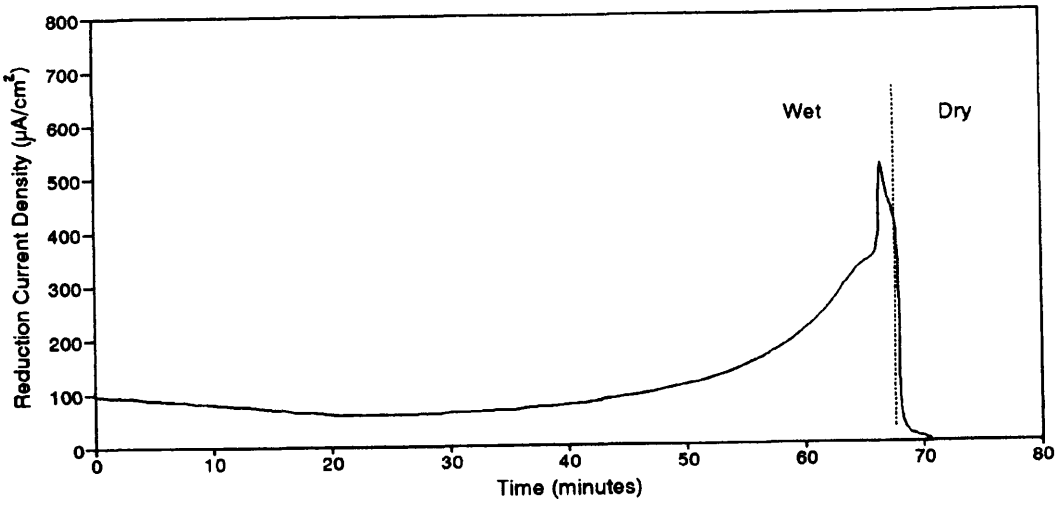

Figure 4-13 The change of oxygen reduction current with the change of the thickness of the water layer covering the surface of copper (at - 0.851 V (SCE) with the initial water layer of 600 μm).

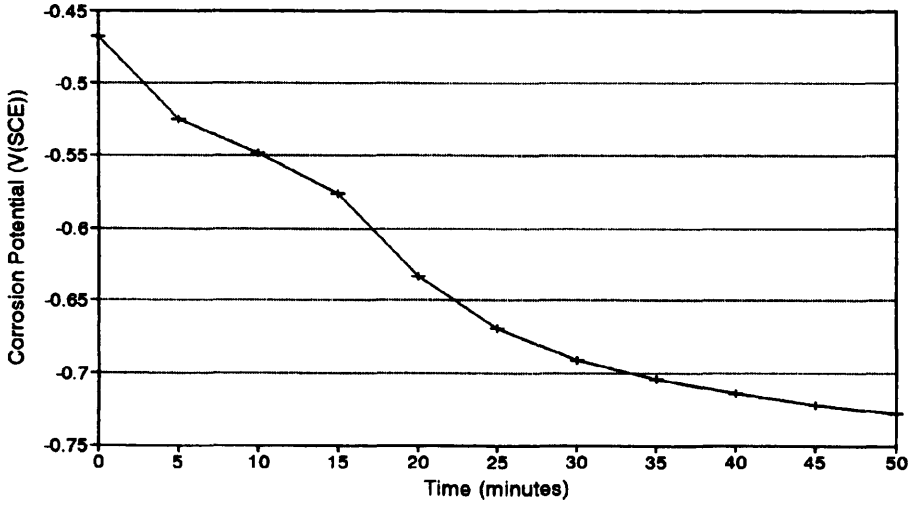

Figure 4-14 Changes in corrosion potential of iron during nitrogen-purged period (water layer: 550 μm).

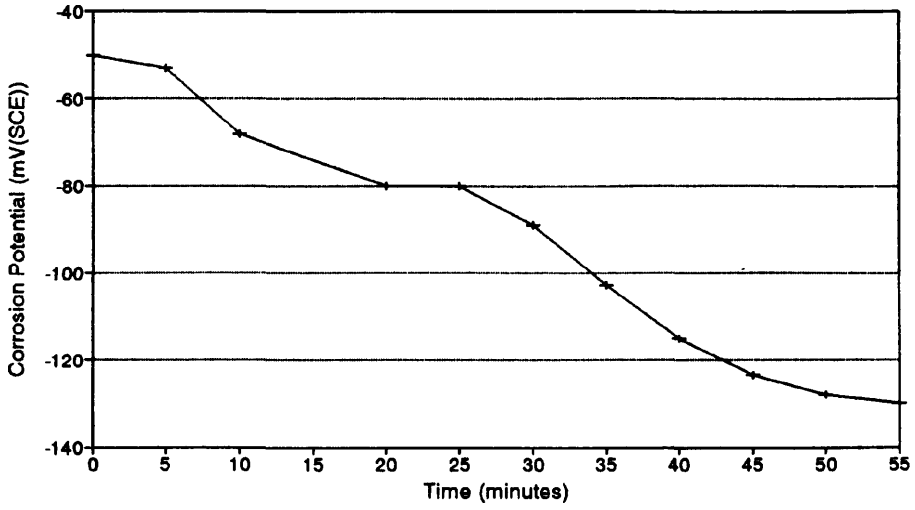

Figure 4-15 The change of corrosion potential of copper during nitrogen purged (water layer: 410 μm).

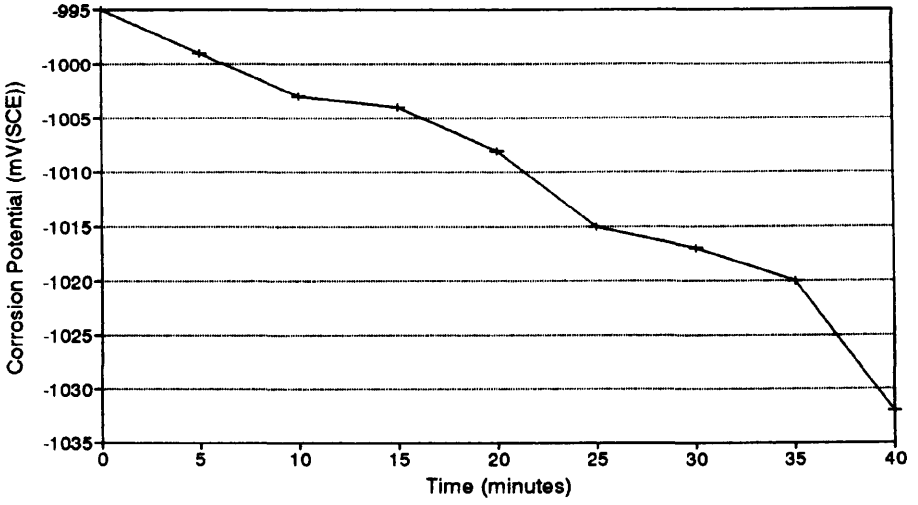

Figure 4-16 The change of zinc corrosion potential during nitrogen purge (water layer: 328 μm).

Finally, if the corrosion system is controlled by the cathodic diffusion process, the decrease in the oxygen concentration will decrease the oxygen reduction rate, thus, decreasing the corrosion potential to the negative.

4.2.3 Discussion

4.2.3.1 The Mechanism of Oxygen Transfer in Thin Electrolyte layers

Before examining the mechanism of oxygen transfer in thin electrolyte layers, it is appropriate to discuss the oxygen transfer in bulk solution for better understanding and comparison. Gaseous oxygen is dissolved in the electrolyte and generally the solubility of oxygen is dependent on the partial pressure of oxygen on the surface of electrolyte, the concentration of the electrolyte and the temperature. The oxygen solubility in water is about 2.645×10^{-7} mol cm^{-3}[129]. Oxygen is transferred to the electrode surface through a diffusion layer by a diffusion process, which is governed by Fick's law. For unagitated electrolytes with natural convection, the thickness of the diffusion layer is between 500 to 700 μm[13,131] quoted by Rosenfeld[5]. However, in the case of thin electrolyte layers, the oxygen in the air is transported through the electrolyte/gas phase boundary first, which may become rate-controlling step in extremely thin electrolytes. The literature data for this transport is about 10000 and 3000 $\mu A/cm^2$[132], quoted by M. Stratmann et al[120] and measured value of this limiting rate of the oxygen reduction is about 8000 $\mu A/cm^2$ obtained by M. Stratmann et al[120]. Oxygen then enters the thin electrolyte layer which is composed of a convective layer and a diffusion layer, suggested by Rosenfeld[5], although the total thickness of thin electrolyte layers is below the thickness of diffusion layer in bulk

solution as discussed above. The thickness of the diffusion layer in the thin film is dependent on the total thickness of the electrolyte. When the thickness of the thin electrolyte layer is decreased further, the thickness of the electrolyte is equal to the thickness of the diffusion layer, due to the adherent (viscosity) property of very thin electrolyte films. Rosenfeld[5] obtained a value of 30 μm for this process.

If the cathodic process is controlled only by the diffusion of the reactant to the surface, the cathodic current density is now inversely proportional to the thickness of the diffusion layer δ according to Fick's law:

$$i_{O_2} = 4FD_{O_2}\frac{C_{O_2}}{\delta} \tag{4-2}$$

By substituting the value of oxygen solubility in water (2.645×10^{-7} mol/cm^3)[129] and of the oxygen diffusion coefficient in water (2.10×10^{-5} cm^2/s)[133] into this equation, the following expression can be obtained,

$$i\delta = 21278.25 \tag{4-3}$$

where i is the limited diffusion current density (μA/cm^2) and δ the thickness of the diffusion layer (μm). From equation (4-3), the true diffusion layer in thin electrolyte layers can be obtained using the respective limiting diffusion current densities obtained in the experiment.

The dependence of the limiting diffusion current (at a potential of - 0.95 V(SCE)) on the reciprocal of total water layer thickness on the surface of iron and copper samples is shown in Figure 4-17 and Figure 4-18 respectively. The correspondent slopes of the lines, obtained by regression of the data in Figure 4-17 and Figure 4-18 are:

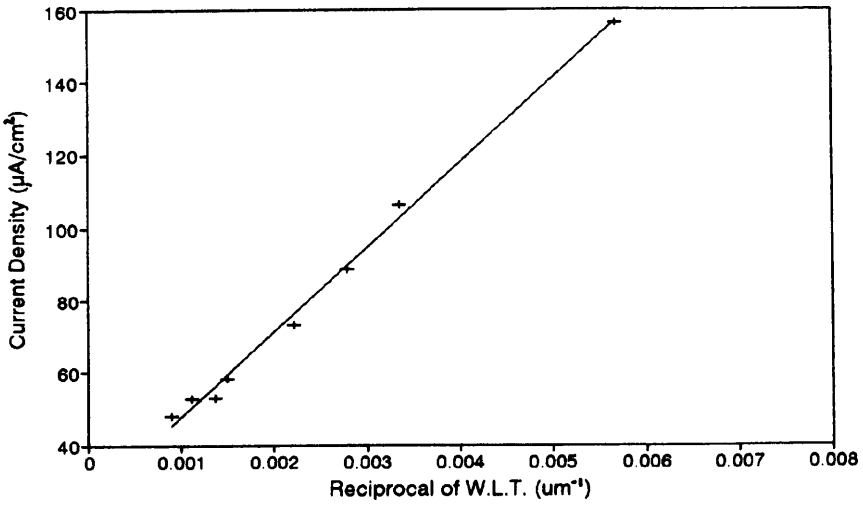

Figure 4-17 Dependence of the limited diffusion current (at - 0.95 V (SCE)) on the reciprocal of water layer thickness on the surface of the iron sample (slope = 23278.25).

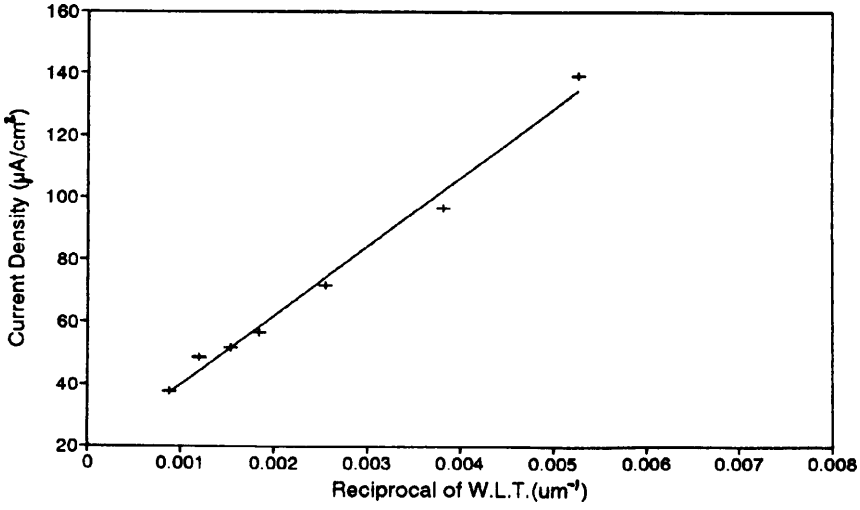

Figure 4-18 Dependence of the limited diffusion current (at - 0.95 V (SCE)) on the reciprocal of water layer thickness on the surface of the copper sample (slope = 22210.06).

$$i = 23278.25\frac{1}{\delta} + 24.43$$

and

$$i = 22210.06\frac{1}{\delta} + 17.69$$

respectively.

From equation (4-3), for a given limiting diffusion current density, a true value for the diffusion layer thickness can be determined. A comparison of the total thickness of the water layers with the calculated diffusion layer thicknesses is listed in table 4-1. From these data, it can be seen that although an excellent linear relation between the limiting diffusion current density and the reciprocal of the water layer thickness is observed, the slopes of the curves (23278.25 in Figure 4-17 and 22210.06 in Figure 4-18) are slightly larger than the theoretical value 21278.25 calculated above. In addition, the results in table 4-1 show that the thin water layers are still composed of two layers, the diffusion layer and the convection layer.

Now a quantitative comparison can be made between the present results and results reported in the literature. Thus, Rosenfeld[5] reported a limiting cathodic reduction current of 620 $\mu A/cm^2$ for the thickness of 30 μm, which is larger than the maximum (about 500 $\mu A/cm^2$) cathodic current obtained in this study during evaporation (Figure 4-12 and Figure 4-13). Stratmann et al[132] reported an even higher cathodic current density (about 2000 $\mu A/cm^2$ for 10 μm thickness at $P_{O2} = 0.2$ Bar), although a strong convection was induced by the vibrating Kelvin probe just above the electrolyte. However, these workers claimed that, for thicknesses < 100 μm, this convection no longer affects the thickness of the adherent diffusion layer and Fick's law can be directly applied in this situation.

Table 4-1 A comparison of the total thickness of electrolyte layers with the true thickness of the diffusion layers (from the results in Figure 4-17)

Total thickness of electrolyte layers $\delta 1$ (μm)	True thickness of diffusion layers $\delta 2$ (μm)	$\delta 1$-$\delta 2$
176	136.06	39.94
298	200.36	97.64
358	240.22	117.78
450	291.62	158.38
668	365.67	302.33
736	402.01	339.99
898	404.71	493.29
1118	443.58	674.44

Therefore, from this comparison, it may be argued that the current distribution may not be uniform on the surface of the electrode and the cathodic reaction may happen just on part of the surface area, instead of on the whole electrode surface area. This would make the current density, which was normalized by whole surface area of the sample, less than true value. In the next section, a smaller electrode (0.5 mm in diameter) was used to study the cathodic reduction process and to verify this argument.

4.2.3.2 Controlling Step in Atmospheric Corrosion

Rosenfeld[5], studying the corrosion behaviour of materials covered with thin film electrolytes, concluded that, under atmospheric conditions, corrosion proceeds basically with cathodic control when the metal surface is covered with a visible electrolyte film. Thus, oxygen diffusion in the thin electrolyte film is still the factor that determines the corrosion rate. When the thickness of the electrolyte film is reduced or dilute electrolytes used, the process was said to proceed with mixed anodic - cathodic control and not with anodic - ohmic control.

Mansfeld[134] suggested that when the electrolyte layer becomes thinner, the control of the mechanism of corrosion changes from diffusion to charge transfer with the value of the cathodic Tafel coefficient becoming lower, and the value of i_{corr} less than the diffusion limiting current.

Justo et al[63] proposed that the control of atmospheric corrosion processes takes place initially by oxygen diffusion through the electrolyte layer and thus by the cathodic reaction, but for longer drying times the control changes to the anodic process.

Barton[10] pointed out that atmospheric corrosion is in no way controlled by the cathodic oxygen reduction process, comparing the high limited current density of oxygen reduction in thin electrolyte layers and long - term corrosion rates of iron in atmospheric corrosion.

Indeed, by comparing the limited current density of oxygen reduction in thin electrolyte layers of 620 $\mu A/cm^2$ for a layer thickness of 30 μm (obtained by Rosenfeld) and the maximum current density ,560 $\mu A/cm^2$, of oxygen reduction on the surface of a fresh sample (shown in Figure 4-12) with corrosion rates found experimentally in long-term corrosion investigations, 0.02-0.1 g/m^2h (2-45 $\mu A/cm^2$)[34], it is clear that the cathodic

reduction current is sufficient to balance the current required to sustain the anodic process. From this point of view, it is impossible for corrosion processes to be significantly controlled by a slowing of the cathodic process, as stated by Barton[10].

However, by examining the recently reported results of Stratmann et al[119], it can be found that the corrosion rate, measured by oxygen consumption, is not constant and fluctuates with wet and dry conditions on the surface. The maximum corrosion rate they measured (about 1000 $\mu A/cm^2$) was observed during wet/dry transitions on the surface. This implies that, in certain conditions, a very high cathodic reaction rate (e.g. 1000 $\mu A/cm^2$) is needed to sustain the operation of the anodic process. On this basis, it is possible that in a few cases, atmospheric corrosion can be controlled by the cathodic process.

4.2.3.3 The Suitability of the Present Device for the Study of Thin Film Electrolyte Electrochemistry

On the basis of the results obtained and discussions made above, the device used in the present study is suitable and well able to study thin layer electrolyte electrochemistry. The experimental techniques can indicate the factors, associated with materials (Fe, Cu, Zn), the thickness of electrolyte layers, the concentration of oxygen, and evaporation. The main disadvantage of this device may concern the non-uniform current distribution, as discussed previously, caused by a relatively large electrode used. However, this can be improved using a smaller electrode and this later work will be studied and discussed in more detail in the next section.

4.2.4 Summary

1. Cathodic reduction processes on Fe and Cu, covered with thin electrolyte layers, mainly involve the reduction of oxygen. Under fairly strong cathodic polarization, the cathodic reduction of oxygen is controlled by the diffusion process of oxygen through a thin electrolyte film on the surface, which is sensitively affected by the concentration of oxygen and the thickness of electrolyte layers.

2. Under cathodic polarization, the cathodic reduction processes on zinc covered with thin layers of electrolyte are concerned with the reduction of zinc oxides, evolution of hydrogen and the reduction of oxygen. The first two effects tend to obscure any systematic trend of the cathodic current density as a function of electrolyte thickness.

3. The maximum cathodic current density of Fe (or Cu) covered with a thin electrolyte film during evaporation is about 560 $\mu A/cm^2$ for the 3 mm diameter sample.

4. By comparing the limiting diffusion current density and the long term corrosion rate of atmospheric corrosion for iron, it can be seen that it is impossible for atmospheric corrosion to be controlled by the cathodic reduction process. This viewpoint will be verified later using a smaller electrolyte sample.

5. Generally, the device used presently is successful and suitable for the study of thin film electrolyte electrochemistry, in respect of effects due to the kind of materials and the environmental factors including the thickness of electrolyte layers, the concentration of oxygen and the evaporation process.

6. Mechanisms of oxygen transfer in thin layer electrolyte, which may be composed of both convective action and diffusion process, will be justified and discussed in more detail in the following section.

4.3 More Detailed Study of Cathodic Reactions on Pure Iron Covered with Electrolyte Layers

4.3.1 Experimental

All experiments discussed in this sub-section were performed on the small electrode (0.5 mm diameter). The samples are either fresh polished pure iron (99.99 %, 0.5 mm diameter) or pre-corroded pure iron which was exposed in Manchester, outdoors, for about 4 months. The other procedures are the same as these described previously.

4.3.2 Experimental Results

4.3.2.1 The Cathodic Polarization Curves of Iron Covered with Thin Electrolyte Layers

The cathodic polarization curves for pure iron covered with relatively concentrated electrolyte layers (0.1 M Na_2SO_4, thickness from 39 μm to 1515 μm) in the normal condition (laboratory air) are shown in Figure 4-19.

Generally speaking, the shape of the cathodic polarization curves is similar to those (in Fig. 4-1) obtained on 3 mm diameter electrode and discussed previously. Except in the case of the thinnest electrolyte, e.g. 39 μm, a clear limiting diffusion current range in the cathodic polarization curves can be observed, indicating the existence of oxygen diffusion processes through the thin electrolyte film to the surface of the electrode. Again, the limiting diffusion current densities increase with decreasing electrolyte thickness, as

expected if cathodic reactions are controlled by the diffusion of oxygen in the electrolyte film. However, comparing the results of Figure 4-19 (smaller electrode and more concentrated electrolyte) with the results of Figure 4-1 (larger electrode and dilute electrolyte), several different points can be recognized. For instance, a smaller overpotential between the open-circuit potential and the potential when the diffusion characteristics begin to emerge is observed in Figure 4-19, which can be attributed to a reduction in IR drop due to smaller electrode and the more concentrated electrolyte. In addition, a larger limiting diffusion current density is found for a given electrolyte thickness, probably due to the more uniform current distribution on the smaller electrode. The magnitude of limiting diffusion current density in Figure 4-19 is approximately four times greater than that of the limiting diffusion current density in Figure 4-1. This may justify the proposition, as mentioned previously, that under the circumstances of thin electrolyte layers, it is quite difficult to obtain uniform current distribution on the surface of the electrode, even on 3 mm diameter electrode which can be considered to be fairly small from the viewpoint of bulk electrochemistry and was often used in previous thin electrolyte film electrochemistry research.

4.3.2.2 The Cathodic Reduction Process During Evaporation of Electrolyte Layers

Figure 4-20 shows the change in cathodic reduction current as a function of changing electrolyte thickness (10^{-4} M Na_2SO_4) represented by the heating time during evaporation on a pure iron surface.

Initially, the result is similar to that in Figure 4-12; thus, an initial cathodic current of about 200 $\mu A/cm^2$ is observed when the surface is covered with about 547 μm of

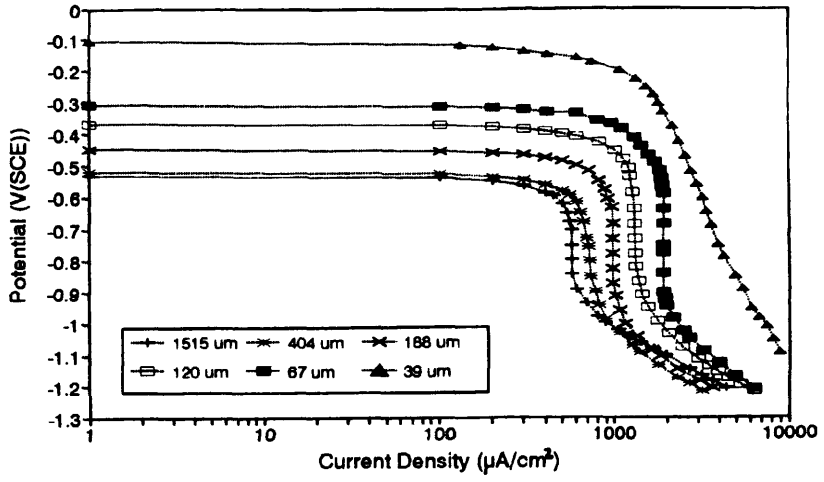

Figure 4-19 The cathodic polarization curves for pure iron (0.5 mm in diameter) covered with 0.1 M Na_2SO_4 layers (thickness from 39 μm to 1515 μm) in the normal condition (laboratory air).

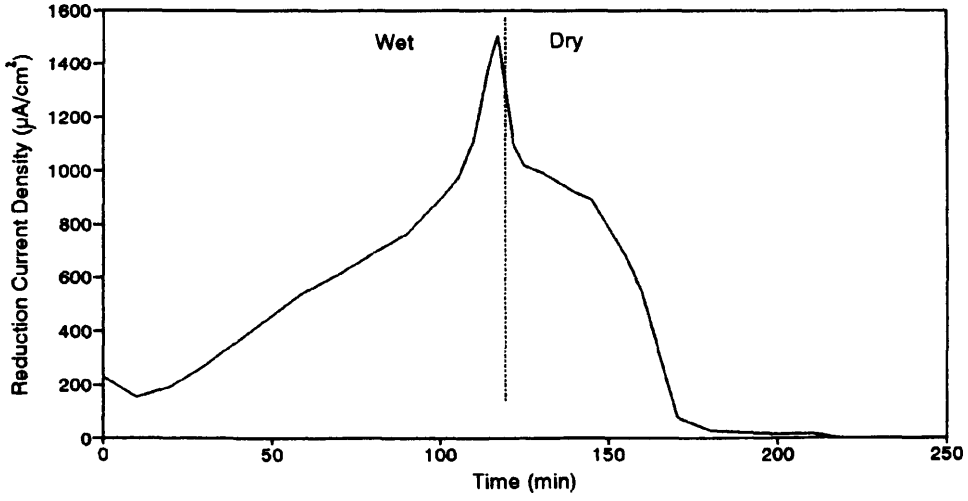

Figure 4-20 The change in cathodic reduction current (at - 0.85 V (SCE)) as a function of changing electrolyte thickness (10^{-4} M Na_2SO_4) represented by the heating time during evaporation on a pure iron surface (initial electrolyte thickness: 547 μm).

electrolyte. With the increase in heating time, the cathodic current increases gradually due to gradually reducing thickness of electrolyte. When the thickness of the electrolyte has decreased to a certain point (i.e. very thin but still can maintain the electrochemical process), a maximum cathodic current about 1500 $\mu A/cm^2$ was found. After this, the cathodic current declined sharply, probably because there is not enough electrolyte on the surface to sustain the electrochemical reduction reaction.

In comparing the present result with the result in Figure 4-12, there are several points worthy of consideration. The heating, in this case, was deliberately slower in order to give a slower evaporation rate of electrolyte. Thus, evaporation took about 250 minutes for complete drying of a 547 μm thick electrolyte layer in the present result while previously it took about 54 minutes for complete evaporation of an 800 μm thick electrolyte layer. In this way, a weaker convective action is expected. So the cathodic reduction current increased linearly with increase of heating time (decrease of electrolyte thickness) at the beginning of evaporation, instead of the constant reduction current observed earlier in the beginning of the evaporation due to the convective action caused by strong heating. This further indicates the sensitivity of the present experiment for the study of thin film electrolyte electrochemistry. On the other hand, a much larger maximum cathodic current about 1500 $\mu A/cm^2$ is found in Figure 4-20, about 3 times larger than that (about 560 $\mu A/cm^2$) in Figure 4-12. This is probably explained by the more uniform current distribution on the surface of smaller electrode used in this experiment. Figure 4-21 shows the result of a similar experiment to that in Figure 4-20, except that a 10 times more concentrated Na_2SO_4 solution (10^{-3} M Na_2SO_4) was used. In this case, the maximum cathodic current is increased further to about 1800 $\mu A/cm^2$, probably due to further improvement of current distribution on the surface of electrode in slightly more

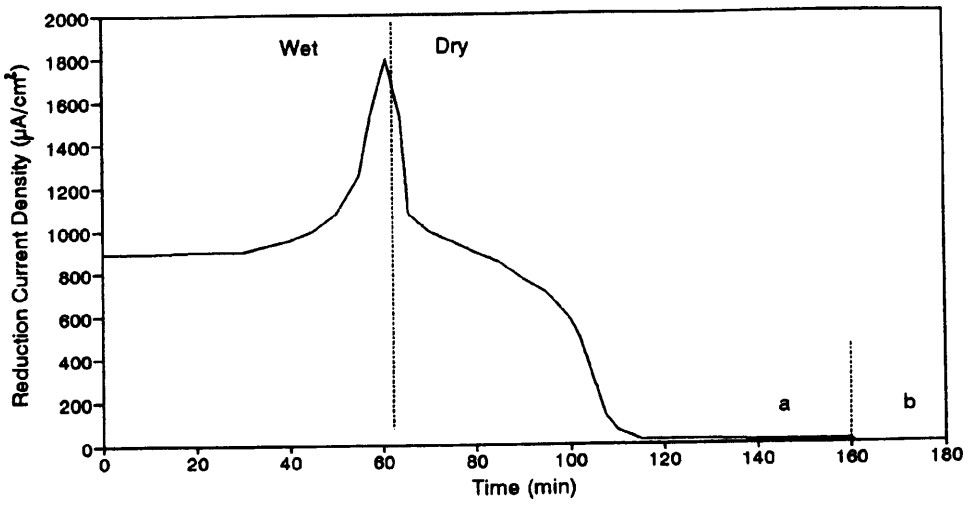

Figure 4-21 The change in cathodic reduction current (at - 0.85 V (SCE)) as a function of changing electrolyte thickness (10^{-3} M Na_2SO_4) represented by the heating time during evaporation on a pure iron surface at the different environmental humidity: (a) in the closed box at R.H. = 89 %; (b) in the open box at R.H. = 47 %, with initial electrolyte thickness: 313 μm.

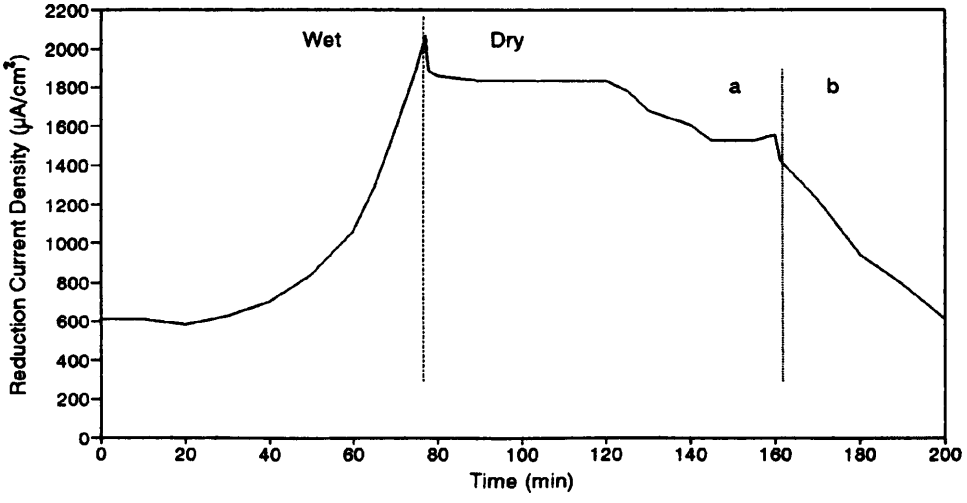

Figure 4-22 The change of cathodic reduction current (at - 0.85 V (SCE)) as a function of changing electrolyte thickness (10^{-1} M Na_2SO_4) represented by the heating time during evaporation on a pure iron surface at the different environmental humidity: (a) in the closed box at R.H. = 89 %; (b) in the open box at R.H. = 47 %, with initial electrolyte thickness: 433 μm.

concentrated solution.

With further increase of concentration of electrolyte to 0.1 M Na_2SO_4, the maximum cathodic current was increased to about 2070 $\mu m/cm^2$. However, an interesting phenomenon was also found, as shown in Figure 4-22. After the surface became nearly dry and the cathodic current passed a maximum value, instead of dropping to zero as observed before, the cathodic current was still at high value, i.e. 1850 $\mu A/cm^2$ as long as the relative humidity inside the experimental chamber was kept at 89 % (by saturated Na_2SO_4). However, when the relative humidity inside the chamber was reduced to 47 % (by opening the cover of the experimental chamber), the cathodic current began to decline with increase in heating time. At a relative humidity of 89 %, it is impossible to completely dry a saturated solution of Na_2SO_4, because the equilibrium relative humidity over the surface of a saturated Na_2SO_4 solution is about 89 %; and, in fact, crystalline Na_2SO_4 was observed on the surface of the sample at these conditions. This phenomena indicates the importance of the critical relative humidity in atmospheric corrosion, at which a very high cathodic current (1850 $\mu A/cm^2$) can still be sustained even in an apparently dry condition.

4.3.2.3 The Cathodic Reduction Process on Pre-corroded Iron During Evaporation of Electrolyte Layer

In this sub-section, the experiments were carried out on pre-corroded iron samples which were prepared by exposure outdoors in the Manchester environment for nearly four months. The purpose of this was to focus on a better understanding of the effect of corrosion products, particularly rust, on atmospheric corrosion, especially on its cathodic

reduction process, as proposed by Evans et al[78].

The typical result of change of cathodic reduction current density (at -0.900 V (SCE)) with decreasing thickness of dilute Na_2SO_4, expressed as the heating time during the evaporation process, is shown in Figure 4-23.

For clarity, a comparison can be made between the present result and the result of a similar experiment on bare iron (in Figure 4-20). There are several different features which can be observed in the present result. The initial cathodic current is about 3 times larger than that on the bare iron, e.g. 600 $\mu A/cm^2$ on the pre-corroded sample and about 220 $\mu A/cm^2$ on the bare iron sample, probably due to the effect of rust on the sample. It is likely that on the one hand, the comparatively larger surface area of rust on the sample could increase the reduction oxygen, if reduction of oxygen on rust is possible, and on the other hand, the rust itself may be reduced under these circumstances. The latter point may be verified by the fact that there are two cathodic current peaks in the graph, one in earlier stages where the electrolyte film is typically between 557 μm and 484 μm, and the other in the critical wet/dry condition. The first cathodic current peak may be attributed to the reduction of rust because, after this peak, the reduction current declines gradually with increasing time, indicating depletion of the reducible rust components during the reduction process, although the thickness of the electrolyte layer is also decreased during this period of time. The current peak occurring in the critical wet/dry condition is apparently caused by the reduction of oxygen, as discussed previously in the similar experiments on the bare pure iron samples. However, it is noted that a smaller oxygen reduction current peak (about 750 $\mu A/cm^2$) occurs during the wet/dry transition, instead of a larger current peak, as would be expected if a larger surface area of rust on the pre-corroded iron causes the initially increased current. This observation is probably related to the dust on the surface

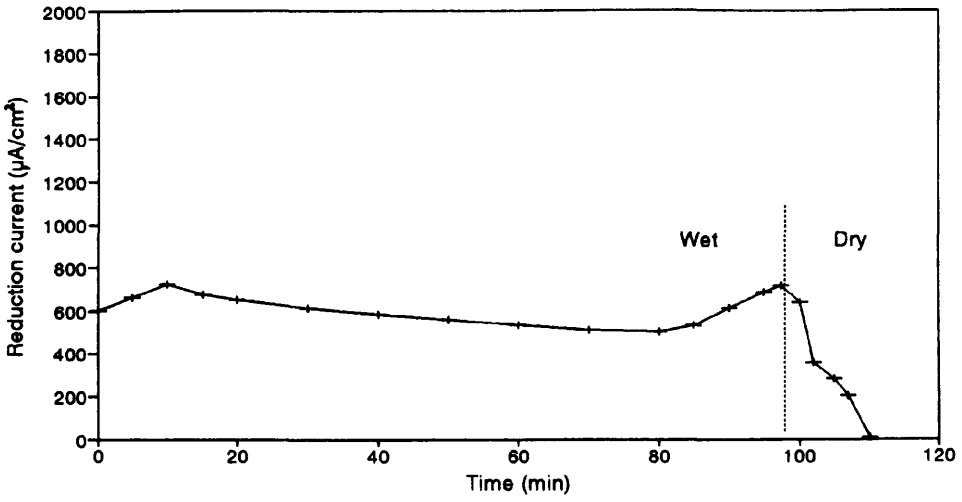

Figure 4-23 The change of cathodic reduction current (at - 0.900 V (SCE)) on the pre-corroded iron sample with decreasing thickness of dilute Na_2SO_4 (10^{-4} M), expressed as the heating time during the evaporation process, with the initial electrolyte thickness 557 μm.

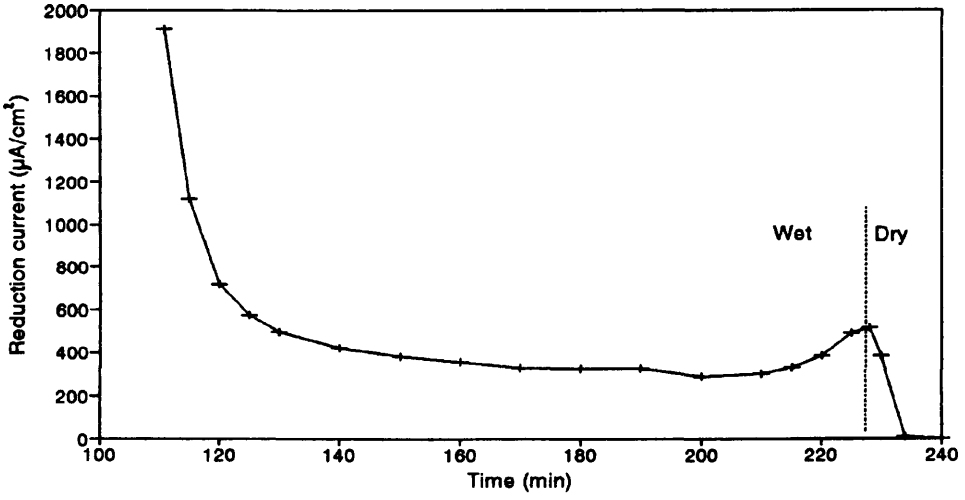

Figure 4-24 After final drying (in Figure 4-23), the sample was immediately re-wetted (to the electrolyte thickness of 787 μm) and a similar evaporation experiment carried out.

of pre-corroded sample after exposure. Although attempts were made to remove these dust particles before each experiment, a thin viscous film of dilute Na_2SO_4 solution and the remaining dust was found, even after a long evaporation time. At the moment just before the completely dry condition, this viscous film has already retarded the transfer of oxygen through this film to the surface of the electrode, making the cathodic reduction current at wet/dry transition on pre-corroded sample less than that on the bare iron sample.

After final drying above, the sample was immediately re-wetted and a similar evaporation experiment carried out. The result obtained is shown in Figure 4-24. An initial cathodic current surge up to about 1960 $\mu A/cm^2$ is observed, followed by a gradual decline in cathodic current. Finally, in the wet/dry transient condition, a cathodic current peak attributed to the reduction of oxygen as discussed previously is revealed.

There may be two reasons for the initial cathodic current surge observed in Figure 4-24. The first explanation seems to be that after the full evaporation of solution in the first experiment, the concentration of electrolyte in porous rust layer increases drastically. The residual reducible rust components could be reduced rapidly in relatively concentrated electrolyte during the following experiment. The second possibility is that, after the first experiment, the interfacial capacity of the electrode, which is related to the state of charge of the rust components, the concentration of electrolyte etc, may be increased. This will introduce the current surge observed in the initial instant of the second experiment. Although it is difficult to provide an exact description to this initial current surge, the one point can be confirmed that the rust components have an effect on the cathodic reduction processes of iron under the thin film electrolyte condition.

In order to identify whether the reduced rust components can be re-oxidized by oxygen in air, the same sample with reduced rust (produced as above) was washed with deionized

water, dried with a cold air stream, and then put in the laboratory air for one day. After these procedures, a further experiment was carried out on this sample, with the result shown in Figure 4-25. In this case two current peaks in the graph are evident, one occurring at electrolyte thickness between 415 μm and 385 μm and the other in the wet/dry transient condition. The latter peak, with approximately the same magnitude as the one observed in Figure 4-23, is apparently ascribed to the reduction of oxygen. The former one with a larger magnitude (the maximum value being about 1080 $\mu A/cm^2$) is probably due to the reduction of re-oxidized rust components. So far, two aspects have been confirmed by these experiments: the reduced rust components in previous experiments can be re-oxidized by oxygen in air, and the re-oxidized rust components in this way are very active and can be further reduced easily (indicated by a larger cathodic current peak in Figure 4-25). The same sample was used again for a repeated experiment, in which electrolyte was dropped on the sample immediately after final drying. The corresponding result is shown in Figure 4-26. As expected, this shows a similar phenomena to Figure 4-24 because very similar conditions were encountered in these two experiments. Therefore, the explanation to this result can be referred to that of Figure 4-24.

In order to identify the effect of rust on the cathodic reduction process of iron in more practical conditions, similar experiments were carried out at electrode potentials of - 0.600 V and - 0.550 V (SCE) respectively on the pre-corroded iron sample. These potentials are closer to the practical conditions of atmospheric corrosion. The variations in cathodic reduction current with evaporating time on the pre-corroded iron sample (washed with deionized water, dried with cold air stream, and placed in the laboratory air for two days after each previous experiment) are shown in Figure 4-27 (at potential -0.600 V (SCE) and

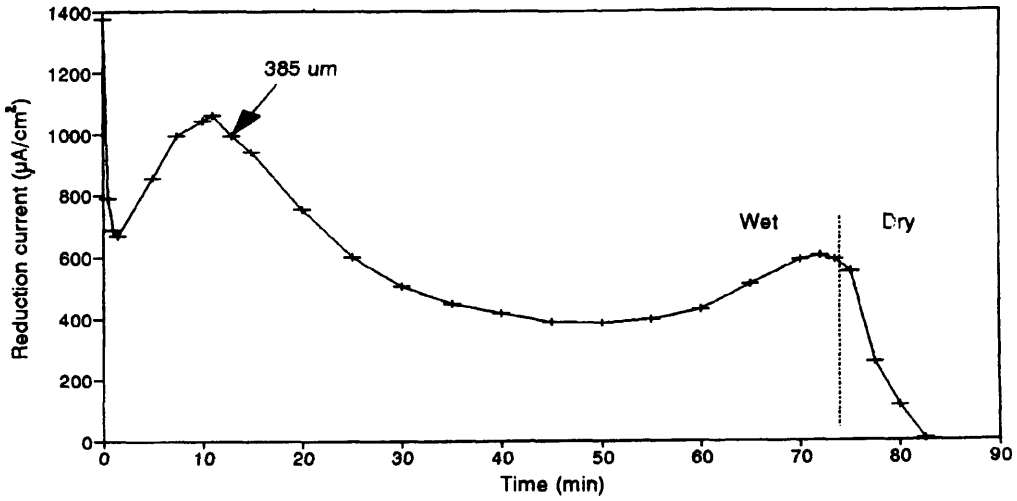

Figure 4-25 After finishing the experiment in Figure 2-24, the same sample with reduced rust was washed with deionized water, dried with a cold air stream, and then put in the laboratory air for one day. After these procedures, a further experiment (as in Figure 2-24) was carried out.

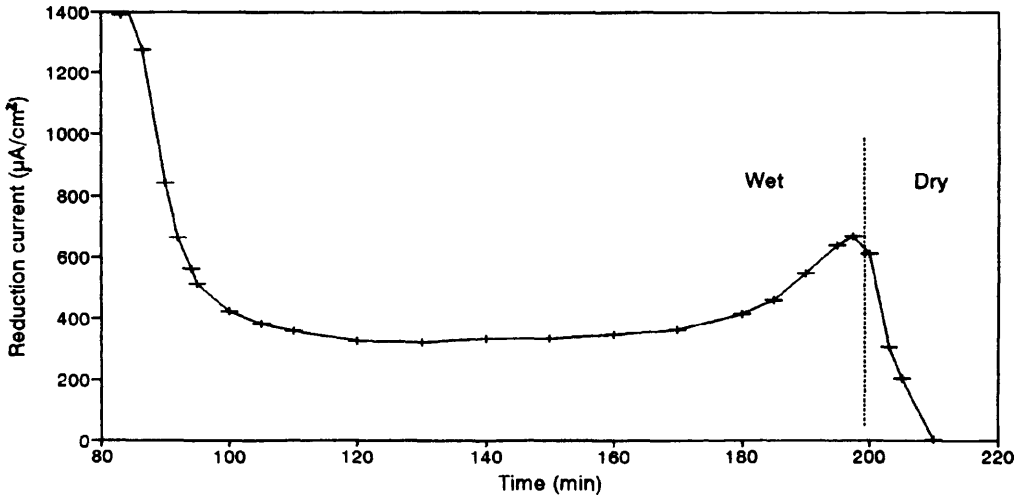

Figure 4-26 The same sample (as in Figure 4-25) was used again for a repeated experiment, in which electrolyte was dropped on the sample (to the thickness of 628 μm) immediately after final drying.

Figure 4-28 (at potential -0.550 V (SCE) respectively. For comparison, the results of similar experiments on bare iron samples are also shown in Figure 4-29 (at potential -0.600 V (SCE)) and Figure 4-30 (at potential -0.550 V (SCE)) respectively. For the pre-corroded sample, a cathodic reduction current peak at the wet/dry transition can still be observed. The relatively smaller magnitude of this peak may indicate that here, this cathodic process could be controlled by mixed electrochemical activation and diffusion processes. However, on the bare iron no cathodic current peak is observed on the graphs, probably due to the fact that the cathodic process at these potentials is controlled by the electrochemical activation, which is not affected by the diffusion process of oxygen (or the change of thickness of electrolyte layer). Therefore, it may be inferred from these observations that the electrochemical activity of oxygen on the surface of rust could be higher than on the surface of iron. In other word, the electrochemical overpotential of oxygen on the surface of rust is smaller than that on the surface of iron.

For the reduction of rust components themselves, no current peak relative to this reaction is observed. This is probably because that in the circumstance, the applied overpotential is not big enough to cause the emergence of the current peak which is normally produced by the slowing of diffusion process of reactants when the applied electrode potential (i.e. applied overpotential) is enough to overcome the electrochemical activation. However, the involvement of rust reduction in the reduction process may be identified by the bigger average cathodic current in Figure 4-27 and 4-28 compared with these in Figure 4-29 and 4-30, or by initial current surge shown in the Figure 4-27 and 4-28 respectively.

Finally, it may be worthy to mention that the cathodic reactions observed in Figure 4-27 and Figure 4-28 when the electrode potential was kept at -0.600 V (SCE) and -0.550

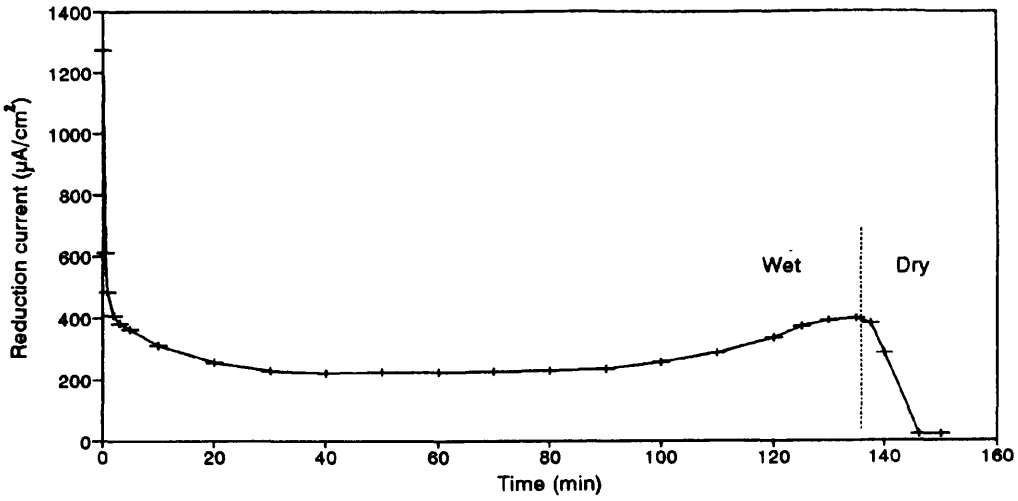

Figure 4-27 The variation in cathodic reduction current (at - 0.600 V (SCE)) with evaporating time on the pre-corroded sample (initial electrolyte thickness:686 μm).

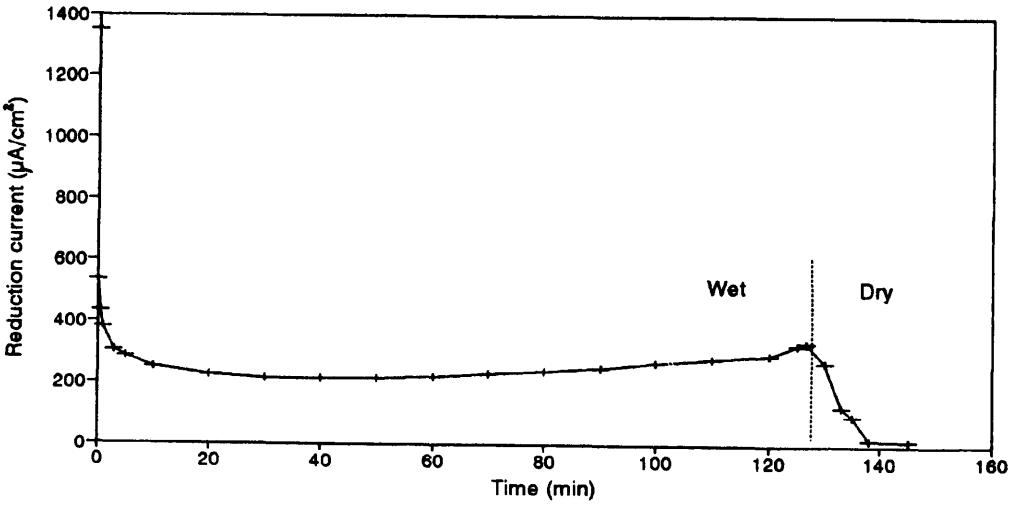

Figure 4-28 The variation in cathodic reduction current (at - 0.550 V (SCE)) with evaporating time on the pre-corroded sample (initial electrolyte thickness: 638 μm).

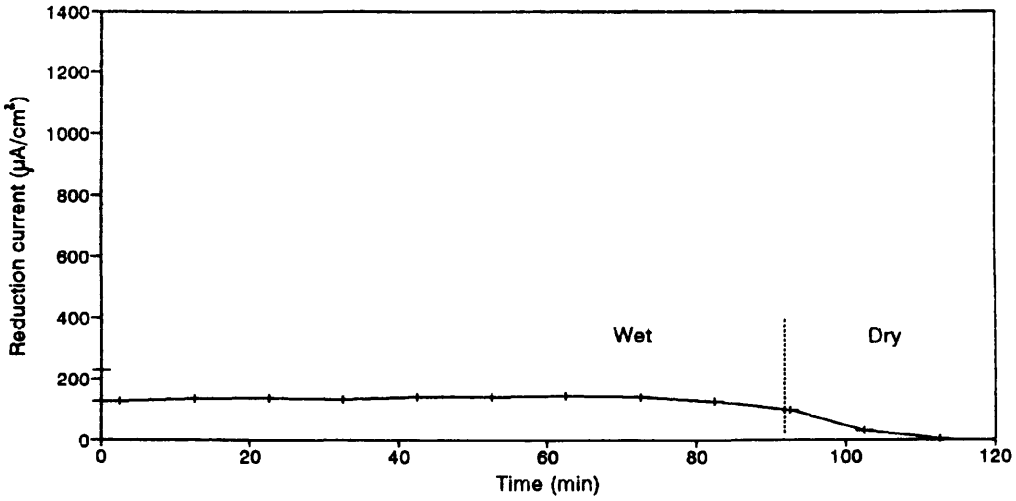

Figure 4-29 The variation in cathodic reduction current (at - 0.600 V (SCE)) with evaporating time on the bare iron (initial electrolyte thickness: 554 μm).

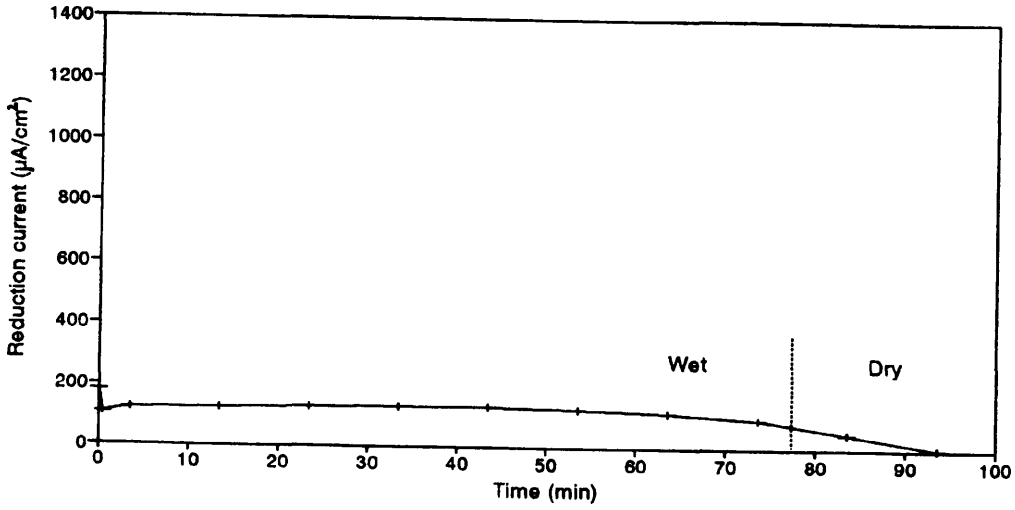

Figure 4-30 The variation in cathodic reduction current (at - 0.550 V (SCE)) with evaporating time on the bare iron (initial electrolyte thickness: 396 μm).

V (SCE) may occur on the interface of electrolyte/rust, instead of on the interface of electrolyte/pure iron. In normal condition (bulk aqueous electrolyte), the corrosion potential of iron with no passive oxide film on the surface would be about -0.600 - -0.700 V (SCE). Therefore, at the electrode potential of -0.550 and -0.600 V (SCE), which is positive to the corrosion potential -0.600 - -0.700 V (SCE) of pure iron, anodic current should be obtained if reactions indeed occur on the surface of the pure iron. However, if reactions occur on the interface of electrolyte/rust, when the electrode was kept at -0.600 V (SCE) and -0.550 V (SCE), cathodic current could still be obtained because the electrode potential is still negative to the open potential of electrolyte/rust system. This explanation is also suited to that of pure iron with an air-formed oxide film, especially in thin film electrolytes where supplies of oxygen is more favoured than that in bulk electrolyte. Once cathodic reaction occurs on the surface of oxides, the more alkaline condition produced by this reaction will further stabilize the existence of oxides, which sustains the continuation of the reaction.

4.3.3 Discussion

4.3.3.1 The Mechanism of Oxygen Transfer in Thin Electrolyte Layers

After the significant improvement of current distribution which was made in the experiments of this section, using a smaller electrode and more concentrated electrolyte, a more specific and more clear description about the mechanism of oxygen transfer in thin electrolyte layers can be made, which makes it possible to better understand the cathodic reduction process of oxygen on the metal surface covered with thin electrolyte film.

From the cathodic polarization curves on iron covered with various thicknesses of electrolyte layers (shown in Figure 4-19), the dependence of limiting diffusion current on the reciprocal of electrolyte layer thickness can be obtained and this is shown in Figure 4-31. There are two important points which can be observed in this graph: one is that a linear relationship between the limiting diffusion current and the reciprocal of thickness of electrolyte layers is revealed, and other is that the slope of the curve is 95713.54, over four times greater than that (21278.25) estimated by the theoretical calculation shown in equation (4-3).

On the basis of the result obtained in this sub-section, the cathodic reduction of oxygen under the thin electrolyte film condition can be described in more detail. In the first place, gaseous oxygen in air enters through air/electrolyte interface and is dissolved in the thin electrolyte. Then, oxygen transfers to the electrode surface through a diffusion layer by a diffusion mechanism. Generally, the mechanism of oxygen transfer in thin electrolyte films is not much different from that in bulk solution, except that the thickness of the diffusion layer in this case is much less than that in bulk solution and dependent on the total thickness of the electrolyte layers. The relationship between the true diffusion layer and the total thickness of electrolyte layer is shown in Figure 4-32. The true diffusion layer thickness is calculated by equation (4-3), using the limiting diffusion current obtained in the experiment (Figure 4-19). From this graph, it can be seen that even in a very thin electrolyte layer, e.g. 67 μm, a large part of the electrolyte within the thin film is still in the convective state, increasing the oxygen transfer significantly.

The convective action in thin electrolyte layers may come from many sources. It may concern the existence of variable surface tension, either due to the non-uniformity of evaporation or to the variation in the temperature and concentration of the electrolyte in

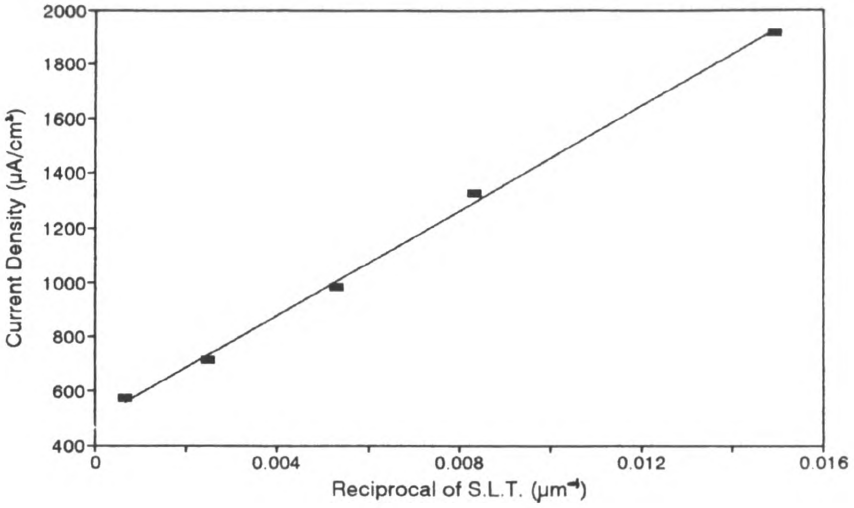

Figure 4-31 The dependence of limiting diffusion current on the reciprocal of electrolyte layer thickness (electrolyte: 0.1 M Na_2SO_4. material: iron. slope: 95713.54).

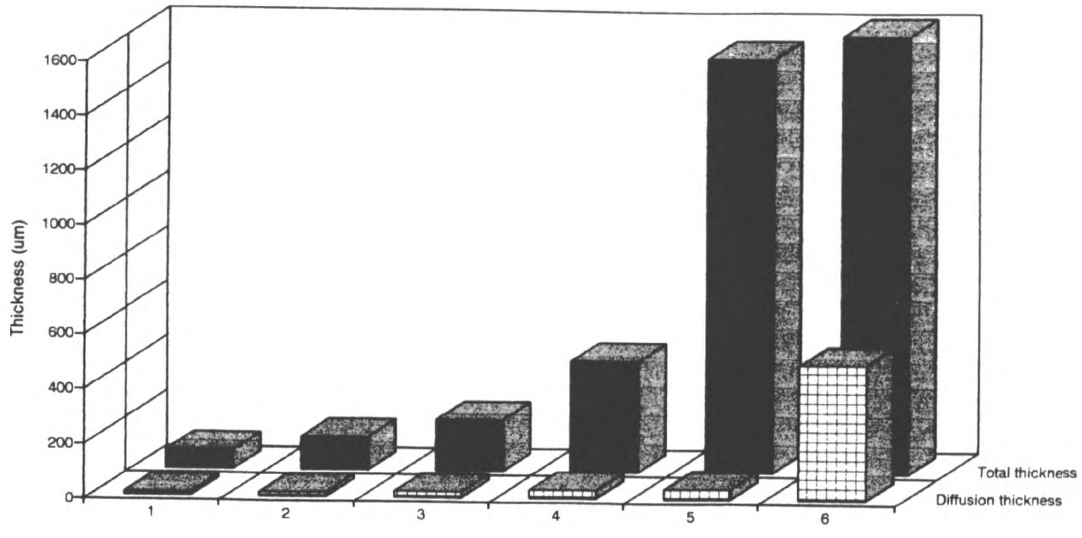

Figure 4-32 The relationship between the true diffusion layer and the total thickness of electrolyte layer. The total thickness is respectively: (1) 67 μm; (2) 120 μm; (3) 188 μm; (4) 404 μm; (5) 1515 μm; (6) bulk solution.

different parts of the electrolyte, as suggested by Rosenfeld[5]. On the other hand, it was found during experiments that it was impossible to keep the experimental device absolutely still because of small external vibration. Finally, the contribution of parallel diffusion from the edge of the electrode should also be taken into account because of the smaller electrode used. This last question will be discussed in the next sub-section.

4.3.3.2 The Controlling Step in Atmospheric Corrosion

As discussed previously in section 4.2.3.2, atmospheric corrosion may be controlled by the cathodic reduction process, e.g. the diffusion of oxygen through thin electrolyte films if the maximum cathodic reduction currents are about 620 $\mu A/cm^2$ obtained by Rosenfeld (and 560 $\mu A/cm^2$ obtained in this work using a 3 mm diameter electrode), because the maximum corrosion rate in atmospheric corrosion can reach over 1000 $\mu A/cm^2$ under some circumstances, as reported by Stratmann[119]. However, under more uniform current distribution using a smaller 0.5 mm diameter electrode, the maximum cathodic current densities have reached about 1500 $\mu A/cm^2$ in 10^{-4} M Na_2SO_4 (Figure 4-20), 1800 $\mu A/cm^2$ in 10^{-3} M Na_2SO_4 (Figure 4-21) and 2070 $\mu m/cm^2$ in 10^{-1} M Na_2SO_4 (Figure 4-22) respectively. This means that at all cases, the cathodic current density is large enough to balance the anodic current density occurring in atmospheric corrosion. This data strongly suggest that atmospheric corrosion is not controlled by the slowing of the cathodic reduction process.

4.3.3.3 The Effect of the Electrode Size and the Concentration of Electrolyte

There are two ways in which the smaller electrode size can affect the cathodic current measurements. First, the reduced size of the electrode can improve the uniformity of the current distribution on the sample of the electrode. Secondly, the smaller size of electrode may change the diffusion of reactant within the thin electrolyte film. In both cases, the net effect is to increase the cathodic reduction current measured.

Comparing the result in Figure 4-12, obtained using a 3 mm diameter electrode, with the results in Figure 4-20, attained using a 0.5 mm diameter electrode, the maximum cathodic current density (using a smaller electrode)in Figure 4-20 is about 3 times larger. It can probably be suggested that in a thin electrolyte film, the current distribution may be limited to a small area on the surface of a larger electrode. Thus, if the cathodic current density was normalized by the whole area of the electrode, the current density is less than its true value. Therefore, the results obtained on the smaller electrode may be more convincing.

On the other hand, one of the consequences arising from the reduction in size of an electrode concerns the increased mass transport rates to and from the electrode because of nonplanar (spherical) diffusion. For micro-disks under extreme polarization in steady state, Saito[135] has calculated the steady state diffusion current, using a discontinuous integral of Bessel functions. This diffusion current, quoted by B. R. Scharifker[136], is

$$I_d = 4nFDC^{\infty}a \tag{4-4}$$

where a is the radius of the micro disk. The correspondent diffusion current density is

$$i_d = \frac{4nFDC^{\infty}}{\pi a} \tag{4-5}$$

Comparing this diffusion current i_d in equation 4-5, obtained by taking into account the effect of edge diffusion, with the Fick's diffusion current i_d' in equation (4-2), we obtain

$$\frac{i_d}{i_d'} = \frac{4\delta}{\pi a} \tag{4-6}$$

It is clear that the contribution of edge diffusion is not significant unless the radius of electrode is far less than the thickness of diffusion layer. In this experiment, the radius of the electrode is 500 μm, comparable to the thickness of diffusion layer. Therefore, the nonplanar diffusion current is insignificant.

With regard to the effect of the concentration of electrolyte on the measurements, two possibilities may be considered. On the one hand, the change of concentration of electrolyte will alter the structure of the double layer of the electrode, which will affect the kinetics of the electrode reaction. However, theoretically this variation in the double layer structure has no effect on the mass transfer process, e.g. oxygen diffusion. From this viewpoint, the effect of change in the concentration of electrolytes on the limiting cathodic reduction current can be ignored in this experiment. On the other hand, it is more likely in this experiment that more concentrated electrolyte may improve the spread of the current, increasing the effective area of reactions on the surface of the electrode. This supposition may be verified by the results in Figure 4-20, 4-21 and 4-22 respectively. The maximum cathodic current densities during evaporation are increased with increasing concentration of electrolyte. From this standpoint, the 0.5 mm diameter electrode used in this investigation is still not small enough to completely eliminate the effect of nonuniform current distribution.

4.3.3.4 The Effect of Rust on Atmospheric Corrosion

Evans[78] has emphasized the important role of rust components in atmospheric corrosion. He proposed that the rust components produced during atmospheric corrosion may take part in the cathodic reduction reactions when the surface of metal was covered with a relatively thicker electrolyte film, where the transfer of oxygen to the metal surface was retarded. The reduced rust components could be re-oxidized by oxygen during dry conditions. Therefore, the redox couple of rust components could sustain the continuation of these reactions under alternating dry/wet conditions.

In this investigation, at least two points which concern the mechanism proposed by Evans[78] have been experimentally identified. One is that the reduction of rust components on iron covered with a thin film of electrolyte is possible, which has been verified by a cathodic reduction current peak occurring under the thin film electrolyte condition. The other is that the reduced rust components can be re-oxidized by oxygen in air and the obtained re-oxidized rust components are very active in terms of their reducibility. In addition, the rust layer formed on iron may be considered as an electrically conductive layer, on which cathodic reduction of oxygen can occur with a smaller electrochemical overpotential than on the surface of pure iron.

However, with regard to the effect of rust on atmospheric corrosion, many questions are still open to be answered. On the one hand, the reduction of rust components in a relatively thick electrolyte film enhances the validity of the view point that atmospheric corrosion is by no means controlled by oxygen diffusion because the reduction of rust components increases the total cathodic current, especially in the case of thick electrolyte films. On the other hand, if the cathodic current produced by the reduction of oxygen is

already big enough to sustain the anodic processes of atmospheric corrosion, the reduction of rust components in cathodic processes should have no significant effect on the whole process of atmospheric corrosion, just in respect of the magnitude of the cathodic current. Of course, the effect of rust on atmospheric corrosion is more complicated than expected, if the factors, in relation to the change of conductivity in the matrix of rust layer, the change of critical humidity, and the change of protective properties of rust, which were caused by the reduction of rust components, are also taken into account.

4.3.4 Summary

1. The thin electrolyte film is composed of the convective and the diffusive parts. The convective layer occupies the major part of the film. Although the thickness of electrolyte layers is smaller than that of the diffusion layer of the bulk electrolyte, the transfer of oxygen through a thin electrolyte layer is significantly enhanced by the convective action occurring in the thin electrolyte film.

2. The maximum cathodic reduction current of oxygen on iron (diameter 0.5 mm) covered with 0.1 M Na_2SO_4 electrolyte layer during evaporation can reach up to 2070 $\mu A.cm^{-2}$.

3. The reduction of rust components is possible on the surface of pre-corroded iron covered with a thin film of electrolyte. The reduced rust components can be re-oxidized by oxygen in air when the surface of pre-corroded sample is dry.

4. It is impossible to atmospheric corrosion to be controlled by the slowing of cathodic processes.

5. The smaller electrode (0.5 mm diameter) is more suitable for the study of thin film

electrolyte electrochemistry in terms of the uniformity of current distribution on the surface of the electrode.

CHAPTER 5
ANODIC PROCESSES ON IRON COVERED BY THIN ELECTROLYTE LAYERS

CHAPTER 5 ANODIC PROCESSES ON IRON COVERED BY THIN ELECTROLYTE LAYERS

5.1 Introduction

In the previous chapter, the cathodic process on materials (iron, copper and zinc) covered by thin electrolyte layers (thickness from 100 to 1132 μm) was discussed in detail based on the cathodic polarization curves and the oxygen reduction current-time (change in water thickness) relationship during evaporation. In relation to the maximum limiting oxygen reduction current (2070 $\mu A/cm^2$) obtained in this investigation and the maximum anodic current (about 1000 $\mu A/cm^2$) which may occur during wet/dry transitions, attained in the research work by Stratmann et al[119], the cathodic reduction current is enough to balance the current required to sustain the anodic process. From this point of view, it is impossible for atmospheric corrosion processes to be significantly controlled by slowing of the cathodic process. Therefore, it is reasonable to assume that anodic processes in atmospheric corrosion may play a critical role in controlling the whole corrosion rate.

This work initially considers the anodic process of pure iron covered by various thicknesses of dilute electrolyte (10^{-4} and 10^{-3} M Na_2SO_4). The emphasis will be focused on the effects of the thickness of the electrolyte layers, which always changes in practice according to the weather condition, and the concentration of SO_4^{2-} in the electrolyte layers, the product formed after the SO_2 adsorption, on the anodic mechanism on iron. The anodic process on pure iron was studied by thin layer electrolyte electrochemical techniques including anodic polarization measurements on a thin film electrolyte electrochemical cell. The corrosion potential-time curves during wet/dry periods are also presented.

Secondly, the anodic process on pure iron covered by more concentrated electrolyte layers (0.1 M Na_2SO_4), which is considered to be encountered occasionally in atmospheric conditions, was investigated using anodic polarization measurement techniques.

Finally, anodic polarization measurements in 0.1 M Na_2SO_4 electrolyte layers are made on a pure iron surface, on which a small amount of copper has already been deposited from dilute $CuSO_4$ solution before the measurements. This work intends to show insight into the mechanisms of copper-enhanced corrosion resistive properties of weathering steels, which have not yet been understood although this phenomenon has already been found in practice for many years.

5.2 Anodic Processes on Iron Covered by Thin, Dilute Electrolyte Layers

5.2.1 Experimental

A three electrode electrochemical system with a small pure iron working electrode (0.5 mm diameter) was used to study the anodic polarization behaviours and the corrosion potential-time relation of iron covered by the dilute electrolyte layers (10^{-4} to 10^{-3} M Na_2SO_4).

5.2.2 Experimental Results

5.2.2.1 Anodic Polarization Curves

Anodic polarization curves measured on pure iron surfaces covered by various

thicknesses of electrolyte layers (thickness from 50 μm to bulk solution, 10^{-3} M Na_2SO_4) are shown in Figure 5-1. Generally speaking, the anodic polarization increases with decreasing thickness of electrolytes. This is especially noticeable in the case of 50 μm thickness of electrolyte. Unlike normal anodic polarization curves without passivation, these curves show characteristics of both partial passivation and pitting. When the polarization potential is more negative than -0.2 V (SCE), the curves reveal a passivation tendency with nearly vertical lines on the potential-current curves. This is not an instrumental limitation of the potentiostat (e.g. voltage limited) as current densities up to 10^5 μA cm^{-2} were measurable. At potentials more noble than -0.2 V (SCE), the current densities increase fairly rapidly, indicating that the passivation begins to break down and pitting occurs. Optical microscopy examinations verified the above explanations. Thus, in all experiments, pits were visible after the tests.

Figure 5-2 shows the anodic polarization measurements obtained on the surfaces of pure iron in 10^{-4} M Na_2SO_4 with the electrolyte thickness ranging from 100 μm to bulk solution. In bulk solution, a similar anodic polarization curve to that described previously (for 10^{-3} M Na_2SO_4) was observed, resulting in the pitting. When the thickness of electrolyte layer is 1160 μm, the competing processes between pitting and passivation are displayed more clearly in that when the potential is less noble than 0 V (SCE), some passivation happens with current density about 12 $\mu A/cm^2$, however for a potential more noble than 0 V (SCE), this passivation begins to break down and pitting occurs. When the thickness decreases to 941 μm, the anodic polarization curve displays a typical passivation characteristic, with the current peak, i.e. the critical current density of passivation (i_{cc}) in this case being about 500 $\mu A/cm^2$ and a passivated current density about 18 $\mu A/cm^2$. With the thickness decreasing further to 600 μm, the critical current density of passivation

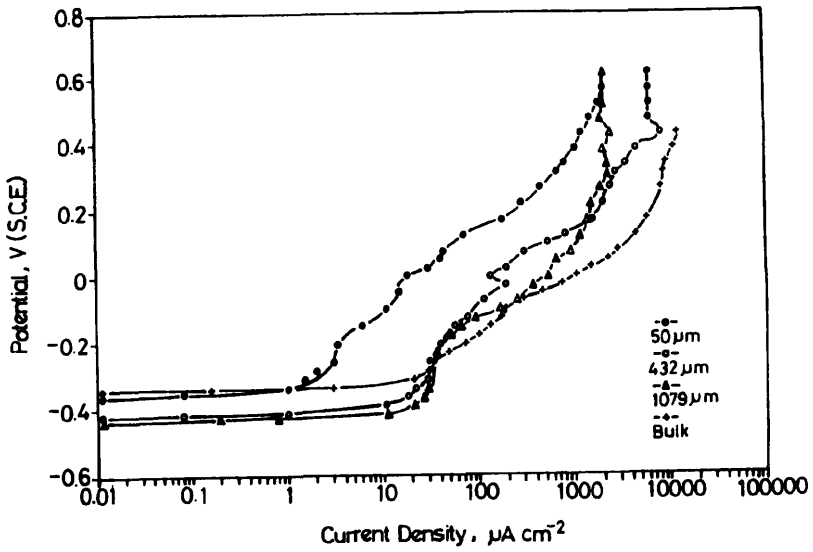

Figure 5-1 Anodic polarization curves for pure iron covered by various thicknesses of electrolyte layers (thickness from 50 μm to bulk solution, 10^{-3} M Na_2SO_4).

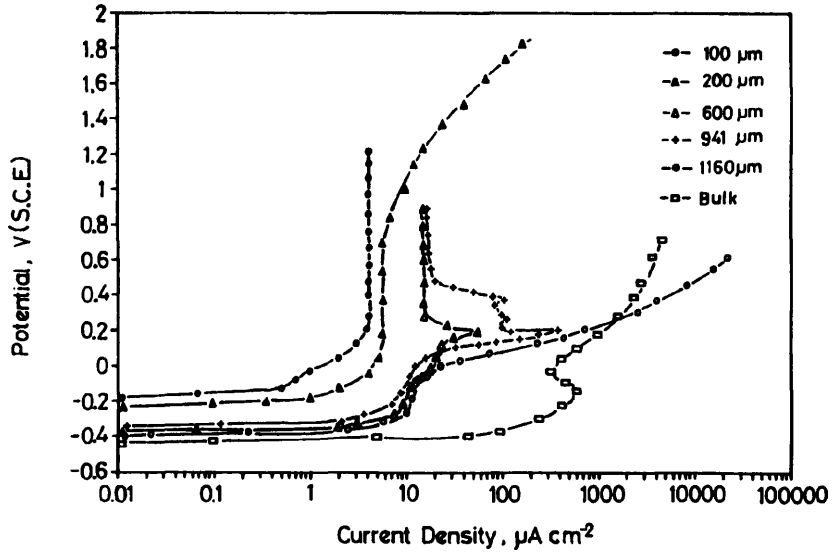

Figure 5-2 Anodic polarization curves for pure iron covered by various thicknesses of electrolyte layers (thickness from 100 μm to bulk solution, 10^{-4} M Na_2SO_4).

reduces to about 65 $\mu A/cm^2$ and passive current density to 16 $\mu A/cm^2$. When the thickness of electrolyte layer is below 200 μm, spontaneous passivation occurs with no critical current observed and finally, at 100 μm, self passivation again occurs with a small passive current density ($4\mu A/cm^2$). Microscopy examinations at the end of anodic polarization measurements showed that the surfaces of the samples remained bright and intact when the thickness of electrolyte layers was below 600 μm but some pitting was found when the thickness was 1160 μm and in the bulk solution.

In order to check the stability of passivation of pure iron covered with thin film of electrolytes, additional experiments were carried out. Samples covered initially with a 150 μm thick layer of 10^{-4} M Na_2SO_4 were polarized to +0.5 V (SCE) and passivity maintained. Two droplets of solution were then added to the surface of the sample to change the composition and concentration of the electrolyte covering the surface of the electrode. After the addition of the solution, the anodic polarization process was continued at the same sweep rate as before.

Figure 5-3 shows the result of the experiment described above, where the initial electrolyte thickness on the surface of iron was 150 μm and final thickness about 450 μm after the addition with two droplets of the solution (0.1 M Na_2SO_4) at the potential of +0.5 V (SCE). It can be seen from Figure 5-3 that even though the concentration of the solution on the surface increased significantly with the addition of the 0.1 M Na_2SO_4, the iron still retains its stable passivation during further anodic polarization. The increase in passive current density from 6.5 $\mu A/cm^2$ to 18 $\mu A/cm^2$ after the addition of two droplets of 0.1 M Na_2SO_4 may be attributed to the increase in the thickness of electrolyte layer from 150 μm to about 450 μm.

In contrast, Figure 5-4 shows the results when two droplets of 10^{-3} M NaCl electrolyte

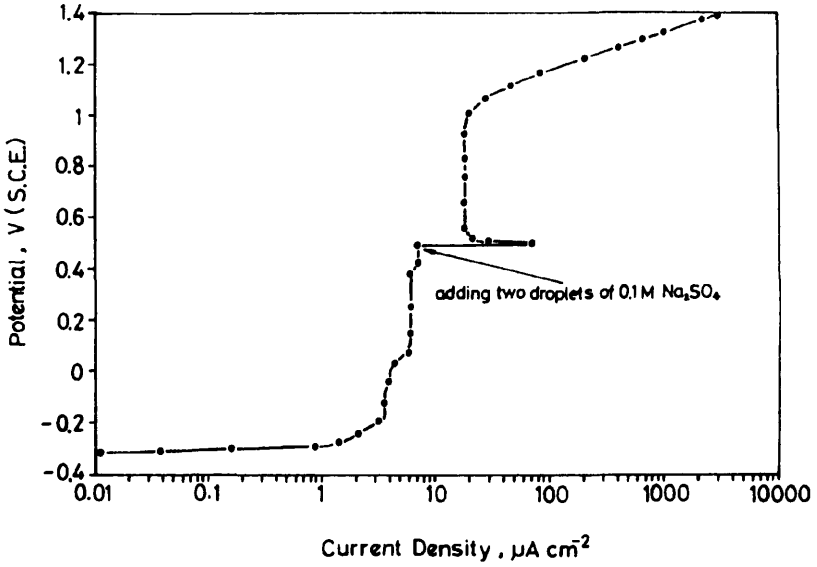

Figure 5-3 Anodic polarization curves for pure iron, where the initial electrolyte thickness on the surface of iron was 150 μm (10^{-4} M Na_2SO_4) and final thickness about 450 μm after the addition with two droplets of the solution (0.1 M Na_2SO_4) at the potential of + 0.5 V (SCE).

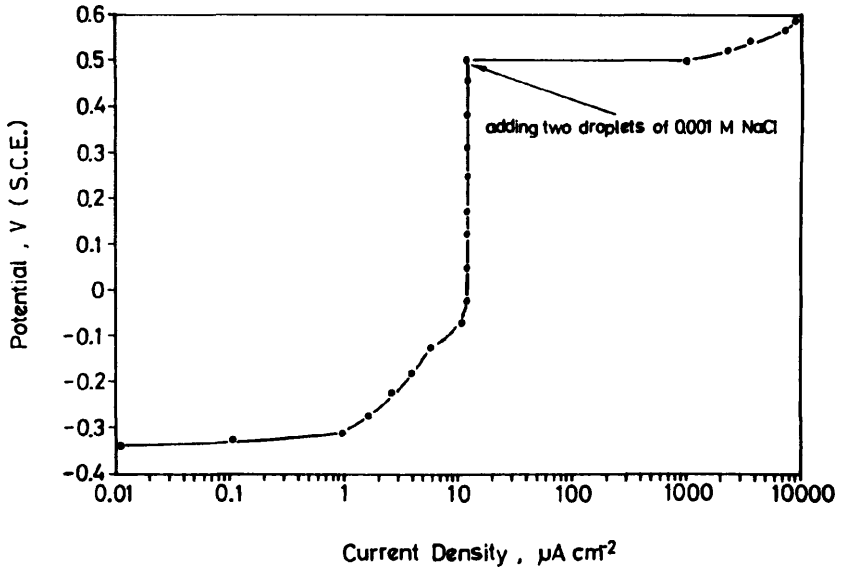

Figure 5-4 Anodic polarization curve for pure iron when two droplets of 10^{-3} M NaCl electrolyte at + 0.5 V (SCE) potential were dropped on the surface of iron covered with 160 μm initial thickness of electrolyte (10^{-4} Na_2SO_4).

at +0.5 V (SCE) potential were dropped on the surface of iron covered with a 160 μm initial thickness of electrolyte. The anodic current suddenly increased from about 12 $\mu A/cm^2$ to 10000 $\mu A/cm^2$, a change of about one thousand times, indicating a total loss of passivity. This occurrence may be caused by the aggressiveness of the Cl^- ion in the NaCl solution, as opposed to any significant change in the concentration of the electrolyte layer. In addition, more importantly, all the results represented in Fig.5-3 and Fig.5-4 confirmed that passivation of iron occurred when covered with a thin layer dilute electrolyte. If the results in Fig.5-2 were attributed to the significant effect of an IR-drop (instead of to passivation) when the solution concentration was increased to 0.1 M Na_2SO_4 and the thickness of the electrolyte layer was changed from an initial 150 μm to a final 450 μm (which two processes will decrease the electrolyte resistance dramatically) the polarization current would, as a consequence, be increased by many more times than it does. In contrast, the addition of 10^{-3} M NaCl changes the anodic current by about one thousand times as pitting commences.

A similar result was obtained in Figure 5-5. But in this case, the added solution was artificial acid rain solution, whose concentration is about $4x10^{-4}$ M. Instead of an instant destruction in passivation after the addition of the acid rain at +0.5 V (SCE) potential, passivity was retained for few minutes, however, eventually it began to collapse with a great increase in current density to about 7000 $\mu A/cm^2$.

5.2.2.2 Corrosion potential-time curves

On the basis of the potential-pH equilibrium diagram for the iron-water system, in which conditions of immunity, general corrosion and passivation of iron are shown, it has

been suggested that the measurement of electrode potentials on steel-rust surfaces can be used for assessing atmospheric corrosion of steel, particularly in relation to the protective properties of steel corrosion products[137,138]. In the presence of oxygen, iron can be active or passive and when passive, generally the more noble the potential the better is the protection given by the oxide film.

Figure 5-6 shows the relation between the corrosion potentials and time obtained in the thin layer electrolyte of 10^{-4} M Na_2SO_4 (thickness 250 μm), a bulk solution of 10^{-4} M Na_2SO_4 and a thin layer electrolyte of 10^{-3} M Na_2SO_4 (thickness 500 μm),respectively. In the case of 10^{-4} M Na_2SO_4, the initial corrosion potential is about -0.255 V (SCE). This potential tends to increase with increasing exposure time up to 180 minutes, the total length of exposure. For iron in bulk solution of 10^{-4} M Na_2SO_4, its initial corrosion potential is also fairly high (about -0.24 V (SCE)). This potential decreases with increasing exposure time and declines sharply after 23 minutes exposure. When the exposure time reaches 180 minutes its potential falls down to about -0.5 V (SCE), at which the iron is in the active state. With a thin layer electrolyte of 10^{-3} M Na_2SO_4, the initial corrosion potential of iron is about -0.35 V (SCE). After about 23 minutes exposure, the corrosion potential begins to decrease sharply and finally approaches -0.53 V (SCE) after 60 minutes. The results of potential-time curves are consistent with that of anodic polarization measurements discussed previously. When passivation occurs the potential remains at a comparatively high value. If the surface activates, the potential will decline to a relatively low value.

In the atmospheric corrosion of iron, the dry/wet cycles play a very important role. Figure 5-7 shows the changes in corrosion potential of iron during evaporation and condensation periods. At the beginning, iron was covered with a thin layer of 10^{-4} M

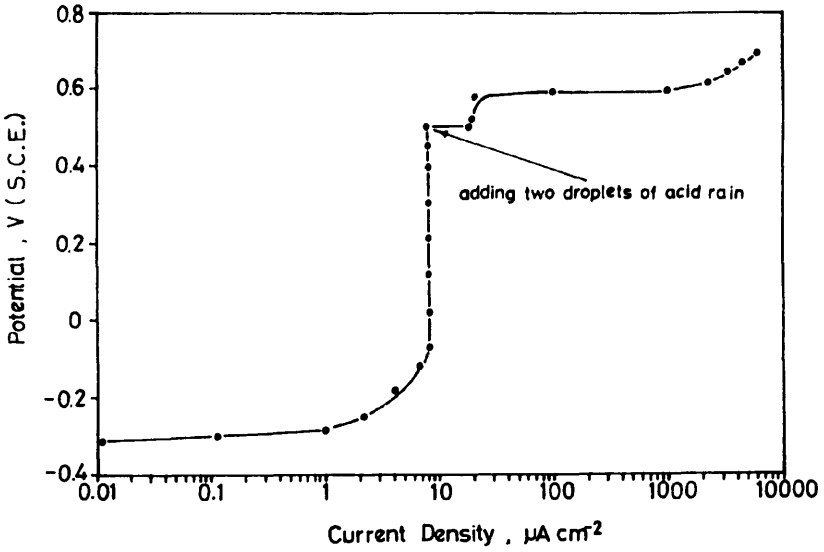

Figure 5-5 Anodic polarization curve for pure iron when two droplets of acid rain solution at + 0.5 V (SCE) potential were dropped on the surface of iron, initially covered with 150 μm thickness of electrolyte (10^{-4} Na_2SO_4).

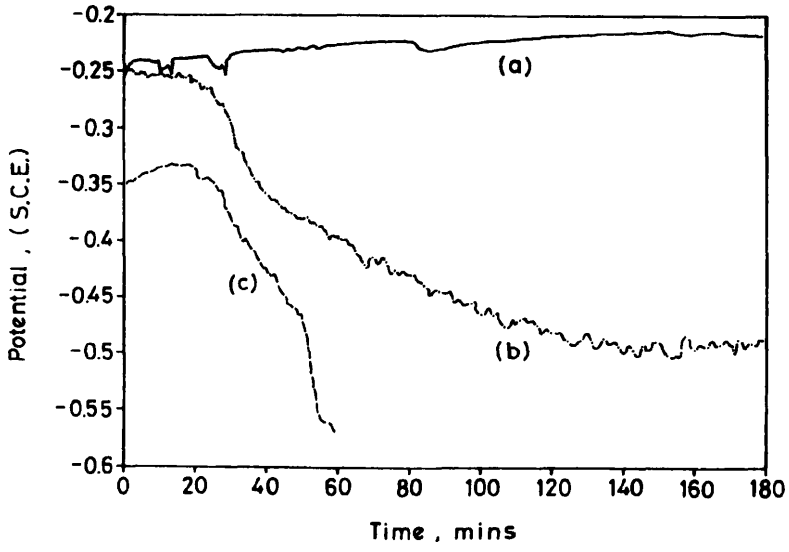

Figure 5-6 The relationship between the corrosion potentials and time, obtained in the conditions: (a) thin layer electrolyte 10^{-4} M Na_2SO_4 (thickness 250 μm); (b) bulk solution 10^{-4} M Na_2SO_4; and (c) thin layer electrolyte 10^{-3} M Na_2SO_4 (thickness 500 μm).

Na_2SO_4 (initial thickness 352 μm). In this condition passivation is likely according to the anodic polarization curves presented earlier and the corrosion potential remains between -0.2 and -0.3 V (SCE). When the electrolyte layer on iron became invisible by the naked eye close to the end of the first evaporation process, a anodic shift of potential from -0.32 V (SCE) to 0 V (SCE) was observed which may be attributed to an acceleration of the transport of oxygen, pH shifts and precipitation of iron ions in so small a volume of electrolyte[119]. Later, with the evaporation proceeding, the surface of iron became completely dry so that random values of potential were measured because of the broken circuit between the working electrode and reference electrode. After a few dry/wet cycles, the corrosion potential remained at a fairly high value (-0.18 V (SCE)). This is evidence that the passivation produced on the iron covered by thin layer electrolyte of 10^{-4} M Na_2SO_4 is stable even after a few dry/wet cycles.

The corrosion potential-time curve during evaporation and condensation for iron initially covered by thin layer of electrolyte 10^{-3} M Na_2SO_4 (initial thickness 216 μm) is shown in Figure 5-8. As long as the electrolyte layer on the surface was visibly thick, activation was observed, identified with the decrease in corrosion potential to between -0.5 V (SCE) and -0.6 V (SCE). In some conditions, where the electrolyte layers were very thin immediately prior to drying and at very beginning of condensation, passivation was also observed with potentials between 0 V (SCE) and -0.3 V (SCE). This phenomenon cannot be identified by anodic polarization measurements due to difficulties of keeping so thin a film of electrolyte while making electrochemical measurements in this condition. A different behaviour happened after the third cycle, the corrosion potential falling straight down to about -0.52 V (SCE) soon after the beginning of condensation.

Figure 5-9 shows corrosion potential-time curve during evaporation and condensation

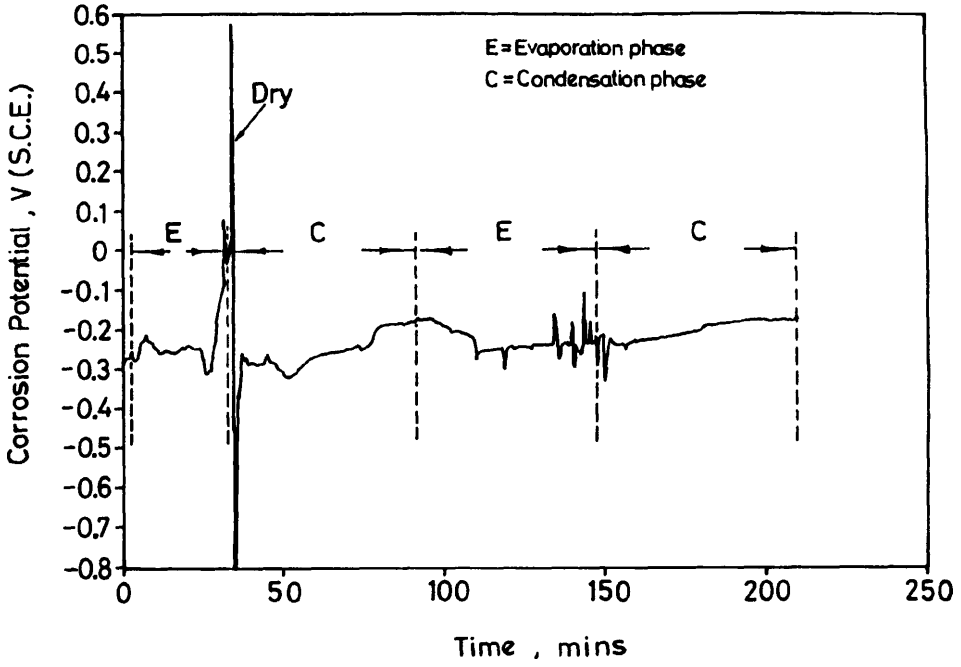

Figure 5-7 Corrosion potential as a function of time during evaporation and condensation period of an iron electrode, initially covered with a thin layer of electrolyte 10^{-4} M Na_2SO_4 (initial thickness 352 μm).

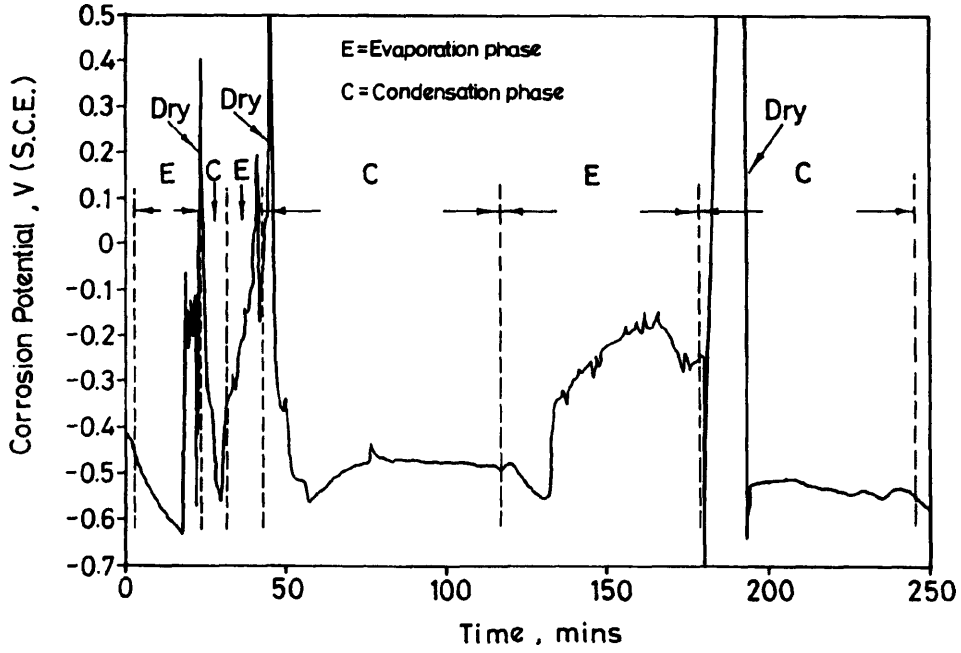

Figure 5-8 Corrosion potential-time curve during evaporation and condensation period for iron initially covered by a thin layer of electrolyte 10^{-3} M Na_2SO_4 (initial thickness 216 μm).

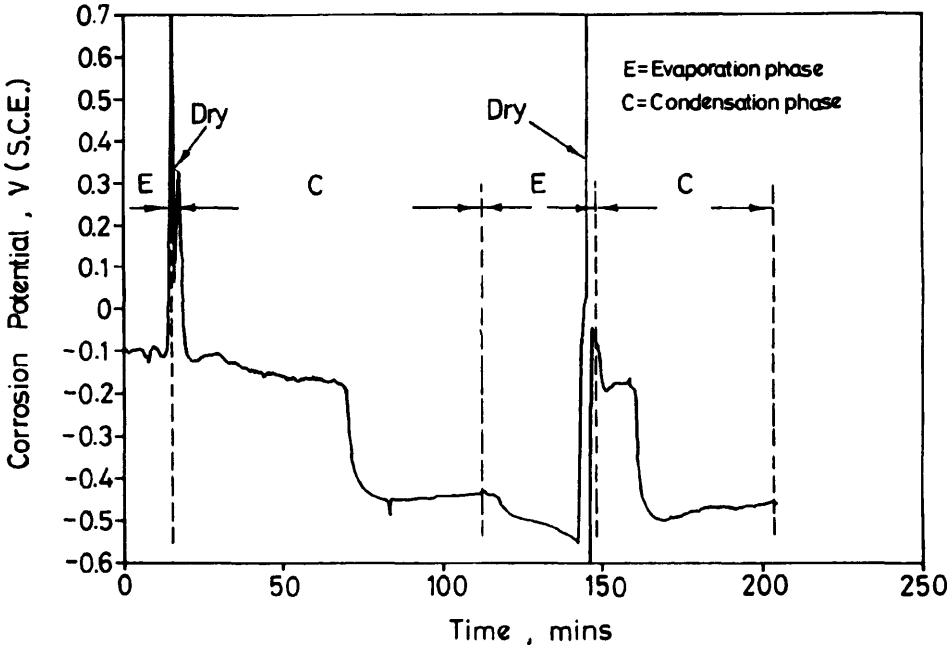

Figure 5-9 Corrosion potential-time curve during evaporation and condensation period on the previously rusted iron sample covered initially with a 10^{-4} M Na_2SO_4 electrolyte layer (initial thickness 156 μm).

on a previously rusted sample covered initially with 10^{-4} M Na_2SO_4 electrolyte layer (initial thickness 156 μm). Compared with the uncorroded sample, the rust on iron has a great effect on its corrosion properties, especially its passivation. In the presence of rust, after one drying process, passivation was retained for only 50 minutes, before the potential dropped down to about -0.5 V (SCE). Moreover, passivation was sustained for an even shorter time after the second cycle.

5.2.3 Discussion

5.2.3.1 Mechanisms of Atmospheric Corrosion

It has long been known that the atmospheric corrosion of iron is accelerated by the presence of sulphur dioxide (SO_2). This accelerating effect of sulphur dioxide eventually involves the sulphate ion produced by the conversion of sulphur dioxide. After the primary adsorption of SO_2, the SO_2 is oxidized to SO_4^{2-} according to[10]:

$$SO_2 + O_2 + 2e^- \rightarrow SO_4^{2-}$$

or the SO_2 is hydrolysized to HSO_3^- and H^+ (thereby increasing the electrolyte acidity). Oxidation of HSO_3^- to SO_4^{2-} is rapid by the reaction:

$$2HSO_3^- + 1\frac{1}{2}O_2 + 2e^- \rightarrow 2SO_4^{2-} + H_2O$$

the electrons coming from the reaction

$$Fe(OH)_2 \rightarrow FeOOH + H^+ + e^-$$

or

$$2Fe(OH)_2 \rightarrow Fe_2O_3 + 2H^+ + H_2O + 2e^-$$

or from metallic dissolution

$$Fe \rightarrow Fe^{2+} \rightarrow + 2e^-$$

The final conversion product of SO_2, existing in the electrolyte layer on the surface of sample, is sulphate (SO_4^{2-}). Therefore, the SO_4^{2-} concentration of electrolyte layer is an important factor affecting the results of the experiments.

In practical conditions of atmospheric corrosion, water films on the surface of steel structures are formed by rain, snow, fog or condensation caused by lowering of temperature in the surroundings. During these processes, some pollutants, for example, SO_2, NO_2 etc are absorbed into a water phase to form the solution,or alternatively, SO_2 adsorption occurs on metal surfaces which are already covered by a thin film of water. The composition of acid rain can contain Na_2SO_4, NaCl, NH_4Cl and its equivalent concentration is about $4x10^{-4}$ M in Manchester. Under normal conditions (i.e. in less polluted areas or rural areas), it is reasonable to assume that the concentration of the water phase formed on steels will be less than that of acid rain formed in more severe conditions. Justo and Ferreira[63] used $FeSO_4.7H_2O$ solution with concentration of $3.1x10^{-4}$, $7.8x10^{-4}$, and $1.2x10^{-3}$ M as experimental electrolytes, corresponding respectively to concentrations of 20, 50, 75 $\mu g\ m^{-3}$ of SO_2. It was also reported that precipitation contains sulphate and chloride ions and hydrogen peroxide molecules, generally in 10 μM to 1mM concentration range[33,72]. Hence, in this experiment, solutions of 10^{-3} M and 10^{-4} M Na_2SO_4 were chosen as research electrolytes therefore making the results obtained more realistic and more easily related to real conditions of atmospheric corrosion. With regard to the effect of SO_2 in air on the atmospheric corrosion, it is suggested that SO_2 is rapidly

oxidized by oxygen to form SO_4^{2-}, following primary adsorption of SO_2 and O_2, as discussed above. The accelerating effect of sulphur dioxide is not due to the amount of gas dissolved in the electrolyte or the acidification of the electrolyte, but involves the sulphate ions formed by conversion of sulphur dioxide. Florianovich, Soklova and Kolotyrkin showed that on iron the anodic dissolution current at constant electrode potential is a function of not just the OH^- activity, but rather of the summed activities of OH^- and SO_4^{2-} ions[75]. When the concentration of electrolytes used in this investigation was increased from 10^{-4} M to 10^{-3} M Na_2SO_4, the environment in the thin film of electrolyte 10^{-3} M Na_2SO_4 became more severe and no passivation occurred even with the very thin films of electrolyte (50 μm) where transport of oxygen was enhanced greatly.

In atmospheric corrosion where thick electrolyte layers are present electrochemical reduction of oxygen is undoubtedly the most important cathodic process which is controlled by diffusion of oxygen through the electrolyte layer. When the layer of electrolyte becomes thinner, the transport of oxygen through the electrolyte layer will be increased. The effect of increasing the transport of oxygen by decreasing the thickness of electrolytes layer on corrosion rates may be twofold. If the rate of the corrosion process is controlled just by the cathodic process, i.e. the diffusion of oxygen, the increased transport of oxygen will increase the rate of corrosion. If the condition is favourable for the occurrence of passivation, the enhancement of oxygen reduction will increase the possibility of passivation of metals. Whether passivation can occur in a particular condition will depend on both the cathodic and anodic processes.

It has to be noted from Figure 5-2 that in contrast to the corrosion in bulk solution, in most atmospheric corrosion (electrolyte thickness < 200 μm), very stable self-passivation of iron can be established. Passivation is the predominant anodic process. This can be

attributed to the easy access of oxygen from air through the very thin layer of electrolyte. In this case, the passivation cannot be interpreted as the result of precipitation of corrosion products caused by excess of solubility of ions produced by the anodic process of corrosion, because before passivation, the anodic process always proceeds at very low rate. In the case of 10^{-3} M Na_2SO_4 solution, passivation is difficult to establish even in very thin layers of electrolyte due to the increased aggressiveness of the environment by increasing concentration of SO_4^{2-}. It indicates the importance of the concentration of SO_4^{2-} in atmospheric corrosion, which is produced by conversion of SO_2 in air.

The result of Figure 5-3 can be explained as once established, passivation of iron is relatively stable and cannot be destroyed by changing the concentration of electrolyte covering the iron to 0.1M (very concentrated compared with 10^{-3} M Na_2SO_4 in Figure 5-1). This indicates that, as evaporation and condensation of the electrolyte occurs, passivity is expected to be retained, a result which is verified in Fig.5-7. The process is related above all to the primary anodic step of the corrosion. As expected (Figure 5-4 and 5-5), the passivation of iron covered with thin electrolyte layer can be easily destroyed by the addition of Cl^- because of the severe aggressiveness of the Cl^- ion.

Barton and Bartonova[76] have investigated the kinetics of atmospheric corrosion of steel, interpreting them by the processes described by the following equations:

$$Fe+H_2O \rightarrow Fe(OH^-)_{ads}+H^+ \qquad (5\text{-}1)$$

$$Fe(OH^-)_{ads} \rightarrow Fe(OH)_{ads}+e \qquad (5\text{-}2)$$

$$Fe(OH)_{ads}+SO_4^{2-} \rightarrow FeSO_4+OH^-+e \qquad (5\text{-}3)$$

Oxidative hydrolysis of $FeSO_4$ leads to formation of hydroxides as the chief component of rust[19,140]:

$$FeSO_4 + H_2O \rightarrow FeOOH + SO_4^{2-} + 3H^+ + e \qquad (5\text{-}4)$$

In these reactions, the processes (5-3), (5-4) are slow, and hence rate-controlling steps. It was expected that the reaction rate is of a second-order dependence on water activity and first order dependence on sulphate concentration. In reaction (5-4), the stimulating sulphate ions are reliberated, so that their activity is independent, within certain limits, of the varying atmospheric SO_2 concentration.

In the condition where there is not much sulphate present or where the supply of O_2 is abundant, atmospheric corrosion can involve another reaction mechanism:

$$2Fe + 2H_2O + O_2 \rightarrow 2Fe(OH)_2 \qquad (5\text{-}5)$$

$$2Fe(OH)_2 + \frac{1}{2}O_2 \rightarrow 2FeOOH + H_2O \qquad (5\text{-}6)$$

In this mechanism, hydroxide is formed directly from the oxidation of iron. Although the final products formed by these two reaction mechanism appear to be similar, the effects on the long term course of atmospheric corrosion are different. In the first case, due to the present of SO_2, the acidity of the electrolyte layer is increased during the period of conversion of SO_2 to SO_4^{2-} (hydrolysis of SO_2 to HSO_3^- and H^-) and following corrosion process (reaction(5-4)), more importantly, SO_4^{2-} is regenerated and its activity keeps nearly constant during the corrosion process. This will increase the possibility of active dissolution for iron at low pH and fairly high SO_4^{2-} concentration conditions. In practice, it should be expected that atmospheric corrosion can happen by either mechanism or by two mechanisms simultaneously. Which mechanism is predominant in the corrosion depends on the concentration of SO_4^{2-} and the supply of O_2 in the system.

In this study, when 10^{-4} M Na_2SO_4 was used and thicknesses of electrolyte layers on

the sample surface was kept fairly low (e.g. < 200 μm in Fig.5-2), the corrosion occurred by the second reaction mechanism (reactions (5-5) to (5-6)), in that a stable hydroxide was directly formed leading to passivation of iron since sufficient oxygen was supplied to the surface of iron through a thinner layer of electrolyte. With the increase in concentration of SO_4^{2-} (Fig.5-1) or increase in thicknesses of electrolyte layer (Fig. 5-2), the mechanism of corrosion changes from one to the other. In this case, the sulphate is primarily formed, instead of the direct formation of hydroxide of iron, followed by the oxidative hydrolysis (reaction 5-4). This finally leads to the formation of a less protective film on the iron surface. Hence, it is suggested that the concentration of SO_4^{2-} and supply of O_2 to the surface of iron, affected greatly by the electrolyte layer thickness on the iron surface, are very important factors determining the mechanism of initial atmospheric corrosion of iron.

After the passivation of iron covered with thin electrolyte layer is established, the increase in concentration of SO_4^{2-} in electrolyte layer has no significant effect on the stability of the passive film (Fig. 5-3). This implies that the effect of SO_4^{2-} on iron corrosion process is concerned only with the initial anodic step of the corrosion. In contrast, passivation of iron covered with a thin electrolyte film can be disrupted by the addition of Cl^--containing solution (Fig.5-4) even when the concentration of Cl^- ion in the solution is relatively low (Fig.5-5).

Finally, it must be mentioned that, with the decrease in the SO_4^{2-} concentration from 10^{-3} M to 10^{-4} M, the kinetics of the electrode reaction would be affected due to the formation of a thicker diffuse layer in the more dilute electrolyte. It is believed that this effect on the dissolution kinetics is relatively unimportant when compared with the obvious passivation already demonstrated by the sensitivity of the polarization curves to changes in electrolyte thickness and composition. This question will be discussed in more detail in

the next sub-section.

In a.c. impedance measurements, reported in the next Chapter, it was found that the responses of a.c. impedance change with time during the first one to two hours of measurement. After that time, stable, reproducible results can be obtained on the iron covered with thin layer electrolyte. This indicates that the establishment of the passivation on iron surface occurs over a period of time, typically one to two hours.

On the basis of the results obtained in this investigation and discussion above, a mechanism in relation to the initial stages of atmospheric corrosion of iron is suggested as follows:

When the fresh iron sample is exposed to the atmospheric environment, a thin layer of water is formed on the iron surface. The formation of this layer may be due to precipitation (e.g. rain) or to condensation of atmospheric moisture on to the surface. The thickness of layers formed by atmospheric precipitation may be up to 200 μm[32]. The absolute magnitude of the thickness of layers formed by condensation on to iron has been variously reported in the range 25-30 molecules (or $< 10^{-2}$ μm) on pure iron at 100% r.h.[38] to < 4 μm on iron with a sulphate-free rust layer[39] at 100% r.h. After the primary adsorption of SO_2, SO_2 is oxidized to SO_4^{2-} in the water layer on the iron surface. The concentration of this dilute electrolyte layer is generally in the range of 10 μM - 1 mM[72]. In normal atmospheric environment, iron is initially kept in its passive state, depending on the composition, concentration and thickness of the electrolyte layer on the surface. The establishment of this initial passivation may occur over one to two hours. Once the iron has passivated, it is stable, even after several wet/cry cycles (Fig. 5-7). When the concentration of SO_4^{2-} in the electrolyte layer increases to 10^{-3} M, passivation may also be established on the iron surface in very thin electrolytes (Fig. 5-8). However, when the

concentration of SO_4^{2-} is increased to 10^{-3} M in the electrolyte layers of thickness > 100 μm or the thickness of the electrolyte layer (10^{-4} M Na_2SO_4) becomes > 880 μm, the initial passivation is difficult to establish and some pitting happens. The corrosion products from the activated area inside the pit is spread around the surface through diffusion. This causes the remaining passivated area to break down further by crevice corrosion. Finally, the whole area becomes activated and comparatively uniform corrosion occurs. When the iron surface is covered with a layer of rust, rain can wash out the surface and dilute the electrolyte layer on the surface. This time, if the rusted iron surface is covered with a thin layer dilute electrolyte (10^{-3} M Na_2SO_4). Passivation can be re-established again on the rusted surface (Fig. 5-9). After each evaporation and condensation cycle, this repassivation can remain some time prior to breaking down. In this way, atmospheric corrosion of iron occurs as a series of alternate passive and active stages. This mechanism may also be elucidated by considering the long term corrosion rate of atmospheric corrosion for iron (from 1.9 μA cm^{-2} to 9.5 μA cm^{-2})[139], which fall in the range of passive current obtained in this investigation by anodic polarization measurements. From the viewpoint of this mechanism, it would be suggested that in order to improve the protective properties of iron in atmospheric environments, increasing the stability of the passivation, or more importantly, the repassivation ability after rusting are the promising avenues of attack. Indeed, Stratmann et al have shown that one effect of the copper in weathering steels is to reduce the critical current density for passivation[119,120].

5.2.3.2 The Validity of the Polarization Curves

The major question is related to the validity of polarization curves, measured in diluted

electrolytes, especially for thin films (Figure 5-2). There are three aspects which must be considered to answer this question, i.e. the uncompensated IR drop, the effect of concentration of electrolytes on the structure of double layer and the non-uniformity of current distribution. These three aspects are discussed as follows.

A. The uncompensated IR drop

The contentious question in regard to the effect of uncompensated IR drop on the results of polarization curves may arise from the observation (Figure 5-2) that for thin films (100 to 200 μm) only negligible O_2-evolution is observed even at very anodic potentials of 1.2 to 1.8 V(SCE). For the 200 μm film a "Tafel-slope" of 0.8 V/decade would result for the "O_2-evolution" beyond +1.2 V(SCE). This may be a consequence of IR drop. In addition, how far is the difference between Figure 5-1 and Figure 5-2 determined by the IR drop?

As discussed previously in sub-section 3.5.1, the appropriate approach to limiting IR drop in this work was to use a semi-micro electrode thus minimising the net current while maintaining current density. In this way, at a current of 10 $\mu A.cm^{-2}$, the absolute value of current is about 20 nA. Thus, for an IR drop of 1 mV, the solution resistance would have to be > 50 kΩ. It is thought that in the worst case (thinnest and most dilute system, i.e. 100 μm and 10^{-4} Na_2SO_4) the IR drop is not significant enough to undermine the explanation to the phenomena of passivation and non-passivation, observed in Figure 5-2.

Concerning the question about the validity of resultant current-voltage curves in this investigation, it is thought that even the exact magnitudes of the uncompensated IR-drops were not known, due to the difficulty, as discussed previously, the validity of the results can be considered by two aspects. First, the significance of the results obtained is just related to the passivation of the iron in the case of thin layer diluted solution and non-

passivation phenomena of iron when the layer of electrolyte is thicker or the concentration of SO_4^{2-} increases. The vertical line portion in current-voltage curve, signifying the passivation phenomena, still remains vertical, without changing the intercept with the x-axis even after the correction for significant IR-drop is made. In Fig.5-10, the different IR-drop compensation processes are simulated by a computer program. It is shown that in certain extreme situations where the IR-drop is very large, the most significant effect of IR-drop on the shape of the current-voltage curve is in reducing the critical current density of passivation (i_{cc}), while, the vertical line portion corresponding to the passive state and the passive current density remain virtually unchanged. Secondly, the passivation phenomena of iron covered with thin diluted electrolyte, described in Fig.5-2, instead of the contribution of significant IR-drop, was confirmed by the experiments, whose results were represented in Fig.5-3 and Fig.5-4. Obviously, if the results in Fig.5-2 were attributed to the significant effect of IR-drop, instead of the passivation phenomena, when the solution concentration was increased to 0.1 M Na_2SO_4 and the thickness of electrolyte layer was changed from initial 150 μm to final 450 μm (Fig.5-3), those two processes decreasing the electrolyte resistance dramatically, the polarization current would be increased largely. In contrast, even though the concentration of electrolyte added in Fig.5-4 (10^{-3} M NaCl) was more dilute than that in Fig.5-3, the anodic current was changed by about one thousand time, because of the aggressiveness of the Cl^- ion in the NaCl solution.

Accordingly, on the basis of the above discussions, the results obtained in this investigation are valid, especially for the passivity of iron covered with thin layer dilute electrolyte, even if a small effect due to IR-drop exists in this experimental set up.

For the observation (Fig.5-2) that, for thin films, only a negligible O_2 evolution is

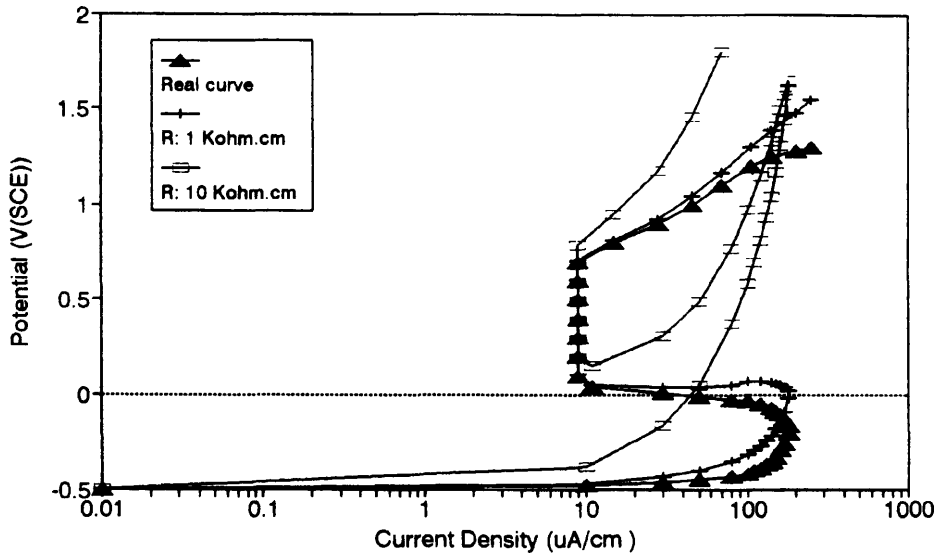

Figure 5-10 The different IR-drop effect on the anodic polarization curve with passive region, simulated by a computer program.

observed even at very anodic potential (+1.2 V) and a large "Tafel-slope" (0.8 V/decade) was obtained, it may be suggested that due to the passivation of iron, the electrochemical kinetics of oxygen evolution was changed from a bare iron/electrolyte system to a unique passive film/electrolyte system, which is not fully understood yet. If an IR drop exists, this is thought to be concerned with the IR drop through oxide coated metal, not electrolyte resistance.

Finally, it must be mentioned that the phenomena discovered in this thin layer electrochemical system (10^{-3} - 1-$^{-4}$ M Na_2SO_4, thickness 100 - 1000 μm) are just related to the passivation and non-passivation (pitting) of iron in some specific conditions. The IR drop may be significant when the current density is above 100 uA.cm^{-2}. However, the main differences in these graphs are below this value and all the evidence indicates that the difference between the non-passivation and passivation phenomena in Fig.5-1 and Fig.5-2 is real.

B. The effect of change in electrolyte concentrations on the double layer

The influence of the SO_4^{2-} concentration on the dissolution kinetics of iron is discussed in section 5.2.3.1. This interpretation would be correct for a constant activity of the supporting electrolyte. However, if the supporting electrolyte is changed between 10^{-3} and 10^{-4} M, then an extensive double layer is formed, which slows down the dissolution kinetics. How can the influence of SO_4^{2-} on the formation of the double-layer be separated from the influence of SO_4^{2-} on the dissolution kinetics in Figure 5-1 and 5-2 respectively?

Indeed, with the decrease in the concentration of the research electrolyte from 10^{-3} to 10^{-4} M, the kinetics of the electrode reaction would be affected due to the formation of thicker diffuse layer in more dilute electrolyte situation. This effect can be interpreted in terms of the variation of potential in the double layer region and the change of the

concentration of electroactive species within the double layer. For example, let us consider the reaction

$$O^z + ne = R^{z-n} \qquad (5-7)$$

and assume that the species undergoing reduction, O^z, is not specifically adsorbed. Its position of closest approach to the electrode is the OHP (outer Helmholtz plane) and the total potential it experiences is $\phi^M - \phi_2$ (ϕ_2 the potential at the OHP), less than the potential between the electrode and the solution by an amount $\phi_2 - \phi^S$, which is the potential drop across the diffuse layer. These potential differences in the double layer can affect the electrode reaction kinetics in two ways.

(1) If $z \neq 0$, the concentration of O^z at x_2 (the position of OHP), $C_o(x_2, t)$, will be different from that immediately outside the diffusion layer, C_o^b. The variation of $C_o(x, t)$ within the double layer can be expressed as the following equation[126]

$$C_o(x_2, t) = C_o^b \exp\left(\frac{-zF\phi_2}{RT}\right) \qquad (5-8)$$

Clearly, the effect of this concentration variation of electroactive species within the double layer on the reaction kinetics can be opposite, depending on the charge polarity on the electrode ($\phi_2 > 0$ or $\phi_2 < 0$) and the kind of electroactive species, e.g. anions ($z = -1$) or cations ($z = +1$).

(2) The potential difference driving the electrode reaction is not $\phi^M - \phi^S$, but instead $\phi^M - \phi^S - \phi_2$; thus the effective electrode potential is $E - \phi_2$.

After taking into account the above effects, the rate equation for a totally irreversible reaction is rewritten as follows:

$$\frac{i}{nF} = K^{o} C_{o}^{b} \exp\left[\frac{-zF\phi_2}{RT}\right] \exp\left[\frac{-\alpha nF}{RT}(E - E^{o} - \phi_2)\right] \qquad (5\text{-}9)$$

Therefore, the K° and i°, are functions of potential, through the variation of ϕ_2 with E, and also functions of supporting electrolyte concentration, C, since ϕ_2 depends on C.

However, corrections for the ϕ_2 effect prove to be difficult, especially for solid electrodes, because of the difficulties in obtaining a value of ϕ_2 for the given experimental condition based on a model for the double-layer structure. In this experiment, for the most simple case, the following reaction was considered in order to elucidate the influence of change of electrolyte concentration on the iron dissolution kinetics based on the above discussions.

$$Fe - 2e \rightleftharpoons Fe^{2+} \qquad (5\text{-}10)$$

First, due to the zero charge carried by a pure iron electrode, the variation of ϕ_2, caused by change of research electrolyte (10^{-3} M to 10^{-4} M), has no effect on the concentration change of Fe within the double layer for the forward reaction (i_1). In contrast, for the backward reaction (i_2), when the electrode is polarized positively ($q^M > 0$, $\phi_2 > 0$), the cations Fe^{2+} will be repelled out of the OHP of the electrode. The concentration of Fe^{2+} at OHP will be lower than that outside the diffusion layer. From this point of view (discussed above as in (1)), rates of the backward reaction ($Fe^{2+} + 2e \rightarrow Fe$) will be decreased due to the effect of ϕ_2. Thus, the net effect is in increasing the dissolution of Fe.

Secondly, the change of concentration from 10^{-3} M to 10^{-4} M will undoubtedly increase the diffuse layer, and thus the ϕ_2, which causes the rate of the reaction (dissolution of iron) to be decreased. The extent of this effect on the reaction rate is not known, due to the lack of information concerning the double-layer structure of the electrode in this

experimental condition. Nevertheless, under some simple limiting conditions, one can show from the theory of the electrical double layer that[141]

$$\phi_2=\phi_2^o+\frac{RT}{z_iF}lnC_i \qquad (5\text{-}11)$$

This relationship indicates that ϕ_2 will change by $0.059/z_i$ V (25°C) when the concentration of solution changes by ten times.

Therefore, according to above discussions, although the dilution of electrolytes would change the electrochemical reaction kinetics, the passivation of iron covered by thin film of dilute electrolyte (10^{-4} M) in Fig.5-2, and sensitivity of polarization curves to the change of electrolyte layer thickness in Fig.5-1 and Fig.5-2 cannot be interpreted as the result of effect of dilution of electrolytes on the electrochemical reaction kinetics under these experimental conditions.

C. The non-uniformity of current distribution

Although a semi-micro electrode (0.5 mm diameter) was used in this investigation, a non-uniformity of current distribution on the surface of the electrode can still be found in the former experiments (refer to the chapter 4). This was verified by the fact that the maximum cathodic current density increased with increasing concentration of the electrolytes. With regard to the anodic polarization measurements in different concentration of electrolytes, as discussed in this chapter, the effect of non-uniformity of current distribution cannot be ignored. The question is how much does this effect have on the validity of the anodic polarization curves obtained and discussed in this chapter.

Comparing the anodic current density obtained in 10^{-4} M Na_2SO_4 electrolyte (Figure 5-2, 200 μm) and the anodic current density obtained in 10^{-1} M Na_2SO_4 (Figure 5-11 of next sub-section), a few thousand times difference between the values of anodic current

density obtained in respective conditions can be found. This cannot be explained as the effect of non-uniformity of current distribution, caused by dilution of the electrolyte, because only a few times difference in the values of the cathodic current density has been found in the cathodic current measurements in 10^{-4} M to 10^{-1} M Na_2SO_4 electrolytes, as discussed in the previous chapter. Generally speaking, in d.c. measurements the main effect of non-uniform current distribution on the polarization curves is just a restriction on the magnitude of the polarization current, not on the shape of the polarization curves, i.e. the passivation and the non-passivation characteristics of the polarization curves. In addition, the result in Figure 5-3 also indicates that the polarization curve in dilute, thin electrolyte film is dominated by the passivation phenomenon, not by any artefact caused by non-uniform current distribution.

Therefore, it can be claimed that the results of anodic polarization curves related to the passivation and non-passivation characteristics in this chapter are valid, despite the existence of the non-uniformity of current distribution.

5.2.4 Summary

In this investigation, a modified electrochemical technique in thin layers of electrolyte has been used to study anodic process on iron covered by thin dilute electrolyte layers (10^{-3} to 10^{-4} M Na_2SO_4). The electrochemical techniques used included anodic polarization, allied with the measurements of corrosion potential-time relationship during wet/dry periods . On the basis of previous discussion, some conclusions can be obtained:

(1) It is reasonable to suggest that in many cases, at least in the condition of thin layer of electrolyte 10^{-4} M Na_2SO_4, passivation is a prevalent

phenomenon.

(2) The initial process of atmospheric corrosion for iron is the establishment of passivation. The establishment of initial passivation depends on the composition, concentration, and thickness of the electrolyte layer on iron. In normal conditions, atmospheric corrosion for iron happens in alternative passive and active stages, with the changes of wet/dry conditions on the surface of iron.

(3) Long-term corrosion rates on iron (22.5-112.3 μm/year) are equivalent to an average current density of 1.9-9.5 $\mu A\ cm^{-2}$, consistent with the passive current densities observed in this study.

5.3 Anodic Processes on Iron Covered with 0.1 M Na_2SO_4 Electrolyte layers

5.3.1 Experimental

In this series of experiments, anodic polarization measurements were conducted on a bare iron surface and a copper-deposited iron surface in 0.1 M Na_2SO_4 electrolyte layers. For the copper-deposited iron sample, a few droplets of 0.01 M $CuSO_4$ were dropped on the surface and retained on the surface for about 30 s before washed in deionized water. In this way, a small amount of copper was deposited on the surface. The other experimental procedures were the same as previously described. The purpose of these experiments were to identify the effect of relatively concentrated electrolyte (0.1 M Na_2SO_4) and copper on the anodic processes of iron in thin electrolyte films.

5.3.2 Experimental Results

5.3.2.1 Anodic polarization Curves of Bare Iron in 0.1 M Na_2SO_4 Films

Figure 5-11 shows the anodic polarization curves of bare iron in 0.1 M Na_2SO_4 films in thicknesses of 133 μm and 1548 μm respectively. In both thin and thick electrolyte layers, the curves show the typical characteristic of passivition for iron. However, from Figure 5-11, it can be seen that the thickness of electrolyte layer has a significant effect on the passive properties of iron. For instance, the critical current density decreases with decreasing thickness of the electrolyte layer, i.e. about 30000 $\mu A/cm^2$ for an electrolyte of thickness 133 μm and more then 100000 $\mu A/cm^2$ for one of 1548 μm thickness. More importantly, more than 25 times reduction in passive current density can be observed when the thickness of electrolyte layer was reduced from 1548 μm to 133 μm. The primary passive potential is not affected by the change of electrolyte layer thickness, implying that the change in the thickness of electrolyte layers does not affect the mechanism of passivity of iron significantly.

5.3.2.2 Anodic Polarization Curves of the Copper-Deposited Iron in 0.1 M Na_2SO_4 Films

Figure 5-12 shows the anodic polarization curve of copper-deposited iron in 135 μm 0.1 M Na_2SO_4 electrolyte. For clarity, comparison of the different anodic polarization curve in 0.1 M Na_2SO_4 electrolyte for copper-deposited iron and the bare iron is made in Figure 5-13. It is clear that, in similar electrolyte thickness (135 μm and 133 μm

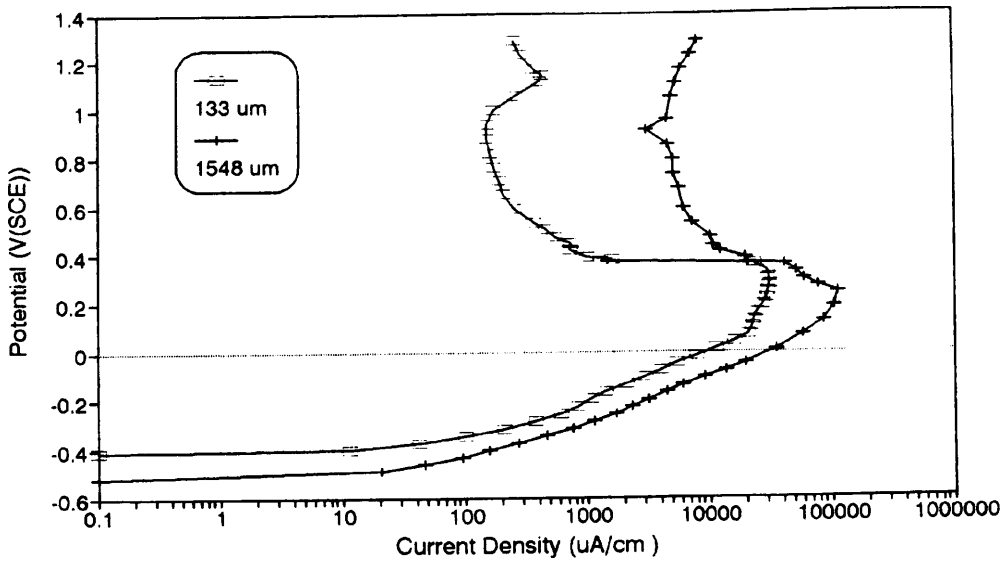

Figure 5-11 Anodic polarization curves of bare iron covered by 0.1 M Na_2SO_4 layers (thickness from 133 μm to 1548 μm).

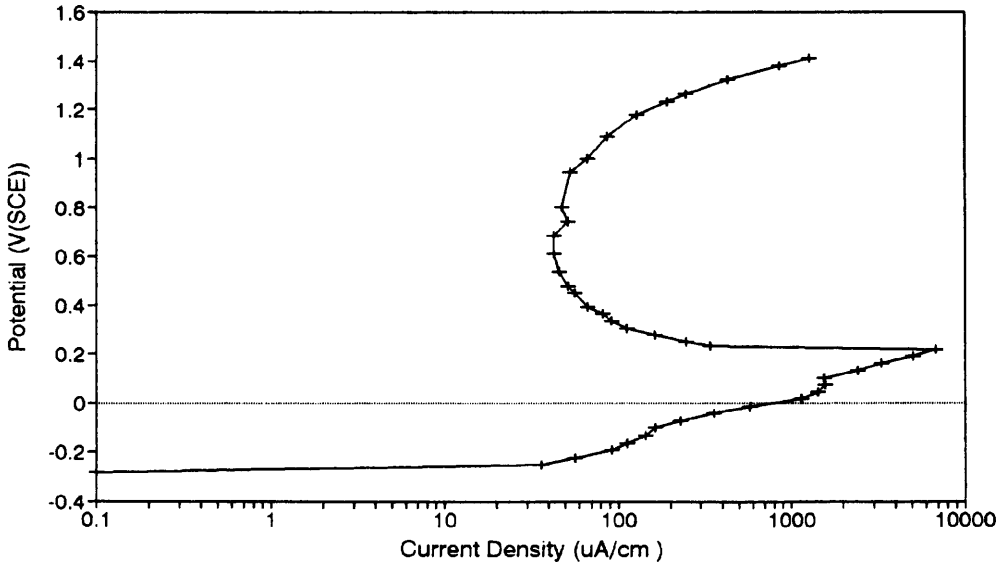

Figure 5-12 Anodic polarization curves of the copper-deposited iron covered by 0.1 M Na_2SO_4 film (thickness 135 μm).

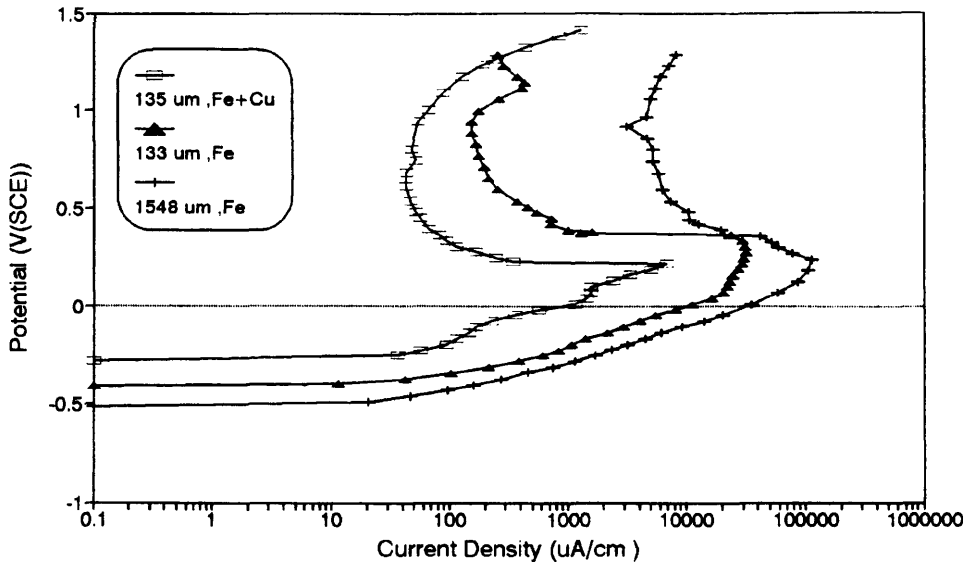

Figure 5-13 Comparison of anodic polarization curves on bare iron and the copper-deposited iron surface.

respectively), the passive current density, the critical passive current density and the primary passive potential for copper-deposited iron were all reduced, indicating a significant effect of copper on the anodic process of iron under these circumstances. For instance, the passive current density for copper-deposited iron is about 60 $\mu A/cm^2$, a reduction of over 3 times compared with that of bare iron. In addition, the negative shift of primary passive potential for copper-deposited iron indicates that the copper on the iron surface may change the mechanism of passivity of iron, rather than reducing the corrosion active area of iron by covering part of the surface.

5.3.3 Discussion

5.3.3.1 Anodic Behaviour of Iron in More Concentrated Electrolyte Films

Although the conditions for materials to be covered with concentrated electrolytes are possibly rare in atmospheric corrosion, as discussed in section 5.2.3.1, there are still several possibilities for the occurrence of this situation. For instance, the concentration of electrolyte films on the surface of material increases in proportion to the reduction of thickness of the electrolyte film due to evaporation. Therefore, if the original thickness of electrolyte film is about 200 μm, as produced by rain, and its original concentration $4x10^{-3}$ M, as occurs in severely polluted areas, it can be calculated that the concentration will be increased to 0.1 M when the thickness decreases from 200 μm to 8 μm during evaporation (assuming that the radius of the droplet is unchanged during evaporation). In addition, in the initial adsorption of SO_2 on the material in high humidity and high SO_2 concentration environment, is highly likely that the concentration of invisible condensed film formed on

the surface of material is very high. Thus, it is clear that a high concentration situation is often concurrent with a very thin electrolyte. On the one hand, the increased concentration (SO_4^{2-}) of electrolyte films will increase the possibility of active corrosion (referred to Fig.5-1, Fig.5-2, and Fig.5-11), and, on the other hand, the decreased thickness of electrolyte films will increase the possibility of passivation for materials.

Due to the limitations of the technique used in this investigation, it is difficult to carry out electrochemical measurements under thin electrolyte films as thin as 8 μm. Thus, direct observation of anodic behaviour for iron covered with extremely thin concentrated Na_2SO_4 electrolyte has not been performed here. However, from the significant decrease of the critical current density and passive current density, caused by thinning of the electrolyte layer, as shown in Figure 5-11, it can be inferred that passivation is probably still the dominant phenomena for iron covered by even a relatively concentrated electrolyte film provided it is sufficiently thin.

Unlike the self-passivation observed on iron covered with dilute electrolyte films (in Fig.5-2), the mechanism of passivation of iron covered with concentrated electrolyte films (in Fig.5-11) may be different. It is likely that after the active dissolution of iron, the iron ions produced may saturate the small volume of electrolyte and precipitate in the form of oxides or hydroxides at the interface of metal/electrolyte. As a consequence, the surface of iron is partially covered and blocked by the corrosion products, and passivation is more easily established in this condition. This point may be verified by the significant effect of thickness of electrolyte on the passive behaviour of iron as shown in Figure 5-11 and discussed previously. Increased supply of oxygen under thinner electrolyte layer may also contribute the establishment of the passivation.

In practice, if iron is covered with a relatively thick concentrated electrolyte layer

(although this situation is rare), the initial stage of atmospheric corrosion is active corrosion rather than the passivation. However, with this corrosion, there is still a trend for the establishment of passivity, depending on the thickness of the electrolyte layer and the duration of active corrosion (the amount of corrosion products produced during active corrosion). The ease for establishment of passivity and the stability of passivity are still important aspects which increase the ability of iron-based materials to resist atmospheric corrosion.

5.3.3.2 Effect of Alloying Element Cu on Atmospheric Corrosion of Steel

It has been known that the addition of copper to steel, as in weathering steels, can improve the protective properties of steels against atmospheric corrosion. This beneficial effect is more significant in long term exposure, especially in industrial areas. The role of copper in these weathering steels is not clear so far, although extensive research has been carried out to try to elucidate the mechanisms of the copper effect. The most attention has been previously paid to the effect of copper on the structure of corrosion products formed during long time exposure in environments.

Misawa, et al[89] pointed out that the amorphous δ-FeOOH formed by the presence of Cu and P in steel is much finer in grain size and crack-free, and provides a compact rust layer to enhance the corrosion resistance of the steel. Later, they[96] stated that the amorphous ferric oxyhydroxide rust acts as a protective barrier against atmospheric rusting of the steels. Thus Cu, P and Cr in low alloy steels are inferred to favour the formation of crack-free, uniform rust layers and help to produce uniform amorphous ferric oxyhydroxide.

Suzuki, et al[81] proposed that beneficial elements added to weathering steel inhibit the formation of crystalline magnetite in the cathodic reduction process of rust and increase the electrical resistance of the rust layer.

Recently, Yamashita, et al[107] studying the rust layers formed on weathering and mild steels exposed in an industrial environment for 26 years, reported that the inner stable and protective rust layer on weathering steel mainly consists of nano-particles of α-FeOOH containing a considerable amount of Cr. It was supposed that Cr, P and Cu which dissolved out from the steel matrix may favour the uniform formation of the protective rust layer.

However, due to the electrochemical nature of atmospheric corrosion, the effect of alloying elements in weathering steels should ultimately be revealed by the electrochemical measurements.

Stratmann, et al[87, 119] have suggested that Cu may change the kinetics of the cathodic reaction. If the addition of copper would retard the kinetics of the O_2 reduction until the overall reaction is under kinetic control, then the enhancement of the transport of O_2 during the drying out period would have no influence on the corrosion rate. On the other hand, Cu may change the kinetics of the anodic reaction. If during corrosion copper is enriched at the metal-electrolyte-interface, it will change the kinetics of the metal dissolution. Their experimental results have provided the evidence of passivation-like features for weathering steels.

In this investigation, a complete anodic polarization curve with passivation characteristic of copper-deposited iron has been obtained using 0.1 M Na_2SO_4 electrolyte. This clearly indicates that the effect of copper on the surface of iron is mainly on the anodic process of iron, e.g. enhancing the passivity of iron. Copper on the surface of iron

can substantially reduce the critical current and passive current of passivity and make the primary passive potential shift negatively.

It may be argued that the amount of copper deposited on the surface of iron in this way may be much greater than that produced on the surface of weathering steel in practical atmospheric corrosion condition. However, this argument does not affect the validity of the result. In fact, the difference of protective properties between mild steels and weathering steels, or the superior resistance of weathering steels against atmospheric corrosion, emerges after a few years exposure. This may indicate that during atmospheric corrosion, Cu is gradually accumulated on a weathering steel surface. When the amount of Cu accumulated on the surface is enough after a long time exposure, then the beneficial effect of Cu on the establishment of passivation of weathering steel is revealed, just as the result shown in Figure 5-12.

Although the effect of Cu accumulated on the surface of iron on the passivation of iron has been found in this investigation, it is still difficult to give an satisfactory explanation for its mechanism. This may be related to the production of hydrogen peroxide during the corrosion process. Hydrogen peroxide is often produced in the course of exposure of metals to water and aqueous solutions under oxygen-or air-saturated condition[142], probably through the cathodic reduction process of oxygen as an intermediate product[143]. Mayne and Burkill[144], studying the role of hydrogen peroxide in inhibition of corrosion of iron, found that when mild steel specimens were cathodically polarized at 100 mA/m^2 for 2 hours in a range of inhibitive and corrosive 0.1 M oxygen-saturated solutions, hydrogen peroxide was always obtained from the inhibitive solutions, but not from those which were corrosive including sodium sulphate. When unpolarized specimens were immersed in solutions saturated with air, hydrogen peroxide was again detected, but in much smaller

quantities and again only in the inhibitive solution. The absence of hydrogen peroxide in corrosive solutions was established from potential measurements that hydrogen peroxide behaves in a similar manner to oxygen in solution of non-oxidizing inhibitors and it was concluded that cathodically formed hydrogen peroxide plays an important part in the process of inhibition, probably via the formation of peroxy compounds.

Recently, Olszowka, et al[145], studying copper dissolution and hydrogen peroxide formation in aqueous media, showed that the rates of copper dissolution and hydrogen peroxide formation upon exposure of copper metal to aerated water or neutral aqueous solutions (including 0.1 M Na_2SO_4) are low but detectable. H_2O_2 formation appears to proceed through copper-oxygen intermediates on the metal surface.

Thus, it may be supposed that during corrosion, Cu on the surface of iron preferentially acts as an cathode, on which cathodic reduction, e.g. reduction of oxygen, occurs and hydrogen peroxide is produced on the surface of iron as an intermediate of cathodic reduction. Hydrogen peroxide produced in this way may change the mechanisms of anodic dissolution of iron, promoting the passivation of iron. Verification of this supposition needs moreinvestigation, such as the overpotential of H_2O_2 formation on copper and iron surfaces respectively, the details of effect of H_2O_2 on the passivation of iron (or on the dissolution mechanisms of iron), and the decomposition of H_2O_2 on copper and iron surface respectively, etc.

5.3.4 Summary

1. Even in a relatively high concentrated electrolyte (0.1 M Na_2SO_4), passivity of iron is still the dominant anodic process. The passive properties of iron

covered with concentrated electrolyte layers are significantly affected by the thickness of electrolytes.

2. The beneficial effect of alloying element Cu on the protective properties of weathering steel in atmospheric corrosion is mainly on the anodic processes, e.g. enhancing the passivity of iron by accumulated Cu on the surface during long time exposure.

CHAPTER 6
A.C. IMPEDANCE MEASUREMENTS ON IRON COVERED BY THIN, DILUTE ELECTROLYTE LAYERS

CHAPTER 6 A.C. IMPEDANCE MEASUREMENTS ON IRON COVERED BY THIN, DILUTE ELECTROLYTE LAYERS

6.1 Introduction

Due to the high impedance of the system caused by the poor conductivity of the electrolyte and the thin film electrolyte characteristic of this study, conventional methods for the measurement of a.c. impedance in electrochemical systems may have problems and limitations if the technique was directly used without any modification. Therefore, in this chapter, an initial discussion of the problems in a.c. impedance measurements of high resistance system in thin film electrolytes is presented. Various factors affecting the accuracy and the reliability of the results are discussed and finally, a two-electrode galvanostatic method, thought to be the most suitable in this case, was chosen to measure the a.c. impedance of the system. With regard to the mechanisms of atmospheric corrosion, attempts were made to answer two questions; first, confirmation and explanation of the results obtained and discussed in the previous chapter; secondly, determination of controlling factors in atmospheric corrosion, especially concerning the resistance polarization caused by the high electrolytic resistance between the anode and cathode.

6.2 Problems in A.C. Impedance Measurements of High Resistance System in Thin-film Electrolytes

6.2.1 Introduction

A.C. impedance techniques are widely used in corrosion studies. The increasing application of this technique relies on the fact that during A.C. impedance measurements very small signals, which do not significantly disturb the electrode system, are applied. Furthermore, the information on the uncompensated solution resistance, electrode polarization resistance as well as double layer capacitance can be obtained in the same measurement. It is also thought that the A.C. impedance technique is more suitable for measurements in poor conductivity media, and does not suffer from the same limitations as D.C. techniques[146]. As a consequence, A.C. impedance measurements are increasingly used in high resistance systems, namely; organic electrolytes[147], dilute aqueous media[146], thin film electrolyte electrochemistry[63], polymer coatings[148] and anodic films on aluminium[149-152]. In these systems, the high frequency limit of the impedance, normally dominated by the solution resistance combined with, for example, a contribution of passive, or paint film resistance, may be affected by interference from the reference electrode when three electrode measurements are made. In addition, the impedance difference between the values for the solution resistance at high frequencies, and the total resistance at low frequencies, is several orders of magnitude which makes it difficult to choose a proper current measuring resistance (ideally this should match the impedance to be measured).

In this section, various factors affecting a.c. impedance measurements, e.g. the

impedance of reference electrode, the counter (current measuring) resistance and stray capacitance etc, are discussed on the basis of the a.c. impedance results obtained from the real electrochemical systems and also a dummy cell, as well as the computer-simulated data using an equivalent circuit which accounted for variations in impedance of the reference electrode and counter (current measuring) resistance as well as stray capacitance, etc. The methods used in real system measurements included three-electrode (potentiostatic) and two-electrode (galvanostatic) technique. Attention was paid to the methodological aspects of a.c. impedance measurements in high resistance system.

6.2.2 Experimental

The configurations of the three-electrode and two-electrode electrochemical cells used in real system measurements have already been described previously in Chapter 3, as shown in Fig.3-1 and Fig.3-2 respectively. Three kinds of commercially available potentiostats, signified as No.1, No.2, and No.3 respectively, were used and connected with a Solartron 1250 frequency response analyzer (FRA) for the measurement of A.C. impedance. A computer with an appropriate program was used for the acquisition of the data.

The circuit connections for potentiostatic control in three electrode system are conventional however, a modified galvanostatic connection was used with the two electrode system, as shown in Fig.6-1, where a potential follower was utilized to increase the input impedance of channel 1 in the 1250 FRA. The dummy cell used to investigate the difference between potentiostatic and galvanostatic methods with different potentiostats is shown in Fig.6-2. Finally, computer simulated data was generated by taking into

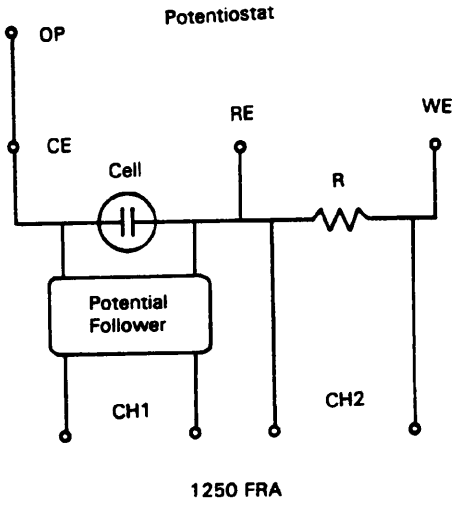

Figure 6-1 The connection of the modified galvanostatic method with two electrode system.

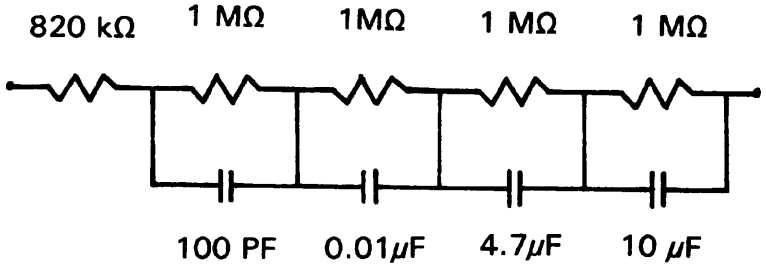

Figure 6-2 The circuit arrangement of the dummy cell.

account factors including the characteristic of the reference electrode, counter resistance, and the input capacitance of the potentiostat and the frequency response analyzer etc.

6.2.3 Experimental Results

6.2.3.1 Real Electrochemical System Measurements

The purpose of these measurements is to find the difference of the results obtained using different methods, i.e. the three electrode potentiostatic and the two electrode galvanostatic method. The detailed explanation of a.c. impedance results in relation to the mechanisms of atmospheric corrosion will be made in section 6.3 below.

Fig.6-3 shows A.C. impedance data obtained from an iron electrode under a 101 μm thick electrolyte layer using the galvanostatic method described previously. Two semi-circles, one in the high frequency portion and the other in the comparatively low frequency part of the impedance spectra, are observed on the Nyquist impedance plot. Optical microscopy examination on the iron surface after the experiment showed that the iron surface remained bright, and in this case the iron was clearly in the passive state, a situation which has also been verified by D.C. electrochemical measurements in Chapter 5. In interpreting this result, two aspects, which may exist in the A.C. impedance response simultaneously, must be examined in detail. In the case where the layers of electrolyte were very thin (101 μm), the value of the real part of the impedance data as $\omega \rightarrow 0$ were more than 30 kΩ.cm^2. This high value of impedance can be explained in terms of passivation of iron. Conventionally, the high frequency semi-circle is frequently taken to represent a characteristic of the passive oxide film. However, in this thin electrolyte

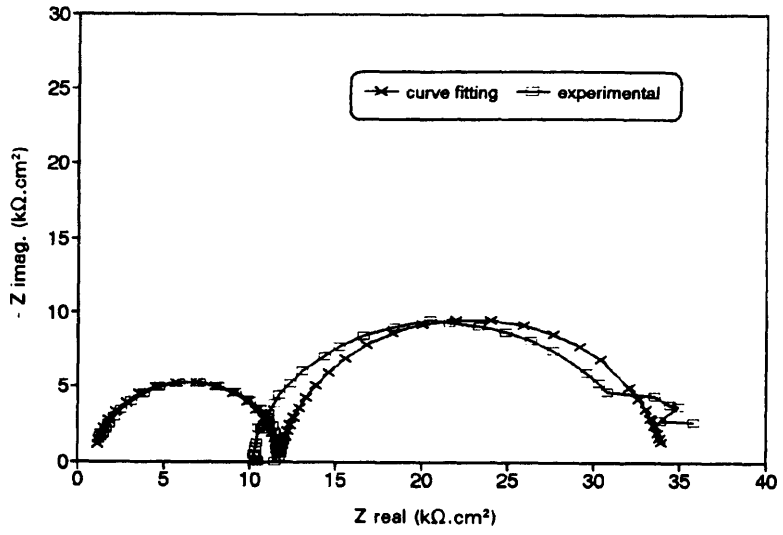

Figure 6-3 The result of a.c. impedance measurement on iron covered by 101 μm thick electrolyte layer by the two-electrode galvanostatic method.

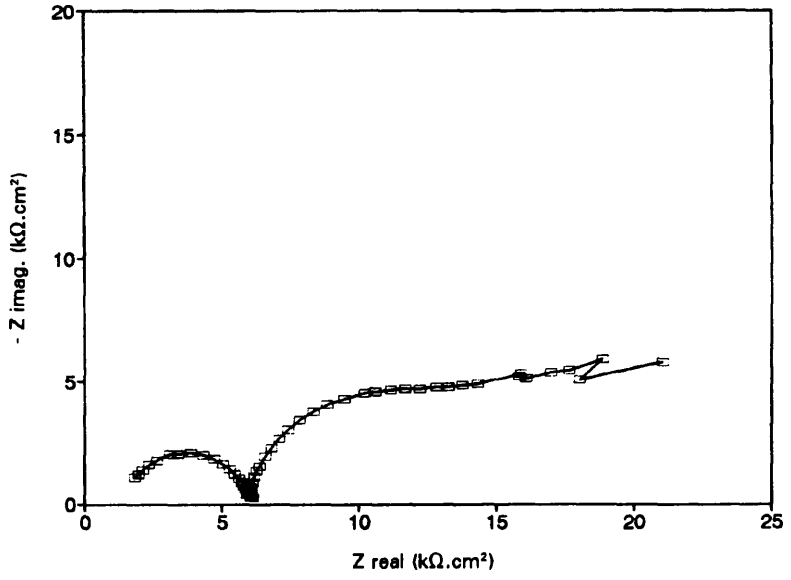

Figure 6-4 The result of a.c. impedance measurement of platinum covered by 130 μm thick electrolyte layer in the same way as in Fig. 6-3.

experiment, or where high solution impedance is present , the current distribution on the electrode may also affect the A.C. impedance response. Thus the first time constant may also be produced by a nonuniform current distribution at the iron electrode.

In order to identify the effect of nonuniform current distribution, a supplemental experiment was performed using the same configuration of the electrochemical cell in Fig.3-2, except that platinum electrodes rather than iron electrodes, were used. In the solution of 10^{-4} M Na_2SO_4, and at the open circuit potential, platinum is likely to be oxide-free. Obviously, if the first time constant in the A.C. impedance data of iron corresponds to the response of an oxide film on the iron surface, this feature should disappear in the A.C. impedance spectra of the platinum. From Fig.6-4 however, it is clear that a high frequency semi circle is present, which is similar to that observed in the iron impedance response with a similar solution electrolyte and thickness. Therefore, it is presumed that the high frequency semi-circles in Fig.6-3 and 6-4 arise from a response produced by non-uniform current distribution.

For comparison, three electrode (potentiostatic) measurements on a similar iron system are illustrated in Fig.6-5 and Fig.6-6. In Fig.6-5, part of a semi-circle in the high frequency region can be seen. However, as the frequency decreased, the magnitude of the system impedance became too large, causing mis-match with the current measuring resistor (180 kΩ) which is too small for the impedance to be measured. Hence, when the frequencies are lower than a certain point, e.g. 316.23 Hz in this case, "random" values, rather than regular impedance values, were recorded. This indicates the importance of the choice of the counter (current measuring) resistance for the correct and sensitive measurement of A.C. impedance. Although a higher counter resistance may be used and signals in the low frequency region are hence increased, distortion of the A.C. impedance

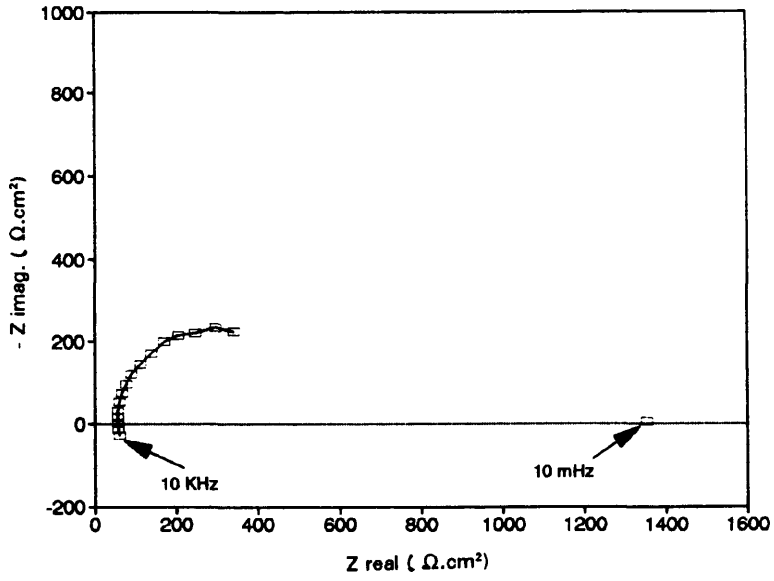

Figure 6-5 The a.c. impedance result of iron covered by 109 μm thick electrolyte layer by the three-electrode potentiostatic method, current measuring resistance: 180 kΩ.

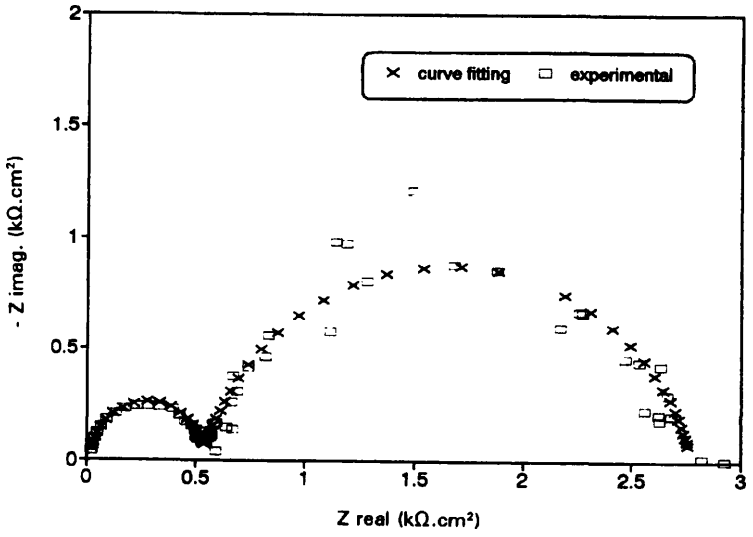

Figure 6-6 The a.c. impedance result of iron covered by 149 μm thick electrolyte layer in the same way as in Fig. 6-5 except that the counter resistance increases to 471 kΩ.

signal in the high frequency region still occurs. In Fig.6-6, with a larger current measuring resistance (471 kΩ), the results are improved significantly, compared with the Fig.6-5 and it appears that the data fits the same circuit model as the two electrode data in Fig.6-3. By using a computer program for circuit simulation in electrochemical systems[153], and the circuit model shown in Fig.6-7, curve fitting for the results of Fig.6-3 and Fig.6-6 was made. The derived values of R_s, R_h, C_h, R_t, C_d for the respective data are tabulated in table 1, where R_s represents the extrapolated high frequency intersect with the real axis; R_h, the resistance of the high frequency semi-circle; the C_h, the capacitance of the high frequency semi-circle; C_d and R_t, the double layer capacitance and charge transfer resistance respectively.

Table 6-1. Values of R_s, R_h, C_h, R_t, and C_d of impedance spectra of Fig.6-3 and Fig.6-6

System	R_s ($\Omega.cm^2$)	R_h ($k\Omega.cm^2$)	C_h ($\mu F.cm^{-2}$)	R_t ($k\Omega.cm^2$)	C_d ($\mu F.cm^{-2}$)
two electrode, galvanostatic	508	5.34	0.029	11.27	64.98
three electrode, potentiostatic	21	0.51	0.307	2.25	159.30

From Table 6-1, it is clear that although the shape of Fig.6-3 and Fig.6-6 are similar (two semi-circles), the values of components, obtained by curve fitting of the A.C. impedance results, are very different.

In this case, which A.C. impedance result, Fig.6-3 or Fig.6-6, best describes the practical situation? If the following definition of the polarization resistance is used[154],

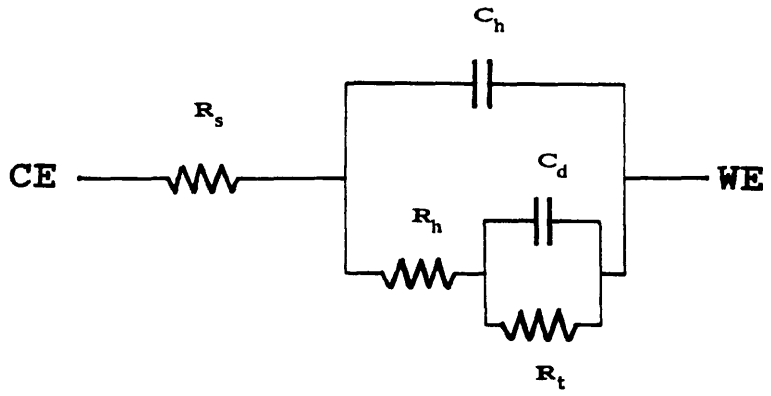

Figure 6-7 The circuit model used to make the curve fitting of the results in Fig. 6-3 and Fig. 6-6.

$$R_p = \lim_{\omega \to 0} R_e\{Z_f\}$$

where $R_e\{Z_f\}$ denotes the real part of the complex faradaic impedance Z_f and ω corresponds to the frequency of the A.C. signal ($\omega = 2\pi f$), the values of R_p, from Fig.6-3 and Fig.6-6 are 17.11 $k\Omega.cm^2$ and 2.78 $k\Omega.cm^2$ respectively for the two electrode galvanostatic system and the three electrode potentiostatic system. As this is a passive system, verified by optical examination and especially, the D.C. electrochemical measurements (referred to Chapter 5), then clearly the A.C. impedance data obtained by the two electrode galvanostatic method is more realistic.

6.2.3.2 The Dummy Cell Measurements

It may be more convincing to identify the advantages of the two electrode galvanostatic method by using dummy cell measurements, because the real electrochemical system measurements may be affected by the reproducibility of the experiments and the unnoticed variation in experimental conditions. In addition, determination of which method is better, based on the results of real system measurements, is limited by the understanding of mechanisms of reactions occurring in the real system. Therefore, in other experiments, a.c. impedance measurements were made using the dummy cell shown in Fig.6-2. As before, the galvanostatic method was found to be better than the potentiostatic method, especially in high resistance systems. Furthermore, there was a surprisingly large difference in results obtained using three different commercial potentiostats. Thus, A.C. impedance results obtained with the potentiostatic method using three different potentiostats are shown in Fig.6-8 to Fig.6-12(a). In some cases, increasing the amplitude (in Fig.6-8(b)), or increasing the values of the counter resistance (in Fig.6-11(b)) can increase the

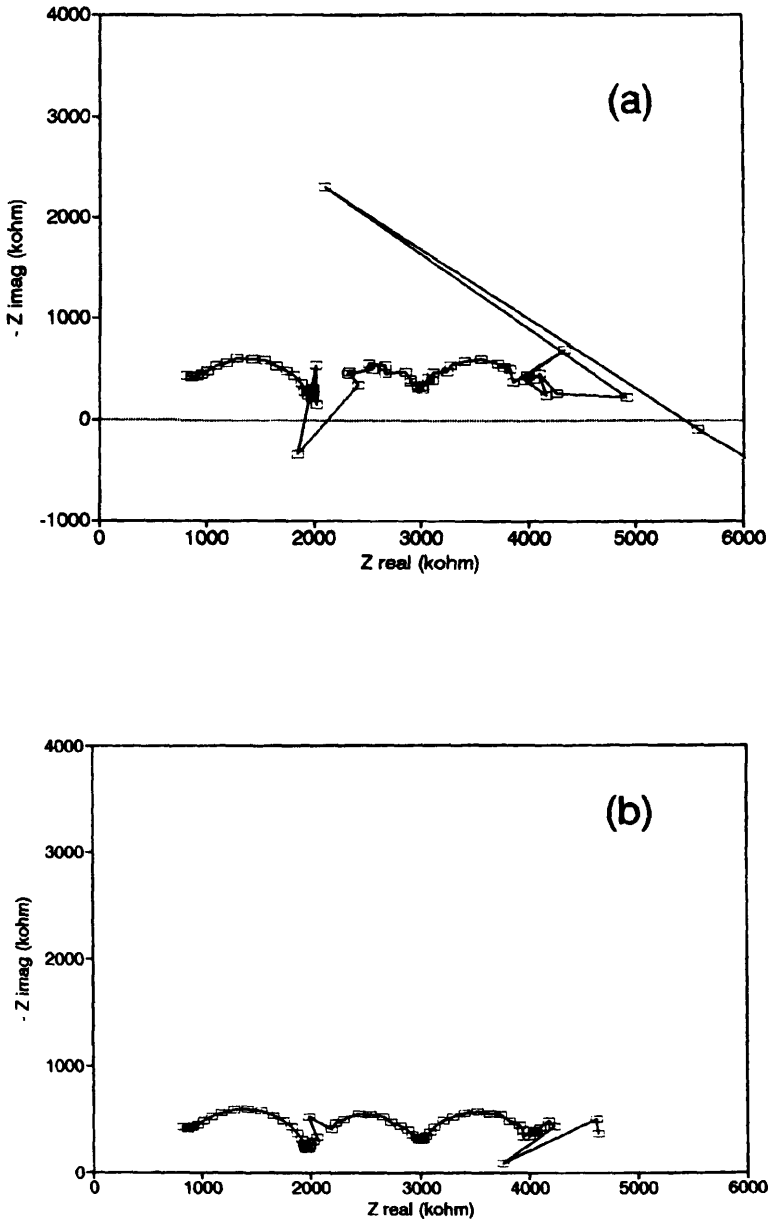

Figure 6-8 The a.c. impedance results of the dummy cell obtained with the No. 1 potentiostat in the potentiostatic way. (a): amplitude = 10 mV, counter resistance = 100 kΩ; (b): amplitude = 50 mV, counter resistance = 100 kΩ.

signal/noise radio, thus improving the measurement. However, in all potentiostatic cases, the A.C. impedance results are not good, though the resistance of this dummy cell (4.82 MΩ) is not very high, compared with real high resistance systems, e.g. anodic films on aluminium (10^5 - 10^8 $\Omega.cm^2$ or more)[149-152], and thin layer dilute electrolyte electrochemistry (maximum absolute value about 17 MΩ, referred to the section 6.3). The best data (Fig.6-8) were obtained by No 1 potentiostat, as long as the amplitudes were kept in the range from 30 mV to 70 mV; out of this range, the results deteriorated. The most questionable results (Fig.6-9) were attained by the No 2 potentiostat, with a large phase shift at high frequencies and the low frequency limit showing a much smaller resistance (1.5 MΩ) than the total true resistance of the dummy cell (about 4.82 MΩ). Concerning the results (in Fig.6-10 and Fig.6-11) obtained by the No 3 potentiostat, besides the serious high frequency phase shift, a far larger resistance (about 7 MΩ) at the low frequency limit was found. Importantly, as all the data appear of reasonable form, these results may easily lead to an erroneous interpretation of mechanisms and kinetics. However, using the same potentiostat as in Fig.6-9, but changing from the potentiostatic to the galvanostatic method as described in Fig.6-1, the measurements can be improved significantly. For example, the result attained by the No 2 potentiostat in this way is given in Fig.6-12(b). As expected, four semi-circles were found, with the high frequency resistance limit at about 820 kΩ, and the low frequency limit at about 4.8 MΩ, agreeing very well with the component values of the dummy cell.

Finally, all these three commercial potentiostats give an accurate A.C. impedance result when the ASTM standard[155] dummy cell (resistance about 210 Ω) is used. However, when a high resistance dummy cell is used as here, the results are sensitively affected by the model and manufacturer of the potentiostat and the way in which the experiments are

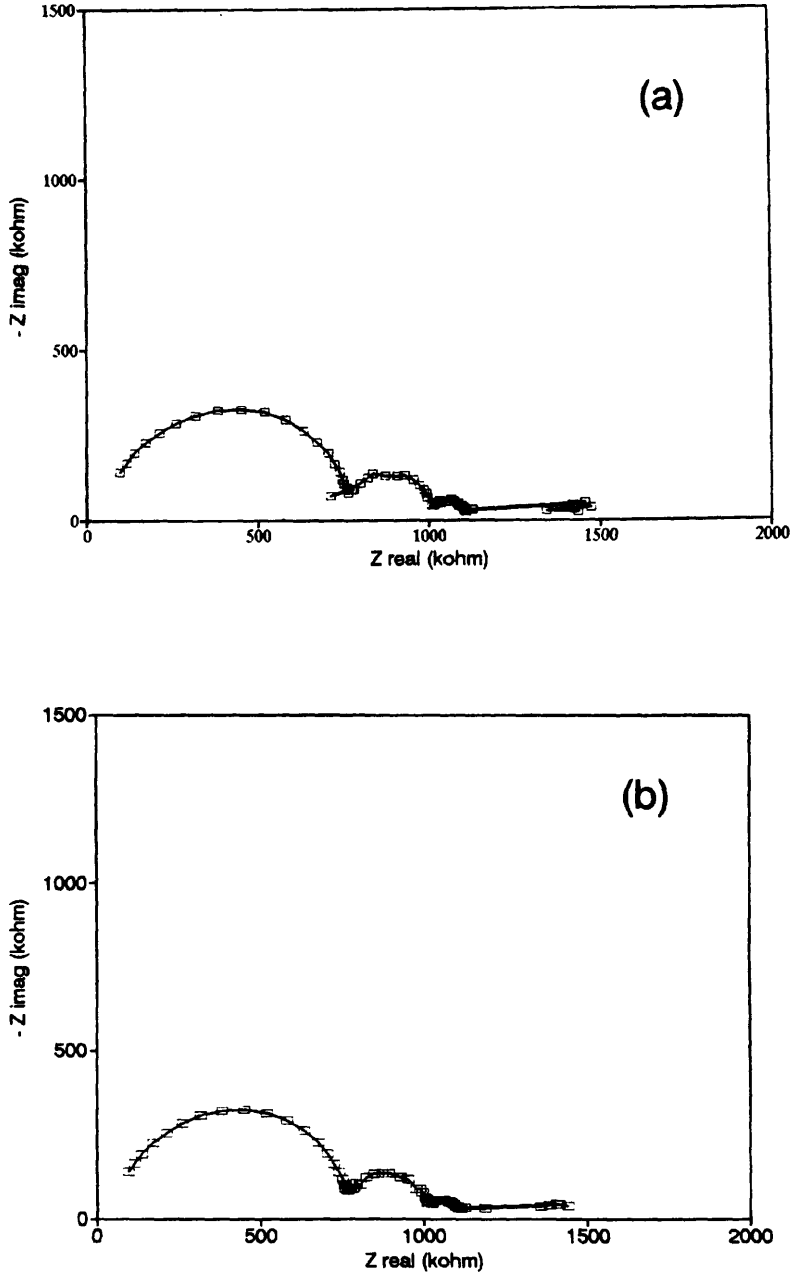

Figure 6-9 The a.c. impedance results of the dummy cell obtained with the No. 2 potentiostat in the potentiostatic way. (a): amplitude = 10 mV, counter resistance = 180 kΩ; (b): amplitude = 50 mV, counter resistance = 180 kΩ.

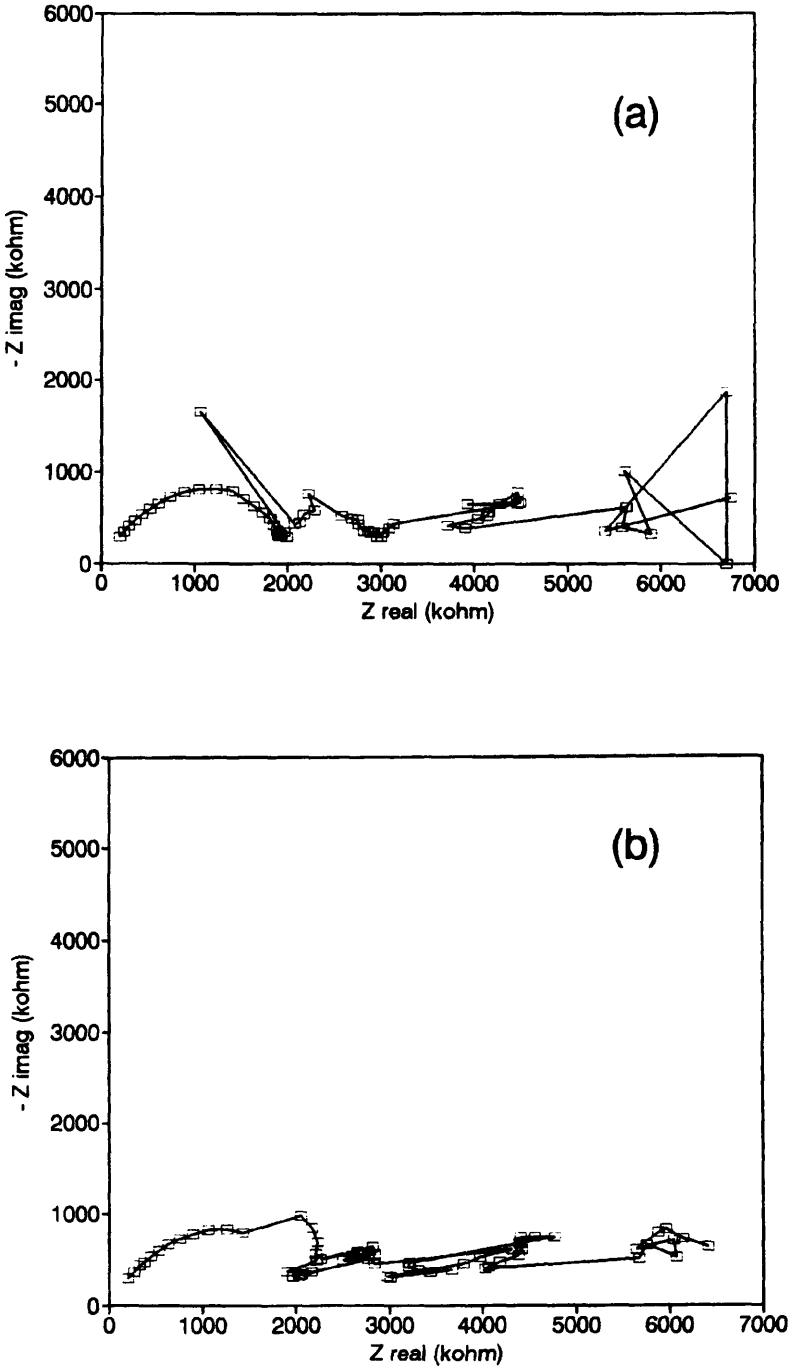

Figure 6-10 The a.c. impedance results of the dummy cell obtained by the No. 3 potentiostat in the potentiostatic way. (a): amplitude = 10 mV, counter resistance = 180 kΩ; (b): amplitude = 50 mV, counter resistance = 180 kΩ.

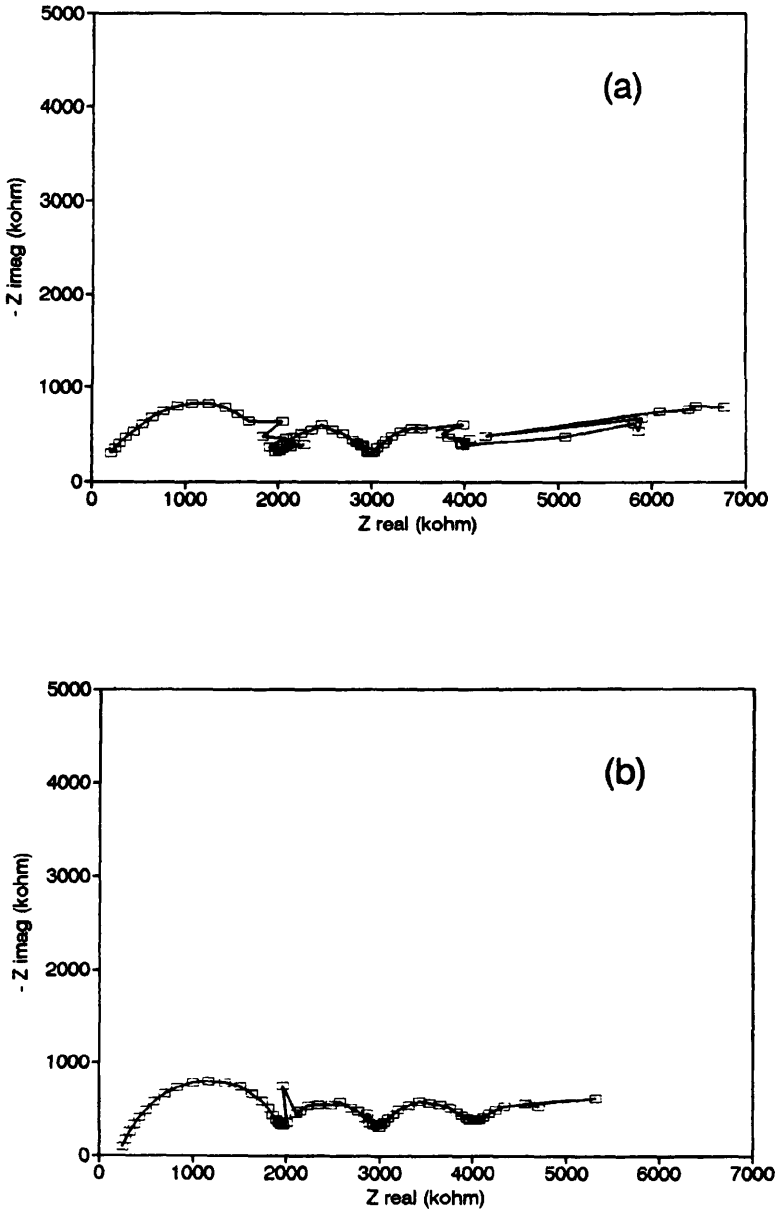

Figure 6-11 The a.c. impedance results of the dummy cell obtained by the No. 3 potentiostat in the potentiostatic way. (a): amplitude = 100 mV, counter resistance = 180 kΩ; (b): amplitude = 100 mV, counter resistance = 985 kΩ.

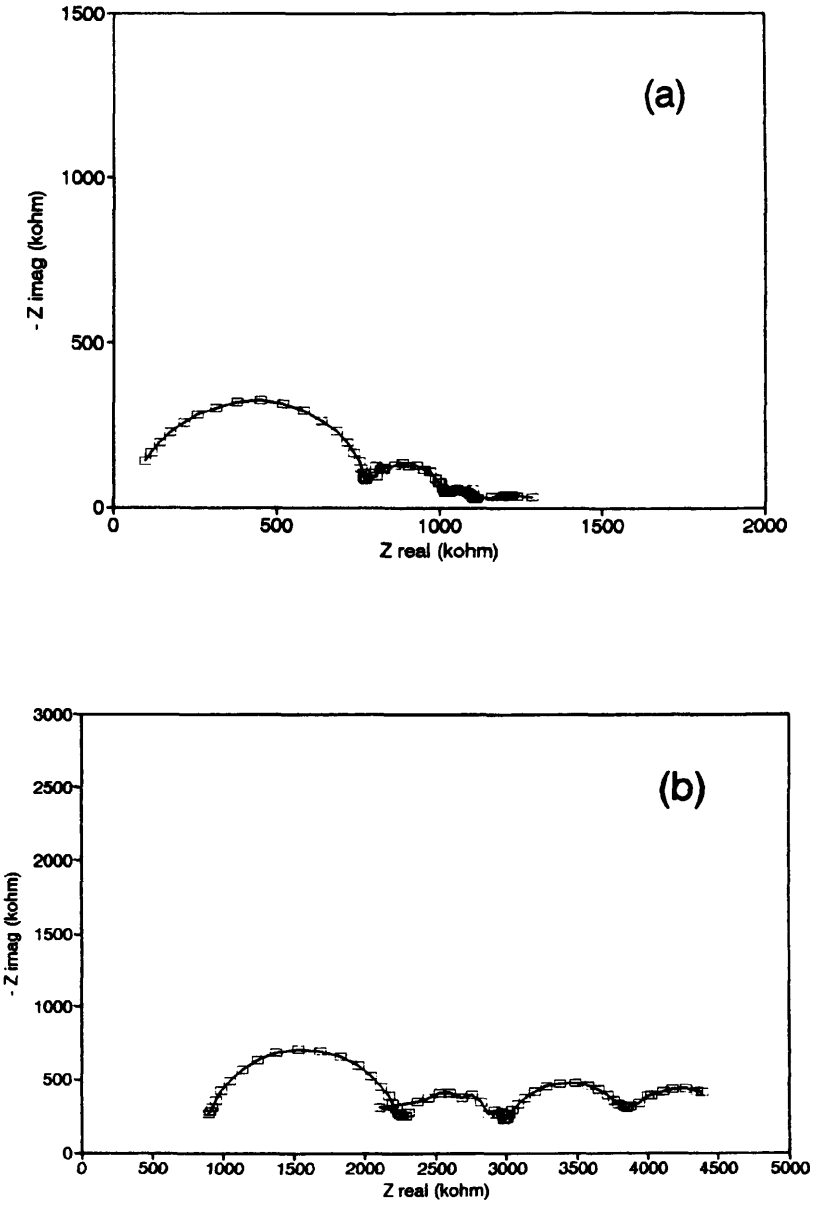

Figure 6-12 The a.c. impedance results of the dummy cell obtained with the No. 2 potentiostat. (a): by the potentiostatic way, amplitude = 100 mV, counter resistance = 180 kΩ; (b): by the galvanostatic way, current = 5 mV/180 kΩ.

performed (galvanostatic or potentiostatic).

6.2.4 Discussion

Normally, A.C. impedance measurements are performed by using a potentiostat and a frequency response analyzer (FRA). The electrochemical cell to be investigated is in the feed-back loop of the main control amplifier in a potentiostatic system. Therefore, the performances of the potentiostat, the FRA and the characteristic of the electrochemical cell can have a large effect on the A.C. impedance response of the system. For the simplest situation, A.C. impedance measurements in a potentiostatic system can be simulated using the equivalent circuit shown in Fig.6-13. In this circuit, R_{cr} is the counter resistance and C_{cr}, is the counter capacitance. If the channel 1 of the FRA is directly connected across the counter resistance for the record of the polarization current, the C_{cr} should include the input capacitance of the channel 1 of the FRA ($<$ 70 pF in Solartron 1250). In high resistance systems, a large counter resistance R_{cr} must be chosen to obtain proper data (Fig.6-5 and Fig.6-6). This will introduce phase shift at high frequencies, the severity of which depends on the values of the resistance R_{cr} and the capacitance C_{cr} ($\tau = R_{cr}.C_{cr}$). This phase shift error can be overcome either by using an additional amplifier to adjust continuously the counter resistors to match the system impedance or by calculation afterwards if the values of C_{cr} are known. On the other hand, as the counter resistance forms part of the load of the potentiostat, a high value counter resistance, compared with a comparatively low impedance of the electrochemical cell at high frequencies, will cause mismatch problems in the system, especially in the high frequency region.

R_e represents the electrolyte resistance between the Luggin probe and the counter

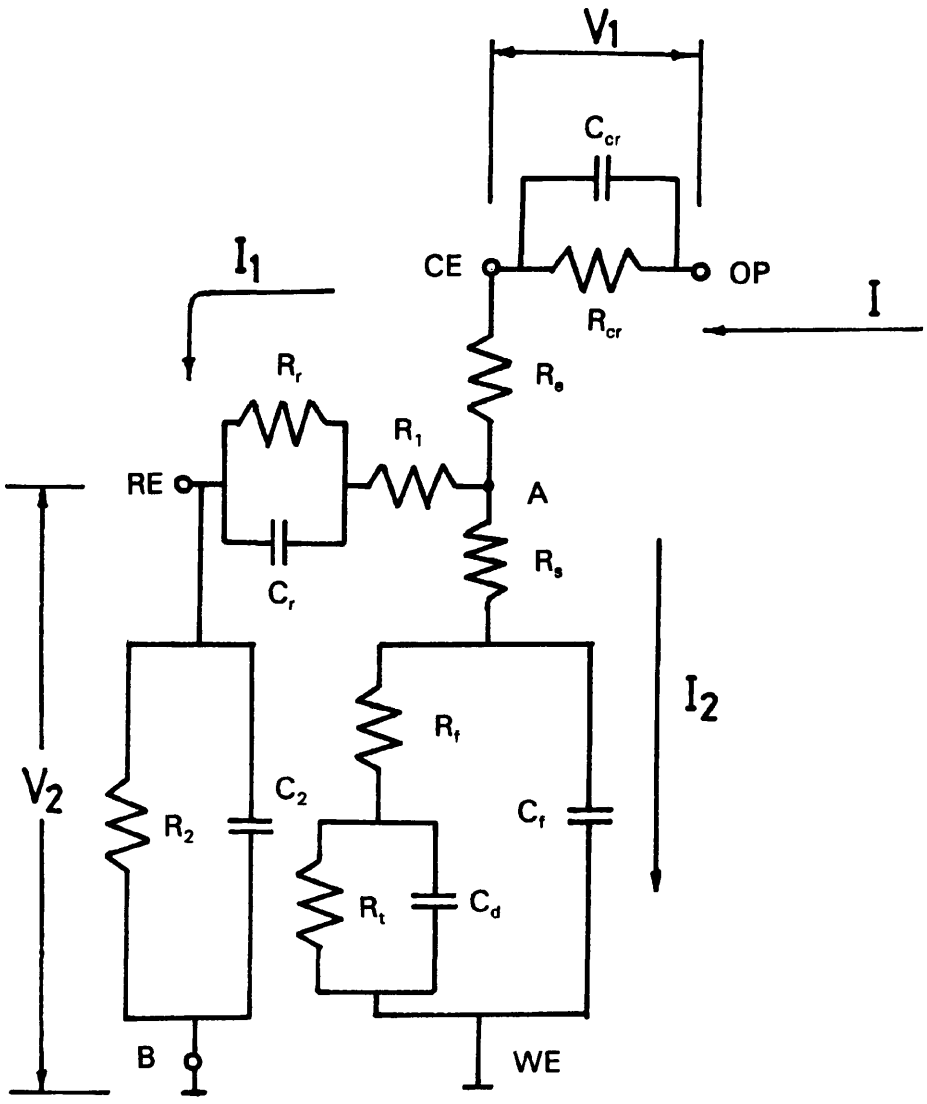

Figure 6-13 The equivalent circuit used to simulate the a.c. impedance measurements in a potentiostatic system.

electrode, R_s, the uncompensated solution resistance between the Luggin probe and the working electrode, R_f and C_f the (passive or coating) film resistance and capacitance respectively, and R_t, the charge transfer resistance, C_d, the double layer capacitance. R_l is the solution bridge resistance between the Luggin probe and the reference electrode. R_r and C_r denote the resistance and capacitance of the reference electrode respectively. Finally, R_2 and C_2 is the input resistance and input capacitance of the potentiostat. During measurement, ideally, the voltage between the point A and WE (working electrode) requires to be controlled within a certain range. However, the controlled voltage is actually that between the RE (reference electrode) and WE (working electrode) terminals of the potentiostat. The actual impedance obtained can be expressed as:

$$Z_{actual} = \frac{V_2}{V_1} R_{cr}$$

This includes the effects of the reference electrode, the counter resistance and the counter capacitance. The effect of the reference electrode depends on the parameters of the close circuit A-RE-B (WE). In low frequencies, R_2 (about 10^{11} to 10^{12} Ω) + R_r + R_l >> R_s + R_f + R_t, I_1 =0, the potential (RE) = potential (A), so the effect of the reference electrode is negligible. In high frequencies, this effect mainly depends on the solution resistance R_s (in some cases, also R_f if C_f is very small), the capacitance of the reference electrode, and potentiostat input capacitance (unfortunately, some manufacturers do not give this value). Fig.6-14 shows the result of simulation in a low resistance system where the uncompensated solution resistance R_s is 10 Ω, the charge transfer resistance R_t, 100 Ω and double layer capacitance C_d = 10 μF. This is the same as the equivalent circuit in the ASTM standard[155]. The other parameters concerning the potentiostat, counter resistance, FRA, etc include R_l =20 Ω, R_r = 820 kΩ, C_r = 100 pF, the input impedance of the

potentiostat = 10^{11} Ω, the input capacitance = 70 pF, R_{cr} = 20 Ω and C_{cr} = 70 pF. The effects of the reference electrode and the counter resistance are not significant. However, in a high resistance system, where R_s increases to 60 kΩ, R_t to 120 kΩ, and the passive film resistance R_f is 20 kΩ (C_f = 0.01 μF), the R_1 (solution bridge resistance) will also increase to 1 kΩ. In order to obtain accurate data, the counter resistance should be increased to about 90 kΩ. The variables concerning the equipment (R_r, C_r, R_2, C_2, C_{cr} etc) remain the same as in Fig.6-14. Clearly, the influence of the reference electrode and the counter resistance is large (Fig.6-15), and is mainly in the high frequency portion of the impedance spectrum. As the high frequency semi-circle contains contributions from the reference electrode, counter resistance and capacitance, uncompensated solution resistance and in some cases, the passive or coating film resistance, the interpretation of A.C. impedance in the high frequency area should be made with great discretion.

In the above analysis and simulation, noise problems, the minimum current control ability of the potentiostat and the measuring sensitivity of the FRA have not been considered. In practice, a higher amplitude signal (e.g. > 20 mV) can often be used, because the system may still be linear due to the potential drop produced by the solution resistance and passive film resistance. This will improve the measuring sensitivity of the FRA but should be used with care to avoid overloading the amplifier input.

In addition, the different designs of potentiostats and different quality of components, especially that of the amplifiers chosen by the manufacturers, affect the power amplifier response, the electrometer input response for reference electrode potential measurement including the bandwidth of the electrometer, common mode rejection ratio and input impedance, and I/E converter response[156]. This is the reason why the different results of a.c. impedance were obtained on the same system by the different potentiostats, as shown

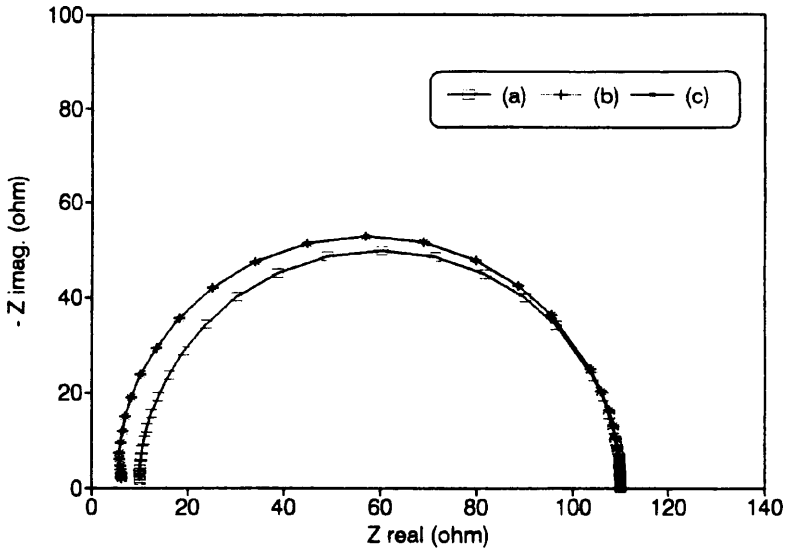

Figure 6-14 The result of the simulated a.c. impedance measurement by using the circuit in Fig.6-13 in low resistance system, where R_s = 10 Ω, R_t = 100 Ω, C_d = 10 μF. Other parameters concerning the potentiostat, counter resistance etc include: R_1 = 20 Ω, R_f = 820 kΩ, C_f = 100 pF, R_2 = 10^{11} Ω, C_2 = 70 pF, R_{cr} = 20 Ω and C_{cr} = 70 pF. (a) true a.c. impedance results; (b) effect of the reference electrode; (c) effect of the reference electrode and counter resistance.

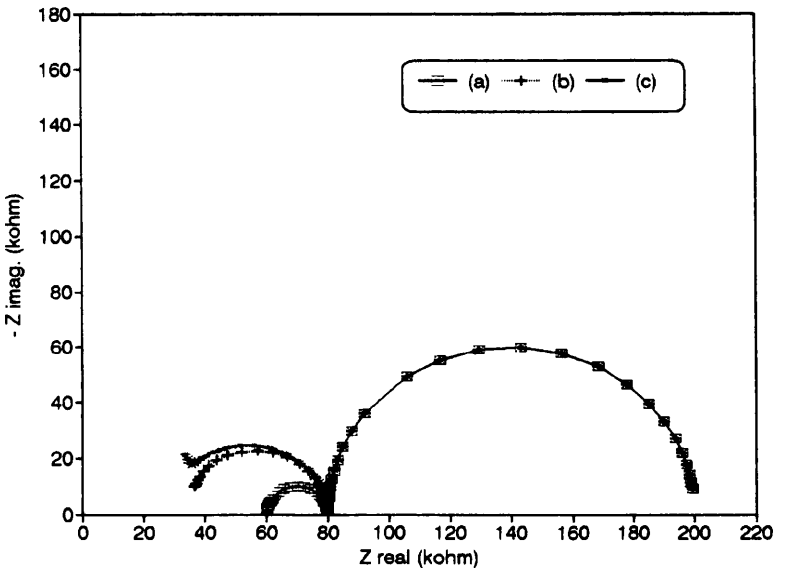

Figure 6-15 The result of the simulated a.c. impedance measurement by using the circuit in Fig. 6-13 in high resistance system, where R_s = 60 kΩ, R_t = 120 kΩ, C_d = 10 μF, R_f = 20 kΩ, C_f = 0.01 μF, R_{cr} = 90 kΩ, R_1 = 1 kΩ. Other parameters concerning the potentiostat ect, are the same as in Fig. 6-14. (a) true a.c. impedance result; (b) effect of the reference electrode;(c) effects of the reference electrode and counter resistance.

by the results discussed above.

A.C. impedance measurements using potentiostatic techniques can thus be affected by many factors, especially in high resistance systems. This partly explains why A.C. impedance measurements are improved significantly by using the galvanostatic techniques. In this method (Fig.6-1), there is no interference of the reference electrode, Moreover, the resistance between the WE and RE terminals (which serves as the potential control resistance) is constant, which makes the feedback loop of the potentiostat more stable.

Finally, it must be mentioned that the factors affecting the results of a.c. impedance measurements in high resistance system, discussed above, are mainly related to effects on the high frequency region. However, a very big difference in the a.c. impedance results of the same dummy cell was also found in the low frequency region, as shown in Fig.6-8 to 6-11. The reason for this problem has not been fully understood yet; maybe it relates to noise, the minimum current control ability of the potentiostat, and corrosion potential variation during the measurement of real systems. From the practical standpoint, it may cause more severe problems because corrosion rates of real systems are normally estimated by the values of a.c. impedance of low frequency.

6.2.5 Summary

1. It must be understood that a.c. impedance measurements by conventional three electrode potentiostatic method in high impedance systems, like coatings, anodic films of aluminium, concretes, high purity water and organic solutions, are easily affected by artifacts, such as the interference of reference electrode, qualities of the instrumentation and the values of counter resistance. Convincing explanation of the results depends on: (a)

a full understanding of the limitation of the instrumentation, (b) confirmation that the data produced comes from the response of the electrochemical system, instead of the instrumentation, (c) it is important that repeated data can be obtained using a dummy cell produced by simulating the results of a.c. impedance obtained on real electrochemical system.

2. The galvanostatic method with two electrode system is better than the potentiostatic method in the measurement of high resistance systems in terms of the stability of the system and the accuracy of the results.

6.3 A.C. Impedance Measurements On Iron Covered By Thin, Dilute Electrolyte Layers

6.3.1 Introduction

Atmospheric corrosion is considered to happen on a metal surface covered by a thin, dilute electrolyte layer, produced either by condensation processes in high humidity conditions or by direct precipitation of rain or snow, etc. The cathodic process in atmospheric corrosion is mainly the reduction of oxygen, transported through thin electrolyte layers on the metal surface by diffusion mechanisms, probably allied with a convection process. The anodic process during atmospheric corrosion is primarily metal dissolution. However, under certain conditions, passivation can occur for iron. Due to the characteristics of thin films and dilute electrolyte layers on the surface, it is reasonable to suppose that under some circumstances resistance polarization during atmospheric corrosion may become significant and control the whole process of atmospheric corrosion.

In the previous chapter, anodic processes of iron covered with thin, dilute electrolyte layers were studied by using D.C. electrochemical methods. It was found that passivation is the dominant phenomena during the initial stages of atmospheric corrosion of iron. However, more information is needed for better understanding and interpretation of this particular phenomena, which has a large effect on the whole process of atmospheric corrosion for iron. Accordingly, in this investigation, A.C. impedance measurements were conducted on a planar two electrode system, covered with thin electrolyte layers (10^{-4} M to 10^{-3} M Na_2SO_4, thickness from 101 μm to 1188 μm). The purpose is to confirm the passivation phenomena discovered in the previous chapter and determine the significance of the resistance polarization of iron covered by thin, dilute electrolyte layers.

6.3.2 Experimental

As discussed in the section 6.2, due to the poor conductivity of the electrolyte in investigation and the thin film electrolyte characteristic of this study, the identification of various items contributing to the measured impedance and the interpretation of the results become rather difficult when a three electrode electrochemical system is used. Partially, this problem may arise from the participation and the interference of the reference electrode with the system A.C. impedance response in high resistance systems. It was found that the situation could be improved greatly by using a two electrode electrochemical system without an additional reference electrode. This makes the A.C. impedance response more accurate and the interpretation of it more easy. Hence, A.C. impedance measurements were performed in this investigation on a planar two electrode sample, covered with a thin layer of electrolyte. The configuration of the two-electrode

electrochemical cell used in this study and the experimental procedures have been described in Chapter 3.

The A.C. impedance was measured under galvanostatic control with approximate polarization current densities of 41 μAcm^{-2} , estimated from anodic polarization data reported in the previous chapter. The circuit connection of a.c. impedance measurements in this study is same as shown in Fig.6-1. A high impedance potential follower was used to increase the input impedance of Channel 1 in the frequency response analyzer.

The equipment used in measurements of A.C. impedance included a Solartron 1250 frequency response analyzer, a "Ministat" potentiostat and a computer for data acquisition.

6.3.3 Experimental results and Discussion

6.3.3.1 A.C. Impedance Measurements

The results of A.C. impedance measurements conducted on pure iron surfaces covered by various thicknesses of electrolyte layers (thicknesses from 101 μm to 818 μm, 10^{-4} M Na_2SO_4) are shown in Figure 6-16 to Figure 6-19. In the case of fairly thin layers of electrolyte (thicknesses below 568 μm), two semi-circles, one in the high frequency portion and the other in a comparatively low frequency part of the impedance spectra, are observed on the Nyquist impedance plots. When the thickness of the electrolyte layer is 101 μm, the plot in Fig.6-16 shows clearly the existence of two complete semi-circles, while in other cases, with the electrolyte layers being thicker, just part of the semi-circle can be observed in the high frequency zone due to the limitation of high frequency response of the potentiostat. Obviously, the diameters of the semi-circles responding to the

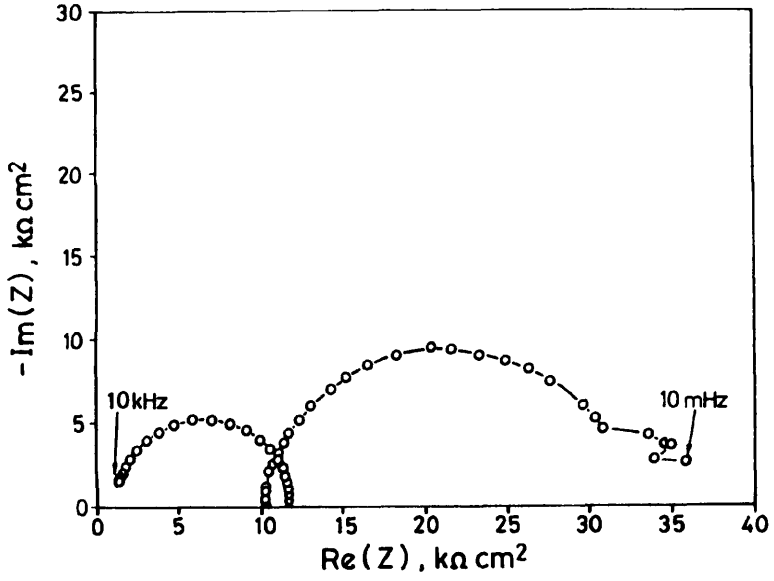

Figure 6-16 The result of a.c. impedance measurement on iron covered by 101 μm thick electrolyte layer (10^{-4} M Na_2SO_4).

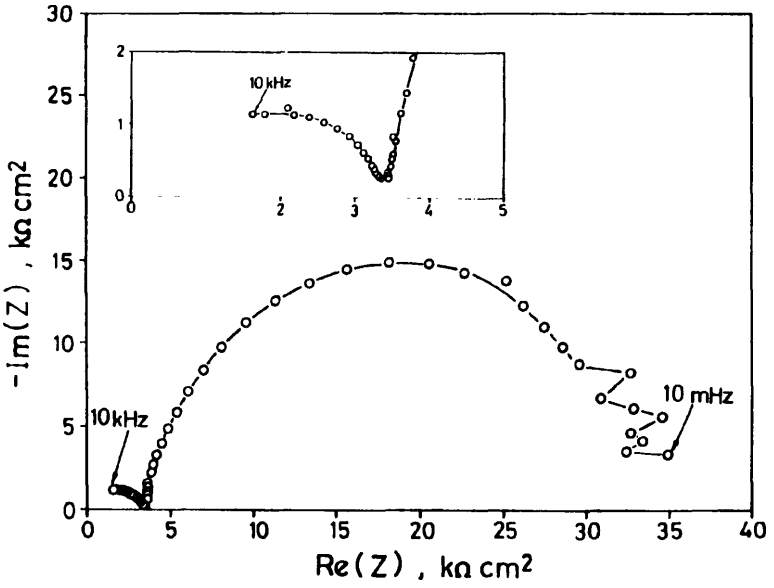

Figure 6-17 The result of a.c. impedance measurement on iron covered by 282 μm thick electrolyte layer (10^{-4} M Na_2SO_4).

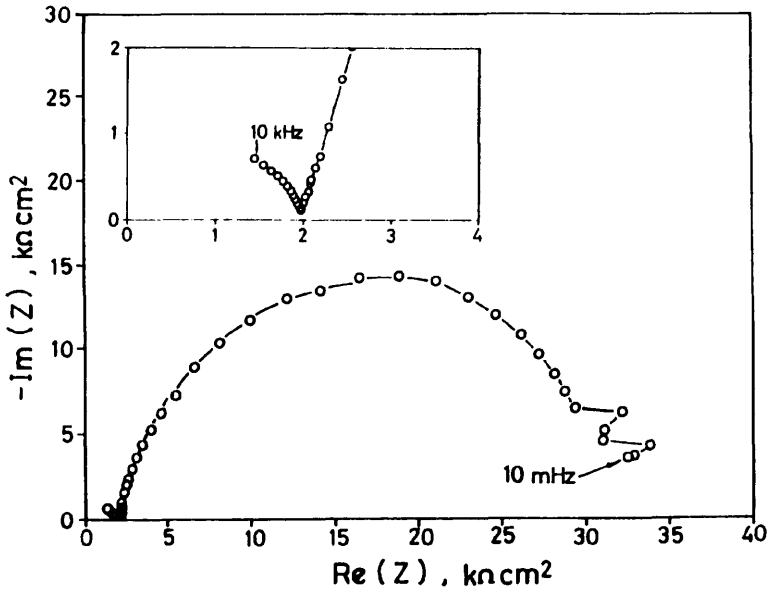

Figure 6-18 The result of a.c. impedance measurement on iron covered by 568 μm thick electrolyte layer (10^{-4} M Na_2SO_4).

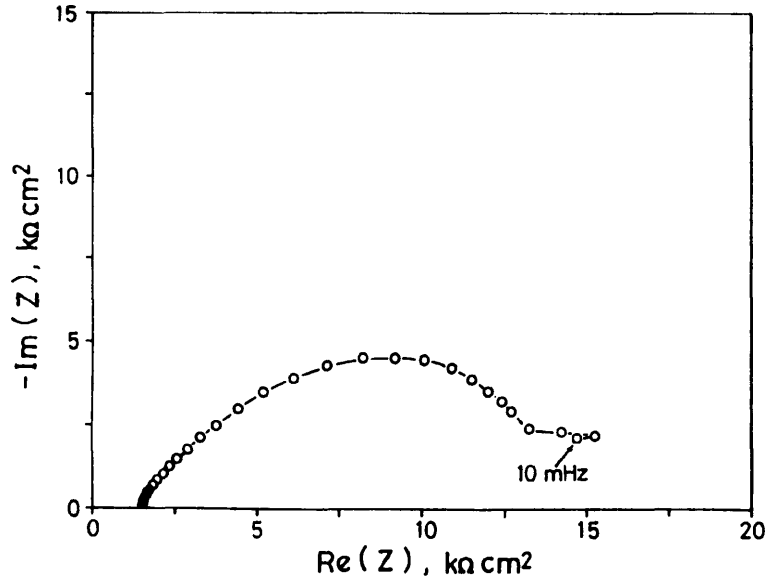

Figure 6-19 The result of a.c. impedance measurement on iron covered by 818 μm thick electrolyte layer (10^{-4} M Na_2SO_4).

high frequency perturbation decrease with increasing thickness of the electrolyte layer on the iron surface. Thus, when the thickness increases, e.g. 818 μm, the semi-circle in the high frequency area of the impedance spectra merged and just one semi-circle was revealed on the impedance plot (Fig.6-19). The optical microscopy examination on the iron surface after each experiment showed that the iron surface remained bright with electrolyte layers below 568 μm while slight pitting occurred on the iron when the thickness of electrolyte layer was increased to 818 μm.

In interpreting these results represented in Fig. 6-16 to Fig. 6-19, two aspects which may exist in these A.C. impedance responses simultaneously, must be examined in detail. In the case where the layers of electrolyte were relatively thin ($< 568\ \mu$m), the values of the real part of the impedance data at a very low frequency ($\omega \rightarrow 0$) were more than 30 kΩ.cm^2. These high values of impedance can be explained in terms of passivation of iron in these situations, which has been verified by visual examination of a bright pit-free surface. A facile interpretation of the high frequency semi-circle, whose diameter increases with a decrease in thickness of the electrolyte layers, is that it is characteristic of the passive oxide film. On the other hand, when the thickness of electrolyte layers was decreased, the current distribution will also be changed significantly for the given experimental set-up. This implies that the first time constant, clearly depending on the thickness of the electrolyte layer, may also be produced by a changing current distribution.

In order to identify the effect of changed current distribution caused by changing the thickness of the electrolyte on the impedance data, a supplemental experiment was performed using the same configuration of the electrochemical cell as described previously in Fig.3-2, except that platinum electrodes, rather than iron electrodes, were used. In the solutions (10^{-4} M, 10^{-3} M Na_2SO_4, respectively) and at the open circuit potential,

platinum is likely to be oxide-free. Obviously, if the first time constants in the A.C. impedance data of the iron correspond to the response of an oxide film formed on the iron surface, these features should disappear in the A.C. impedance spectra of the platinum. The results of A.C. impedance measurements of platinum covered by various thickness of electrolyte layers (thickness from 112 μm to 1248 μm , 10^{-4} - 10^{-3} M Na_2SO_4) are shown in Fig.6-20 and Fig.6-21. In the case of thin layers of dilute solution (10^{-4} M Na_2SO_4, thickness from 130 - 809 μm), the A.C. impedance plots in Fig.6-20, similar to that of iron covered with the same electrolyte layers, are composed of two parts, one semi-circle in the high frequency region, whose diameter clearly depends on the thickness of the solution layers, and the other part in a relatively low frequency zone of the impedance spectra, whose features are obviously independent of the thickness of the solution layer. In contrast, when the concentration of solution was increased to 10^{-3} M Na_2SO_4, the high-frequency semi-circles (Fig. 6-21) disappear, while the low frequency regions shows nearly the same trends as described in Fig.6-20, irrespective of the thickness of the solution layer. As the effect of changes in the concentration of solution on the A.C. impedance results obtained is mainly in regard to the current distribution on inert (Pt) electrodes and largely affect the high frequency portion characteristic of the A.C. impedance[112,113], therefore, according to the above discussion and the comparison between Fig.6-20 and Fig.6-21, it is presumed that the high frequency semi-circles in Fig.6-20, when the dilute solution was used, may arise from a response produced by non-uniform current distribution. Thus, by analogy, when the results of A.C. impedance measurements in Fig.6-16 and Fig.6-19 are examined, one cannot rule out the possibility of the effects of non-uniform current distribution, particularly when dilute electrolyte is used.

Although the effects of non-uniform distribution on the A.C. impedance results may

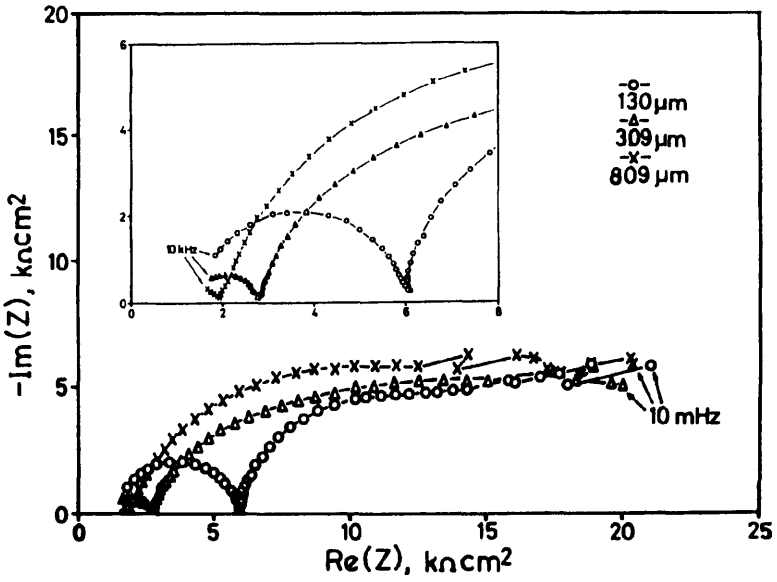

Figure 6-20 The results of a.c. impedance measurements on platinum covered by 130, 309 and 809 μm thick electrolyte layers (10^{-4} M Na_2SO_4), respectively.

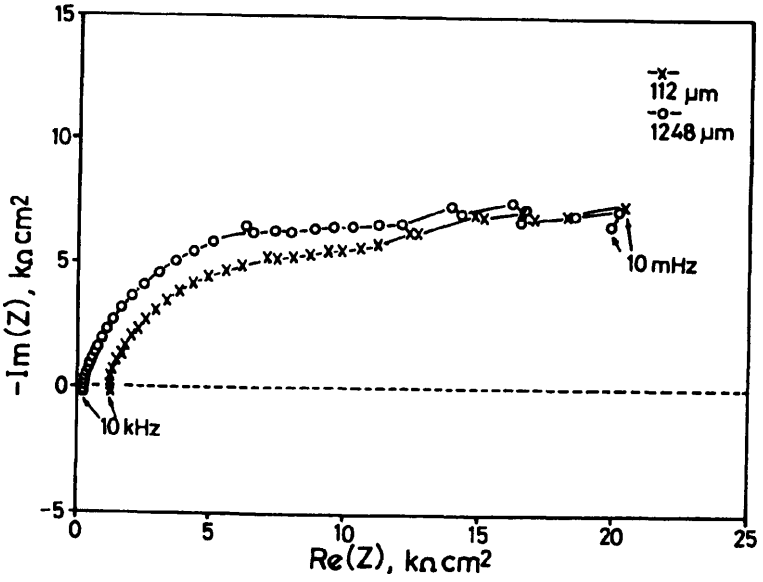

Figure 6-21 The results of a.c. impedance measurements on platinum covered by 112 and 1248 μm thick electrolyte layers (10^{-3} M Na_2SO_4), respectively.

exist, it is still appropriate to produce an equivalent circuit model to simulate the impedance results obtained, and this was done by using a computer program for equivalent circuit simulation in electrochemical system[153]. The resulting equivalent circuit model, composed of capacitances and resistances, is shown in Fig.6-22, where R_s represents the extrapolated high frequency intersect with the real axis; R_h, the resistance of the high frequency semi-circle; the C_h, the capacitance of the high frequency semi-circle; C_d and R_t, the double layer capacitance and change transfer resistance respectively. The definition of R_p will be discussed later in this section. The derived values of R_s, R_h, C_h, R_t, C_d, R_p are tabulated in Table 6-2.

Table 6-2.* Values of R_s R_h , C_h , R_t , C_d , and R_p of impedance spectra for iron covered with various thicknesses of 10^{-4} M Na_2SO_4 layers.

Thickness (μm)	R_s ($\Omega.cm^2$)	R_h ($k\Omega.cm^2$)	C_h ($\mu F.cm^{-2}$)	R_t ($k\Omega.cm^2$)	C_d ($\mu F.cm^{-2}$)	R_p ($k\Omega.cm^2$)
101	1016	10.67	0.014	22.53	32.492	34.22
282	231	3.29	0.068	28.89	17.254	32.41
568	-31	2.09	0.029	29.66	23.655	31.72
818	1572			13.30	11.76	

* N.B. Due to the application of the two electrode method, the above values are referred to that of the total electrochemical cell. The values of resistance and capacitance for individual electrode can be calculated by the following relations: $R_{individual} = 0.5\ R_{cell}$ and $C_{individual} = 2\ C_{cell}$.

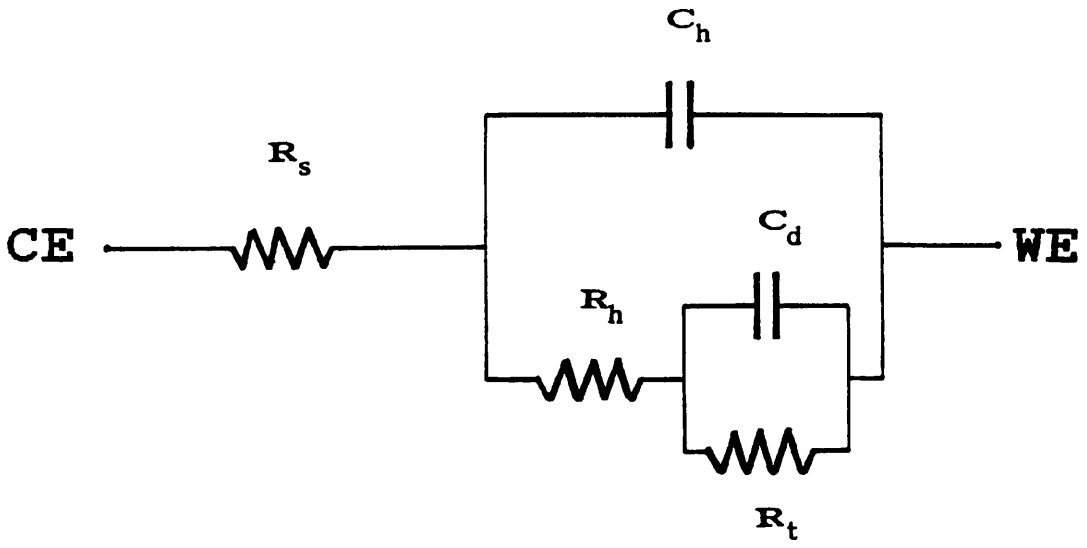

Figure 6-22 The equivalent circuit model to simulate the impedance results

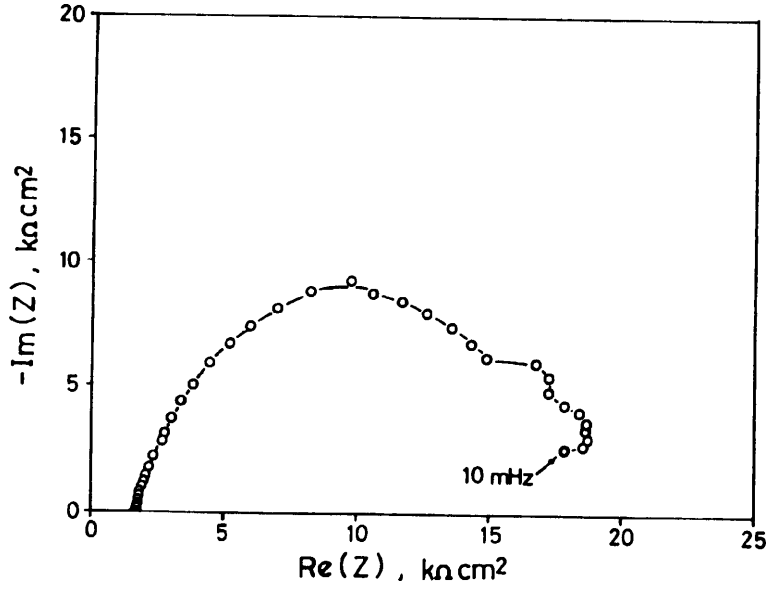

Figure 6-23 The result of a.c. impedance measurement on iron covered by 123 μm thick electrolyte layer (10^{-3} M Na_2SO_4).

With regard to the values of R_s in Table 6-2, if R_s is really the solution resistance between the two electrodes, it should have a linear relationship with the reciprocal of the thickness of solution. However, the values of R_s in Table 6-2 do not exhibit such a relation (see next section). This deviation may arise from the effects of non-uniform distribution of current on the sample. Thus, R_s, C_h and R_h in this equivalent circuit model could be interpreted as due to the geometric effect of non-uniform current distribution on the electrode, produced by reduction of the concentration and the thickness of electrolyte layer being used. However, the values of R_h, C_h in Table 6-2 do seem to be appropriate to the response of oxide films on the iron.

Now, the problem appears to be how to identify the polarization resistance R_p, related to the total corrosion rate of the sample, from the A.C. impedance results obtained. Judging from the values of R_t concerned, when the thickness of electrolyte layers is below 568 μm, the system remains in a stable passive state, identified by the relatively larger R_t values ranging from 22.53 kΩ.cm^2 (thickness 101 μm) to 29.66 kΩ.cm^2 (thickness 568 μm). In the case of thickness of electrolyte layer being 818 μm, slight pitting had developed and this behaviour is revealed by the sharp decrease of relevant R_t, to 13.30 kΩ.cm^2 in this situation. However, estimations of R_p by taking values of R_t are questionable, by considering that the values of R_t are slightly increased with increase in thickness of electrolyte, which disagrees with increased stability of passivation for the iron in thinner electrolytes (referred to Chapter 5). Thus, in this situation, it seems to be more reasonable to use the following definition of the polarization resistance to determine the total corrosion behaviour[154]

$$R_p = \lim_{\omega \to 0} R_e\{Z_f\}$$

where $Re\{Z_f\}$ denotes the real part of the complex faradaic impedance Z_f and ω

corresponds to the frequency of the A.C. signal ($\omega = 2\pi f$). The values of R_p, determined in this way are shown in Table 6-2. The magnitudes of R_p slightly decrease with increase in thickness of dilute electrolyte layers, although the iron retains its passivity, as long as the thickness of the electrolyte layers remain below a certain value (e.g. 568 μm).

Figure 6-23 and Figure 6-24 give the results of a.c. impedance spectra for iron covered by thin layers of 10^{-3} M Na_2SO_4 electrolyte, thicknesses being 123 μm and 1188 μm respectively. Due to the increased aggressiveness of the environment by increasing concentration of SO_4^{2-} to 10^{-3} M, passivation is difficult to produce and pitting is the dominant phenomena in this situation. However, the change in thickness of electrolyte layer on the surface has a great effect on the severity and sensitivity to the pitting. It was found that when the electrolyte layer thickness was decreased the severity and sensitivity to pitting were also reduced, verified by the R_p values calculated from a.c. impedance results and microscopy examination after experiments. In the case of iron covered with thinner electrolyte layers (thickness 123 μm), the R_p value obtained from Figure 6-23 can approach 18.78 kΩ.cm^2, very close to the value (20 kΩ.cm^2) required for the establishment of passivation for normal electrochemical system, and just one pit was observed after the experiment. When the thickness of electrolyte layer increased (thickness 1188 μm), the R_p value from Figure 6-24 drops down to 1.5 kΩ.cm^2, more than ten times less compared with that of thinner electrolyte layer (in Figure 6-23). Microscopy examination showed that severe pitting had happened.

In this case, the severe pitting causes a heavily depressed semi-circle, instead of a normal semi-circle with its centre on the real resistance axis, to appear in the a.c. impedance spectra in Figure 6-24. This depressed semi-circle impedance spectra is best described by:[61]

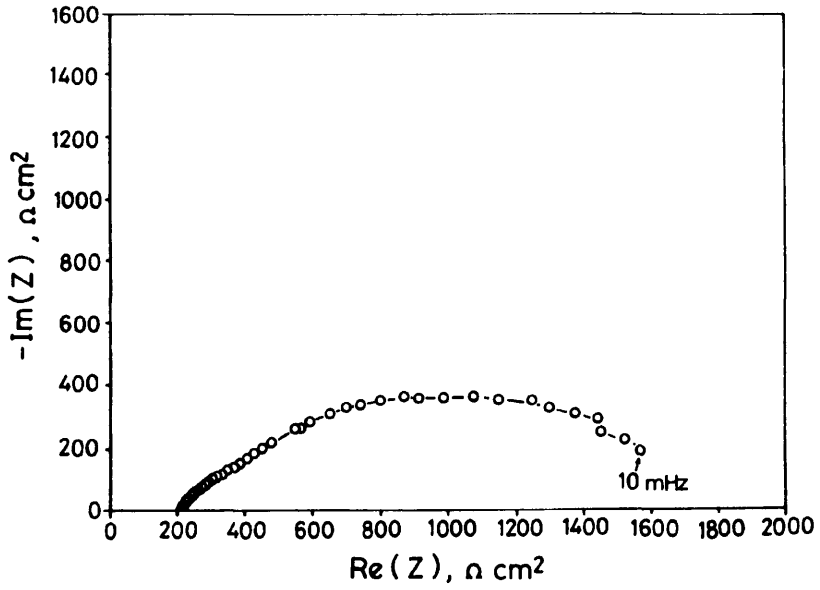

Figure 6-24 The result of a.c. impedance measurement on iron covered by 1188 μm thick electrolyte layer (10^{-3} M Na_2SO_4).

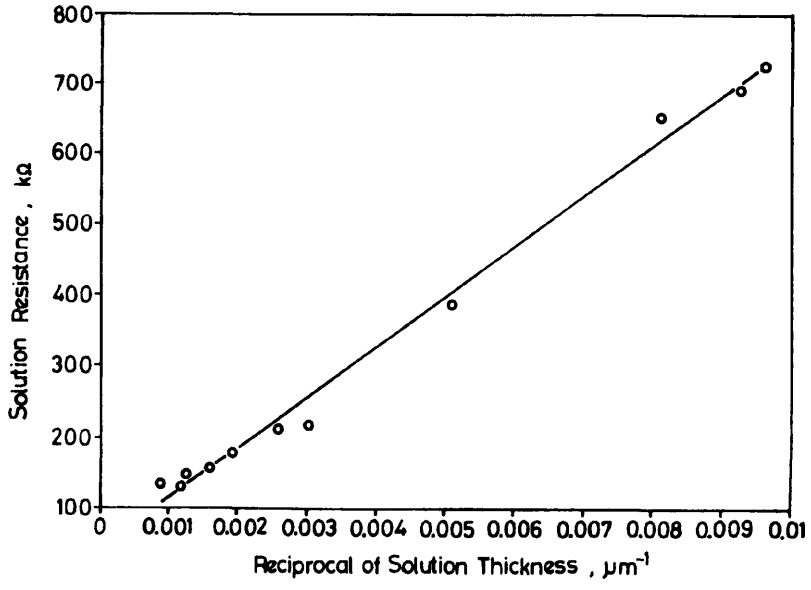

Figure 6-25 The relationship between the solution resistance and reciprocal of the electrolyte thickness (10^{-3} M Na_2SO_4).

$$Z = R_s + \frac{R_p}{1 + (j\omega\tau)^{\beta}}$$

In this equation, the phenomenological term $(j\omega\tau)^{\beta}$ replaces the $j\omega R_pC$ for the case when $\beta < 1$. In normal condition, $\beta = 1, \tau = R_pC$. Two explanations have been offered to this unique behaviour. The depression may be caused by increased surface roughness or by geometrical effects leading to a nonuniform repartioning of the current density on the surface[62].

According to the above discussion, the results obtained by a.c. impedance measurements agree very well with that discussed in the anodic polarization curves section obtained in Chapter 5. As in the a.c. impedance technique a small signal is used to disturb the system, the results were obtained in the vicinity of corrosion potential. Therefore the results are more close to that of real conditions.

Thus, in normal conditions with a very dilute electrolyte layer covering bare iron, passivation is a dominant phenomena, indicated by both anodic polarization measurements and now confirmed by the A.C. impedance measurements. However, A.C. impedance results obtained indicate more detailed changes of passive stability for iron with the change of thickness and composition of electrolyte layers on the surface. The establishment of the passivation for iron depends on the concentration of SO_4^{2-} and supply of O_2 to the surface of iron, affected by the electrolyte layer thickness on the surface.

6.3.3.2 Ohmic Resistance Polarization

Generally speaking, in a corrosion cell with a specific electromotive force the total corrosion rate is controlled either by the cathodic polarization, anodic polarization or

ohmic resistance polarization, which is caused by current flowing through a poor conductivity electrolyte path between the anode and cathode. Due to the fact that most atmospheric corrosion of metals happens in a thin, poor conductivity electrolyte layer, it is understandable to suppose that the corrosion rate of metals in atmospheric corrosion may be controlled by the ohmic resistance polarization, which is greatly affected by the conductivity and the thickness of the electrolyte on the surface.

In practice, the determination of the ohmic potential drop caused by dilute electrolytes in atmospheric corrosion is difficult because the geometry and the distribution of anode and cathode in microcells are not known. Here, a effort is made to explain the role of ohmic resistance in atmospheric corrosion on the basis of the a.c. impedance results in this paper.

It is assumed that in atmospheric corrosion a small anode (with radius r_1) is surrounded by a number of small cathodes in a circular distribution (with radius r_2). The resistance between a central anode and an annular cathode covered by a film of electrolyte can be estimated by the formula for the resistance between two coaxial cylindric electrodes:[122,125]

$$R=(2\pi\lambda\delta)^{-1}\ln\frac{r_2}{r_1}$$

where λ is the conductivity of the electrolyte; δ the height of the cylinder (in the present case thickness of electrolyte); r_1 the radius of the internal cylinder (in the present case the radius a central anode); r_2 the radius of the external cylinder (in the present case the radius of the annular cathode).

Although the value of R increases with decreasing anode radius, in practice when the radius of the anode is decreased, the radius of surrounding cathodes should be reduced at the same time because of the potential drop due to the electrical field distribution. Thus,

the radio of r_2 to r_1 should remain nearly constant. So the predicted resistance between electrodes has a reciprocal relation with electrolyte layer thickness.

Figure 6-25 shows the measured relationship between electrolyte resistance R between the two electrodes and the reciprocal of the electrolyte layer thickness. This result was obtained by a.c. impedance measurement carried out on the planar two electrodes (dia.0.5mm and distance 2.8 mm) sample covered with a thin layer electrolyte (10^{-3} M Na_2SO_4), which is not an identical situation to the proposed model. The electrolyte resistance R was determined by the value of the extrapolated intercept at the high frequency limit of the a.c. impedance curve with the real axis. It is clear from Figure 6-25 that a good relation of electrolyte resistance and reciprocal of electrolyte layer thickness can be observed as expected and discussed above.

Concerning the cathodic polarization share in atmospheric corrosion, Rozenfeld[5], by measuring the curves of potential distribution over the surface of the corrosion cell with different metal couples and surface area ratio, found that both in the bulk and in thin electrolyte films the initial potential difference essentially overcomes the cathodic potential resistance. The potential drop due to the anodic polarization resistance is 1.5-4.5 percent and the ohmic potential drop equalled only 2 percent in a 70 μm electrolyte film. Therefore, he concluded that in the case of atmospheric corrosion where the metal is covered with a visible electrolyte layer, the corrosion is mainly controlled by the cathodic process of oxygen reduction.

However, by considering the limited current density of oxygen reduction in thin electrolyte layers (620 $\mu A\ cm^{-2}$ for a layer thickness of 30 μm[5]) and corrosion rates found experimentally in long term corrosion investigation (0.02 g $m^{-2}\ h^{-1}$ (1.9 $\mu A\ cm^{-2}$) to approximately 0.1 g $m^{-2}\ h^{-1}$ (9.5 $\mu A\ cm^{-2}$) and exceptionally 0.5 g $m^{-2}\ h^{-1}$ (47.5 $\mu A\ cm^{-}$

$^{2)}$[39]), Barton[10] pointed out that everything thus seems to indicate that atmospheric corrosion is in no way controlled by the cathodic oxygen reduction process.

In fact, due to the large specific surface area of rust layers (51 m^2 g^{-1} rust[41]), the cathodic processes of oxygen reduction on the rusted sample can be increased significantly. M. Stratmann and H. Streekel[119] reported that the cathodic current density of oxygen reduction (consumption of oxygen) can reach as high as about 1000 μA cm^{-2}, during the critical wet to dry transition period on the rusted sample.

In Chapter 4, the cathodic process of oxygen reduction was studied by decreasing the thickness of electrolyte layer on the sample. The result showed that the maximum current density of oxygen reduction on the surface of fresh sample is about 560 μA cm^{-2}. In normal conditions, very stable self-passivation of iron covered with fairly thin electrolyte layer can be produced with a very small passive current density (4-7 μA cm^{-2} in Fig.5-2). Even when the thickness of electrolyte layer is thicker, e.g. 600 μm, about 70 μA cm^{-2} current density is enough to cause the iron to passivate[5]. Therefore, the cathodic current density of oxygen reduction is enough to balance the requisition of the current for sustaining the anodic process. It appears to be impossible for the corrosion process to be controlled by cathodic processes in normal atmospheric environment.

Additionally, the A.C. impedance results discussed above show that there is no feature characteristic of diffusion; e.g. a straight line existing in the low frequency region, which is related to the diffusion process of electroactive species in the electrolyte layer-the Warburg impedance. This indicates that the electrochemical processes occurring in the thin film electrolyte electrochemical cell are in no way controlled by the diffusion process of certain species.

In determining the contribution of ohmic resistance polarization in the total polarization

occurring on the sample covered with thin electrolyte film, two planar electrodes were used. In this system, two electrodes were separated by a certain distance with one assumed to act as anode and the other as cathode. The polarization on one electrode (e.g. the cathode) can be neglected due to the fact that cathodic polarization is not significant in normal atmospheric corrosion condition as discussed above. The polarization on the other electrode (e.g. the anode), which was identified by A.C. impedance measurement, is supposed to be caused mainly by the anodic polarization due to the passivation of the sample. The ohmic resistance is considered as the resistance of electrolyte between two electrodes, which is bigger than that of the real micro-corrosion-cell since a point cathodic electrode was used to simulate the ring cathodic electrode. Hence, the percentage of Rs in total polarization resistance can be calculated by using following equation:

$$R_s\% = \frac{R_s}{\frac{1}{2}R_{cell} + R_s}$$

where R_s is the resistance of electrolyte path between two electrodes; 0.5 R_{cell} the polarization resistance of individual electrode in two electrodes system; R_{cell}, the polarization resistance of same two electrodes system.

In the 10^{-3} M Na_2SO_4 solution, the above equation and the a.c. impedance results in Fig.6-23 and Fig.6-24 show that when the thickness of electrolyte layer is 123 μm where R_{cell} is 18.78 kΩ cm^2; the resistance of electrolyte path between two electrodes, referred as R_s in the above equation, is 1.678 kΩ cm^2, the ohmic resistance is about 15.16% and that this value increases to 21.55% with an electrolyte thickness of 1188 μm, where R_{cell} is 1.562 kΩ cm^2 and R_s is 214.6 Ω cm^2. It is interesting to note that as the electrolyte layer thins, the percentage of ohmic resistance in the total polarization resistance reduces. This phenomenon can be explained by the fact that although the ohmic resistance increases as

the electrolyte layer thins, however, at the same time, the anodic polarization also increases due to the favourable conditions for passivation. In contrast, with thicker electrolytes (e.g. 1188 μm) where active corrosion or pitting is likely, leading to the decrease of anodic polarization, the percentage of ohmic resistance contributed to the total cell resistance increases.

The question arises to what extent this result can be extended to the real micro-corrosion cell in normal atmospheric corrosion. This question is considered by the following aspects:

It was reported that[5,6] the radius of microcells is usually within 10^{-4} to 10^{-5} cm, and is same order of magnitude of electrode separation distance. The ratio of electrode separation distance to radius is about 1. In this experiment mentioned above this ratio is about 5.6 (2.8/0.5). On the other hand, in real corrosion cells the anode is surrounded by numerous small cathodes, while in the experiment only two electrodes are used, which implies that the real solution resistance is likely to be smaller than that calculated by this two electrode method. Finally, the above calculation for ohmic resistance percentage just includes the one electrode polarization (e.g. anode), ignoring the polarization happening on the other electrode (e.g. cathode). Therefore, the percentage of ohmic resistance calculated above is probably a maximum compared with realistic corrosion cells. So the ohmic resistance polarization is not very significant in the initial stages of atmospheric corrosion of bare iron. The corrosion rate is mainly controlled by the anodic process, the passivation of the material.

6.3.4 Summary

(1) The results of A.C. impedance obtained in this investigation confirm the result reported in Chapter 5. In many cases, at least in the condition of thin layer of electrolyte 10^{-4} M Na_2SO_4, the passivation is a prevalent phenomenon.

(2) The initial process of atmospheric corrosion for iron is the establishment of passivation. The establishment of initial passivation depends on the composition, concentration, and thickness of the electrolyte layer on iron.

(3) The anodic process in atmospheric corrosion of iron during initial stages is the predominant controlling process. The ohmic resistance polarization is not very significant on bare iron, even with relatively thin films of electrolyte.

CHAPTER 7
RETENTION OF PASSIVITY ON SELECTED IRON SAMPLES AFTER SEVERAL MONTHS ATMOSPHERIC EXPOSURE

CHAPTER 7 RETENTION OF PASSIVITY ON SELECTED IRON SAMPLES AFTER SEVERAL MONTHS ATMOSPHERIC EXPOSURE

7.1 Introduction

The original aim of the atmospheric exposures described herein were to prepare a natural rust film in order to investigate its electrochemical behaviour in-situ. When several electrodes refused to corrode after 4 months the exposure was repeated to confirm the effect. This chapter reports the observations made and provides a comment on likely reasons.

Samples of iron were exposed during 1993 in two batches; firstly over the summer and early autumn, and also during the winter and early spring periods. In each case, and as intended, a large majority of the samples were covered in thick adherent corrosion product "rust" after the end of the exposure period. However, and unexpectedly, a few samples from each batch remained visually uncorroded remaining their original bright appearance. This observation is presented as an interesting insight into, and as supporting evidence for, mechanisms of atmospheric corrosion of iron involving passivation.

7.2 Experimental

High purity iron (99.99%) was obtained from Goodfellow Metals in the form of wire 0.5 mm in diameter. Short lengths of this wire were then used to prepare semi-micro electrodes, initially for atmosphere exposure but ultimately for electrochemical measurements, as follows. Each cut section was initially coated over its length using a thin

layer of epoxy adhesive; this was done to avoid subsequent crevicing of the electrode. After curing for 48 hours at 25 °C, the wires were then mounted in standard metallographic moulds using an epoxy resin. After full curing, the electrodes were polished to 800 grit on SiC paper, dried and stored in a desiccator prior to exposure.

An initial batch of ten samples was prepared and exposed for 4 months commencing on June 1st, 1993. Subsequently, a further batch of sixteen samples was prepared and placed outdoors for 3 months commencing February 20th, 1994. Samples were thus exposed outdoors, unsheltered and in a garden environment, over the summer and early autumn periods as well as (separately) during the winter and early spring. The weather was typical of Manchester for the time of year; i.e. generally cool and damp. After exposure, the sample was removed from the exposure site on a dry day, dusted with a soft artists' brush, and stored in a desiccator over dry silica gel prior to photography.

7.3 Observation and Discussion

Examination of the first batch, i.e. that exposed for 4 months during the summer and early autumn, indicated that one of the samples was visually uncorroded (bright). All the other samples in this batch were corroded to a similar degree. As this was such an unexpected occurrence, this first observation was initially discounted and the specific sample discarded. Nevertheless, a second batch of samples was exposed and examined at more frequent intervals in case the phenomena repeated and , if so, to obtained an estimate of the onset of corrosion. Thus, after 3 months, two (out of sixteen) samples remained apparently uncorroded (bright) with the balance corroded as expected.

This information is summarized below:

Exposure time	No. corroded	No. uncorroded
1 weeks	4	12
4 weeks	13	3
8 weeks	14	2
12 weeks	14	2

Figure 7-1 and Figure 7-2 show, respectively, low magnification images of a corroded (i.e. rusty) and an apparently uncorroded (i.e. bright) sample after the 4 month exposure period. Figure 7-3 shows the other bright sample at higher magnification. The bright samples all show scratches from the initial grinding. On close inspection in can be seen that the "bright" samples do, in fact, have evidence of corrosion product on their surfaces. Thus, in Figure 3, very small, darker areas on the surface can be seen although, to the naked eye, they could not be discerned. About 20-30% of the surfaces of the two bright samples were slightly darkened in this way, with 70-80% completely of the surface completely bright.

That bare, untreated iron remains largely uncorroded and passive for several months in a wet Northern climate is a remarkable result. The reasons for the observations can only be speculative at this stage. In particular, the small size of the exposed area is clearly important as a macroscopic surface could be normally expected to develop a visible patina of rust in a few hours or days depending on the weather. Another factor is the relatively high purity of the iron which limits the presence of second phase particles, especially sulphide. A third reason may well be the wire form of the metal as heavy drawing will tend to reduce the dimensions of secondary phase particles and string them out. Finally, the smaller exposed area of the sample may reduce the possibility of contamination of

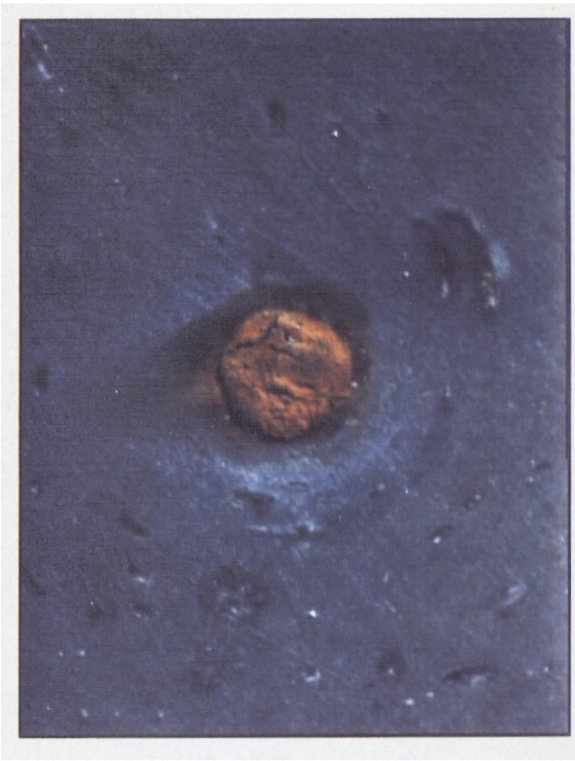

Figure 7-1 Low magnification image of a corroded sample after 4 months exposure period.

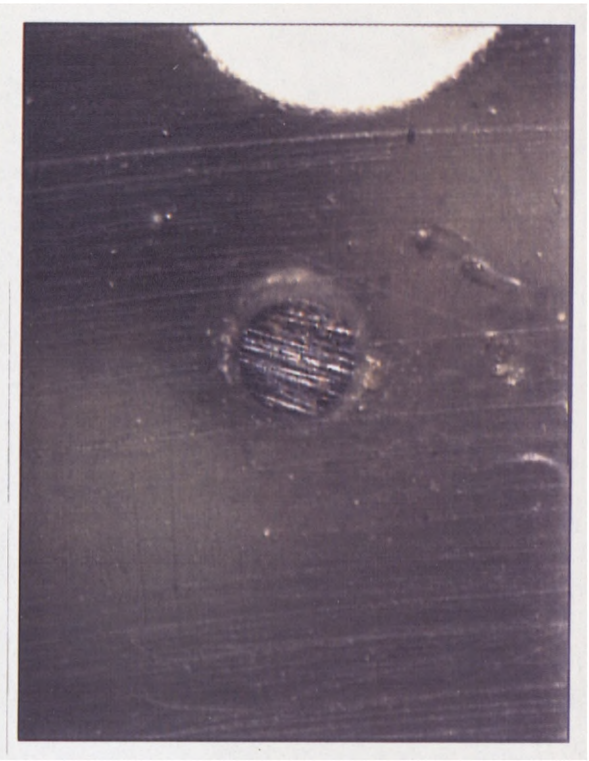

Figure 7-2 Low magnification image of an apparently uncorroded sample after 4 months exposure period.

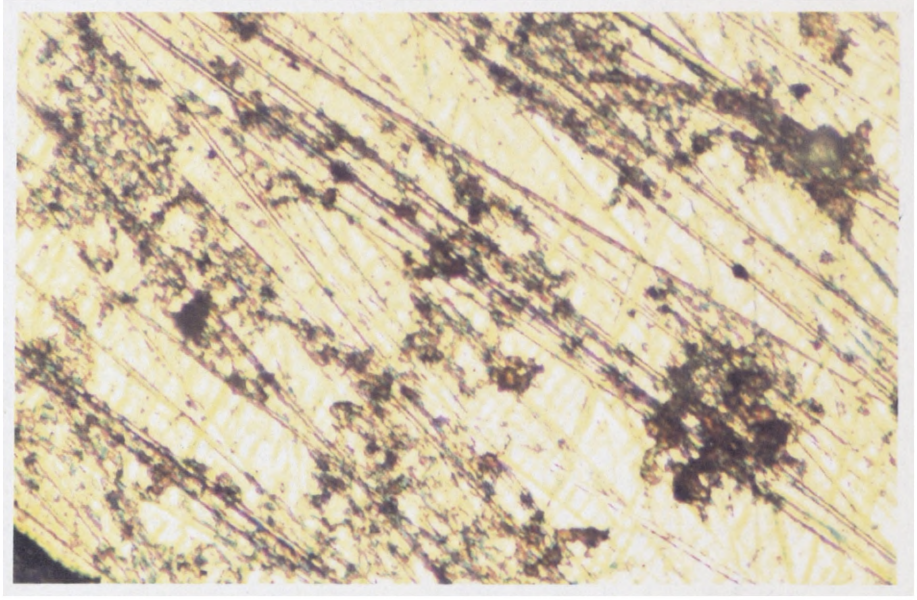

Figure 7-3 Higher magnification image of the other bright sample after 4 months exposure period.

dusts on the surface, which will easily induce the corrosion.

Whatever the reason, this observation is strong evidence that the corrosion on iron and steel in the atmosphere proceeds by disruption of an initially passive film and that the film is repairable under conditions of atmospheric exposure.

7.4 Summary

About 10-14% of high purity small diameter iron wire samples, exposed to the atmosphere for period of up to 4 months, remain uncorroded. This retained passivity is evidence that atmospheric corrosion on iron proceeds by disruption of a passive film and, under normal conditions, the film is normally self-repairing.

CHAPTER 8
CONCLUSIONS AND SUGGESTIONS

CHAPTER 8 CONCLUSIONS AND SUGGESTIONS

8.1 Conclusions

8.1.1 Mechanisms of Atmospheric Corrosion

(1) In relation to the maximum limiting oxygen reduction current (2070 $\mu A/cm^2$) obtained in this investigation and the maximum anodic current (about 1000 $\mu A/cm^2$) which may occur during wet/dry transitions, attained in the research work by Stratmann et al[119], the cathodic reduction current is more than enough to balance the current required to sustain the anodic process. From this point of view, it is impossible for atmospheric corrosion processes to be generally controlled by slowing of the cathodic process.

(2) It is reasonable to suggest that in many cases, at least in the condition of thin layer of electrolyte 10^{-4} M Na_2SO_4, passivation is a prevalent phenomenon. Therefore, the initial process of atmospheric corrosion for iron is the establishment of passivation. The establishment of initial passivation depends on the composition, concentration, and thickness of the electrolyte layer on iron. In normal conditions, atmospheric corrosion for iron happens in alternative passive and active stages, with the changes of wet/dry conditions on the surface of iron.

(3) Long-term corrosion rates on iron (22.5-112.3 μm/year) are equivalent to an average current density of 1.9-9.5 $\mu A\ cm^{-2}$, consistent with the passive current densities observed in this study.

(4) Even in a relatively high concentrated electrolyte (0.1 M Na_2SO_4), passivity of iron is still the dominant anodic process. The passive properties of iron covered with

concentrated electrolyte layers are significantly affected by the thickness of electrolytes.

(5) The beneficial effect of alloying element Cu on the protective properties of weathering steel in atmospheric corrosion is mainly on the anodic processes, e.g. enhancing the passivity of iron by accumulated Cu on the surface during long time exposure.

(6) The anodic process in atmospheric corrosion of iron during initial stages is the predominant controlling process. The ohmic resistance polarization caused by the thin electrolyte film between anode and cathode is not very significant on bare iron, even with relatively thin films of electrolyte.

(7) About 10-14% of high purity iron wire samples, exposed to the atmosphere for period of up to 4 months, remain uncorroded. This retained passivity is evidence that atmospheric corrosion on iron proceeds by disruption of a passive film and, under normal conditions, the film is normally self-repairing.

(8) The thin electrolyte film is composed of the convective and the diffusive parts. The convective layer occupies the major part of the film. Although the thickness of electrolyte layers is smaller than that of the diffusion layer of the bulk electrolyte, The transfer of oxygen through a thin electrolyte layer is significantly enhanced by the convective action occurring in the thin electrolyte film.

(9) The reduction of rust components (at potential - 0.9 V(SCE)) is possible on the surface of pre-corroded iron covered with a thin film of electrolyte. The reduced rust components can be re-oxidized by oxygen in air when the surface of pre-corroded sample is dry.

8.1.2 Methodology

(1) Currently, the electrochemical cell used here was is successful and suitable for the study of thin film electrolyte electrochemistry, in respect of effects due to the kind of materials and the environmental factors including the thickness of electrolyte layers, the concentration of oxygen and the evaporation process.

(2) Cells with a smaller diameter electrode (0.5 mm diameter) was found to be more suitable for the study of thin film electrolyte electrochemistry in terms of the uniformity of current distribution on the surface of the electrode.

(3) It must be understood that a.c. impedance measurements by conventional three electrode potentiostatic method in high impedance systems, like coatings, anodic films of aluminium, concretes, high purity water and organic solutions, are easily affected by artifacts, such as the interference of reference electrode, qualities of the instrumentation and the values of counter resistance. Convincing explanation of the results depends on: (a) a full understanding of the limitation of the instrumentation, (b) confirmation that the data produced comes from the response of the electrochemical system, instead of the instrumentation, (c) it is important that repeated data can be obtained using a dummy cell produced by simulating the results of a.c. impedance obtained on real electrochemical system.

(4) The galvanostatic method with two electrode system is better than the potentiostatic method in the measurement of high resistance systems in terms of the stability of the system and the accuracy of the results.

8.1.3 Data

(1) The maximum cathodic reduction current of oxygen on iron (diameter 0.5 mm) covered with 0.1 M Na_2SO_4 electrolyte layer during evaporation can reach up to 2070 $\mu A/cm^2$.

8.2 Suggestions

(1) Using the two-electrode system designed and produced in this investigation, a.c. impedance measurements on iron can be carried out either outdoors or in controlled laboratory conditions (controlled parameters including the concentration of SO_2 and relative humidity). The final purpose is in developing this electrochemical cell into an atmospheric corrosion monitor. The success of this development depends on the further reduction of electrode size, the avoidance of crevice corrosion and the reduction of distance between the two electrodes.

(2) Anodic polarization measurements of weathering steel (electrode size < 0.5 mm in diameter) in thin layer of electrolytes (10^{-4} to 10^{-1} M Na_2SO_4).

(3) Anodic polarization measurements of copper-deposited iron in thin layer electrolytes (10^{-4} to 10^{-1} M Na_2SO_4) to find the relationship between the anodic properties and the different copper-deposition time (quantity of copper on the surface).

(4) Cathodic polarization measurement of micro-electrode (< 500 μm in diameter) in thin layer electrolyte (10^{-4} to 10^{-1} M Na_2SO_4) to find the maximum oxygen reduction current.

(5) Detailed study of the cathodic process on pre-corroded samples and bare iron

samples (for comparison), e.g. the reduction of a pre-corroded sample at different potentials under different thin films of electrolytes (10^{-4} to 10^{-1} M Na_2SO_4).

(6) Galvanostatic current measurements between bare iron and rusts under thin layer electrolyte conditions.

(7) Anodic polarization measurements on pre-corroded sample in thin layer electrolytes (10^{-4} to 10^{-1} M Na_2SO_4) to study the re-passivation of rusted samples.

(8) A.C. impedance measurements of two pre-corroded electrode system to find the redox reactions of rusts at the corrosion potential condition.

REFERENCES

REFERENCES

(1) J.C. Hudson, The Corrosion of Iron and Steel, Chapman & Hall Ltd, London (1940)

(2) Testing in Natural Atmospheres, Corrosion in Natural Environments, ASTM STP 558, 1974

(3) Atmospheric Factors Affecting the Corrosion of Engineering Metals, ASTM STP 646, S.K. Coburn, Ed., 1978

(4) F. Mansfeld, J.V. Kenkel, Corros. Sci., **16**, 111(1976)

(5) I.L. Rozenfeld, Proc. 1st Int. Cong. on Metallic Corrosion, London, Butterworths, 243(1961)

(6) I.L. Rozenfeld, Atmospheric Corrosion of Metals, NACE, Houston, Texas 1972

(7) Report of the Committee on Corrosion and Protection, A Survey of Corrosion and Protection in the U.K., Chairman, T.P. Hoar, H.M.S.O., London, (1971)

(8) L.H. Bennett, J. Kruger, R.L. Parker et al., Economic Effects of Metallic Corrosion in the United States, Report NBS SP 511-1, National Bureau of Standards, Washington DC (1978)

(9) J.H. Payer, D.G. Dippold, W.K. Boyd, et al., Economic Effects of Metallic Corrosion in the United States, Report NBS SP 511-2, National Bureau of Standards, Washington DC (1978)

(10) K. Barton, Protection Against Atmospheric Corrosion: Theories and Methods, John Wiley and Sons, London (1976)

(11) H.H. Uhlig, Corrosion, **6**, 29(1950)

(12) K. Daeves and K. Trapp, Stahl und Eisen, **59**, 169(1937)

(13) M.G. Fontana, Corrosion Engineering, McGraw-Hill Book Company, pp.372(1987)

(14) A. Cox, Ph.D Thesis, UMIST, pp.2(1991)

(15) Corrosion: Industrial Problems, Treatment and Control Techniques, Proc. of 1st Arabian Conf. on Corros., V. Ashworth, Ed., Pergamon Press, Kuwait, pp.17(1984)

(16) D. Knotkova-Cermakova, K. Barton, "Corrosion Aggressivity of Atmospheres (Derivation and Classification)," Atmospheric Corrosion of Metals, ASTM STP 767, S.W. Dean, Jr., and E.C. Rhea, Eds., American Society for Testing and Materials, pp.225(1982)

(17) E.A. Baker, T.S. Lee, "Calibration of Atmospheric Corrosion Test Sites," Atmospheric Corrosion of Metals, ASTM STP 767, S.W. Dean, Jr., and E.C. Rhea, Eds., American Society for Testing and Materials, pp.250(1982)

(18) Physical Chemistry-Developing a Dynamic Curriculum, Eds. R. W. Schwenz and R. J. Moore, American Chemical Society, Washington DC pp.381(1993)

(19) G. Schikorr, Werkst. Korros., **14**, 69(1963); **15**, 457(1964); **18**, 514(1967)

(20) A. Kutzelnigg, Werkst. Korros., **8**, 492(1957)

(21) M. Eisenbud, Science, **170**, 706(1970)

(22) M. Manning, "Corrosion of Building Materials due to Atmospheric Pollution in the United Kingdom," Central Electricity Research Laboratories, C.E.G.B., Leatherhead, Surrey, (1987)

(23) F.L. LaQue, "Corrosion Testing," Proc. ASTM, 51, 495(1951)

(24) P.J. Sereda, "Weather Factors Affecting Corrosion of Metals," Corrosion in Natural Environment, ASTM STP 558, American Society for Testing and Materials, pp.7(1974)

(25) K. Barton, Werkst. Korros., **9**, 547(1958)

(26) W.H.J. Vernon, Trans. Faraday Soc., **31**, 1668(1935)

(27) P.J. Sereda, "Measurement of Surface Moisture and Sulphur Dioxide Activity at Corrosion Sites," ASTM Bulletin, American Society for Testing and Materials, No. 246, May 1960, pp.47

(28) P.J. Sereda, S.G. Croll and H.F. Slade, "Measurement of the Time of Wetness by Moisture Sensors and Their Calibration," Atmospheric Corrosion of Metals, ASTM STP 767, S.W. Dean, Jr., and E.C. Rhea, Eds., American Society for Testing and Materials, pp.267(1982)

(29) P.R. Grossman, "Investigation of Atmospheric Exposure Factors that Determine Time of Wetness of Outdoor Structures," Atmospheric Factors Affecting the Corrosion of Engineering Metals, ASTM STP 646, S.K. Coburn, Ed., American Society for Testing and Materials, pp.5(1978)

(30) F. Mansfeld, J. Electrochem. Soc., **135**, 1354(1988)

(31) J.A. Gonzalez, E. Otero, C. Cabanas and J.M. Bastidas, Br. Corros. J., **19**, 89(1984)

(32) D.K. Cermakova, J. Vlckova, Werkst, Korros., **21**, 16(1970)

(33) T.E. Graedel, J. Electrochem. Soc., **133**, 2476(1986)

(34) Corrosion volume 1 : Metal/Environment Reactions, L.L. Shreir, Ed., Newnes-Butterworth, pp.2:33(1976)

(35) H. Kaesche, Werkst. Korros., **15**, 379(1964)

(36) F.P. Bowden, W.R. Throssell, Proc. Roy. Soc. (A), **209**, 297(1951); Nature, **167**, 601(1951)

(37) K.A. Chandler, J.F. Stanners, Proc. Second Int. Cong. on Metallic Corros., New

York, NACE (1966), pp.325

(38) V.V. Skorchelletti, S.E. Tukachinskii, J. Appl. Chem., USSR, **26**, 27(1953)

(39) K. Barton and Z. Bartonva, Werkst. Korros., **21**, 85(1970)

(40) S.B. Lyon, C.W. Wong, P. Ajiboye, "An Approach to the Modelling of Atmospheric Corrosion," Atmospheric Corrosion, ASTM STP in press, W.W. Kirk and Herbert H. Lawson, Eds., American Society for Testing and Materials, Philadelphia, 1994

(41) M. Stratmann, K. Bohnenkamp and H.J. Engell, Corros. Sci., **23**, 969(1983)

(42) J.R. Duncan, D.J. Spedding, Corros. Sci., **14**, 241(1974)

(43) U.R. Evans and C.A.J. Taylor, Corros. Sci., **12**, 227(1972)

(44) M. Stratmann and H. Streckel, Corros. Sci., **30**, 697(1990)

(45) H.E. Townsend and J.C. Zoccola, "Eight-Years Atmospheric Corrosion Performance of Weathering Steel in Industrial, Rural, and Marine Environments," Atmopheric Corrosion of Metals, ASTM STP 767, S.W. Dean, Jr., and E.C. Rhea, Eds., American Society for Testing and Materials, pp.45(1982)

(46) D.K. Cermakova, J. Vlakova and J. Honzak, "Atmospheric Corrosion of Weathering Steels," Atmospheric Corrosion of Metals, ASTM STP 767, S.W. Dean, Jr., and E.C. Rhea, Eds., American Society for Testing and Materials, pp.7(1982)

(47) J.C. Hudson and J.F. Stanners, J. Appl. Chem., **3**, 86(1953)

(48) F.H. Haynie, J.W. Spence and J.B. Upham, "Effects of Air Pollutants on Weathering Steels and Galvanized Steel: A Chamber Study," Atmospheric Factors Affecting the Corrosion of Engineering Metals, ASTM STP 646, S.K. Coburn, Ed., American Society for Testing and Materials, pp.30(1978)

(49) "The OECD Programme on Long Range Transport of Air Pollutants," OECD, Paris,

1977, 2nd Ed.

(50) A. Eliassen, Atmos. Environ., **12**, 479(1978)

(51) G. Howells, Acid Rain and Acid Waters, Ellis Horwood Limited, 1990

(52) The Acid Rain Sourcebook, T.C. Elliott, R.G. Schwieger, Eds. McGraw-Hill, Inc., New York (1984)

(53) Materials Degradation Caused by Acid Rain, ACS Symposium Series 318, R. Baboian, Ed., American Chemical Society, Washington, DC 1986

(54) B. Ottar, "Acidification of Precipitation," Materials Degradation Caused by Acid Rain, ACS Symposium Series 318, R. Baboian, Ed., American Chemical Society, Washington, DC, pp.2(1986)

(55) J.S. Gamble and C.I. Davidson, "Measurement of Dry Deposition onto Surrogate Surfaces: A Review," Materials Degradation Caused by Acid Rain, ACS Symposium Series 318, R. Baboian, Ed., American Chemical Society, Washington, DC, pp.42(1986)

(56) D.J. Spedding, Br. Corros. J., **7**, 281(1972)

(57) T. Sydberger and N.G. Vannerberg, Corros. Sci., **12**, 775(1972)

(58) J.R. Duncan, D.J. Spedding and E.E. Wheeler, Corros. Sci., **13**, 69(1973)

(59) J.R. Duncan and D.J. Spedding, Corros. Sci., **13**, 993(1973)

(60) J.R. Duncan and D.J. Spedding, Corros. Sci., **14**, 241(1974)

(61) M.W. Kendig, E.M. Meyer, G. Lindberg and F. Mansfeld, Corros. Sci., **23**, 1007(1983)

(62) C. Gabrielli, Identification of Electrochemical Proc. Instrumentation Group, Solartron, Farnborough, Hampshire, U.K. 1980

(63) M.J. Justo and M.G.S. Ferreira, Corros. Sci., **29**, 1353(1989)

(64) M. Stratmann, H. Streckel, K.T. Kim and S. Crockett, Corros. Sci., **30**, 715(1990)

(65) G.G. Koschelev, G.B. Klark, Trudy Inst. Fiz. Chim., **8**, 84(1960)

(66) J.E.O. Mayne, J. Appl. Chem., **9**, 673(1959)

(67) A.G. Tanner, Chem. Ind., 1027(1964)

(68) H. Schwarz, Werkst. Korros., **16**, 93, 208(1965)

(69) T.K. Ross and B.G. Callaghan, Corros. Sci., **6**, 337(1966)

(70) U.R. Evans, Nature, Lond., **206**, 980(1965)

(71) K. Barton, D. Kuchynka, Z. Bartonova and E. Beranek, Corros. Sci.,**11**, 937(1971)

(72) T.E. Graedel and R.P. Frankenthal, J. Electrochem. Soc., **137**, 2385(1990)

(73) P.F. Wieser, in "Atmospheric Corrosion," W.H. Ailor, Editor, John Wiley & Sons, Inc., New York, pp.453(1982)

(74) G.K. Singhania and B. Sanyal, Br. Corros. J., **8**, 224(1973)

(75) G.M. Florianovich, L.A. Sokolova and Y.M. Kolotyrkin, Electrochim. Acta, **12**, 879(1967)

(76) K. Barton and Z. Bartonova, Werkst. Korros. **20**, 216(1969)

(77) J.R. Duncan, Werkst. Korros., **25**, 420(1974)

(78) U.R. Evans, Nature, **206**, 980(1965)

(79) U.R. Evans, Tran. Inst. Met. Finishing, **37**, 1, esp. 5 (1960)

(80) U.R. Evans, The Corrosion and Oxidation of Metals: First Supplementary Volume, Edward Arnold (Publishers) Ltd., London, 195(1968)

(81) I. Suzuki, N. Masuko and Y. Hisamatsu, Corros. Sci., **19**, 521(1979)

(82) I. Matsushima and T. Ueno, Corros. Sci., **11**, 129(1971)

(83) M. Cohen, K. Hashimoto, J. Electrochem. Soc., **121**, 42(1974)

(84) J.E. Hiller, Werkst. Korros., **17**, 943(1966)

(85) L. Formaro, Corros. Sci., **20**, 1251(1980)

(86) J. Dunnwald and A. Otto, Corros. Sci., **29**, 1167(1989)

(87) M. Stratmann, K. Bohnenkamp, T. Ramchandran, Corros. Sci., **27**, 905(1987)

(88) C.F. Barrett, D.H.F. Atkins, J.N. Cape, et al, Acid Deposition in the United Kingdom: Second Report of the UK Acid Rain Review Group, Department of the Environment, London, U.K.(1987)

(89) T. Misawa, T. Kyuno, W. Suetaka and S. Shimodaira, Corros. Sci., **11**, 35(1971)

(90) B.R. DE Meybaum and E.S. Ayllon, Corrosion, **36**, 345(1980)

(91) J.T. Keiser and C.W. Brown, Corros. Sci., **23**, 251(1983)

(92) S. Okamoto, J. Am. Ceram. Soc., **51**, 594(1968)

(93) P. Keller, Werkst. Korros., **18**, 865(1967)

(94) H. Leidheiser, Jr. and Svetozar Music, Corros. Sci., **22**, 1089(1982)

(95) H. Leidheiser, Jr. and Ilona Czako-Nagy, Corros. Sci., **24**, 569(1984)

(96) T. Misawa, K. Hashimoto and S. Shimodaira, Corros. Sci., **14**, 131(1974)

(97) T. Misawa, K. Asami, K. Hashimoto and S. Shimodaira, Corros. Sci., **14**, 279(1974)

(98) A.K. Singh, T. Ericsson, L. Haggstrom, Corros. Sci., **25**, 931(1985)

(99) P. Keller, Werkst. Korros., **20**, 102(1969)

(100) M. Kiyama, T. Akita, S. Shimizu, Y. Okuda and T. Takaa, Bull. Chem. Soc. Jpn., **45**, 3422(1972)

(101) D.C. Smith and B. McEnaney, Corros. Sci., **19**, 379(1979)

(102) Ph. Refait and J.M.R. Genin, Corros. Sci., **34**, 797(1993)

(103) A.A. Olowe and J.M.R. Genin, Corros. Sci., **32**, 965(1991)

(104) Ph. Refait and J.M.R. Genin, Corros. Sci., **36**, 55(1994)

(105) T. Misawa, Corros. Sci., **13**, 659(1973)

(106) I.L. Roikh, 3rd Int. Cong. on Mettallic Corros., Moscow(1966)

(107) M. Yamashita, H. Miyuki, Y. Matsuda, H. Nagano and T. Misawa, Corros. Sci., **36**, 283(1994)

(108) U.R. Evans, The Corrosion and Oxidation of Metals: Second Supplementary Volum, Edward Arnold, 248(1976)

(109) G.D. Bengough, Proc. Roy. Soc. A. **131**, 494(1931)

(110) W.I. Whitton, Trans. Faraday Soc., **46**, 927(1950)

(111) S.G. Fishman, C.R. Crowe, Corros. Sci., **17**, 27(1977)

(112) C. Fiaud, R. Chahrouri, M. Keddam, G. Maurin, H. Takenouti, Proc. 8th Int. Cong. on Mettallic Corrosion, 18(1981)

(113) C. Fiaud, M. Keddam, A. Kadri, H. Takenouti, Electrochimica Acta, **32**, 445(1987)

(114) A. Cox and S.B. Lyon, Corros. Sci., **36**, 1167(1994)

(115) A. Cox and S.B. Lyon, Corros. Sci., **36**, 1177(1994)

(116) A. Cox and S.B. Lyon, Corros. Sci., **36**, 1193(1994)

(117) M. Stratmann, Corros. Sci., **27**, 869(1987)

(118) M. Stratmann, H. Streckel, Corros. Sci., **30**, 681(1990)

(119) M. Stratmann, H. Streckel, Corros. Sci., **30**, 697(1990)

(120) M. Stratmann, H. Streckel, K.T. Kim, S. Crocket, Corros. Sci., **30**, 715(1990)

(121) Yu.P. Gladkikh, Yu.N. Mikhailovskii, L.A. Shuvakhina, R.I. Nazarova, Zashchita Mettallov, **6**, 505(1970)

(122) A.R. Basman, L.I. Freiman, British Corros. J., **27**, 119(1992)

(123) A.R. Basman, S.B. Adeloju, L.I. Freiman, British Corros. J., **27**, 121(1992)

(124) M. Keddam, A. Hugot-Le-Goff, H. Takenouti, D. Thierry, M. C. Arevalo, Corros. Sci., **33**, 1243(1992)

(125) K. Vetter, Electrochemical Kinetics, New York, London, Academic Press, 394(1967)

(126) A.J. Bard and L.R. Faulkner, Electrochemical Methods: Fundamentals and Applications, John Wiley & Sons, 1980

(127) D. Britz, J. Electroanal. Chem., **88**, 309(1978)

(128) G.K. Berukschtis and G.B. Klark, Korrosija i zaschtschtita Splavov (Corrosion and Protection of Alloys), Metallurgia, Moscow, 1965

(129) Annual Book of ASTM standards, vol. 11.01, p. 454(1989)

(130) U.R. Evans and T.P. Hoar, Proc. Roy. Soc. A, **137**, 343(1932)

(131) S. Glasstone and A. Hickling, Electrolytic Oxidation and Reduction, 1935(London)

(132) Gmelins Handbuch der Anorganischen Chemie, Sauerstoff, System 3, Lieferung 3, Seite 469, Weinheim (1958)

(133) CRC Handbook of Chemistry and Physics, p.f-49, CRC Press, Boca Raton, FL (1990)

(134) F. Mansfeld, Corrosion Processes, (ed. R.N. Parkins), p.1, Applied Science Publications London (1982)

(135) Y. Saito, Rev. Polarogr. (Japan), **15**, 177(1968)

(136) B.R. Scharifker, Modern Aspects of Electrochemistry, No 22, Eds. J.O'M. Bockris, B.E. Conway and R.E. White, Plenum Press, New York and London P467(1992)

(137) M. Pourbaix, Corros. Sci. **12**, 161(1972)

(138) M. Pourbaix, Corros. Sci. **14**, 25(1974)

(139) K. Barton and Z. Bartonova, Werkst. Korros., **21**, 25(1970)

(140) K. Barton and E, Beranek, Werkst. Korros., **10**, 377(1959)

(141) J.O'M. Bockris and A.K.N. Reddy, Modern Electrochemistry, Vol. 2, Macdonald & Co. (Publishers) Ltd, P913(1970)

(142) J.R. Churchill, Trans. Electrochem. Soc., **76**, 341(1939)

(143) P. Delahay, J. Electrochem., **97**, 198(1950)

(144) J.E.O. Mayne and J.A. Burkill, Br. Corros. J., **21**, 221(1986)

(145) S.A. Olszowka, M.A. Manning and A. Barkatt, Corrosion, **48**, 411(1992)

(146) F. Mansfeld, M.W. Kendig and S. Tsai, Corrosion/82, The International Corrosion Forum Sponsored by the NACE, Paper 179(1982)

(147) J.P. De Souza, O.R. Mattos, L. Sathler and H. Takenouti, Corros. Sci., **27**, 1351(1987)

(148) F. Mansfeld and M. W. Kendig, Organic Coatings Science and Technology, 8, 513(1986).

(149) F. Mansfeld and M. W. Kendig, Aluminium Surface Treatment Technology (ed. R. S. Alwitt and G. E. Thompson). The Electrochemical Society Softbound Series, PV-86, p 263.

(150) J. Hitzig, K. Jrttner, W. J. Lorenz and W. Paatsch, Corr. Sci. **24**, 945(1984).

(151) J. Hitzig, K. Juttner and W. J. Lorenz, J. Electrochem. Soc. **133**, 887(1986).

(152) J. L. Dawson, G. E. Thompson and M. B. H. Ahmadun, Electrochemical Impedance: Analysis and Interpretation, ASTM STP 1188, p 257(1993).

(153) Equivalent Circuit, Version 3.97, May 1989, Bernard A. Boukamp, Faculty of Chemical Technology University of Twente.

(154) W. J. Lorenz and F. Mansfeld, Corr. Sci. **21**, 647(1981).

(155) Annual Book of ASTM Standards, Vol. 03.02 p432(1992).

(156) Technical Note 201, EG & G Princeton Applied Research, Electrochemical Instruments.